Impact of High Pressure - Low Temperature Processes on Cellular Materials Related to Foods

vorgelegt von
Diplom-Ingenieur
Oliver Schlüter

von der Fakultät III – Prozesswissenschaften
der Technischen Universität Berlin
zur Erlangung des akademischen Grades

Doktor der Ingenieurwissenschaften
- Dr.-Ing. -

genehmigte Dissertation

Promotionsausschuss:

Vorsitzender: Prof. Dr.-Ing. Dr. e. h. Friedrich Meuser
Berichter: Prof. Dr. Dipl.-Ing. Dietrich Knorr
Berichterin: Dir'in. u. Prof'in. Dr.-Ing. Heike Schuchmann

Tag der wissenschaftlichen Aussprache: 28.07.2003

Berlin 2003
D 83

ACKNOWLEDGEMENTS

This thesis is an extract of my work during the years from 1998 to 2003 in the Department of Food Biotechnology and Food Process Engineering, Berlin University of Technology and I would like to take this opportunity to thank the people who contributed in all sorts of ways to this thesis.

First of all I am very grateful to Prof. Dr. Dipl.-Ing. Dietrich Knorr for inspiring me to focus on high pressure-supported phase transitions, for his constant enthusiasm concerning this interesting field of research and his extensive scientific support. I would like to express my gratitude to Dir'in. and Prof'in. Dr.-Ing. Heike Schuchmann, her generous reviewing with critical comments and alternative views greatly added to the quality of this thesis. I would also like to thank Prof. Dr.-Ing. Dr. e. h. Friedrich Meuser for being the chairman of my thesis defence.

I wish to express my heartfelt thanks to Dr.-Ing. Volker Heinz and Dr. Ing. Alexander Angersbach for being a constant source of help, encouragement and inspiration to me. I especially acknowledge the substantial contribution of Mr. Sujith George, Mr. Edwin Ananta, Mr. Cornelius Luscher and Mr. Gabriel Urrutia Bennet. I gratefully acknowledge the help rendered by all my friends and colleagues, especially Mr. Stefan Boguslawski.

Furthermore, I would like to acknowledge Dr. Carsten Meyer and Dr. Reinhard Schubring for the fruitful co-operation within the "Hochdruck-Verbundprojekt" and the impressive experiences during our high pressure experiments on the Atlantic ocean.

The financial support provided by the German Research Foundation (DFG), the German Federal Ministry of Education and Research (BMBF) and the European Commission (EC) is thankfully acknowledged.

Dedicated to my inner source of love, sunshine and lightness:
Christine, Paul Linus and Julina Fee

LIST OF NOTATIONS **VIII**

ABSTRACT **XI**

KURZFASSUNG **XII**

1 INTRODUCTION **1**

2 THEORY AND LITERATURE REVIEW **8**

2.1 LOW TEMPERATURE PRESERVATION **8**
2.1.1 PHASE TRANSITIONS 8
2.1.2 PRINCIPLE AND PROCESSING STEPS 11
2.1.3 PRODUCTS AND FREEZING SYSTEMS 13
2.1.4 QUALITY AND SAFETY ASPECTS 16
2.1.5 SUBSEQUENT THAWING 19
2.1.6 HEAT TRANSFER AND MODELLING 21
2.2 APPLICATION OF HIGH HYDROSTATIC PRESSURE **28**
2.2.1 GENERAL ASPECTS 28
2.2.2 PHYSICAL PROPERTIES OF WATER 30
2.2.3 WATER-ICE TRANSITION 32
2.2.4 BIOMOLECULAR COMPOUNDS 35
2.2.5 CELLULAR SYSTEMS 37
2.3 HIGH PRESSURE - LOW TEMPERATURE PROCESSES **38**
2.3.1 INDUCTION OF PHASE CHANGES 38
2.3.2 PRESSURE SUPPORTED FREEZING 39
2.3.3 PRESSURE SUPPORTED THAWING 42
2.3.4 MODELLING OF HIGH PRESSURE SUPPORTED FREEZING/THAWING 45
2.3.5 SUBZERO TREATMENT IN THE LIQUID STATE 48
2.3.6 SPECIAL APPLICATIONS 49
2.3.7 REQUIREMENTS FOR THE TECHNICAL EQUIPMENT 50

3 MATERIAL AND METHODS **54**

3.1 TEST SAMPLES **54**
3.1.1 POTATO TISSUES 54
3.1.2 FISH FILLETS 54
3.1.3 MICROORGANISMS 55
3.2 HIGH PRESSURE UNITS **55**
3.2.1 MULTI-VESSEL-SYSTEM 55
3.2.2 LOW TEMPERATURE SYSTEM I 57
3.2.3 LOW TEMPERATURE SYSTEM II 58
3.2.4 PILOT SCALE SYSTEM I 60
3.2.5 PILOT SCALE SYSTEM II 61
3.3 PROCESS EVALUATION **61**
3.3.1 PHASE TRANSITION POINTS 61
3.3.2 DESCRIPTION OF MELTING CURVES 63

3.3.3 CALCULATION OF PHASE TRANSITION TIMES 64
3.3.3.1 Modelling 64
3.3.3.2 Thermodynamic properties 64
3.3.3.3 Stability criteria 65
3.3.3.4 Treatment & procedure 66
3.4 QUALITY ASSESSMENT 68
3.4.1 PLANT DERIVED TISSUE 68
3.4.1.1 High pressure treatments 68
3.4.1.2 Impedance measurement 69
3.4.1.3 Texture measurement and analyses 70
3.4.1.4 Colour measurement and visual appearance 71
3.4.1.5 Thermal analyses 71
3.4.2 ANIMAL DERIVED TISSUE 72
3.4.2.1 Thawing experiments 72
3.4.2.2 Water holding capacity 72
3.4.2.3 Thawing loss 72
3.4.2.4 Sensory tests 73
3.4.2.5 Texture analyses 73
3.4.2.6 Colour changes 73
3.4.2.7 Calorimetric analyses 73
3.4.2.8 Viable count of microorganisms 73
3.4.2.9 Parasites 74
3.4.2.10 Statistical analysis 74
3.4.3 INACTIVATION OF MICROORGANISMS 74
3.4.3.1 Sample preparation 74
3.4.3.2 Treatment 75
3.4.3.3 Enumeration of viable cells 75
3.4.3.4 Regression analysis 76

4 RESULTS AND DISCUSSION 78

4.1 PROCESSING CRITERIA FOR CONTROLLED PRESSURE-SUPPORTED PHASE TRANSITIONS 78
4.1.1 INTRODUCTION 78
4.1.2 PHASE TRANSITION LINES OF PLANT TISSUE 78
4.1.2.1 Melting curve ice I 78
4.1.2.2 Melting curve ice III 80
4.1.2.3 Melting curve ice V 81
4.1.2.4 Solid-solid phase boundary 83
4.1.2.5 Phase diagram 84
4.1.2.6 Liquid-solid contour plot 85
4.1.3 MODELLING HIGH PRESSURE SUPPORTED FREEZING OF PLANT TISSUE 87
4.1.3.1 Relevant aspects 87
4.1.3.2 Pressure assisted freezing to ice I 88
4.1.3.3 Pressure assisted freezing to ice III 91
4.1.3.4 Pressure assisted freezing in metastable zones 92
4.1.3.5 Pressure shift freezing 94
4.1.3.6 Discussion on temperature profiles 95
4.1.3.7 Supercooling and instantaneously formed ice 97
4.1.4 HIGH PRESSURE SUPPORTED THAWING OF PLANT TISSUE 99
4.1.4.1 Temperature evolution during pressure-assisted thawing 99
4.1.4.2 Modelling thermophysical properties 100

4.1.4.3 Calculation of pressure-assisted thawing times 103
4.1.4.4 Impact of sample size 105
4.1.4.5 Prediction of thawing profiles 107
4.1.4.6 Pressure assisted and pressure induced thawing 108
4.1.4.7 Critical parameters for pressure supported melting 109
4.2 QUALITY AND SAFETY ASPECTS OF HIGH PRESSURE - LOW TEMPERATURE PROCESSES 113
4.2.1 IMPACT OF HIGH PRESSURE-LOW TEMPERATURE PROCESSING ON PLANT TISSUE 113
4.2.1.1 Characteristic pressure and temperature plots 113
4.2.1.2 Indication of phase transitions by impedance spectra 116
4.2.1.3 Process induced changes of the cell membrane 118
4.2.1.4 Effects of phase transitions on textural properties 120
4.2.1.5 Evaluation of changes in colour and visual appearance 122
4.2.2 IMPACT OF HIGH PRESSURE THAWING ON ANIMAL TISSUE 125
4.2.2.1 Evaluation of the required processing time 125
4.2.2.2 Effects of thawing and subsequent heating on sensory attributes 126
4.2.2.3 Pressure and heat induced changes in texture 127
4.2.2.4 Evaluation of processing effects on colour and proteins 128
4.2.2.5 Treatment effects on water loss and pH value 130
4.2.2.6 Effect on microorganisms and parasites 132
4.2.3 IMPACT OF HIGH PRESSURE-LOW TEMPERATURE PROCESSING ON MICROORGANISMS 134
4.2.3.1 Inactivation kinetics of Listeria innocua 134
4.2.3.2 Bacteria inactivation in frozen solutions 136
4.2.3.3 Influences of p,T-combinations on the rate constant 137
4.2.3.4 Pressure resistance of Listeria innocua in food matrix 138

5 SUMMARY AND CONCLUSION 140

5.1 MODELLING OF HIGH PRESSURE SUPPORTED WATER-ICE TRANSITIONS 140
5.2 DEFINITION OF METASTABLE STATES IN THE PHASE DIAGRAM 143
5.3 IMPROVEMENT IN HIGH PRESSURE – LOW TEMPERATURE PROCESSES 144
5.4 IMPACT OF PROCESS PARAMETERS ON QUALITY AND SAFETY ASPECTS 146
5.5 PERSPECTIVES OF HIGH PRESSURE – LOW TEMPERATURE PROCESSES 149

6 REFERENCES 154

LIST OF PUBLICATIONS 170

LIST OF NOTATIONS

Symbols

α	thermal diffusivity	$m^2\ s^{-1}$
α	thermal expansion coefficient	K^{-1}
β	isothermal compressibility	Pa^{-1}
λ	thermal conductivity	$W\ m^{-1}K^{-1}$
φ	electrical conductivity	$\mu S\ cm^{-1}$
ρ	density	$kg\ m^{-3}$
Θ	temperature quotient	-
α, χ	adjustable coefficient (equation 3.1)	-
β, δ	adjustable exponent (equation 3.1)	-
ΔG_{act}	activation energy	$J\ mol^{-1}$
ΔH	enthalpy	J
ΔT_{sup}	degree of supercooling	K
ΔV_{act}	reaction volume	$cm^3\ mol^{-1}$
μ	viscosity	Pa s
A	peak parameter (equation 3.7)	
A	constant (equation 2.10)	-
A_i	cross-sectional area of a cylindrical sample before compression	mm^2
A_x	heat flux area normal to the direction of heat flow	m^2
B	scale parameter (equation 3.5, 3.6, 3.7)	
B	constant (equation 2.10)	-
Bi	Biot number	-
C	reaction order	
C	shape parameter (equation 3.5, 3.6, 3.7)	
c_p	specific heat at constant pressure	$J\ kg^{-1}\ K^{-1}$
e_q	rate of heat generation per unit volume	$W\ m^{-3}$
F	force	N
Fo	Fourier number	-
F_p	fractional pore area	%
G	Gibbs energy	$J\ mol^{-1}$
H	sample height	mm
H	surface heat transfer coefficient	$W\ m^{-2}K^{-1}$
J	temperature dependence	-
K	rate constant	s^{-1}
K	equilibrium constant	-
$k_{1,2,3...20}$	coefficients	-
L	latent heat	$J\ kg^{-1}$
l_c	length of the cell	m
l_m	thickness of the cell membrane	m
m_i	mass of ice	g
m_w	mass of liquid water	g
N	nucleation rate	$mol^{-1}\ s^{-1}$
N_0	initial number of cells	ml^{-1}
$o_{1,2,3}$	adjustable coefficients (eqn. in table 2.3)	-
P	pressure	MPa
p_m	melting pressure (equation 3.1)	MPa

p_N	pressure to normalise another pressure value	MPa
q_c	rate of heat flow by convection	W
q_x	rate of heat flow in the x-direction	W
R	universal gas constant	8.314 J mol^{-1} K^{-1}
R	radius	m
S	entropy	J K^{-1}
T	time	s, h
T	temperature	°C, K (T [K]=T [°C]+273.16)
T_∞	temperature of the surrounding fluid	K
T_f	freezing temperature	°C
T_g	glass transition temperature	°C
T_m	melting temperature	°C
T_N	temperature to normalise another temperature	K
U	concentration of microorganisms	
V	volume	m^3
X	mass fraction	%
X	radial distance	m
ε_c	true compressive strain	-
σ_c	true compressive stress	N mm^{-2}

Abbreviations

AC	alternating current
ADP	adenosine diphosphate
AF	atmospheric freezing
AMP	adenosine monophosphate
AT	atmospheric thawing
ATP	adenosine triphosphate
CFU	colony forming unit
DMSO	dimethylsulphoxide
DNA	deoxyribonucleic acid
DSC	differential scanning calorimetry
FSE	fit standard error
HHP	high hydrostatic pressure
IAPWS	International Association for the Properties of Water and Steam
OD	optical density
PAF	pressure-assisted freezing
PAT	pressure-assisted freezing
PIF	pressure-induced freezing
PIT	pressure-induced thawing
PSF	pressure-shift freezing
PST	pressure-shift thawing
QIM	quality index method
TVC	total viable count

Sub/superscripts

0, 1	denote the time moments before and after the chosen time interval
A	ash
Act	activation
B	bound water

C	compressive
C	carbohydrate
E	denotes final state
Exp	experimental
F	freezing
F	failure
H	at high frequency
I	denote initial state
I	Cartesian space coordinates
I, III, V	denotes polymorphs of ice
L	at low frequency
M	melting
m	denotes the location of the volume element along the radial *x*-direction
N	denotes a value to normalise another value
O	other components
P	protein
Tr	denotes phase transitions
Treat	treated sample
W	water

ABSTRACT

The currently established methods used for processing and producing food primarily concentrate on combining different processes to achieve desired qualities and shelf-life. With the exception of fermentation and the addition of permitted preservatives, the processes used primarily have a purely physical effect on the food matrix. However, with the use of conventional thermal processes the properties of the complex system "food" and/or single food components could be influenced, with respect to the process target. On one hand different aggregate states are used for drying, steaming, crystallising, melting and extracting, on the other hand the reactive state of high and low molecular organic substances, enzymes and microorganisms are selectively influenced (e.g. blanching, pasteurisation, sterilisation, coagulation). The phase or state changes are not only influenced by temperature but also directly effected by the acting pressure. With the application of high hydrostatic pressure there arises a new opportunity to specifically control phase changes during treatment of foods especially in the low temperature domain. Increased hydrostatic pressure influences the phase transition of water by way of depressing the freezing/melting point as well as reducing the latent heat of fusion. Furthermore different solid states of pure water with a higher density than the fluid exist under hydrostatic pressure above 209 MPa.

Consequently, this thesis work was carried out to estimate the potential of application of high hydrostatic pressure at low temperature with special regard to high pressure supported water-ice transitions for innovative food processing. The processing effects on cellular materials related to food, i.e. plant tissue (potato), animal tissue (fish) and on microorganisms (*Listeria innocua*) were evaluated. In the first step of this study the phase transition lines of water in potato tissue was examined, as an example for cellular food matrices. An empirical model was adapted to accurately describe the melting curves of different ice polymorphs (ice I, ice III and ice V) for pressure levels up to 400 MPa. In the second step, high pressure-supported freezing was investigated, considering also the formation of higher ice polymorphs, with the intention of developing a model enabling the calculation of freezing times. The mathematical model was based on the solution of differential equations governing heat transfer. The apparent specific heat and thermal conductivity were modelled as functions of the pressure-dependent freezing point using the Density- and Cumulative-Weibull distribution functions. In the third step this mathematical model was adapted to also calculate temperature profiles during high pressure-supported thawing. Significant shortening of freezing/thawing times was observed for pressure supported phase transitions processes when compared to conventional processes. Different metastable states of water (liquid and solid) were experimentally observed and defined according to their process dependent stability.

Based on the results of the experiments on process evaluation, specific process parameters were selected for the investigation of the impact of high pressure - low temperature processes on quality attributes of cellular foods. The impact on potato tissue was investigated by texture analysis and impedance analysis, a non-destructive method which measures the state of the cellular membranes throughout the whole sample after treatment. Using impedance analysis, special attention could be paid to the kinetic development of the state of the membranes after the treatment. Macroscopic changes, and browning reactions of the potato tissue were documented by photographs and colour measurements. Considerable improvements compared to conventional freezing were found for some pressure supported freezing processes. Beside pressure-shift freezing, the processes of freezing to different solid states (ice I, ice III and ice V, as well as storage at –28 °C and 250 MPa up to 24 h) of potato samples as well as solid-solid transformations were examined. The effects of high pressure-supported thawing on the quality of fish fillets were investigated. The influences of pressure assisted thawing at 200 MPa and of conventional thawing on the quality of both the thawed product and the subsequently cooked sample was compared. Using several commercially important fish species, the quality was evaluated by sensory, physico-chemical and microbiological methods. An improved product safety was indicated by high pressure inactivation of specific microorganisms and parasites. Furthermore, the effect of relevant pressure-temperature combinations on *Listeria innocua* (as indicator for *Listeria monocytogenes*) dispersed in different media was investigated in order to estimate the potential for increasing the product safety by applying high pressure supported freezing/storing/thawing processes. The inactivation kinetics obtained was modelled using an empirical formula. On the basis of the accumulated results and with respect to critical processing criteria several process strategies were proposed to effectively use the potential of high pressure application in the low temperature domain for innovative food processing.

KURZFASSUNG

Bei den gegenwärtig im industriellen Maßstab eingesetzten Verfahren zur Herstellung und Verarbeitung von Lebensmitteln handelt es sich überwiegend um Kombinationen verschiedener Prozessschritte, die zur Erzielung der gewünschten Produkteigenschaften und zur Gewährleistung einer bestimmten Lagerungszeit angewendet werden. Neben Fermentationsverfahren und der Beimengung zugelassener Hilfs- und Konservierungsstoffe handelt es sich dabei vorrangig um rein physikalische Einflussnahmen auf die Lebensmittelmatrix. Abgesehen von den mechanischen Verfahren, wird besonders bei thermischen Prozessen der Zustand des komplexen Systems „Lebensmittel“, bzw. einzelner Bestandteile durch die Verarbeitung dem vorgegebenen Prozessziel entsprechend verändert. Einerseits werden unterschiedliche Aggregatzustände genutzt wie etwa beim Trocknen, Verdampfen, Kristallisieren, Schmelzen und Extrahieren, andererseits werden möglichst selektiv die reaktiven Zustände von nieder- und hochmolekularen organischen Substanzen, von Enzymen sowie von Mikroorganismen beeinflusst (Blanchieren, Pasteurisieren, Sterilisieren, Koagulieren, usw.). Die Phasen- bzw. Zustandsänderungen sind jedoch nicht nur von der Temperatur abhängig, sondern werden auch maßgeblich vom wirkenden Druck beeinflusst. Mit der Anwendung von hohem hydrostatischem Druck bietet sich eine neuartige Möglichkeit zur gezielten Steuerung zahlreicher Phasenumwandlungsprozesse bei der Lebensmittelverarbeitung, besonders im Bereich niedriger Temperaturen. Ansteigender hydrostatischer Druck beeinflusst den Phasenübergang von Wasser, wobei die Gefrier- bzw. Schmelztemperatur erniedrigt wird und begleitend eine Reduzierung der ab- bzw. zuzuführenden Kristallisationswärme erfolgt. Bei Drücken oberhalb von 209 MPa existieren zusätzliche Eiskristallformen mit einer höheren Dichte als die des Wassers.
Die vorliegende Arbeit beschäftigt sich daher mit der Einschätzung des Potentials von Anwendungen hoher hydrostatischer Drücke im Bereich niedriger Temperaturen zur Umsetzung innovativer Lebensmittelverarbeitungsschritte unter besonderer Berücksichtigung von Wasser-Eis-Transformationen. Dabei wurde der Einfluss verschiedener Prozesse auf zellulare, lebensmittelrelevante Materialien, d.h. pflanzliches Gewebe (Kartoffel), tierisches Gewebe (Fisch) sowie Mikroorgansimen (*Listeria innocua*) bewertet. Beispielhaft für das Verhalten zellularer Matrices wurden zunächst die Phasengrenzlinien von Wasser im Kartoffelgewebe untersucht. Die Schmelzkurven für verschiedene Eismodifikationen (Eis I, Eis III und Eis V) konnten durch Adaption eines empirischen Models mit guter Übereinstimmung für einen Druck bis 400 MPa beschrieben werden. Unter Berücksichtigung der Bildung höherer Eisformen wurden in einem zweiten Schritt unterschiedliche druckunterstützte Gefrierverfahren untersucht, mit der Intention, ein Model zur Berechnung von Gefrierzeiten zu entwickeln. Das mathematische Model basiert auf einer nummerischen Lösung von Differentialgleichungen zur Beschreibung relevanter Wärmetransportprobleme. Die notwendige Einbindung der scheinbaren spezifischen Wärmekapazität sowie der Wärmeleitfähigkeit am druckabhängigen Gefrierpunkt erfolgte unter Verwendung der Funktion der Weibull-Dichte-Verteilung bzw. der Kumulierten-Weibull-Verteilung. In einem dritten Schritt wurde das mathematische Modell modifiziert, um die Berechnung der Temperaturprofile bei hochdruckunterstützten Auftauprozessen zu ermöglichen. Im Vergleich zu konventionellen Prozessen konnten für die hochdruckunterstützten Phasenumwandlungsprozesse deutliche Verkürzungen der Gefrier- und Auftauzeiten festgestellt werden. Verschiedene metastabile Zustände von Wasser (flüssig und fest) wurden experimentell nachgewiesen und entsprechend ihrer prozessabhängigen Beständigkeit definiert.
Basierend auf den experimentellen Ergebnissen zur Prozessbetrachtung wurden bestimmte Prozessparameter ausgewählt, um die Auswirkung von Hochdruck–Niedrigtemperatur Anwendungen auf qualitative Merkmale von zellularen Lebensmitteln zu untersuchen. Der Einfluss auf Kartoffelgewebe wurde mittels Texturanalyse und Impedanzanalyse, einer zerstörungsfreien Untersuchungsmethode, bewertet. Die Messung des Impedanzspektrums ermöglichte eine Aussage über den Zustand der Zellmembran innerhalb der gesamten Probe im Anschluß an eine Behandlung, wobei insbesondere die fortschreitenden Änderungen des Membranzustands beachtet werden konnten. Makroskopische Veränderungen sowie Bräunungsreaktionen wurden fotografisch bzw. durch Farbmessungen dokumentiert. Für einige hochdruckunterstützte Verfahren konnten merkliche Verbesserungen im Vergleich zu einem herkömmlichen Gefrierprozess aufgezeigt werden. Neben dem Druckwechselgefrieren wurde dabei das Gefrieren zu unterschiedlichen Eismodifikationen (Eis I, Eis III und Eis V), die Lagerung von Kartoffelproben bei –28 °C und 250 MPa (bis zu 24 h) sowie Kristall-Umwandlungen untersucht. Am Beispiel von verschiedenen, kommerziell bedeutsamen Fischarten wurde der Qualitätseinfluss des hochdruckunterstützten Auftauens bei 200 MPa im Vergleich zum konventionellen Auftauen bei 0.1 MPa beschrieben. Die qualitativen Merkmale der aufgetauten sowie der anschließend erhitzten Proben wurden anhand von sensorischen, physiko-chemischen oder auch mikrobiologischen Methoden einander gegenübergestellt. Die Hochdruckinaktivierung von fischspezifischen Mikroorganismen sowie von Parasiten deutete auf eine Erhöhung der Produktsicherheit. Um das Potential von hochdruckunterstützten Gefrier-, Auftau- und Lagerprozessen zur Steigerung der Produktsicherheit bewerten zu können, wurde zusätzlich der Einfluss relevanter Druck-Temperatur-Zeit-

Kombinationen auf *Listeria innocua* (als Indikatorkeim für *Listeria monocytogenes*) in verschiedenen Medien untersucht. Die aufgezeichneten Inaktivierungskinetiken konnten unter Verwendung einer empirischen Formulierung beschrieben werden. Basierend auf der Gesamtheit der gewonnenen Resultate konnten unter Berücksichtigung einzelner Verarbeitungskriterien mehrere Prozessstrategien vorgeschlagen werden, um das Potential der Anwendung hohen hydrostatischen Drucks im niedrigen Temperaturbereich effizient bei innovativen Lebensmittelverarbeitungskonzepten nutzen zu können.

1 INTRODUCTION

The complexity of foods arises from their biological origin and their spatial heterogeneity on a variety of scales which one can even find in single cell units. Fruit, vegetables, meat, poultry and fish are all derived from living organisms which are composed of cells. It is this cell structure which is one of the major contributors to the characteristic texture of a food (Christensen, 1984). Plant and animal related tissues are cellular networks, in which the occurrence and the amount of nutritive and essential compounds are strongly dependent on environmental, agricultural and processing factors. The selective prevention and/or the controlled damage (e.g. bacteria, yeast, moulds) of various food related cellular systems with regard to their specific and functional quality are main targets of several food processing steps. To ensure the distribution of high quality, fresh-like products several preservation methods are being applied in the food industry extending the shelf-life and overcoming seasonal and site–specific limitations of availability of plant and animal derived food.

Changes in consumers' desires in recent years have led to requirements for foods that are more convenient to store and prepare for consumption, are higher in quality and freshness, are more natural, and are nutritionally healthier than before (Gould, 2000). The reactions of food scientists and technologists to these changed requirements have included research and development into less severe "minimal" preservation and processing methods (Ohlsson, 2000). Many of these methods have been based on the use of existing preservation methods in new ways, particularly in new combinations according to "hurdle concepts" (Leistner, 2002). A number of novel physical processes like high electric field pulses, manothermosonication (combined ultrasonic, heat and pressure), electron beam and gamma irradiation, laser and non-coherent light pulses, and high magnetic field pulses offer exciting alternative possibilities to heat treatments (Gould, 2002). Among the investigated non-thermal physical techniques for food preservation the application of high hydrostatic pressure was industrially established recently (Thakur and Nelson, 1998; Rovere, 2002). Examples of commercial pressure treated products in Europe and US are: Orange juice by UltiFruit®, Pernod Ricard Company, France; avocado puree (Guacamole) by Avomex Company in US (Texas/Mexico); and sliced ham (cured-cooked and/or raw-cooked) by Espuna Company, Spain (Tewari *et al.*, 1999). The attractive effects of application of high hydrostatic pressure to food processing include inactivation of microorganisms and enzymes, quality retention (such as colour and flavour), changes in product functionality and modifications of biopolymers (Knorr, 1993). From a food processing/engineering perspective, key advantages of high pressure application to food systems are the independence of size and geometry of the sample during processing, possibilities for low temperature treatment and the availability of a waste-free, environment-friendly technology (Knorr, 1996).

However, numerous interesting effects of high pressure on the solid-liquid and solid-solid phase transitions of water (the major constituent of most food materials), which have been studied in detail by Bridgman (1912) have been neglected by food R&D until recently. Besides a depression

of the freezing-point to a minimum of –22°C at 209.9 MPa (Wagner *et al.*, 1994) a reduced enthalpy of crystallisation can be observed, thereby accelerating phase transition processes (Kalichevsky *et al.*, 1995). Furthermore, different solid forms of pure water exist under pressure with a higher density than the fluid. Taking advantage of the phase diagram of water, various pathways of changing the physical state of food can be followed using external manipulations of temperature and/or pressure. Definitions on possible high pressure-low temperature processes can be given based on a terminology introduced by Knorr *et al.* (1998). The processing steps are shown in Figure 1.1. The processes ranges from storing food under high pressure at subzero temperatures without freezing (A-B-C-D-C-B-A) to freezing at temperatures above 0°C (A-B-C-K-ice VI). Some of the more interesting possibilities are: pressure assisted freezing (A-B-H-I, i.e., pressurisation of an unfrozen sample, cooling, freezing at nearly constant pressure, pressure release) and pressure assisted thawing (I-H-B-A, i.e., pressurisation of a frozen sample, heating, thawing at nearly constant pressure, warming, pressure release). Pressure shift freezing (A-B-C-D-E) is another process of increasing interest where crystallisation is induced simultaneously in the whole subcooled sample by fast pressure release, with the intention of obtaining small and uniform ice crystals in the sample with minimum damage to the tissue. The reverse of this process is pressure induced thawing (E-D-C-B-A), where the phase change is induced by pressurisation. Freezing of tissue water to different ice modifications is also possible with lesser mechanical damage to the tissues expected (because of the higher density of these ice forms compared with the liquid), but these solid forms are stable only under high pressure.

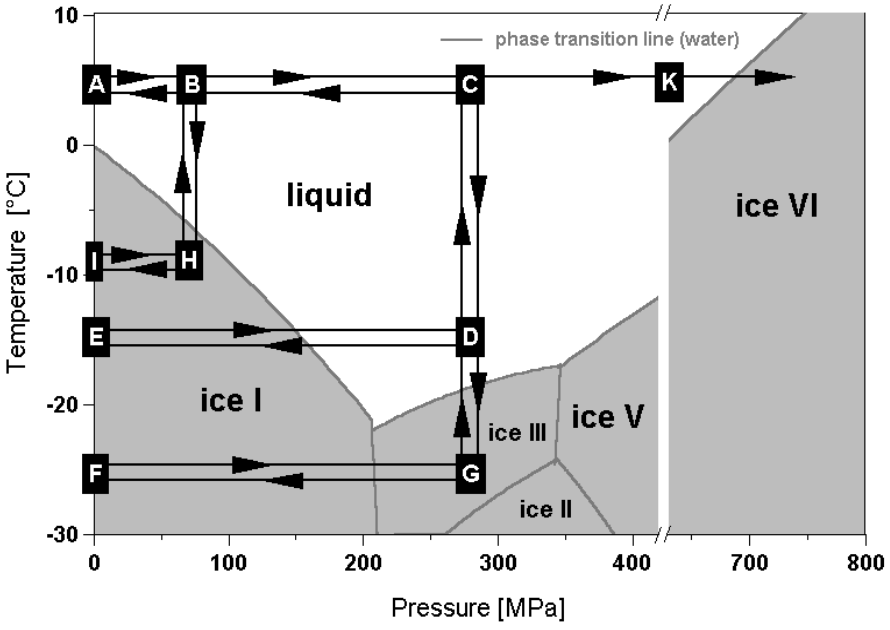

Figure 1.1: Possibilities and definitions of high pressure processing on phase transitions of water modified according to Knorr *et al.* (1998). 1: subzero storage without freezing (A, B, C, D, C, B, A); 2: pressure assisted[1] freezing (A, B, H, I); 3: pressure assisted thawing (I, H, B, A); 4: pressure shift[2] freezing (A, B, C, D, E); 5: pressure induced[3] thawing (E, D, C, B, A); 6: pressure assisted[1] freezing to ice III (A, B, C, D, G) and subsequent transformation to ice I (G, F); 7: solid-solid (ice I/ice III) transformation (F, G) and subsequent pressure assisted[1] thawing of ice III (G, D, C, B, A); 8: freezing above 0°C (A, B, C, K, ice VI). Note: [1]assisted: phase transition under constant pressure; [2]shift: phase transition due to pressure change; [3]induced: phase transition initiated with pressure change continued at constant pressure.

It is widely established that freezing of food provides a safe and convenient way of shelf life extension without negative effects on the nutritional quality. The subsequent thawing of the frozen food is a process assuming no meagre importance. However, parameters like product geometry, the flow rate of the surrounding fluid, the thermophysical properties, as well as the temperature difference between the product and the environment have significant influences on the rate of phase transition. Conventionally, the choice of important process parameters is defined by product specific qualities (e.g. cooling rate and supercooling before freezing by sample size, thawing-medium temperature by protein denaturation in fish and meat). Recent investigations to improve freezing and/or thawing processes of foods showed an increasing interest in the use of high hydrostatic pressure to support phase transitions (Cheftel *et al.*, 2000; Cheftel *et al.*, 2000; Denys *et al.*, 2002; Cheftel *et al.*, 2002; Li and Sun, 2002 a).

With respect to the food quality parameters, the advantages of pressure-assisted and pressure shift freezing have been widely reported and prevention of food damages was shown (Sanz *et al.*, 1997; Otero *et al.*, 1998; Levy *et al.*, 1999; Teramoto and Fuchigami, 2000; Chevalier *et al.*, 2001). Koch *et al.* (1996) observed that pressure-shift freezing of potato cubes resulted in less damage of the cell structure, less drip loss, and less enzymatic browning than conventionally frozen cubes. Fuchigami *et al.* (1997a; 1997b) reported that improvements in texture and histological damage are achieved in pressure-shift frozen carrots. Otero *et al.* (1998) compared the damage to the microstructure of eggplants frozen by conventional air freezing and by pressure-shift freezing. Pressure-shift frozen samples had the appearance of fresh samples, and no differences between centre and surface cell structure were observed (indicating uniform nucleation). Chevalier *et al.* (2000c) studied the increase in tail muscle toughness and the decrease in myofibrillar protein extractability when pressure-shift freezing Norway lobsters at 200 MPa, attributing these changes to myosin or actin aggregation under pressure. These reported effects on muscle foods are not expected when processing vegetable foods due to different morphological structures of animal and plant tissues. Otero *et al.* (2000b) confirmed the beneficial effects of pressure-shift freezing on whole peaches and mangoes as compared to air-blast frozen samples. The authors reported that the cell damage at sample centre was much less in pressure-shift frozen samples than in air blast frozen, evidenced from scanning electron microscopic analysis. This beneficial effect might result from the formation of smaller ice crystals due to enhanced supercooling and homogeneous nucleation during pressure release. Fuchigami and co-workers (1997a, 1997b, 1997c, 1998a, 1998b) also reported experiments on the formation of other ice polymorphs like ice III and V but the sample temperature was not measured during the high pressure treatments. Less damage to structured biomaterials is expected as compared to conventional freezing, mainly because of a decrease in volume during the phase transition (Kalichevsky *et al.*, 1995; Knorr *et al.*, 1998; Cheftel *et al.*, 2000). However, since freezing of water to ice III and ice V required a high degree of supercooling (Evans, 1967a) the formation of ice III or ice V during the experiments of Fuchigami *et al.* (1997a, 1997c, 1998a, 1998b) remains questionable under the process conditions applied (Teramoto and Fuchigami, 2000; Denys *et al.*, 2002). However, Cheftel *et al.* (2000) pointed out that it is likely that high pressure

ices convert to ice I upon pressure release. Due to this solid-solid phase transition, the expected advantages of freezing to ice III might be neutralised. Edebo and Hedén (1960) reported the disruption of *E. coli* suspended in ice by repeated solid-solid phase transitions between ice I and III, indicating severe structural damage. No attempt was made to investigate the effect of solid-solid transformations on food related tissues.

Research on high pressure-assisted thawing of frozen fish and meat has shown the possibilities of significantly reducing the thawing time (Deuchi and Hayashi, 1992; Murakami *et al.*, 1994; Zhao *et al.*, 1998; Massaux *et al.*, 1999a) as well as of minimising the drip volume after thawing (Murakami *et al.*, 1992; Okamoto and Suzuki, 2001) and subsequent cooking (Massaux *et al.*, 1999b; Chevalier *et al.*, 1999; Rouillé *et al.*, 2002). Using whiting fillet, the minimisation of drip volume, in comparison to atmospheric thawing was observed only when the pressure was maintained for a longer duration than that strictly required for thawing (Chevalier *et al.*, 1999). However thawing drip, calculated on a dry basis, was reduced by 70% for spiny dogfish and by 31% for scallops under the best conditions, which were 150 MPa. Total loss after thawing and cooking was reduced by 20% for spiny dogfish at 150 MPa while it increased by 25% for scallops (Rouillé *et al.*, 2002). Also Murakami *et al.* (1992) reported that the volume of free drip from thawed tuna muscle under high hydrostatic pressure was less than that of thawed tuna muscle under atmospheric pressure. Total drip volume decreased when increasing pressure was used for thawing. When pork meat was thawed by high pressure the drip decreased and the water-holding capacity of the meat improved (Okamoto and Suzuki, 2001). Therefore, reducing the drip loss and lowering the processing time can be seen as major advantages of high pressure-assisted thawing. However, high pressure treatment is also connected with colour and texture changes. These are obviously dependent on the level of pressure applied as well as on the pressurisation time. While almost no changes in colour or penetration force of a pressure-thawed (210 MPa) beef product were observed (Zhao *et al.*, 1998), discoloration and toughening of a pork sample occurred and increased with an increasing working pressure (Massaux *et al.*, 1999a). Therefore, it was concluded that the freezing-thawing process under a pressure of 100 MPa seems to be an advantageous treatment for pork because there is no exudate, and only a slight discoloration and toughening of meat (Massaux *et al.*, 1999b). Furthermore, meat softening was found to be induced during high pressure treatment. At 200 MPa unfavourable changes were provoked by high pressure thawing of pork meat (Okamoto and Suzuki, 2001). When frozen tuna back muscle was thawed under various hydrostatic pressures at various temperatures, the colour of thawed samples was changed (Murakami *et al.*, 1992). Carp muscles treated by high pressure in the range of 100 to 300 MPa lost their transparency, together with an increase of the *L*-values and an increase of pressurisation. In a DSC thermogram, each carp muscle showed endothermic peaks corresponding to the changes of raw carp meat. The endothermic peaks shifted to higher temperature regions with increases of pressure at 200 and 300 MPa. Compared to unfrozen fish muscle, high pressure thawed muscles showed a similar breaking stress. Elasticity was also maintained in the muscle. Based on the above results regarding flesh colour and DSC thermograms, high pressure thawing appears to be a better thawing method for fish muscle as long

as the pressure required for thawing is properly adjusted (Yoshioka *et al.*, 1996). Although there are several data available on pressure-assisted thawing and its effect on food quality, there is a lack of data regarding sensory changes and the potential of high pressure to inactivate undesired microorganisms and fish parasites during the phase transition process. Furthermore, it remains unclear as to what extent the results are influenced by differing properties of the fish species treated.

From an engineering point of view, a theoretically based heat transfer model which could predict the temperature history of a product undergoing high-pressure supported phase transition processes, would be very useful with respect to optimisation procedures and subsequent process design. Freezing/thawing time prediction essentially involves modelling based on unsteady-state heat transfer principles (Pham, 2001). Though abundant literature is available on modelling of freezing and thawing under atmospheric pressure (Delgado and Sun, 2001), reports on modelling of freezing and thawing under high pressure are scarce, the reasons being that potential food-applications of high pressure was neglected until recently and also, the calculation of temperatures is complicated by the fact that the thermophysical and transport properties vary with the temperature, the variations depend on the pressure applied and means for measuring them under high pressure have just partly been invented (Denys and Hendrickx, 1999; ; Först *et al.*, 2000). Otero *et al.* (1997) modelled thermodynamic properties of water and the relationship among pressure, temperature, and specific volume in the liquid water region, the ice I region, and the boundary between both regions. Their disagreement between the theoretical model and experimental data was related to supercooling of samples not considered by the theory. Chourot *et al.* (1997) used Crank Nicholson's finite difference scheme as a numerical approximation to model pressure-assisted thawing based on experimental work with pure water and with an aqueous solution of 4.3% NaCl as a model food. They concluded that lack of knowledge of thermophysical as well as transport properties did not allow accurate predictions of the temperature distributions within the samples. Denys *et al.* (1997) modelled heat transfer during high-pressure-shift freezing and thawing of a test substance (thylose) by extending an existing theoretical method for predicting product temperature profiles during freezing and thawing. The method did not take into account the contribution of convection heat transfer by the pressure transmitting fluid. However, no models were developed to calculate the freezing and thawing times in real food matrices like plant or animal tissues.

Recent studies on pressure phase transition processes focused mainly on the triple point of water/ice I/ice III at 209.9 MPa and -22 °C, where the lowest onset temperature for pressure shift freezing and the highest temperature difference (sample - pressure transmitting medium) by decreasing the melting point of a food sample due to pressurisation is expected. Furthermore this triple point defines the lowest temperature for storing food under high pressure without freezing. To date, storage processes of foodstuffs at subzero temperatures under pressure have not been carried out extensively, but the data on enzyme inactivation at subzero temperatures (Indrawati *et al.*, 1998; Indrawati *et al.*, 2000) suggest that denaturation of some enzymes under pressure might be enhanced by low temperature. Although substantial literature is available on high pressure

inactivation of microorganisms at elevated temperatures there is still a lack of data in the subzero temperature range. However, commonly an analogous slope of the melting curve of food compared to that of pure water was assumed for melting curve of ice I (Denys *et al.*, 1997; Chevalier *et al.*, 2000b) but no data were available describing accurately the melting curves of higher ice polymorphs (e.g. ice III and ice V) in real food matrices. Nevertheless, phase transition processes in the region of thermodynamic stability of ice III was not satisfactorily investigated with respect to food processing. Summarising the available data, it can be concluded that successful application of high pressure – low temperature treatment is strongly dependent on the food matrix treated and the process parameters applied. It seems that vegetable tissues are more susceptible to benefits of pressure-assisted or pressure-shift freezing processes than muscle tissues, especially at pressure levels above 200 MPa.

To estimate the potential of high pressure treatment in the low temperature range and in order to contribute to the understanding and development of high pressure supported phase transitions for food application, and keeping the above perspectives in view, this thesis was organised with the following objectives:

The first part of the thesis (Chapter 4.1) aims at evaluating the processing criteria for controlled pressure-supported phase transitions using potato cylinders as primary model systems. According to (Franks, 1982) and (Denys *et al.*, 2002) the range of investigation was defined for temperatures between –40 °C and +40 °C at pressure levels between 0.1 MPa and 400 MPa. The first step was to determine the phase transition lines of water in the cellular food matrix. The second step was to investigate high pressure supported freezing, considering also the formation of higher ice polymorphs, with the intention of developing a model enabling the calculation of freezing times. The third step was to examine high pressure-supported thawing and thus to adapt this mathematical model to also calculate temperature profiles during relevant thawing processes.

The second part of this thesis (Chapter 4.2) aims at selecting specific process parameters for the investigation of the impact of high pressure low temperature processes on quality attributes of cellular foods, based on the results of the experiments on process concepts. Here the processing effects on plant tissue, animal tissue and on microorganisms were evaluated. To examine the storage of plant tissue (potato) at subzero temperatures without ice formation, compared to pressure shift freezing and freezing to different solid states (ice I, ice III and ice V) at pressures up to 400 MPa, as well as the impact of solid-solid transformation. The impact on the tissue was investigated by texture analysis and impedance analysis, a non-destructive method which measures the state of the cellular membranes throughout the whole sample after treatment. Special attention was paid on the kinetic development of the state of the membranes after the treatment, since ongoing cytolysis after high pressure treatments seems to be possible (Kalchayanand *et al.*, 2002). Furthermore, macroscopic changes, and browning reactions of the potato tissue was documented by photographs and colour measurements. To investigate high pressure supported thawing with respect to its effects on the quality of fish fillets, since high pressure supported thawing seems to have the highest

potential regarding high pressure – low temperature processing of animal tissues. The objective was to compare the influences of pressure assisted thawing at 200 MPa and of conventional thawing on the quality of both the thawed product and the subsequently cooked sample. Using several commercially important fish species, the quality was evaluated by sensory, physico-chemical and microbiological methods. In order to estimate the potential for increasing the product safety by applying high pressure supported freezing/thawing processes without additional heat treatments (e.g. blanching) the effect of relevant pressure-temperature combinations on microorgansims was investigated. *Listeria innocua* was chosen for the experiments since it serves as an indicator for the human pathogen species (*Listeria monocytogenes*). The inactivation kinetics obtained was modelled using an empirical formula.

The final objective was to characterise critical process parameters on basis of the data generated in this study and available literature data, allowing for design of controlled pressure-supported phase transition processes and to consequently present suggestions for improved process concepts. An overview of the current state of the art on high pressure-low temperature processing is presented in the Literature review.

2 THEORY AND LITERATURE REVIEW

2.1 Low temperature preservation

2.1.1 Phase transitions

The term *phase* applies to a homogeneous subsystem of a composite (heterogeneous) system. The phases of a heterogeneous system differ from one another in at least one chemical or physical property. A phase may consist of a single kind of particles (molecules, ions or atoms) or represent a mixture (solution) of different kinds of particles (Hemminger and Höhne, 1984). In pure substances, phases correspond to the states of aggregation. In a heterogeneous system, on the other hand, a number of phases in the same state of aggregation may coexist. For example, all gases and mixtures of gases, water, ice (single crystal), solutions and juices can be defined as homogeneous systems (single phase systems), while a water/ice mixture at 0 °C, oil-water emulsions, some copper-zinc alloys (brass), plant related cells and tissues are heterogeneous systems (multiphase systems).

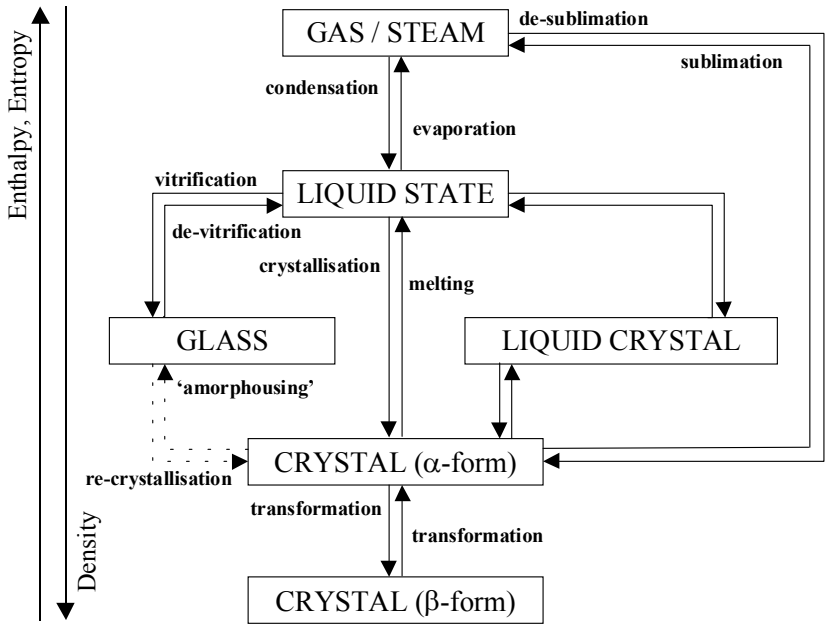

Figure 2.1: Scheme of aggregation states and phase transitions (modified according to Hemminger and Cammenga (1998))

Phase transitions govern changes in the physical state of all materials. They occur at temperatures specific to a given material, depending on pressure. In foods, phase transitions are important in determining physical state during processing, storage and consumption. Possibilities of changing the physical state are summarised in Figure 2.1. However, a system is in a stable state if its thermodynamic potential function has a minimum at the specified boundary conditions. The most commonly occurring boundary conditions stipulate that the pressure p and the temperature T are

specified from the exterior (Hemminger and Höhne, 1984). In such a case the Gibbs function G is a thermodynamic potential function.

$$G = G(T, p)\,. \tag{2.1}$$

The Gibbs free energy can be given as a function of pressure and temperature

$$dG = Vdp - SdT\,. \tag{2.2}$$

The first derivative according to pressure or temperature

$$dG = \left(\frac{\partial G}{\partial T}\right)_p dT + \left(\frac{\partial G}{\partial T}\right)_T dp \tag{2.3}$$

leads to following relations for the entropy S and the volume V:

$$\left(\frac{\partial G}{\partial T}\right)_p = -S\,, \tag{2.4}$$

$$\left(\frac{\partial G}{\partial T}\right)_T = V\,. \tag{2.5}$$

Thermodynamic classification of phase transitions into first-order, second-order, and higher order transition was made by Ehrenfest, (1933). First-order phase transitions govern the changes in the physical state between solid, liquid and gaseous states. In first-order phase transitions, Gibbs energy is the same in both phases ($\Delta G=0$). The Gibbs energy G is a continuous function of temperature and pressure, but it suffers a break at the transition temperature. Therefore, at least one of the first derivatives of Gibbs energy G shows a discontinuous change at the transition temperature, and the transition is noted as a discontinuity in volume, entropy, and other thermodynamic functions (Roos, 1992). At a first-order transition temperature (e.g., crystallisation, melting, condensation, and evaporation temperature), changes in the physical state occur isothermally, and a certain amount of heat is either released (latent heat of crystallisation) or required (latent heat of melting, or enthalpy of melting) as the latent heat (ΔH_{tr}) for the transition. The entropy change can be defined as

$$\Delta S = \frac{\Delta H_{tr}}{T_{tr}}\,, \tag{2.6}$$

In second-order phase transitions both Gibbs energy and its first derivatives are continuous functions of temperature and pressure. At least one of the following second derivatives of G has a discontinuity at the transition temperature:

$$\alpha = \frac{1}{V}\left(\frac{\partial^2 G}{\partial p \partial T}\right)\,, \text{ the thermal expansion coefficient } \alpha \tag{2.7}$$

$$\beta = -\frac{1}{V}\left(\frac{\partial^2 G}{\partial p^2}\right)_T\,, \text{ the isothermal compressibility } \beta \tag{2.8}$$

$$c_p = -T\left(\frac{\partial^2 G}{\partial T^2}\right)_p$$, and/or the specific heat c_p. (2.9)

Second-order transitions occur in amorphous food components as they are transformed from the solid "glassy" state to the more liquid-like "rubbery" state during heating over the glass transition temperature T_g (Tant and Wilkes, 1981; Roos and Karel, 1990). No latent heat is involved for the phase change at the glass transition temperature. The existence of amorphous food materials (in dehydrated, low-moisture and frozen foods) and second-order phase transitions in them increase the complexity of various physical and chemical changes occurring in food systems as functions of temperature and water content, which have been reviewed by (Slade and Levine, 1991). Foods are not chemically pure compounds, and their phase transitions and transition temperatures depend also on composition, and they often exhibit a non-equilibrium, metastable, amorphous state with time-dependent phenomena (Roos, 1992).

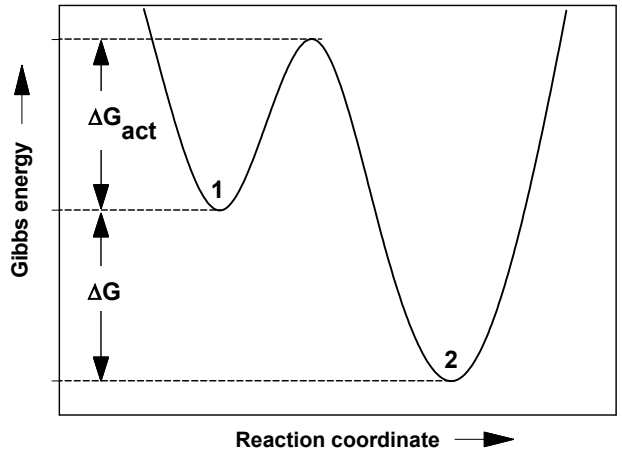

Figure 2.2: Gibbs function of a system in a metastable state and in phase equilibrium with respect to the Gibbs energy of activation ΔG_{act}; ΔG describes the difference of Gibbs function between the metastable state 1 and the stable equilibrium state 2 (redrawn from Hemminger and Höhne, 1984) .

States at which the thermodynamic potential function is at a relative minimum are designated metastable states. They remain stable and simulate an equilibrium state up to the introduction of the activation energy. Figure 2.2 shows a functional path of the Gibbs function with two minima. The system remains at the relative minimum (1) until the Gibbs function rises by ΔG_{act} owing to the introduction of energy (activation energy), whereupon the system overcomes the barrier and reaches the absolute minimum (2), thus releasing the introduced activation energy together with an additional amount of energy (corresponding to ΔG) (Hemminger and Höhne, 1984). The observability of metastable states implies that, at the equilibrium phase transition temperature, the metastable state can be entered on a time scale which is short with respect to the time scale for leaving it. With increasing departure from equilibrium the increasing thermodynamic driving force in favour of the stable states acts to reduce the time scale for escape from metastable states. Thus, unless the time scale for entropy fluctuations within the metastable phase itself becomes long with respect to observation time scales (implying vitrification in the case of supercooled liquids), a condition will finally be reached at which the escape time scale will cross the observation time scale

and a phase change will occur, corresponding to crystallisation in the supercooled liquid case (Angell, 1982).

2.1.2 Principle and processing steps

Temperature is a fundamental descriptor of the state of the system. At high temperatures, molecular motions are more rapid, as described by the Boltzmann relationships. Since molecular motions are more rapid, collision frequencies at the same molecular densities are greater. Thus there is an enhanced kinetics of change. As temperature is reduced, the molecular motions decrease, as do the reaction rates (Reid, 1997). At temperatures below 0 °C there is a significant reduction in growth rates for microorganisms and in the corresponding deterioration of the product due to microbial activity. The same temperature influence applies to most other reactions that might normally occur in the product, such as enzymatic and oxidative reactions. In addition, the formation of ice crystals within the product changes the availability of water to participate in reactions. As the temperature is reduced and more water is converted to a solid state less water is available to support deteriorative reactions (Singh and Heldman, 2001). Thus frozen products benefit from two stabilising factors: reduced temperature and reduced effective moisture content. The primary advantage of frozen products is that of guaranteed long-term stability. At the higher temperatures of storage or shelf-stable products, chemical change is much more rapid, and high quality life is much shorter.

The freezing process consists of freezing, frozen storage and thawing, each of which must be properly conducted to obtain optimum results when preserving foods and living specimens. Freezing involves lowering the product temperature generally to -18 °C or below (Fennema *et al.*, 1973). The temperature reduction process can be divided into three distinct phases: a pre-cooling or chilling phase in which the material is cooled from its initial temperature to the freezing point temperature; a phase change period which represents the crystallisation of most of the water; and a tempering phase in which the product reaches the final established temperature (Delgado and Sun, 2001).

The crystallisation step is started by nucleation. Two categories of nucleation process have been identified which are termed primary and secondary nucleation. Under the heading of primary nucleation the processes of homogeneous nucleation where the seed is spontaneously generated within the system, and heterogeneous nucleation, where some form of catalytic surface exists upon which a nucleus can form are identified (Reid, 1998). The heterogeneous nucleation is the more common process in complex biological systems. An important parameter when studying nucleation of ice is the rate of kinetics at which nuclei appear per volume per unit time: the nucleation rate, *N(T)*. The generalised relationship is:

$$N(T) = A \cdot \exp(B \cdot J), \tag{2.10}$$

where *N(T)* is the steady-state rate of nucleation at temperature (T), *A* and *B* are constants representing several physical parameters of ice and the aqueous water, and *J* describes the

temperature dependence, $((\Delta T_{sup})^2 T^3)^{-1}$, where ΔT_{sup} is the degree of supercooling and T is the absolute temperature (Charoenrein *et al.*, 1991). Since J is dependent on the reciprocal of the square of ΔT_{sup}, low nucleation rates are seen at small levels of supercooling (Sahagian and Goff, 1996). Before nucleation generally supercooling takes place because of a barrier in free energy which has to be overcome to form the initial nucleus of the ice phase. Small clusters of solid-like ice are thought continually to be being formed and destroyed in water even above the freezing temperature, due to thermal fluctuations. The lifetime of these clusters, however, is very small, of the order 10 ps as described by neutron scattering experiments (Kennedy, 1998). Once the temperature falls below T_m, the melting temperature it is possible for an ice nucleus to be stable if it is large enough. Since each nucleus promotes the formation of one ice crystal, the degree of supercooling (ΔT_{sup}), which also is a function of the cooling rate, largely determines the amount and distribution of ice crystals in the product (Sahagian and Goff, 1996). Rapid nucleation rates, favourable during food freezing, are primarily a function of heat removal from the material before phase change (Reid, 1983). However, secondary nucleation describes processes where the growth centres are produced by some form of fragmentation of an existing crystal into a large number of growth centres (more relevant with freeze-concentration of fluid foods in batch crystallisers).

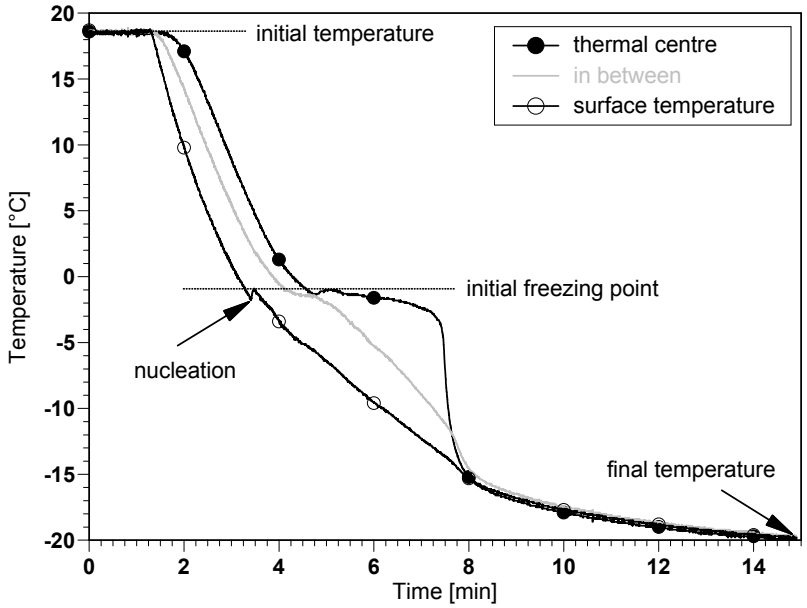

Figure 2.3: Typical temperature history during cryogenic freezing of a potato cylinder (diameter: 13 mm) at atmospheric pressure.

From a typical cooling curve during freezing (Figure 2.3) it can be seen that after the nucleation the temperature increases instantly to the initial freezing temperature. The freezing point of food is depressed compared to pure water due to dissolved solutes. The freezing point depression can be predicted using different kind of models derived from empirical curve fitting, theoretical considerations or semi-empirical estimations (Sahagian and Goff, 1996). The following regression equation to estimate the freezing point T_f of foods from composition data was presented by Pham, (1996):

$$T_f = -4.66 \cdot \frac{x_o}{x_w} - 46.4 \cdot \frac{x_a}{x_w}, \tag{2.11}$$

where x is the mass fraction of water w, ash a (mainly salt content) or other components o (mainly sugar content).

The presence of solute greatly decreases the amount of supercooling for two reasons: faster nucleation and lowered freezing point (Franks, 1985). After crystallisation is completed, the temperature drops as the sensible heat is released in case of water. In case of solution supersaturation continues due to the freezing of water and solute crystals may form by releasing latent heat of solute crystallisation, causing a slight jump in the temperature. The temperature dependent ice fraction x_{ice} in frozen foods can be calculated using different prediction methods (Fikiin, 1998). The relation between ice content and the sample temperature T can be given with:

$$x_{ice} = (x_w - x_b) \cdot \left(1 - \frac{T_f}{T}\right), \tag{2.12}$$

where T_f is the initial freezing point, x_w is the mass fraction of water, and x_b the mass fraction of bound water which can be calculated from composition data (Miles, 1991):

$$x_b = 0.3 \cdot x_p + 0.1 \cdot x_c, \tag{2.13}$$

where x_p is the mass fraction of protein and x_c the mass fraction of carbohydrate. In most cases, approx. 10 % of the water remains in the liquid state at the storage temperature of the frozen food (Singh and Heldman, 2001).

2.1.3 Products and freezing systems

Technological innovations as early as 1869 led to the commercial development and marketing of some frozen foods. Pigeon was one of the first commercially marketed frozen food products and was soon followed by fish, poultry, other meats, liquid eggs and fruits (Jones, 1997). The frozen food industry, one of the largest and most dynamic sectors of the food industry, has grown to a value of over $ 75 billion during the 90s in the USA and Europe alone (Mallett, 1993). The per capita consumption of frozen food products for selected European countries is given in Table 2.1. The evolution of the German frozen foods market during the years 1990 and 2000 is given in Table 2.2. The market studies of the consumption of frozen foods indicate that frozen vegetables and potatoes form a very significant proportion of the German frozen food market, even of the world frozen food market (Cano, 1996). Animal related products, like fish and meat also form a remarkable proportion of the frozen food market.

Table 2.1: Per capita consumption of frozen foods in different European countries (without ice cream)

Country	Per capita consumption [kg]
UK	47.6
Sweden	44.6
Norway	42.1
Germany	32.8
France	30.0*
Finland	25.4
Spain	22.1
Belgium	21.6
The Netherlands	20.0*
Greece	18.0*
Italy	11.7

*: do not include raw poultry
Reference: Deutsches Tiefkühlinstitut e.V., Köln (Stand 2.1.2002), www.tiefkuehlinstitut.de

Table 2.2: The frozen food market in Germany – comparison of the years 1990 and 2000

Products	Household and industrial packages		
	1990 [t]	2000 [t]	Difference %
Vegetables	281 170	408 527	45.3
Fruits and juice	22 169	60 992	175.1
Fish, seafood, molluscs	127 328	218 021	71.2
Potato products	332 443	359 403	8.1
Grain and flour products	8 348	13 505	61.8
Bakery products	93 303	457 340	390.2
Meals, soups, hotpots	131 660	389 666	196.0
Pizza	67 818	159 687	135.5
Baguettes, snacks, etc.	30 854	48 875	58.4
Milk products and sweets	2 260	8 187	262.3
Meat and venison	84 566	240 481	184.4
Total (without poultry)	**1 181 919**	**2 364 684**	**100.1**
Poultry	434 400	324 000	-25.4
Total (incl. poultry)	**1 616 319**	**2 688 684**	**66.3**

Reference: Deutsches Tiefkühlinstitut e.V., Köln (Stand 2.1.2002), www.tiefkuehlinstitut.de

To achieve freezing of a food product, the product must be exposed to a low-temperature medium for sufficient time to remove sensible heat and latent heat of fusion from the product. In general, the type of freezing system used will depend on the product characteristics, both before and after freezing is completed. To accomplish the freezing process in desired short times, the low-temperature medium is at much lower temperature than the desired final temperature of the product, and large convective heat transfer coefficients are created. Freezing systems may be categorised in many ways, namely by batch or in-line operation, by heat transfer systems (air, contact, cryogenic), or by product suitability. A convenient characterisation may be made according to the rate of freezing or the rate of movement of the ice front from the product surface to the thermal centre of the food. This is related to the properties of the food product and also to the efficiency of heat transfer from the freezing medium to the food product surface. The realisable surface heat transfer

coefficients increase with the following convention systems depending on selected conditions (George, 1997): sharp freezer, air-blast freezer, tunnel freezer, contact freezer, fluidised-bed freezer, cryogenic freezer, liquid immersion, scraped-surface freezer.

Furthermore novel freezing methods are under development. To reduce freezing time and water loss during the process a cryomechanical freezing process was developed for freezing of delicate products, i.e. products not having a good mechanical resistance (strawberries, raspberries, shrimps), products that otherwise change their appearance (chicken, scallops) or products that tend to stick or clump (diced potatoes) (Londhal and Goranson, 1995). Cryomechanical freezing consists of the association of two freezing systems: an on-line cryogenic immersion freezer (using a cryogenic fluid like liquid N_2 or CO_2 to form a thin frozen crust) combined with a mechanical freezer (air-blast freezer to complete freezing) (Agnelli and Mascheroni, 2001). Dehydrofreezing is a variant of freezing in which a food is dehydrated osmotically to desirable moisture and then frozen (Robbers *et al.*, 1997). A reduction in moisture content would reduce the amount of water to be frozen, thus lowering refrigeration load during freezing. In addition, dehydrofrozen products could lower cost of packaging, distribution and storage, and maintain product quality comparable to conventional products (Biswal *et al.*, 1991). Power ultrasound is promising to be applied in combination with immersion freezing due to its direct effects on heat transfer (Lima and Sastry, 1990) and crystallisation process (Mason, 1998). Immersion freezing of potatoes showed improved freezing rates with the aid of power ultrasound, but the thermal effects of ultrasound must be considered (Li and Sun, 2002 a). The potential of high pressure to support freezing processes and to improve the size and distribution of ice crystals throughout the frozen product is discussed in section 2.3.2. Controlling the growth of ice crystals can also be achieved by using certain additives. Antifreeze protein and ice-nucleation protein can be directly added to food and interact with ice, therefore influencing ice crystal size and crystal structure within the food, which are two functionally distinct and opposite classes of proteins (Hew and Yang, 1992; Li and Lee, 1995). Antifreeze proteins can lower the freezing temperature and retard recrystallisation on frozen storage, while ice nucleating proteins raise the temperatures of ice nucleation and reduce the degree of supercooling (Feeney and Yeh, 1998; Li and Lee, 1998).

Beneath food products further biological materials are subjected to low temperatures for preservation purposes. The availability of stable and healthy seed cultures is important for a wide variety of processes (e.g. brewing or dairy production). Genetically engineered strains are used for various industrial processes (e.g. sludge and toxic waste treatment). The organisms may be patented and become commercially valuable, requiring secure storage facilities. Freezing followed by cryogenic storage in liquid nitrogen seems to be the best method for preserving the viability of microorganisms, but survival rates depend on the species treated and freezing condition chosen (Darvall, 2000). Cryoprotectants (e.g. glycerol or dimethylsulphoxide (DMSO)) are employed in most freezing methods to improve survival rate. They protect the cell by minimising the effects of extracellular solution changes, and penetrate the cell membrane, lowering the intracellular freezing

point and protecting against solute concentration. For animal cells and more complex microorganisms that cannot tolerate the desiccation of freezing or freeze drying (lyophilisation), vitrification would seem to be a useful alternative (Song *et al.*, 2000). After vitrification a solution is said to become a glass, and if it is held at a low enough temperature (below –136 °C for an aqueous solution), it will remain in this state. Although the cryopreservation of cells is well established for many cell types, cryopreservation of engineered or natural functional tissues is far more complicated (Pegg *et al.*, 1997). The tissue is first loaded with cryoprotecting agents and the temperature of the tissue is then reduced to a predefined temperature for long term storage. Before the tissue is implanted, it must be thawed and the added cryoprotecting agents removed (Cui *et al.*, 2002).

2.1.4 Quality and safety aspects

The water-ice transition has the advantage of fixing the tissue structure and separating the water fraction in the form of ice crystals in such a way that it is not available either as solvent or reactive component. Consequently, the diffusion of other solutes in the tissue is very slow, which together with temperature reduction helps to diminish the reaction rate. However, the size and location of the ice crystals may damage cell membranes and break down the physical structure. Thus, the cause of the undesirable physical-chemical modifications during freezing is the crystallisation of water and sometimes solutes (Delgado and Sun, 2001).

Minimising the time of the phase change period contributes to optimum product quality. It is also recognised that the quality of frozen products is largely dependent on the rate of freezing (Ramaswamy and Tung, 1984). Slow freezing generally causes ice crystals to form exclusively in extracellular areas, while high freezing rates produce small crystals evenly distributed all over the tissue. The presence of intracellular ice is undesirable, since the lack of semipermeability will cause losses of water (drip) and turgidity (Grout *et al.*, 1991). The existence of growing ice crystals may exert stresses on fragile structures, but the popular picture of ice spearing through structures is incorrect, as ice propagates by addition of water molecules to the growing surfaces (Reid, 1993). The crystal size may vary depending on the location in the frozen mass, thus smaller crystals are quickly formed at the periphery, while those growing inside are bigger since the heat transfer is more difficult. Frequently, crystallisation at the same freezing temperature is very different from one tissue to another (Delgado and Sun, 2001). However, some products may crack or even shatter if the freezing rate is too high, or products are exposed directly to extremely low-temperature freezing media. The fundamental aspects of freeze-cracking have been reviewed (Hung and Kim, 1996) and even modelled (Shi *et al.*, 1999).

Plant material is generally recognised as being more difficult to freeze satisfactorily than animal material because of the wide range of tissues in a fruit or vegetable; they also have a variety of enzyme systems and substrates, and so a wide range of enzyme reaction sequences is possible (Edwards, 1995). There are four contributory processes that are particularly important when

considering the mechanisms of freezing damage in plant tissues, namely chill damage, solute-concentration damage, dehydration damage and damage from ice crystals (Reid, 1993). Damage of the internal membrane allows enzymes and substrates to mix which are normally separated. This results in a wide range of chemical reactions leading to breakdown of the cells and the development of off-flavours and colours (Edwards, 1995). Colour changes can result in irreversible browning or darkening of the tissues. The enzyme related to this biochemical reactions is polyphenoloxidase, which can be found in most plant tissues but in especially high amounts in mushrooms and potato tubers. Consequently, heat treatment (e.g. blanching) is partially used prior to freezing to inactivate the enzymes and certain microorganisms (Cano, 1996).

Bacterial cells are sensitive to freezing, which usually leads to a slow rate of death. Indeed, freeze/thaw cycles are often used to kill bacterial cells. Membrane damage and DNA denaturation are the proposed causes of cell death following freezing and thawing but proteins are also damaged by the increase in intracellular solute concentration (Panoff *et al.*, 1998). However, microorganisms differ considerably in their sensitivity to freezing. Since freezing does not kill all microorgansims, care must be taken during harvesting and handling of the fresh product to prevent contamination and growth of bacteria, yeast, and moulds prior to freezing (Skrede, 1996). Frozen foods are not sterile but pathogenic organisms cannot grow at such low temperatures and therefore frozen foods pose no hazard to health provided that they were clean and free from contaminants when frozen (Arthey, 1993). The main concern is organisms that are likely to survive the freezing treatment and grow when the product is thawed. It was demonstrated that populations of various strains of *L. monocytogenes* were not appreciably reduced after storage for 14 days at –18 °C, although up to 82% of the surviving population was injured during freeze treatment (Golden *et al.*, 1988).

Unlike plant cells, animal cells do not possess a structurally strong cell wall. The mechanisms of freezing damage described in the case of plant tissues are still operational, but the relative importance can be very different. In many animal cell systems the most important contributor to freezing damage is solute-concentration damage. In the absence of rigid cell walls, mechanical damage is less common, although dehydration damage is still seen (Reid, 1993). Freezing is effectively a dehydration process in which water is removed from its original location within the foodstuff and collected in the form of ice crystals. During thawing, the water may or may not be reabsorbed into its original location within the food's microstructure. The underlying factors that determine thawing drip loss include the size and location of ice crystals with respect to tissue microstructure, the rate of thawing, the rate and extent of water reabsorption, and the physiological/biochemical status of the tissue prior to freezing (Pham and Mawson, 1997). Some fish species exhibit other problems, notably the disruption of connective tissue integrity called gaping, and toughening of texture due to denaturation and crosslinking of myofibril proteins (Lavety, 1991). However, unlike bacteria, molds, and viruses, most parasites are relatively easy to destroy by holding the raw fish material or finished fish product at freezing temperatures for a specified period of time; of course, this is dependent upon the internal temperature of the material.

To ensure product safety, EU regulations (European Commission, 1991) require freezing at a temperature of no more than -20 °C in all parts of the product for not less than 24 h in order to control parasites in fish. Some published studies support the effectiveness in controlling parasites by freezing at -20 °C in all parts of the product for not less than 24 h. Very early studies by Gustafson (1953) demonstrated that temperatures of less than -17 °C for 24 h could kill nematodes (*Anisakis* larvae). Higher temperatures or shorter times were not as effective. Studies in herring (Houwing, 1969) demonstrated that at -20 °C, nematodes were killed in 24 h, but if the product temperature reached -30 °C by a cryogenic method, the inactivation was immediate, and no further storage was necessary. A more recent study by Deardoff and Throm (1988) used blast freezing to freeze salmon and rockfish at -35 °C. Fish were stored frozen for 15 h and then at -18 °C for up to 48 h. Out of 3545, they found no viable larvae after 1 h of storage at -18 °C. Similar results were found in herring by Karl and Leinemann (1989). They investigated the effect of freezing and cold storage on survival of *Anisakis simplex* in herring and herring fillets at -20 °C for 24 h and found no surviving parasites. While the parasites can be killed by freezing the finished product, it is generally considered more appropriate to freeze the raw material prior to processing. Nematodes in particular will attempt to depart the gut during processing and will then establish themselves in the muscle during salting or smoking (Hauck, 1977). However, the anisakid nematodes seems to vary in their ability to survive at low temperatures and consequently other time and temperature regimes have been prescribed (e.g. holding the fish at -23 °C for 60 h) to accomplish the inactivation of parasites (Ching, 1984).

Ice crystals are relatively unstable and undergo changes in number, size and shape during frozen storage, known collectively as recrystallisation. The principal mechanisms of recrystallisation in frozen foods are iso-mass recrystallisation, migratory recrystallisation (Ostwald ripening), and accretion. The driving force behind all forms of recrystallisation is the minimisation of surface energy. The free energy of a crystal is inversely proportional to its radius of curvature. Surfaces with negative curvature (concave surfaces) will have lower energy than plain surfaces, which have lower energy than convex surfaces (Pham and Mawson, 1997). Although the amount of ice remains relatively constant, over time this phenomenon can be extremely damaging to the texture of frozen food products, such as ice cream (Hartel, 1998). Recrystallisation processes can occur in cold storage, distribution and retail stages of product life, particularly when the storage temperature fluctuates. The result is that the equipment designer not only must adopt a freezing rate that minimises process cost, but also provide all the conditions to assure proper product quality (Delgado and Sun, 2001).

Changes in food quality during its frozen and thawed stages play a major role in the success of products to be marketed as frozen foods. The quality changes in the frozen foods are due mainly to the rate of freezing, storage temperature and temperature abuse during storage, and length of storage. The quality changes can be quantified using various physical (e.g. colour, texture, microscopic structure (Mallikarjunan and Hung, 1997) and chemical measurement methods (e.g.

spectrometric, titrimetric, fluorometric, chromatographic and electrophoretic analyses (Erickson, 1997)) and even sensory evaluation (Resurreccion, 1997). Other studies have demonstrated the possibility of determining the morphological and structural properties of cell systems through the study of electrical behaviour of biological matter (Hayden *et al.*, 1969; Pething and Kell, 1987). Electrical characteristics of plant tissues can be derived from impedance measurements. The technique is rapid, non-destructive and simple to operate. The presence of intact membranes with very low electrical conductance in a cellular sample (with conductive inner and outer phases) produce alternating current (AC)- frequency dependent changes of the macroscopically detectable electrical conductivity (Angersbach *et al.*, 1999). For biological systems it is more pronounced in a frequency range between 1 kHz and 100 MHz which is known as β–dispersion (Zimmermann, 1982). The β–dispersion is the result of the repeated charging process of the membranes in the altering electrical field. Based on an electrophysical model of cellular systems for biological tissues and suspensions, a procedure with general applicability was derived by Angersbach *et al.* (2002) for the determination of local damage of cell membranes also during freeze-thaw cycles.

2.1.5 Subsequent thawing

The thawing process is not the inverse of the freezing process. Water has a higher heat capacity and lower thermal conductivity than ice, hence a worse thermal diffusivity. It therefore performs an insulating function during the thawing process. As a consequence, during thawing the internal temperature rapidly raises to around –5 °C (ice is a better thermal conductor than water), then remains close to this temperature for an extended period as surface melting commences (Figure 2.4). Since this temperature range is one where change can be rapid, the characteristics of the material tend to reduce the quality of the thawed product (Reid, 1993).

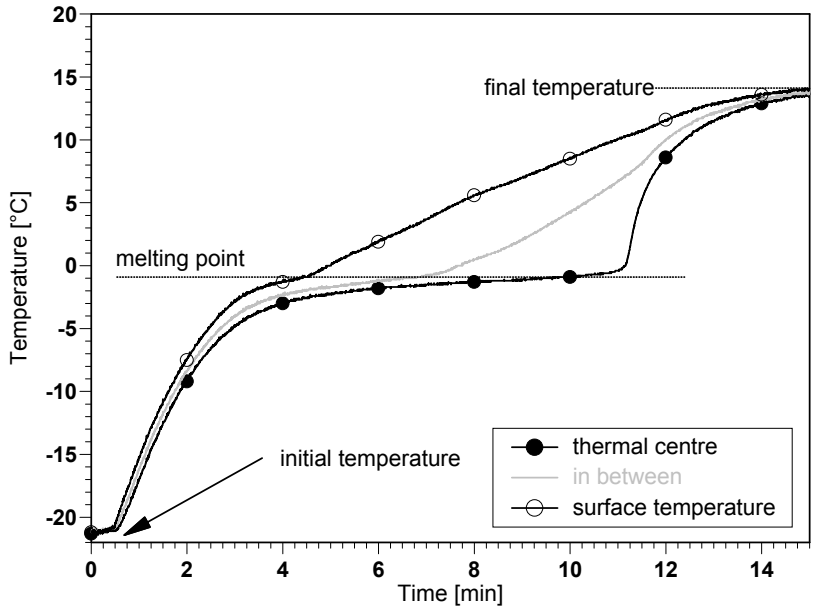

Figure 2.4: Typical temperature profile during thawing of a potato cylinder (diameter: 13 mm) in a water bath at atmospheric pressure.

Thawing of high moisture products such as tomatoes and courgettes can result in a spongy texture, which may result in their rejection. This is due to the destruction of the ultrastructure of plant cells and a loss of moisture during thawing, brought about by ice crystal growth in the thawing zone. As a consequence, water and enzymes are released through the broken cell walls. Those enzymes which had become inactive owing to the low temperature will also start working again (Edwards and Hall, 1988).

Care must be taken in the choice of thawing process used as food in general is a poor conductor of heat, and it is possible to have the outside boiling with ice remaining on the inside. Microwave techniques were investigated to provide a solution, however, ice does not absorb electromagnetic energy. Other material will begin to get hot, and the hotter they become, the more energy they absorb. This produces a phenomenon known as "thermal runaway", with extremely hot spots being created, which may burst the product. In certain cases, such as fruits, which are particularly prone to softening, it is possible to eat them in a semi-thawed state. The firmness of the remaining ice crystals will then help to compensate for loss in texture due to cell damage (Jones and Beckett, 1995). After thawing, fruits are even more susceptible to microbial invasion than the more firm fresh fruit. Thawed material must therefore, be processed immediately to prevent the surviving microorganisms from multiplying (Skrede, 1996).

With respect to the microbial quality of meat and fish, the thawing process restores the potential for the proliferation of both pathogenic and spoilage microorganisms. In general, there is poor agreement on whether the rate of thawing has a significant effect on the survival of microorganisms during thawing (Ingram and Mackey, 1976). However, repeating freezing and thawing cycles do lead to greater loss in microbial viability than does a single freezing-thawing treatment (Meyer *et al.*, 1975; El-Kest and Marth, 1992). Regardless of the thawing rate, the temperature during thawing is of tremendous importance. During thawing, the surface of large frozen products will reach higher temperatures sooner and will be exposed longer than interior portions of the product (Golden and Arroyo-Gallyoun, 1997). In a hygienically acceptable thawing process, the meat surface time-temperature history prevents microbial proliferation from exceeding acceptable limits. Regulatory authorities generally advocate that commercial thawing be undertaken at low temperatures (<10 °C) to ensure that the hygienic status of the meat is not compromised by the growth of mesophilic pathogens (Devine *et al.*, 1996). However, the potential health or quality hazard poses by specific thawing regimes requires individual assessment (Lowry *et al.*, 1989).

Due to the different thermal properties of water and ice, the thawing process is likely to take at least three to four times as long as freezing (Fennema *et al.*, 1973). In addition, unlike freezing, a large temperature differential cannot be used if spoilage, or in extreme cases, cooking has to be avoided. This is further complicated when thawing whole fish. The tail portion is much thinner than the head end, and will thaw out faster. As soon as this happens, the fish must be chilled to prevent bacterial and enzymatic spoilage. Incomplete thawing, where ice crystals are still present in the deep tissue, is liable to produce gaping (separation of the flakes) and structural damage on filleting unless

exceptional care is taken to avoid flexing the fillet (Lavety, 1991). Simple thawing solutions work well in some cases. If circumstances permit, a spray of water at 5 °C to 8 °C will effectively thaw whole fish. Alternatively the fish can be immersed in a bath of water but problems with cost, hygiene, circulation and effluent disposal exist. Various systems using vacuum, high humidity, infra-red and electrical resistance have been found effective for many applications but have had very limited success with fish and fish products. A system using acoustic vibration to assist heat transfer has had conflicting reports. Microwave radiation is used successfully to temper fish but attempts to thaw completely tend to thermal runaway with localised heating (Lavety, 1991), as mentioned above.

There is a variety of strategies available to attempt to overcome this inherent problem of the thawing process. It is necessary to maximise heat transfer at the product surface, since the internal properties of the product are not amenable to manipulation (Reid, 1993). To improve temperature uniformity during microwave thawing, Tong *et al*. (1993) designed a microwave oven with variable continuous power and feedback temperature controller to maintain a desired temperature gradient within a model food system. Using this apparatus, thawing time was reduced by as much as a factor of seven compared to convective thawing at atmospheric temperature when appropriate conditions were used. Ohmic heating technology shows also potential in improving the thawing step (Li and Sun, 2002b). Miles *et al*. (1999) applied high power ultrasound to thaw meat and fish, their work indicated that acceptable ultrasonic thawing was achieved at frequencies around 500 kHz, which conformed to relaxation mechanisms of ice crystals. Recent work on high pressure supported thawing is discussed in section 2.3.3.

2.1.6 Heat transfer and modelling

Freezing implies the removal of heat while thawing implies absorption of heat. The rate at which heat can be exchanged is a function of many factors, most of which can be placed into one or two categories. The first category comprises factors intrinsic to the object to be frozen/thawed, including the object's size, surface area and internal thermal properties. The second category comprises factors characteristic of the freezing/thawing system such as the temperature of the heat transfer medium, and the heat transfer coefficient between the cooling/heating medium and the object to be frozen/thawed (Reid, 1997).

Freezing/thawing process inside a food material can be treated as heat conduction with phase change. The actual phase change takes place over a wide range of temperatures and the food properties change considerably over this temperature range. Freezing/thawing time calculation methods are often classified into two groups: numerical methods (finite difference and finite elements), and simple formulae. Within the latter group there are methods based on adaptation of analytically derived formulae, and those derived by curve fitting experimental data. Numerical methods are regularly used to model heat transfer during food freezing/thawing processes. The advantage of numerical methods over simple equations is that complex initial boundary conditions,

effects of the phase change over a range of temperature, changing thermal properties, and heterogeneity of food products can be analysed (Delgado and Sun, 2001). In this study, radial, one dimensional heat balancing at the different volume elements within a cylindrical sample was calculated following the finite difference method described by Marek and Götz (1995). The derivation of the final equation starts from Fourier's law for heat conduction, which states that,

$$q_x = -\lambda \frac{\partial T}{\partial x} A_x \tag{2.14}$$

where, q_x : rate of heat flow in the x-direction, [W]; λ: thermal conductivity, [$Wm^{-1}K^{-1}$]; T: temperature, [K]; x: distance, [m]; A_x: heat flux area normal to the direction of heat flow, [m^2].

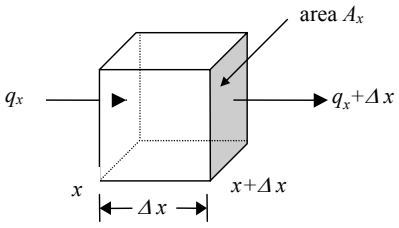

Figure 2.5: Unsteady-state balance for one-dimensional heat transfer in control volume

Making an unsteady-state heat balance for the x-direction only on the elemental volume shown in Figure 2.5, rate of heat accumulation = rate of heat input - rate of heat output + rate of heat generation, i.e.,

$$\frac{\partial U}{\partial t} = q_x - q_{x+\Delta x} + e_q \Delta V \tag{2.15}$$

where, $\partial U/\partial t$: rate of heat accumulation, [W], q_x: rate of heat input, [W] (given by Eqn 2.23), $q_{x+\Delta x}$: rate of heat output, [W], e_q: rate of heat generation per unit volume, [W m^{-3}], ΔV: volume of the element, [m^3].

The rate of heat output, $q_{x+\Delta x}$ is given by Taylor-series expansion as follows:

$$q_{x+\Delta x} = q_x + \Delta x \frac{\partial q_x}{\partial x} + \frac{\Delta x^2}{2} \cdot \frac{\partial^2 q_x}{\partial x^2} + \text{.....} \tag{2.16}$$

Neglecting the terms with 2nd order and higher derivatives,

$$q_{x+\Delta x} \approx q_x + \Delta x \frac{\partial q_x}{\partial x} \tag{2.17}$$

The rate of heat accumulation $\partial U/\partial t$ is given by,

$$\Rightarrow \qquad q_x - q_{x+\Delta x} = -\Delta x \frac{\partial q_x}{\partial x} \tag{2.18}$$

$$q_x - q_{x+\Delta x} = \Delta x \frac{\partial}{\partial x}\left(\lambda \frac{\partial T}{\partial x} A_x \right) \tag{2.19}$$

$$q_x - q_{x+\Delta x} = \lambda \frac{\partial^2 T}{\partial x^2} \Delta V \qquad (\because \quad A_x . \Delta x = \Delta V) \tag{2.20}$$

$$\frac{\partial U}{\partial t} = \rho \cdot c_p \Delta V \frac{\partial T}{\partial t} \tag{2.21}$$

where, ρ: density, [kg m^{-3}], c_p: specific heat, [Jkg^{-1}K^{-1}].

Substituting Eqns 2.20 and 2.21 in eqn. 2.15,

$$\rho \cdot c_p \Delta V \frac{\partial T}{\partial t} = \lambda \frac{\partial^2 T}{\partial x^2} \Delta V + e_q \Delta V \qquad \Rightarrow \qquad \frac{\partial T}{\partial t} = \frac{\lambda}{\rho \cdot c_p} \cdot \frac{\partial^2 T}{\partial x^2} + \frac{e_q}{\rho \cdot c_p} \tag{2.22}$$

Assuming no heat generation within the body (i.e., $e_q = 0$),

$$\frac{\partial T}{\partial t} = \alpha \frac{\partial^2 T}{\partial x^2} \tag{2.23}$$

where α : $\lambda/\rho.c_p$ is the thermal diffusivity, [m^2 s^{-1}].

From the definition of the partial derivative,

$$\frac{\partial T}{\partial t} = \frac{T(t+\Delta t) - T(t)}{\Delta t} \tag{2.24}$$

and,

$$\frac{\partial^2 T}{\partial x^2} = \frac{T(x+\Delta x) - 2T(x) + T(x-\Delta x)}{2\Delta t} \tag{2.25}$$

eqn. 2.25 relates the temperature T with the position x and time t. The solutions of this equation for the specific case of cylindrical elements are considered in the remainder of this section. The heat balancing for the various cylinder elements are considered as follows:

Central element:

Figure 2.6 depicts the central element of the cylinder.

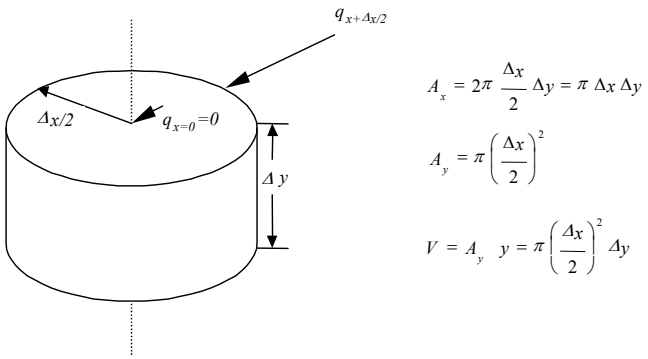

Figure 2.6: Heat balance for the central cylinder element

The heat balance for the central element is given by,

$$\frac{\partial U}{\partial T} = q_{x+\Delta x} = \lambda \frac{\partial T}{\partial x} A_x \tag{2.26}$$

Substituting for $\partial U/\partial t$ and A_x,

$$\rho \cdot c_p \Delta V \frac{\partial T}{\partial t} = \lambda \frac{\partial T}{\partial x} \pi \cdot \Delta x \cdot \Delta y = \lambda \frac{\partial T}{\partial x} \Delta V \frac{4}{\Delta x}$$

$$\Rightarrow \quad \frac{\partial T}{\partial t} = \frac{\lambda}{\rho \cdot c_p} \cdot \frac{4}{\Delta x} \cdot \frac{\partial T}{\partial x} = \alpha \frac{4}{\Delta x} \cdot \frac{\partial T}{\partial x} \tag{2.27}$$

Substituting for $\partial T/\partial t$ and $\partial T/\partial x$ as per eqn.2.24,

$$\frac{T(t+\Delta t) - T(t)}{\Delta t} = \alpha \frac{4}{\Delta x} \left(\frac{T(x+\Delta x) - T(x)}{\Delta x} \right) \tag{2.28}$$

Adopting the following nomenclature,

$T(x) = T_m^0$

$T(x+\Delta x) = T_{m+1}^0$

$T(x-\Delta x) = T_{m-1}^0$

$T(t) = T_m^0$

$T(t+\Delta t) = T_m^1$

where the subscript '*m*' denotes the location of the volume element along the radial *x*-direction and the superscript '0' and '1' denote the time moments before and after the chosen time interval, eqn. 2.28 can be re-written as,

$$T_0^1 - T_0^0 = \frac{\alpha \cdot \Delta t}{\Delta x^2} \left[4T_1^0 - 4T_0^0 \right] \tag{2.29}$$

The Fourier number *Fo* is defined as,

$$Fo = \frac{\alpha \cdot \Delta t}{\Delta x^2} \quad \left(= \frac{\lambda \cdot \Delta t}{\rho \cdot c_p \Delta x^2} \right) \tag{2.30}$$

On re-arranging eqn. 2.29,

$$T_0^1 = 4FoT_1^0 - T_0^0(4Fo - 1) \tag{2.31}$$

eqn. 2.31 is the iterative equation used to calculate the temperature of the central cylinder element.

Intermediate element:

Figure 2.7 depicts an intermediate cylinder element which differs from the central and the boundary elements in having an area A_x which increases with the radius. The radial distance *x* of an intermediate element is defined as $x = i \cdot \Delta x$, for i = 1, 2, 3, ...

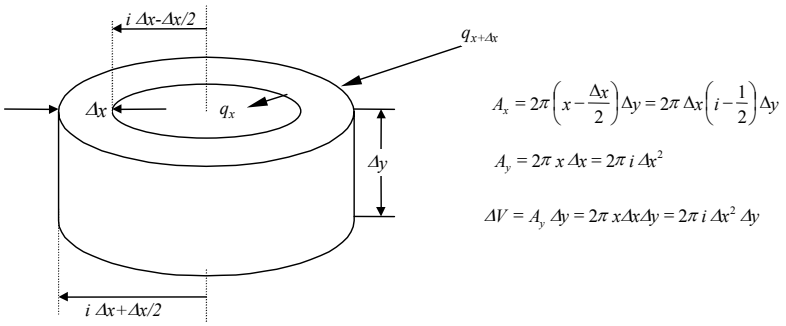

Figure 2.7: Heat balance for the intermediate element

Making a heat balance on the element shown in Fig 2.7,

$$\frac{\partial U}{\partial t} = q_{x+\Delta x} - q_x \tag{2.32}$$

From eqns. 2.19 and 2.21,

$$\begin{aligned}
\rho \cdot c_p \Delta V \frac{\partial T}{\partial t} &= \Delta x \frac{\partial}{\partial x}\left(\lambda \frac{\partial T}{\partial x} A_x\right) \\
&= \lambda \cdot \Delta x \frac{\partial}{\partial x}\left[\frac{\partial T}{\partial x} A_x\right] \\
&= \lambda \cdot \Delta x \cdot \left[\frac{\partial^2 T}{\partial x^2} A_x + \frac{\partial T}{\partial x} \cdot \frac{\partial A_x}{\partial x}\right] \\
&= \lambda \cdot \Delta x \cdot \left[\frac{\partial^2 T}{\partial x^2} \cdot \left(2\pi \cdot \Delta x\left(i-\frac{1}{2}\right)\Delta y\right) + \frac{\partial T}{\partial x} \cdot \frac{\partial}{\partial x}\left(2\pi \cdot \left(x-\frac{\Delta x}{2}\right)\Delta y\right)\right] \\
&= \lambda \cdot \left[\frac{\partial^2 T}{\partial x^2} \cdot \left(2\pi \cdot \Delta x^2\left(i-\frac{1}{2}\right)\Delta y\right) + \Delta x \frac{\partial T}{\partial x} 2\pi \cdot \Delta y\right] \\
\rho \cdot c_p \Delta V \frac{\partial T}{\partial t} &= \lambda \cdot \left[\frac{\partial^2 T}{\partial x^2} \Delta V\left(\frac{i-\frac{1}{2}}{i}\right) + \frac{\partial T}{\partial x} \cdot \frac{\Delta V}{x}\right] \\
\frac{\partial T}{\partial t} &= \frac{\lambda}{\rho \cdot c_p}\left[\frac{\partial^2 T}{\partial x^2} \cdot \left(\frac{i-\frac{1}{2}}{i}\right) + \frac{\partial T}{\partial x} \cdot \frac{1}{x}\right] \\
&= \alpha \cdot \left[\frac{\partial^2 T}{\partial x^2} \cdot \left(\frac{i-\frac{1}{2}}{i}\right) + \frac{\partial T}{\partial x} \cdot \frac{1}{x}\right]
\end{aligned} \tag{2.33}$$

Setting up the finite differences in eqn. 2.33,

$$\frac{T(t+\Delta t) - T(t)}{\Delta t} = \alpha \cdot \left[\left(\frac{T(x+\Delta x) - 2T(x) + T(x-\Delta x)}{\Delta x^2}\right) \cdot \left(\frac{i-\frac{1}{2}}{i}\right) + \frac{1}{i \cdot \Delta x}\left(\frac{T(x+\Delta x) - T(x)}{\Delta x}\right)\right] \tag{2.34}$$

Adopting the same nomenclature as before, eqn. 2.34 can be re-written as,

$$T_m^1 - T_m^0 = \frac{\alpha.\Delta t}{\Delta x^2} \cdot \left[\left(T_{m+1}^0 - 2T_m^0 + T_{m-1}^0\right) \cdot \left(\frac{i-\frac{1}{2}}{i}\right) + \frac{T_{m+1}^0 - T_m^0}{i}\right] \tag{2.35}$$

which on re-arranging, gives,

$$T_m^1 = Fo \cdot \left[\left(\frac{i+0.5}{i} \right) \cdot T_{m+1}^0 + \left(\frac{i-0.5}{i} \right) \cdot T_{m-1}^0 \right] - (2Fo - 1) \cdot T_m^0 . \tag{2.36}$$

Eqn.2.36 is the iterative equation used for the calculation of the temperature of the intermediate cylinder elements.

Boundary element:

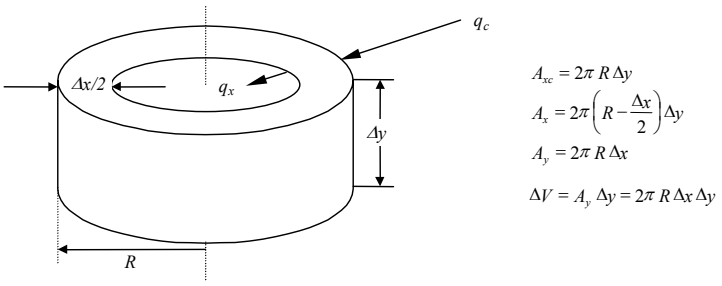

Figure 2.8: Heat balance for the boundary cylinder element

Figure 2.8 depicts a boundary cylinder element. Heat flows into this element by convection at a rate given by,

$$q_c = h \cdot \left(T_\infty - T_m^0 \right) \cdot A_{xc} \tag{2.37}$$

where, h: surface heat transfer coefficient, [W $m^{-2}K^{-1}$], A_{xc}: surface heat transfer area, [m^2], T_∞: Temperature of the surrounding fluid, [K], T: Temperature of the boundary cylinder element, [K].

Making a heat balance on the boundary element,

$$\begin{aligned}
\rho \cdot c_p \Delta V \frac{\partial T}{\partial t} &= q_c - q_x \\
&= h \cdot \left(T_\infty - T_m^0 \right) \cdot A_{xc} - \lambda \frac{\partial T}{\partial x} A_x \\
&= h \cdot \left(T_\infty - T_m^0 \right) \cdot 2\pi \cdot R \cdot \Delta y - \lambda \frac{\partial T}{\partial x} 2\pi \cdot \left(R - \frac{\Delta x}{2} \Delta y \right) \\
&= h \cdot \left(T_\infty - T_m^0 \right) \cdot 2\pi \cdot R \cdot \Delta y - \lambda \frac{\partial T}{\partial x} \left(2\pi \cdot R \cdot \Delta y - 2\pi \frac{\Delta x}{2} \Delta y \right) \\
\rho \cdot c_p \Delta V \frac{\partial T}{\partial t} &= h \cdot \left(T_\infty - T_m^0 \right) \cdot \frac{\Delta V}{\Delta x} - \lambda \cdot \frac{\partial T}{\partial x} \cdot \left(\frac{\Delta V}{\Delta x} - \frac{\Delta V}{2R} \right)
\end{aligned}$$

$$\Rightarrow \qquad \frac{\partial T}{\partial t} = \frac{1}{\rho \cdot c_p} \cdot \frac{h}{\Delta x} \left(T_\infty - T_m^0 \right) - \frac{\lambda}{\rho \cdot c_p} \cdot \frac{\partial T}{\partial x} \cdot \left(\frac{\Delta V}{\Delta x} - \frac{\Delta V}{2R} \right) \tag{2.38}$$

Setting up the finite differences,

$$T_m^1 - T_m^0 = \frac{\alpha}{\lambda} \cdot \frac{h.\Delta t}{\Delta x}\left(T_\infty - T_m^0\right) - \frac{\alpha}{\Delta x^2} \cdot \left(T_m^0 - T_{m-1}^0\right) + \frac{\alpha}{2\Delta x \cdot R}\left(T_m^0 - T_{m-1}^0\right) \tag{2.39}$$

The Biot number *Bi* is defined as follows:

$$Bi = \frac{h \cdot \Delta x}{\lambda}. \tag{2.40}$$

Eqn. 2.39 can be re-written as,

$$T_m^1 - T_m^0 = Fo \cdot Bi \cdot \left(T_\infty - T_m^0\right) - Fo \cdot \left(T_m^0 - T_{m-1}^0\right) + \frac{Fo \cdot \Delta x}{2R}\left(T_m^0 - T_{m-1}^0\right) \tag{2.41}$$

On re-arranging,

$$T_m^1 = T_m^0 + Fo \cdot \left(1 - \frac{\Delta x}{2R}\right) \cdot \left(T_{m-1}^0 - T_m^0\right) - Bi \cdot Fo \cdot \left(T_m^0 - T_\infty\right) \tag{2.42}$$

eqn. 2.42 is the iterative equation used to calculate the temperature of the boundary cylinder element.

The gradual phase change can be incorporated in the heat conduction process in many ways (Mannapperuma and Singh, 1988). The finite difference method includes: (i) simple explicit schemes where thermal conductivity λ and heat capacity c_p are combined and thermal diffusivity is taken as a function of temperature; (ii) explicit solutions where λ and c_p are taken as separate functions of temperature; (iii) explicit difference formulae based on the enthalpy transformation; fully implicit, two time level implicit schemes and three time level implicit solutions (Cleland *et al.*, 1986).

Wherever any freezing/thawing time prediction method is used some imprecision will be inevitable. This imprecision may arise from one of three sources: (i) uncertainty in thermal data for the material being frozen/thawed (thermal conductivity, specific heat and density); (ii) imprecise knowledge of the freezing/thawing conditions, particularly the surface heat transfer coefficient; and (iii) inaccuracy arising from assumptions or approximations made in the derivation of the prediction method (Cleland and Earle, 1984). It was reported also that supercooling can affect the freezing time significantly (Pham, 1989). A detailed review on available heat transfer models for predicting freezing processes was published recently (Delgado and Sun, 2001).

2.2 Application of high hydrostatic pressure

2.2.1 General aspects

Pressure has an effect on the environment of biological systems in a continuous, controlled way by changing only intermolecular distances. Temperature produces simultaneous changes in both volume and thermal energy and there has been a long history of heating and freezing in food processing. During the past several years, pressure and temperature effects on biological systems have been used in research into high pressure processing in the food industries, especially since the Japanese Research Association for High Pressure Technology in Food Industry was established in 1989 (Taniguchi *et al.*, 2002). Extensive research is in progress to possible applications of high hydrostatic pressure (HHP) for preservation purposes or as a method to change the physical and functional properties of food systems. The capability and limitations of high pressure have recently been reviewed by many food scientists and food engineers (Knorr, 1995a; Thakur and Nelson, 1998; Tewari *et al.*, 1999; Palou *et al.*, 1999). HHP offers the possibility of preserving quality related factors (vitamins, pigments, and flavour components), while inactivating microorganisms and quality related enzymes, changing the functionality of food proteins and changing the structure of food systems (Knorr, 1993; Knorr, 2000).

High hydrostatic pressure can be generated either by direct compression and indirect compression. In the case of direct, piston-type compression, the pressure medium in the high pressure vessel is directly pressurised by a piston, driven at its larger diameter end by a low pressure pump. The indirect compression method uses a high pressure intensifier which pumps the pressure medium from the reservoir into the closed and de-aerated high pressure vessel, until the desired pressure is reached. Most of industrial cold, warm and hot isostatic pressing systems use the indirect pressurisation method (Mertens, 1994). There are two major types of high pressure processing of food products: the (conventional) batch systems, derived from cold isostatic processing, and semicontinuous systems. Batch systems can process both liquid and solid products, but these have to be prepacked. In-line systems can be applied only to pumpable products (e.g. fruit juice). The product is pumped into the pressure vessel and pressurised using a floating piston, which separates the product from the pressure medium. For batch systems, the overall cycle time is the sum of a number of single steps: filling, closing, pressure built up, pressure holding, pressure releasing, opening, taking out. For liquid products continuous treatment also is possible using tube reactors or special valve systems (Van den Berg *et al.*, 2002).

In a packed product immersed in a compressed liquid, the pressure is transferred homogeneously and instantaneously throughout the product. Under these conditions, the product is iso-pressed, since its internal pressure becomes equalised to the external one. In practical terms the gaseous part of the product nearly disappears completely while the liquids and solids remain according to their compressibility (eqn. 2.8). The *pT*-diagram of air and its main components is given in Figure 2.9.

Because of the low volume contraction of liquids and solids, particulate products such as foods are not mechanically damaged during pressurisation. The elastic capacity of many foods helps them to recover their original structure and shape (Rovere, 2002).

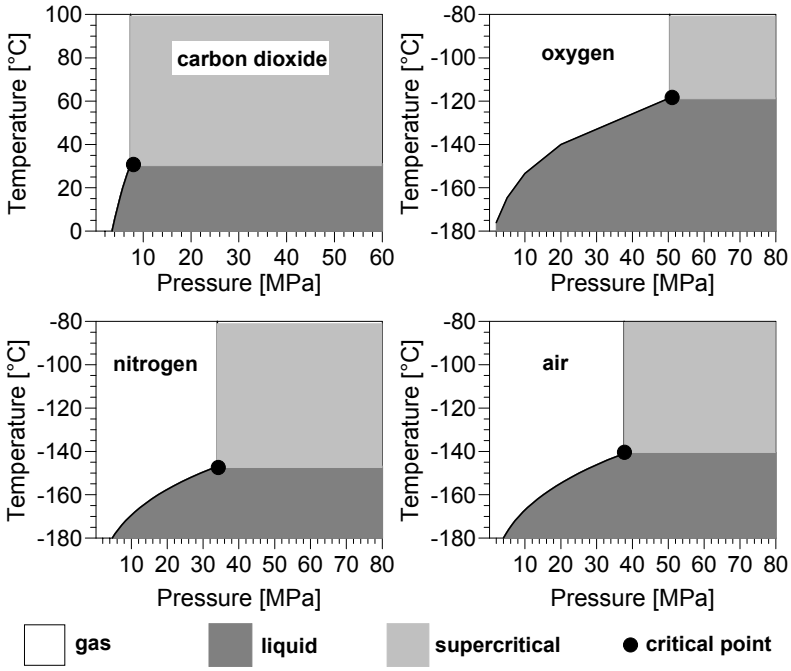

Figure 2.9: Solid, liquid and supercritical state shown in the phase diagram for air and its main components (N_2, O_2 and CO_2). (Data from VDI-Wärmeatlas (1994)).

The pressure transmitting medium should be a suitable liquid for food application processes. Typically, water mixed with a small percentage of soluble oil for pump lubrication is used. The compressibility of water is considerable less than that of most organic liquids. The volume of water is reduced by 10% at 300 MPa and by 15% at 600 MPa, while at the same pressure levels the volume of hexane is reduced by 20% and 25% respectively (Heremans, 2002). If one performs the compression under adiabatic conditions, then the temperature increase is given with the following equation:

$$\left(\frac{\partial T}{\partial P}\right)_S = \left(\frac{T}{C_p}\right) \cdot \left(\frac{\partial V}{\partial T}\right)_p = \frac{\alpha \cdot T}{\rho \cdot C_p}, \tag{2.43}$$

where α is the thermal expansion coefficient, ρ the density and C_p the heat capacity of the system. The temperature increase (ΔT) under adiabatic conditions depends on the maximum pressure reached as well as on the initial temperature of the system before compression. Using this equation for water, the temperature increases by 2 K MPa^{-1} at 25 °C, and there is no temperature increase at 4 °C (Heremans, 2002). In real (non-adiabatic) situations, thermal equilibration with the environment occurs, which produces a time and spatially varied temperature field (Heinz and Knorr, 2002). Consequently, the thermal phenomena occurring during high pressure treatment should be taken into account since temperature influences reaction kinetics.

2.2.2 Physical properties of water

Biological systems are regulated by the basic thermodynamic parameters of pressure and temperature. Life exists only within a closed range of pressure and temperature parameters: a pressure range from 0.1 to more than 1000 MPa, and a temperature range from –22 to more than 100 °C, depending on the phase behaviour of liquid water as the pressure and temperature change (Taniguchi *et al.*, 2002).

Water as the major constituent of most living organisms and plant/animal related food products is of special interest when considering the impact of high pressure processing of cellular biological materials. As mentioned before, water is also often employed as pressure transmitting medium due to its mechanical properties and sanitary safety. In 1995 the International Association for the Properties of Water and Steam (IAPWS) adopted a new formulation for water thermodynamic properties. Software implementations of these international formulations are available (e.g., NIST/ASME Steam Properties). Values for some relevant water properties in the range 0.1 to 400 MPa and temperatures as low as –22 °C, according to the IAPWS release, are presented in Figure 2.10.

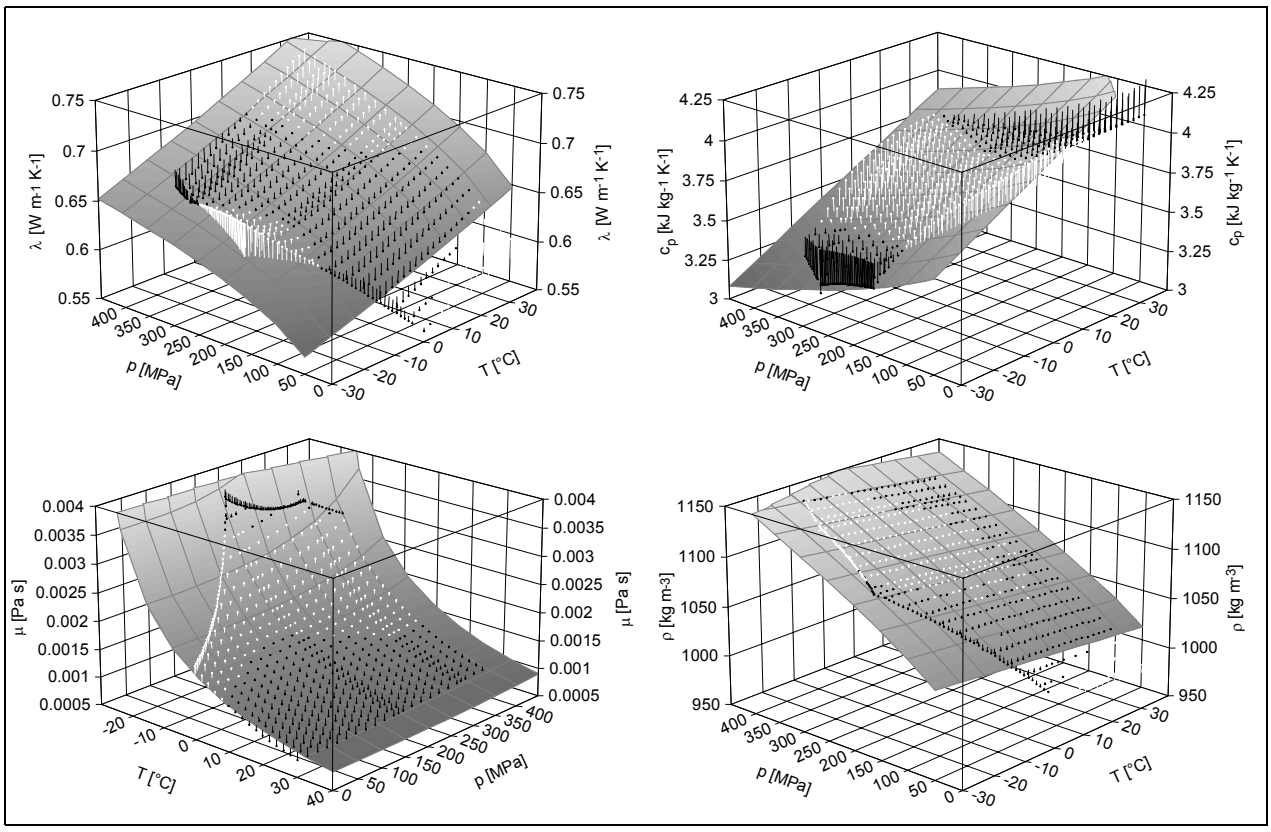

Figure 2.10: Values for some relevant water properties in the range 0.1 to 450 MPa and at temperatures from –30 °C to 40 °C according to NIST/ASME software. The *pT*-dependent tendencies of thermal conductivity λ, specific heat c_p, viscosity μ, density ρ for liquid water in the range below the melting curves was obtained by fitting the calculated data (in the range of validity) with the help of a fitting procedure using Table Curve 3D. Differences of single calculated values and the fitted mesh are indicated by z-lines (white: underestimation; black: overestimation). The relevant equations, fitting parameters and fitting errors are given in Table 2.3.

Especially, along the liquid-solid phase boundary the thermal conductivity does not follow a simple function, leading to obvious discrepancies of calculated values and fitted mesh in Figure 2.10a. However, the effect of high pressure on λ is more pronounced below 200 MPa and subzero temperatures. In the range of consideration the thermal conductivity increases with pressure and temperature. The specific heat c_p seems to be more affected by temperature than pressure (Figure 10b). The specific heat decreases with increasing pressure but increases with increasing temperature. While pressure up to 400 MPa shows no significant effect on viscosity in Figure 2.10c, lowering the temperature to subzero values support a strong increase of the water viscosity, especially of interest when taking into account supercooling and ice formation. As expected, the density values (Figure 2.10d) increase with increasing pressure and decreasing temperature. Here the effect of temperature is smaller than that of pressure. The obtained equations describing the pressure-temperature effect on thermal conductivity, specific heat, viscosity, density and the belonging model parameters fitted to the data calculated using the NIST software are given in Table 2.3.

Table 2.3: Equations and model parameters to describe considered thermophysical properties as a functions of temperature *T* and pressure *p* as presented in Figure 2.10. Precision of the proposed models are indicated by the Fit Standard Error (FSE) and the squared regression correlation coefficient (r^2).

Physical property	**Equation**	**Value o_1**	**Value o_2**	**Value o_3**	**FSE**	**r^2**
thermal conductivity λ [W m^{-1} K^{-1}]	$\lambda^{-1} = o_1 + o_2 T + o_3 (\ln p)^2$	1.8290585	-0.0031504039	0.010455623	0.008	0.946
specific heat c_p [kJ kg^{-1} K^{-1}]	$c_p = o_1 + o_2 T + o_3 p^{0.5} \ln p$	4.0501716	0.011311442	0.004858828	0.103	0.854
viscosity μ [Pa s]	$\mu^{-1} = o_1 + o_2 T + o_3 p^3$	609.73804	15.361378	-1.2739e-06	6.5e-05	0.993
density ρ [kg m^{-3}]	$\rho^{-1} = o_1 + o_2 T + o_3 p^{0.5} \ln p$	0.0010028	3.18e-07	-1.0413e-06	1.7e-05	0.998

For ordinary liquid water, thermodynamic and other properties have been studied thoroughly in an extended temperature and pressure range and a great amount of data is available. For example, Ter Minassian and Pruzan (1981) have reported values of the compressibility, expansivity, and specific heat of water up to 500 MPa for an extended temperature range, also in the supercooled region down to –40 °C. Lüdemann (1994) reviewed the properties of water and aqueous solutions under high pressure. Measurements carried out with two different types of viscosimeter led to new experimental data for the viscosity of water at high pressures up to 700 MPa and at subzero temperatures (Först *et al.*, 2000). According to the data obtained the viscosity significantly increases when lowering the temperature or when increasing the pressure (also indicated in Figure 2.10c).

2.2.3 Water-ice transition

The water substance exhibits a range of solid phases, and all of these are referred to as forms of 'ice'. Ice possesses 12 different crystal structures, plus two amorphous states. At ordinary (low) pressures the stable phase is termed ice I. There are two closely related variants: hexagonal ice Ih, whose crystal symmetry is reflected in the shape of snowflakes, and cubic ice Ic. Ice Ih is obtained by freezing water; ice Ic is formed by depositing vapour at low temperatures (-130 °C). Amorphous ice can be obtained by depositing vapour at still lower temperatures and by compressing ice Ih at liquid nitrogen temperature. In addition to the elemental phases are clathrate hydrates. These are crystalline compounds composed of a large H_2O cage in which Xe, Ar, or CH_4, for instance, is entrapped. Clathrates are of economic interest because they offer an abundant source of natural gas (Schulson, 1999).

Generally, the effect of pressure on the melting temperature T_m of compounds is described by the Clausius-Clapeyron equation:

$$\frac{dT_m}{dP} = \frac{T_m \Delta V}{\Delta H}. \tag{2.44}$$

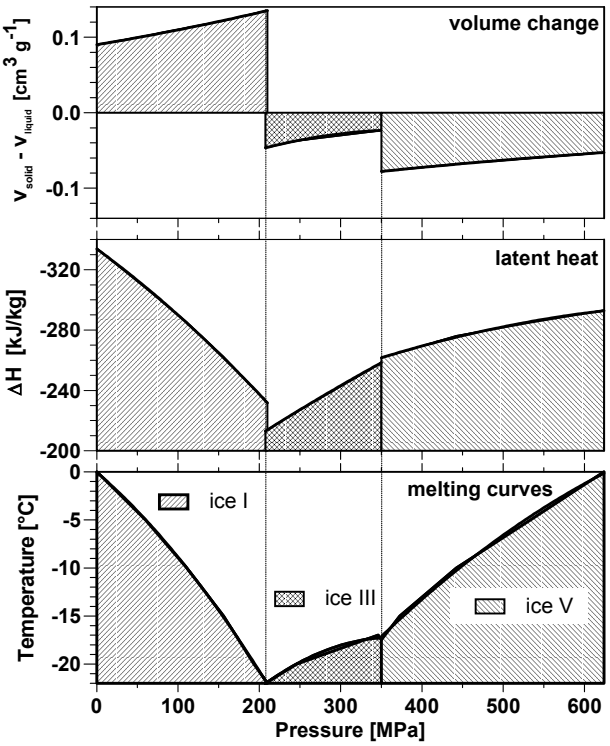

Figure 2.11: Volume change, latent heat and phase transition temperature as functions of pressure

Hexagonal ice (ice 1h, common solid state of water) contracts on melting, making ΔV negative and dT_m/dp also negative as seen in the pT-diagram (Figure 2.11). The expansion on freezing is not unique to ice I; it occurs also in silicon and germanium which have similar low-density structures in the solid state (Petrenko and Withworth, 1999). For all other solid phases of water that have a boundary with the liquid the ice is denser than the liquid and the phase boundary line slopes the other way. However, internationally adopted empirical equations for the melting curves of the

phases of ice are given by Wagner *et al*. (Wagner *et al.*, 1994). The most important effects of high pressure on phase transitions of water are presented in Figure 2.11. The volume change (liquid-solid), the latent heat of fusion and the phase transition temperatures are plotted versus pressure. Besides the depression in the freezing point, a reduction in the enthalpy of crystallisation can also be observed in a range up to 210 MPa. Experimental data obtained by Bridgman (1912) and Karino *et al*. (1994) for water-ice and ice-ice transitions are shown in Table 2.4.

Table 2.4: Thermodynamic properties of the phase transitions of water*

Phase transition **liquid-solid**	Transition temperature T (°C)	Transition pressure P (MPa)	Volume change ΔV (cm^3g^{-1})	Enthalpy change ΔH ($kJkg^{-1}$)
Liquid→ice I	-20	193.3	+0.1313	-241
	-15	156.0	+0.1218	-262
	-10	110.9	+0.1122	-285
	-5	59.8	+0.1016	-308
	0	0.1	+0.0900	-334
Liquid→ice III	-22	207.5	-0.0466	-213
	-20	246.2	-0.0371	-226
	-17	346.3	-0.0241	-257
Liquid→ ice V	-20	308.0	-0.0828	-253
	-15	372.8	-0.0754	-265
	-10	442.4	-0.0679	-276
	-5	533.7	-0.0603	-285
	0	623.9	-0.0527	-293
Liquid→ ice VI	-10	518.0	-0.0960	-264
	0	623.9	-0.0916	-295
	10	749.5	-0.0844	-311
	20	882.9	-0.0751	-320
solid-solid				
Ice I→ice II	-35	212.3	-0.2177	-42.5
Ice I→ice III	-30	211.5	-0.1919	+14.6
	-20	206.3	-0.1773	+23.4
Ice II→ice III	-25	330.6	+0.0148	+68.2
Ice II→ice V	-25	350.2	+0.0401	+66.5
Ice III→ice V	-25	341.1	+0.0546	-3.64
	-20	345.5	+0.0547	-3.72
Ice V→ ice VI	-20	624.4	-0.0381	-0.76
	0	626.0	-0.0389	-0.83

* data obtained from Bridgman *et al*. (1912) and Karino *et al*. (1994)

The first high pressure phases were discovered almost a century ago by Tammann (1900) in a programme to study the pressure-volume-temperature relationships of various materials, and he named ‘ice II’ and ‘ice III’. His discovery was extended in experiments by Bridgman (1912), in which pressures of 2 GPa were reached and led to the discovery of ices V and VI. Ice IV was not assigned by Bridgman until 1935 (Bridgman, 1935), because of uncertainty with regard to some unstable forms, the existence of which was suspected by Tammann. The phases of ice have been

labelled with the Roman numerals I-XII in the approximate order in which they were produced experimentally. Each phase (except IV, IX, and XII) is stable over a certain range of temperature and pressure, but it is a feature of the ice systems that many phases are metastable well outside their regions of stability (Petrenko and Withworth, 1999).

There is often some difficulty in nucleating a new phase, so that one phase can continue to exist where another phase would have a lower free energy. Broken lines in the *pT*-diagram of water represent the equilibrium between two phases within the region of stability of another. For example, if ice III has not formed, ice Ih can convert to liquid on the extrapolation of the ice Ih-liquid line (Bridgman, 1912). When the liquid is cooled there is often supercooling and the phase eventually formed may depend on the nucleation site rather than which of several phases has the lower free energy (Petrenko and Withworth, 1999). Appropriate nucleating agents can promote the formation of a certain ice polymorph (Evans, 1967a).

The structures of the relevant ices are shown in Figure 2.12. Different ice polymorphs (I, III, V, and VI) were optically identified at high pressure using an hydrothermal diamond-anvil cell (Haselton *et al.*, 1995). Images are included in Figure 2.12. An equation of state for certain ice polymorphs from which various thermophysical properties can be derived is described by Chizhov (1993).The ice polymorphs considered in this study can be characterised as follows.

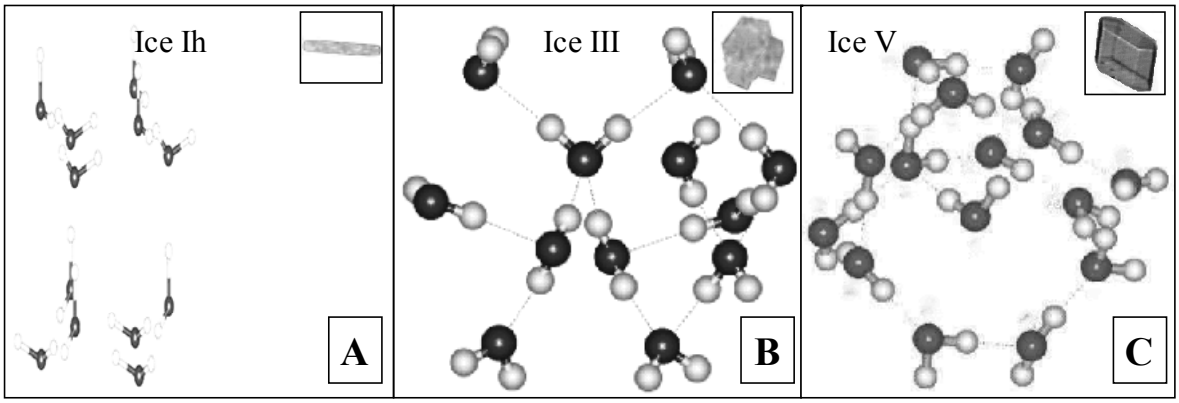

Figure 2.12: Images of ice polymorphs ice Ih, ice III and ice V and arrangement of the water molecules in their crystal units. Images of ice Ih and ice III modified according to Haselton *et al*. (1995), ice V modified according to Chou *et al*. (1998). Scale of the images is about 150 μm.

Hexagonal ice has triple points with liquid and gaseous water (0.01 °C, 612 Pa), liquid water and ice III (-22.0 °C, 209.9 MPa) and ice II and ice III (-35 °C, 213 MPa). Ice Ih is the normal form of ice and snow, as evidenced in the six-fold symmetry in ice crystals grown from water vapour (i.e. snow flakes). Hexagonal ice possesses a fairly open, all-gauche, low-density structure, where the packing efficiency is comparably low (~1/3). The crystals may be thought of as consisting of sheets lying on top of each other. The basic structure consists of a hexameric box where planes consist of chair-form hexamers (the two horizontal planes below) or boat-form hexamers (the three vertical planes below). Ice II is formed by compressing ice Ih at –60 to –80 °C (or by decompression of ice V at –30 °C), and if heated it transforms to ice III which has a totally different arrangement of

oxygen atoms. Ice II is not easily formed on cooling ice III, which remains metastable and finally orders to ice IX (Petrenko and Withworth, 1999).

Ice III is formed from water at 300 MPa by lowering its temperature to 250 K. Its unit cell, which forms tetragonal crystals, is shown in Figure 2.12. In the crystal, all water molecules are hydrogen bonded to four others, two as donor and two as acceptor. Ice III contains five membered rings joined as bicyclo-heptamers and has a density of 1.16 g cm^{-3} (at 350 MPa where water density = 1.13 g cm^{-3}). Ice III is the least dense of the high pressure phases of ice, but is more dense than the liquid so that the melting temperature rises with pressure. The hydrogen bonding is disordered and constantly changing as in hexagonal ice. The tetragonal crystal is pseudo-cubic and contains 12 water molecules. Its structure consists of tight right-handed four-fold helices, containing two thirds of the water molecules, connected by the remaining water molecules which, thus, experience a differing molecular environment (Kamb and Prakash, 1968). Ice III has triple points with liquid water and ice 1h (-22.0 °C, 209.9 MPa), liquid water and ice V (-17.0 °C, 350.1 MPa), ice 1h and ice II (-35 °C, 213 MPa) and ice II and ice V (-24 °C, 344 MPa).

Ice V is formed from liquid water at 500 MPa by lowering its temperature to 253 K. Its unit cell, which forms monoclinic crystals, is shown in Figure 2.12. Ice V contains four-, five-, six- and eight-membered rings (i.e. the opposite sub-structure has two of each) and groups of seven molecules at four different lattice sites (three consisting of two molecules and one of a single molecule) with each experiencing a differing molecular environment. All molecules form one connected lattice with a density of 1.24 g cm^{-3} (at 350 MPa where water density = 1.13 g cm^{-3}). The hydrogen bonding is disordered and constantly changing as in hexagonal ice. The crystal unit cell contains 28 water molecules. Ice-five has triple points with liquid water and ice III (-17.0 °C, 350.1 MPa), liquid water and ice VI (0.16 °C, 632.4 MPa), ice II and ice III (-24 °C, 344 MPa) and ice II and ice VI (-70 °C, 626 MPa) (Kamb *et al.*, 1967).

2.2.4 Biomolecular compounds

The effect of pressure on chemical or biochemical systems is described by the reaction or activation volume ΔV_{act}, the change of partial molar volume between initial and final state at constant temperature:

$$\left(\frac{\delta \Delta G}{\delta P}\right)_T = -RT \cdot \left(\frac{\delta \ln K}{\delta P}\right)_T = \Delta V_{act}, \tag{2.45}$$

where ΔG is the Gibbs free energy, R is the universal gas constant, and K the equilibrium constant of active and inactive state of a certain compound. The principle of Le Châtelier-Braun predicts that application of pressure shifts equilibrium to the state that occupies the smallest volume. Hence, pressure favours reactions accompanied by a volume decrease (Heremans, 1982).

The first systematic observations about the denaturation of proteins by high pressure was made by Bridgman (1914) treating egg albumen. He observed that the appearance of the pressure induced

coagulum is quite different from that induced by temperature and the ease of pressure induced coagulation increases at low temperatures. Suzuki (1960) conducted detailed studies of the effects of pressure and temperature on the kinetics of ovalbumin and haemoglobin denaturation. If the conditions for equilibrium or isokineticity are plotted against temperature and pressure, a stability phase diagram is obtained with an elliptical shape (Hawley, 1971). Not only has this been observed in several proteins (Taniguchi and Suzuki, 1983; Heinisch *et al.*, 1995; Weingand-Ziadé *et al.*, 1997) and enzymes (Ludikhuyze *et al.*, 1998), but it also applies to the effect of pressure on the heat gelation of starch (Rubens *et al.*, 1999). One of the practical consequences of this phenomenon is the stabilisation against heat denaturation by low pressures (Heremans, 2002). Figure 2.13 shows a schematic *pT*-diagram of proteins. Proteins can be denatured using heat, pressure, and low temperatures. The data on enzyme inactivation at subzero temperatures (Indrawati, 1998; Indrawati, 2000) also give a certain hint on cold denaturation of some enzymes under pressure.

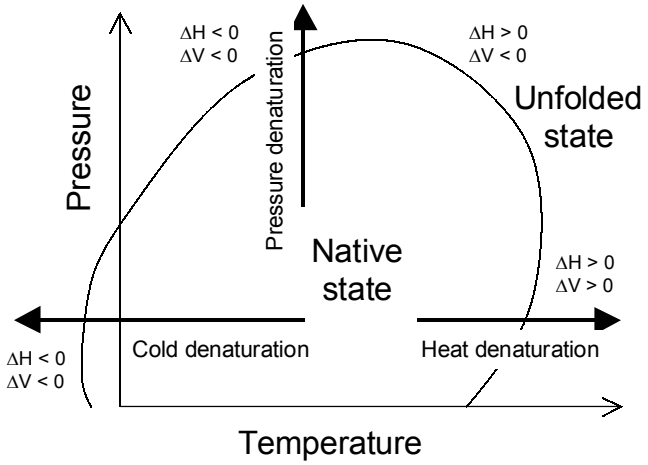

Figure 2.13: Typical phase transition curve of proteins in the *pT*-diagram. The relation between heat-, cold- and pressure-denaturation of proteins is presented by the sign of enthalpy changes (ΔH) and volume changes (ΔV). Redrawn from Heremans (2002).

In biomembranes, the physical state of the lipids that surround the membrane proteins play a crucial role in the activity of membrane-bound enzymes. Pressure favours the crystalline state of lipids, as a result of the Le Châtelier-Braun principle (Czeslik *et al.*, 1998). Buchheim *et al*. (Buchheim *et al.*, 1998) studied the solidification and melting of some edible fats and oils (milkfat, lard, coconut fat, cocoa butter, rapeseed oil), food emulsifiers (acetic esters and propylene glycol esters of monoglycerides) and model lipid systems (stearic and oleic acid, tristearin, triolein) under high pressure (100-400 MPa). The authors reported that the pressure-induced shifts of major phase transition temperatures as derived from linear heating or cooling regimes at isobaric conditions amounted to approx. 16 K/100 MPa for milkfat, coconut fat and lard but 21 K/100 MPa for acetic esters of monoglycerides. According to Heremans (1982) the transition temperature of the lipids depends on the length of the hydrocarbon chain, whereas the rate at which the temperature changes with pressure is almost independent of the chain length (dT/dp = 20 K/100 MPa). A high degree of unsaturation of the hydrocarbon chain lowers dT/dp values of the lipids (dT/dp = 14 K/100 MPa).

The dT/dp values have very little relationship to the pressure, except for the formation of lipid interdigitated phases (Winter and Czelik, 2000). The integrity of the membrane of living organisms such as bacteria is very sensitive to pressure, partially explaining the sterilisation effect of pressure (Heremans, 2002).

2.2.5 Cellular systems

Microorganisms as well as tissues of plant and animal origin can be defined as cellular systems. A challenge when preserving fresh foods is to retain the characteristically structure and functionality of the tissues while affecting food related enzymes and microorganisms. The application of high hydrostatic pressure has the potential to reach this goal, provided that the impact of the selected process parameter (p, T, t) on the relevant systems is known. Besides pressure level and treatment time, the critical parameters for high pressure induced microbial inactivation are pH, water activity (a_w) and the treatment temperature. Various combinations of these parameters have been investigated and the general rules can be described as follows: (i) Microorganisms become more susceptible to pressure at lower pH. Further, sublethally injured microorganisms induced by HHP can be reactivated in nutrition-rich environments, but fail to repair at acidic conditions (Linton *et al.*, 1999); (ii) A reduction of water activity exerts a protective effect for microorganisms against pressure treatments (Palou *et al.*, 1997); (iii) The treatment temperatures above or below room temperature tend to increase the inactivation rate of microorganisms (Knorr and Heinz, 1999).

Vegetative forms of eukaryotes, such as yeast and moulds, are inactivated by pressures between 200 and 300 MPa (Cheftel, 1995a). Gram-positive bacteria (e.g. *Listeria* and *Staphylococcus*) are more resistant to heat and pressure than Gram-negative bacteria (Smelt, 1998) and psychrotrophic bacteria are generally sensitive to heat and also to pressure (Yuste *et al.*, 1998). Pressure treatment almost always involves a permeabilisation of the bacterial membrane. Cellular membranes of bacteria (Ulmer *et al.*, 2002) are subjected to proven phase transitions from the liquid-crystalline phase to a more rigid gel phase when they are treated with high pressure or low temperature processes. In bacteria, the inactivation of membrane bound enzymes is attributed to cell death (Wouters *et al.*, 1998). Nevertheless also a (sub-)lethal permeabilisation of the membranes of bacteria (Hauben *et al.*, 1996; Kalchayanand *et al.*, 2002), cultured plant cells (Dörnenburg and Knorr, 1998) and vegetable tissue (Préstamo and Arroyo, 1998; Tangwongchai *et al.*, 2000; Fuchigami *et al.*, 1998a) was reported after high pressure treatment.

The spoilage bacteria in vegetables come from soil and the varieties of them are extremely wide. Application of 350 MPa was able to reduce indigenous microflora in lettuce and tomato, but the treatment did cause some changes in appearance and structure (Arroyo *et al.*, 1997). However, it was reported that pressure up to 350 MPa can be applied to plant systems without any major effect on texture and structure (Knorr, 1995b). An extensive study on the effect of pressure on the texture of fruits and vegetables has been carried out by Basak and Ramaswamy (1998). They observed the change of firmness of treated samples to be dependent on both pressure level and pressurisation

time. In general, the softening curves revealed that texture changes caused by pressure occurred in two phases: (1) a sudden loss as a result of the pulse action of pressure, followed by (2) further loss or gradual recovery during pressure-holding phase depending on the product treated (Ludikhuyze and Hendrickx, 2002).

The high content in free amino acids and nitrogenous materials make fresh fish quite susceptible to spoilage microorganisms. A number of studies have demonstrated that HHP can extend the shelf life of fish products such as cod (Ohshima *et al.*, 1993), minced mackerel (Fuji *et al.*, 1994), prawns (Lopez-Caballero *et al.*, 2000) or creamed salmon (Capri *et al.*, 1995). However, increasing changes of colour and visual appearance was reported according to the pressure level applied (Ohshima *et al.*, 1993). Fresh minced meat is a highly perishable product, whose shelf life is limited by the growth of different strains of spoilage bacteria contaminated during different steps of processing such as mincing, mixing or packaging. High pressure treatments inactivated *Citrobacter*, *Pseudomonas* and *Listeria* in minced meats (Carlez *et al.*, 1993). *Listeria* was the most resistant among the three species. Higher (50 °C) or lower (4 °C) temperature enhanced the effects of pressure treatments. However, partial discoloration of minced beef was observed above 150 MPa. Processed meat product such as spreadable sausage may be more suitable for pressure treatment than fresh meat. Inactivation kinetics of *E. coli* and *Listeria innocua* inoculated in spreadable sausage were investigated and pressure-time contours for 5 log cycle reductions of microorganisms were established, ensuring the high quality of the product (Zenker *et al.*, 2000). Pressure treatment of meat in pre-rigor as well as in post-rigor can induce changes of texture, depending on the temperature and pressure level applied (Cheftel, 1995b).

Results on inactivation of microorganisms indicate that the medium in which the microorganisms are treated is an important determinant factor of the level of inactivation by HHP. The protective effect of a certain food matrix against HHP were observed with various species of microorganisms (Styles *et al.*, 1991; Patterson and Kilpatrick, 1998). However, the effects of food constituents on pressure resistance are complicated and some of the effects are the result of pressure on the molecules and especially water (Smelt *et al.*, 2002).

2.3 High pressure - low temperature processes

2.3.1 Induction of phase changes

Generally, a phase transition can be obtained either by external manipulation of pressure at constant temperature (e.g. pressure-shift freezing/thawing, pressure induced freezing/thawing (Figure 2.14) or external manipulation of temperature at constant pressure (pressure assisted freezing/thawing (Figure 2.14)). Since the pressure level of a system can be influenced much faster and more homogeneous than the temperature, processes due to pressure shifts are of certain interest especially when considering the scale-up to industrial standards. However, heat transfer and temperature distribution cannot be neglected.

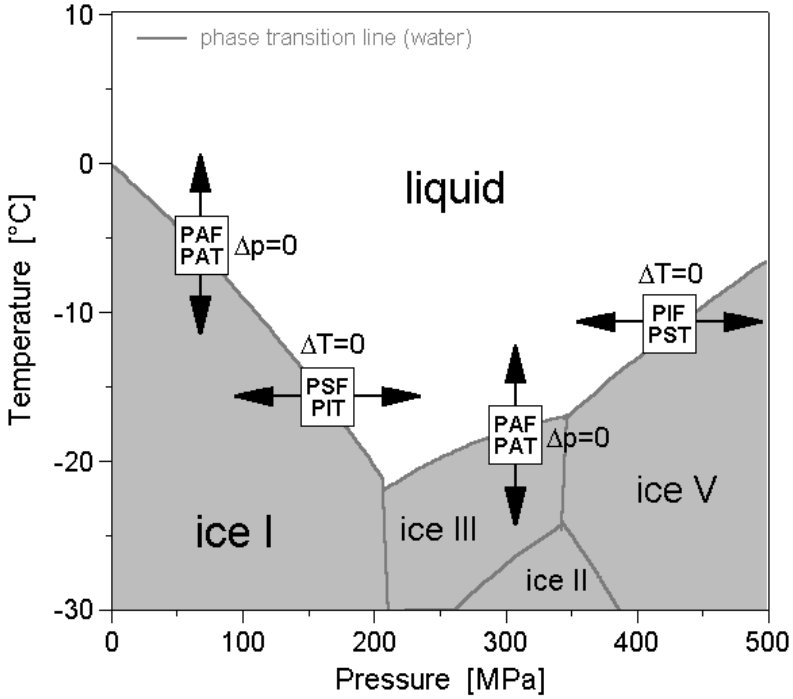

Figure 2.14: Definition of phase transition processes with respect to external manipulation of the process parameters pressure and temperature. Phase transformation at constant pressure is generated due to temperature manipulation in pressure assisted freezing (PAF) and pressure assisted thawing (PAT). Phase transformations at constant temperature (ideally) are to be obtained due to pressure increase in pressure induced thawing (PIT) and pressure induced freezing (PIF) or due to pressure release in pressure shift freezing (PSF) and pressure shift thawing (PST).

2.3.2 Pressure supported freezing

The heading 'pressure-supported freezing' implies different freezing methods possible when combining high pressure and freezing: (i) pressure-shift freezing, (ii) pressure-assisted freezing, and (iii) pressure-induced freezing (see section 2.3.6). When freezing foods, the general purpose of food technologists is to create a homogeneous matrix of small ice crystals. This state arises from rapid nucleation, caused by supercooling. In this context, the above described effect of pressure on the water - ice I phase equilibrium has attracted attention consequently leading to the pressure-shift freezing process. When a product initially is kept in the liquid state at subzero temperature combined with high pressure, upon sudden pressure release, a very high degree of supercooling can be obtained, promoting rapid ice nucleation (Kennedy, 1998). In theory, 22 °C supercooling can be obtained when the expansion is achieved very quickly starting from 210 MPa. In the case of pressure-shift freezing, pressure release and the corresponding supercooling are obtained uniformly and immediately throughout the sample and a uniform matrix of small ice nuclei results (Thiebaud *et al.*, 2002). According to Sanz *et al*. (1999), about 36 % of the total water content can be instantaneously converted to ice during expansion from 200 MPa to 0.1 MPa. A practical problem faced in pressure-shift freezing is that, depending on the size of the product, a large amount of latent heat must be released for completing the freezing process and thus, additional cooling is required to complete crystal growth (Kalichevsky *et al.*, 1995). After pressure release, the product temperature

remains at the ambient freezing temperature value until all latent heat is removed, since simultaneous removal of all latent heat is impossible in large food samples (Denys *et al.*, 1997).

Food applications of pressure shift freezing are still under development and the amount of available data increases accordingly. Most of these studies focus on the advantageous effects of pressure-shift freezing on texture and structure of products, as a result of smaller ice crystals. Japanese studies on tofu revealed that pressure-shift freezing resulted in better structure than air-blast frozen counterparts. Air-blast frozen tofu developed drip, shape deformation, formed a rigid core in the centre and made spongy texture when thawed (Kanda *et al.*, 1992). Pressure shift freezing produced fine ice crystals in tofu to result in lower structural damage. The tofu was restored to the original shape and homogeneous structure and its taste and texture were the same as the original one (Kanda and Aoki, 1993a). Koch *et al*.(1996) observed that pressure-shift freezing of potato cubes resulted in less damage of the cell structure, less drip loss and less enzymatic browning than conventionally frozen cubes.Fuchigami *et al*. (1997a, 1997b) reported on textural and histological changes in pressure-shift frozen carrots, suggesting that specific pressure-temperature conditions (e.g., 200 MPa, -20 °C) are particularly suitable. Otero *et al*. (1998) compared damage to microstructure of eggplants frozen by conventional air freezing and by pressure-shift freezing. Pressure-shift frozen samples had the appearance of fresh samples and no differences between centre and surface cell structure were observed (indicating uniform nucleation). Still-air and air-blast freezing caused cell separation and rupture of cell walls in the product centre. Firmness decreased after freezing in descending order of magnitude: still-air frozen (75%) > air-blast frozen (69%) > pressure-shift frozen (56%). Similar results were observed for drip losses. Martino *et al.* (1998) studied the size and location of ice crystals in large meat pieces of pork muscle as a result of pressure-shift freezing and compared them to those obtained by air-blast and liquid N_2. In the case of pressure-shift freezing, similar small sized ice crystals were observed both in the centre and at the surface of the treated samples. In contrast, air-blast and cryogenic fluid freezing showed non-uniform ice crystal distributions. Levy *et al.* (1999) studied freezing kinetics of oil-in-water emulsions. Pressure-shift freezing produces an extensive supercooling and the shortest freezing plateau, compared to conventional freezing and freezing by slow pressure release resulting in small irregularly shaped ice crystals without specific orientation. The influence of fructose and sodium alginate on pressure-shift freezing of o/w emulsions was reported by Thiebaud *et al*. (2002). The presence of fructose decreases the degree of supercooling, but the crystal clusters were more numerous, smaller and more spherical, resulting from a smaller number of nuclei per crystal cluster. The presence of sodium alginate did not significantly affect the freezing kinetics and did not enhance nucleation nor reduce crystal growth compared to the control sample. Although pressure-shift freezing resulted in a better preserved gel structure, as observed by scanning electron microscopy, and in smaller ice crystals than conventional freezing, it was observed the gel strength was affected (Kalichevsky-Dong *et al.*, 2000). Beneficial effects of pressure-shift freezing for plant tissues, as compared to those of air-blast (-40 °C air) or liquid N_2 freezing were confirmed with whole peaches or mangoes (Otero *et al.*, 2000b). Studies with Norway lobsters indicate that pressure-shift freezing of non-

shelled lobsters induced a significant increase in tail muscle toughness (measured after thawing, boiling, cooling and shelling the lobster) and a marked decrease in myofibrillar protein extractibility (Chevalier *et al.*, 2000c). Increased toughness was accompanied by a decrease in salt-soluble myofibrillar proteins mainly attributed to myosin or actin aggregation under pressure. Similar effects were observed with pressure-shift frozen turbot fillets (Chevalier *et al.*, 2000c).

During the pressure-assisted freezing process, the phase transition occurs under nearly constant pressure. Thus, the advantageous effects of shifting the pressure along the freezing line (uniform nucleation and partial freezing as in pressure-shift freezing) are not exploited. Haas *et al*. (1972) found that is was possible to retain quality when freezing fruits, vegetables and meat products under gaseous pressure of 0.3 to 10 MPa at –20 to –25 °C. Strawberries, pineapple and banana frozen under these conditions had a softer structure and could be eaten without thawing. When samples were air-dried after the pressure treatment, less textural damage, larger size and less shrivelling, more rapid dehydration and more uniform rehydration were the main advantages as compared to conventional freeze-drying. According to the authors, these advantageous effects were a result of tiny gas bubbles visible in the product after pressure treatment. It appears that this gas remains within the tissue during drying and prevents collapse which otherwise occurs due to capillary forces. In case of hydrostatic pressure, these effects are not expected. However, others comprehensively studied effects of phase transitions conducted at constant pressure on the texture and histology of several products: raw and blanched carrots (Fuchigami *et al.*, 1997a; Fuchigami *et al.*, 1997b), kinu-tofu (Fuchigami and Teramoto, 1997c), and chinese cabbage midribs (Fuchigami *et al.*, 1998a). Those processes were conducted by pressurising to the desired pressure for a certain time at –18 °C to –20 °C and then releasing pressure. Besides phase transitions to ice I, transitions to other ice polymorphs (ice III (340 MPa), ice V (400 MPa), and ice VI (700 MPa) were also focused upon in their work. Furthermore, compressions to 200 MPa, where no transition occurs at the temperature under investigation, were also conducted. Cheftel *et al*. (2000) mentioned that, in view of the freezing point depression of liquid water at pressures up to about 600 MPa, and considering the relative high cooling temperatures used in the above described studies, probably the products did not reach complete freezing and nucleation occurred upon expansion (as in pressure-shift freezing), rather than complete phase transition at constant pressure (low ΔT). This could be the case for runs where pressures of 200 to 400 MPa were reached. After treatment, the product was thawed at 20 °C (atmospheric conditions). In summary, the authors reported loss of texture and histological damage when pressure-assisted freezing to ice I or ice VI was conducted (Fuchigami *et al.*, 1997a). In contrast, treatments at 200 to 400 MPa (where pressure-shift freezing probably occurs upon pressure release) of raw carrots yielded a better texture and smaller ice crystals (Fuchigami *et al.*, 1997b). Pressure-assisted freezing to ice III and ice V also appeared to be effective in improving both texture and histological structure of frozen carrots (Fuchigami *et al.*, 1997b). Analogous conclusions were drawn for the texture of frozen tofu (Fuchigami and Teramoto, 1997c) and frozen chinese cabbage (Fuchigami *et al.*, 1998a). For chinese cabbage, use of pressure enhanced de-esterification of pectin and increased firmness and rupture strain (a

'pliable' structure resulted). To eliminate additional nucleation effects caused by pressure release, Fuchigami *et al*. (Fuchigami *et al.*, 1998b) conducted analogue freezing experiments at –20 °C on tofu (compressed to the same pressures as in the author's former work), but the product was thawed at the applied pressure (i.e., pressure-assisted thawing was applied). When tofu was frozen at 200-500 MPa and then thawed at atmospheric pressure, the size of ice crystals slightly increased due to phase transition when pressure was reduced. However, the pore size in tofu thawed at high pressure was the same as untreated tofu. The textural quality of tofu treated at 200, 340 and 400 MPa was better than tofu frozen at 100 MPa or above 500 MPa, regardless of the thawing method. Again, it should be mentioned that probably complete freezing was not reached in these samples. In an additional study, detrimental effects of freezing on gel structure and texture were noted with konjac glucomannan gels frozen at –20 °C and different pressure levels (Teramoto and Fuchigami, 2000).

In summary, the primary advantage of pressure-shift freezing is the possibility of achieving uniform and rapid nucleation, whereby a considerable amount of water is converted to ice I. The subsequent part of the process is analogous to classic freezing processes, and temperature profiles follow the same course as conventional freezing curves. To enable products of large size to be successfully pressure-shift frozen, the removal of latent heat assumes major importance to prevent recrystallisation. A practical remark on pressure-shift freezing is that operating costs probably can be reduced by keeping products in the high pressure chamber only when high pressure is necessary, for instance by removing the products from the high pressure unit after nucleation is achieved and completing the freezing process in conventional freezing equipment. This poses interesting prospects with a view to increase the economic benefits of the pressure-shift freezing process. Phase transitions conducted at constant pressure lack the advantages of pressure-shift freezing and pressure-induced thawing and therefore, these processes are unlikely to reach the commercial potential of the formerly discussed processes. However, these processes seem very useful as a research tool since they allow eliminating effects caused by pressure changes and therefore improving accuracy of experimental data (Denys *et al.*, 2002).

2.3.3 Pressure supported thawing

As described for pressure supported freezing 'pressure supported thawing' also defines different thawing processes in combination with high pressure: (i) pressure-induced thawing where the phase change is induced by pressurisation and (ii) pressure-assisted thawing where the phase transition is obtained by heating at constant pressure (Knorr *et al.*, 1998). A frozen product can be forced to the liquid area in the phase diagram by applying high pressure, thus allowing faster thawing (see also section 2.3.6). For example, pressure treatments of 200 MPa for 30 min at 5 °C were found to be sufficient to completely thaw ice prepared at temperatures in the range –10 to –30 °C (Deuchi and Hayashi, 1992). Reduced treatment time (20 min) produced a 'state of sherbet' (small ice crystals in liquid water), apparently indicating the uniform nature of pressure-induced thawing, but this may also have been caused by recrystallisation in a fully thawed sample on depressurisation, as a result

of insufficient heating (Kalichevsky *et al.*, 1995). A temperature decrease is generally observed when forcing a frozen sample to the liquid region in the phase diagram. This phenomenon was also observed when compressing ice I (Kanda and Aoki, 1993b), and can be attributed to the absorption of latent heat required for the melting process, and the inability to simultaneously supply this amount of heat. The product melts at the melting temperature associated with the applied pressure and heating is required to provide the latent heat of fusion and to prevent recrystallisation on depressurisation. Kanda *et al*. (1993b) also reported partial melting of ice I upon compression, analogous to the partial freezing observed at expansion in pressure-shift freezing. In summary, a high pressure supported thawing process seems to be a combination of both pressure induced and pressure assisted thawing, depending on the initial temperature of the sample, rate of pressurisation, working pressure, sample size and other conditions regarding process control. Eshtiaghi and Knorr (1996) investigated pressure-induced thawing at 600 MPa (25 and 50 °C; 15 min) of frozen strawberries as a pre-treatment in thermal processing of strawberry preparations. They observed increases in sucrose uptake and reduction of microbial counts by two log cycles. In their study the effect of possible solid-solid phase transitions was not discussed and the sample temperature was not measured.

Effects of pressure-supported thawing on food products are studied more thoroughly than pressure-supported freezing. Most studies in the field are on animal related tissues or foods. Effects of pressure-supported thawing on meat products generally include a relevant reduction of the time required to completely thaw the product and better retention of quality factors as compared to conventional methods. The increase of the thawing rate associated to pressure-induced thawing is mainly attributed to the larger temperature gradient between the melting product and the ambient pressure transmitting medium, resulting after compression. Negative effects are generally discoloration and whitening of the meat, depending on the pressure level applied. Frozen beef at -20 °C was thawed at 50 MPa without changing original colour and with low drip (Deuchi and Hayashi, 1991). Considering the low pressure applied in this study, it is questionable whether partial thawing occurred upon compression. Higher pressures caused denaturation of protein resulting in whitening of the meat. Thawing times for frozen beef at -10 °C, thawed at 120 MPa, were one third shorter as compared to a process at atmospheric pressure, with sensory qualities comparable to those of conventionally frozen products (Makita, 1992). Again, toughening and surface whitening were observed at lower temperatures and higher pressures. The most pronounced thawing time reduction was observed by Pothakamury *et al*. (1995): according to these authors, 2 kg of frozen beef could be thawed in 80 min when pressurised to about 200 MPa, while thawing at atmospheric pressure at 5 °C required 7 hours. The flavour and juiciness of the thawed beef were about the same as after thawing under low humidity at 5 °C, but the surface of the beef was slightly discoloured. Obviously, when comparing thawing times and quality effects, a number of factors should be accounted for (initial temperature of the frozen product, ambient temperature, applied pressure level, size and thermal properties of the product). A detailed study was performed by Zhao *et al*.(1998), who compared sensory properties of meat, thawed using high pressure and

conventionally thawed meat. They focused on different pressure levels (140, 210, 280 and 350 MPa), processing times (5, 15 and 30 min), sample diameters (55, 65 and 80 mm), and initial temperatures (-7, -11, -18 and –22 °C) and compared properties of pressure-induced thawed beef and conventionally thawed beef (in a cooler at 3 °C at atmospheric pressure). Pressures of 210 to 280 MPa provided the processing range necessary for thawing. Pressure-induced thawing occurred much faster than controls and resulted in similar texture and colour. They also observed the above explained temperature reduction in frozen beef during pressurisation resulting from the partial conversion of ice to water and the inability to immediately supply the latent heat necessary for thawing the product.

Murakami *et al*. (1994) observed a decrease of drip for frozen tuna fish muscle, thawed at high pressure, with no effect on the microbial quality. However, they observed no effect on the thawing rate. Depending on the pressure level applied, they also observed a discoloration of the tissue. Next to colour changes, a reduced solubility of sarcoplasmic proteins (due to protein denaturation) was obtained with increasing thawing pressure (from 50 to 150 MPa). Yoshioka *et al*. (1996) compared pressure-induced thawed carp (100 – 300 MPa; 10 min) with carp thawed under running water at 15 – 17 °C. They reported that pressure-induced thawing maintained a better quality of the fish muscle than running-water-thawing. Chevalier *et al*. (1999) studied the influence of the pressure level (0.1 – 200 MPa), the freezing rate (prior to thawing), the pressurisation rate, and the pressure holding time for pressure-induced thawing in comparison with thawing at atmospheric pressure on whiting filets. They observed a reduction of the thawing time for the pressure-induced thawing processes by a factor of four. Freezing rate is recognised as being a significant factor in tissue damage: the higher the freezing rate, the lower the drip losses. The authors also observed lower drip losses when higher pressurisation rates were applied at a given pressure. Seemingly, as in slower thawing, ice crystal recombination occurs during the partial thawing when pressurisation rates are lower. However, according to Chevalier *et al*.(1999), the use of high pressure for thawing did not minimise thawing drip in comparison to atmospheric thawing. A decrease of drip volume for high pressure thawing compared to atmospheric thawing was obtained by prolonging the pressure holding time. This was explained as a result of an osmotic pressure gradient and a mass counterflow diffusion (of water into the cells and solutes out of the cells), when physically compressing cells. Rouillé *et al*. (2002) showed that for aiguillat (Spingy dogfish) and scallops the thawing drip was significantly reduced when thawed under pressure. The authors reported best results at a pressure level of 150 MPa.

The advantages of pressure-supported thawing are related to the shortened process time and the low process temperature. The risk of detrimental phenomena such as recrystallisation, solute concentration effects, and microbial growth is markedly reduced (Cheftel *et al.*, 2000). It is likely that pressure-induced thawing will have many applications in the food and medical fields, especially in cases where significant sample deterioration occurs during thawing. Next to food products, also the study of packaging materials appropriate for pressure-induced thawing applications has been initiated. Fradin *et al*. (1998) tested six different packaging materials on

resistance to piercing and delamination due to residual air during pressure-induced thawing. Only one material, BB4L (Cryovac Grace, Epernon, France), containing EVA copolymer, was found to be resistant to piercing. Le Bail *et al*. (1997) proposed an economical calculation for a pressure-induced thawing application. Based on the cost of an installation capable of treating a charge of 300 kg, maintaining a temperature of 10 °C, reaching a pressure of 100 MPa in 5 min, and based on the assumption that drip losses are 5% less than with a conventional method, they calculated the time necessary for recuperating the investment. Recuperation times of 16 to 64 months were reported depending on the annual tonnage treated and the primary cost of the treated product.

2.3.4 Modelling of high pressure supported freezing/thawing

Divergent results concerning the processing time can be found in literature due to different definitions of the freezing time. Reductions in the freezing times of high pressure-supported freezing experiments have been described (Knorr *et al.*, 1998) in comparison with the times required to complete the same processes at atmospheric pressure, but the opposite has been reported also (Levy *et al.*, 1999). Consequently, to compare the various results a differentiation of "processing time", "freezing time" and "crystallisation time" is required. Delgado and Sun (2001) suggested two definitions for freezing times: the "nominal freezing time" for a given product, with uniform initial temperature of 0 °C is the time that the thermal centre takes to reach a temperature of 10 °C below the initial freezing point; the "effective freezing time", also known as "standard freezing time" or "holding time" is the total time required to lower the product temperature from its initial value to a given final one at the thermal centre. The former definition is related to the product quality since it considers the time for ice formation, while the latter is related to the total time in which the product remains in the equipment.

For pressure supported freezing processes the overall "processing time" can be defined as the sum of several time steps due to: loading (initial product temperature), pressure build up, pressure holding (temperature decrease, pressure assisted freezing), pressure release (temperature decrease, pressure shift freezing), taking-out and subsequent storing (final freezing step, final product temperature). Since the phase transition is assumed to mainly affect the tissue, the freezing step in particular is of practical importance. Here, the "freezing time" will be defined for all the cases as the time in which the temperature of the sample centre reaches a value 18 °C lower than the corresponding phase transition temperature starting from the initial temperature experimentally set to 25 °C above the freezing point independent of the applied pressure level. These temperature difference would be more appropriate than the already reported value of 10 °C (Delgado and Sun, 2001) as food products are defined as frozen stored foods at temperatures below –18 °C. The crystallisation time ("plateau" time) will be defined as time span between nucleation and reaching a sample temperature (centre) 5 °C below the corresponding initial freezing point. This definition is based on results given by Fikiin (1998) who calculated the ice content during freezing as a function

of temperature using different models. An ice content of approx. 80 % can be estimated, when the product reaches a temperature 5 °C below the initial freezing point.

Related to the processing time, several numeric prediction methods were reported in the literature, but mainly for atmospheric conditions (Cleland and Earle, 1984; Pham, 1985; Pham, 1987; Mannapperuma and Singh, 1988; Miyawaki *et al.*, 1989; Chung and Merritt, 1991; Sanz *et al.*, 1999; Franke, 2000; Agnelli and Mascheroni, 2001; Martens *et al.*, 2001). Just few reports have been published for numerical modelling of high pressure supported freezing processes.

Denys *et al*. (1997) used a numerical solution for two-dimensional heat transfer for finite tylose (23% (hydroxymethyl) cellulose gel) cylinders, at 66.4, 114.5, 168.6 and 230.8 MPa. Here, pressure-shift freezing was studied, thus, no higher ice modifications were obtained, and all the curves (therefore all the plateaus) had the same freezing temperature corresponding to atmospheric pressure. Sanz and Otero (2000) applied a mathematical model in three steps (precooling, phase change and tempering) based on Chung and Merritt (1991) transient state heat transfer equations for finite agar gel (99% water) cylinders and based on the Newmann's rule for finite geometry, at 92, 130, 180 and 210 MPa. In this case, as the model was divided in three steps, the predictability of the jump to the plateau temperature after supercooling is lost, and only pressure-shift freezing was studied to compare the overall process times with higher or lower degree of supercooling.

According to Le Bail *et al*. (1997) the amount of ice instantaneously formed in a pressure-shift freezing process can be described after a heat balance:

$$m_w \cdot c_p \cdot \Delta T_{\text{sup}} = L \cdot m_{ice} \tag{2.46}$$

where m_w is the mass of liquid water, c_p is the specific heat capacity of liquid water at atmospheric pressure and 0 °C, ΔT_{sup} is the supercooling attained, L is the latent heat of water and m_{ice} is the mass of ice. They estimated that 25% of the water converted to ice I after adiabatic expansion from 200 MPa and –20 °C, assuming the latent heat released by nucleation is equal to the sensible heat absorbed by liquid water to pass from metastable conditions to its freezing point at atmospheric pressure. Similar balances to calculate the amount of ice instantaneously formed after expansion was presented by Barry *et al*. (1998) taking into account the sensible heat absorbed by ice crystals just formed and by Otero *et al*. (2000a) considering a sample temperature decrease due to expansion.

Chourot *et al*. (1997) presented the first paper about heat transfer during high-pressure assisted thawing. They used Crank Nicholson's finite difference scheme as a numerical approximation to model high-pressure thawing based on experimental work with pure water and with an aqueous solution of 4.3% NaCl as a model food. They concluded that lack of knowledge of thermophysical as well as transport properties did not allow accurate predictions of the temperature distributions within the samples. Denys *et al*. (1997) modelled heat transfer during pressure-assisted thawing of a test substance (tylose) by extending an existing theoretical method for predicting product temperature profiles during freezing and thawing. The method did not take into account the

contribution of convection heat transfer by the pressure transmitting fluid. At that time, the authors solved the problem using an increased "apparent thermal conductivity" value for the high pressure surrounding the sample to get a good fit of the experimental thawing profiles. Later, Denys *et al*. (2000a) presented an improved model considering the pressure dependence of the latent heat of the product. Additionally the model allows a non-uniform initial temperature distribution in the sample before compression.

In contrast to pressure-shift freezing, the major part of the phase transition during pressure-induced thawing takes place at high pressure. Thus, the effect of pressure on the properties determining the rate of phase transition becomes more important (as for pressure assisted freezing). Based on thermodynamic P-V-T relations, the latent heat required for the transition ice I – liquid water was reported to decrease with pressure (Bridgman, 1912, Karino *et al.*, 1994). Karino *et al*. (1994) reported a reduction from 333 kJ/kg at atmospheric pressure to 241 kJ/kg at 194.7 MPa. In addition to the large temperature gradient resulting after compressing a frozen sample, the reduced latent heat will also contribute to a shorter thawing time. Denys *et al*. (2000a) determined the pressure dependence of the latent heat of tylose, based on an optimisation procedure that fits temperature profiles recorded during freezing processes at different pressure levels. The pressure dependent melting point depression of several food model systems was reported to be almost parallel to that of pure water (Levy *et al.*, 1999; Thiebaud *et al.*, 2002) and was calculated using polynomial equations fitted to experimental data (Denys *et al.*, 1997; Chevalier *et al.*, 2000b). Probably, this will be the case for most real foodstuffs but has to be quantified. However, since the enthalpy difference between initial state (frozen product at temperature T_i) and final state (thawed product at temperature T_e) is the same whatever pathway is followed, additional enthalpy must be provided as sensible heat necessary for heating the thawed product to its final temperature.

The main difficulty when modelling heat transfer in high pressure supported phase transition processes is the lack of thermophysical data of food products under high pressure. The determination of these properties under pressure through conventional techniques is hampered by practical problems. Just for water, the main component of foods, there exists an extensive set of experimental and theoretical data. Selected thermophysical properties of water and ice are presented in section 2.2.2. Otero *et al*. (2002) have made a review about some thermophysical properties of liquid water and ice I (thermal expansion coefficient, isothermal compressibility coefficient, specific volume and specific isobaric heat capacity) including supercooled water. Due to the complexity of foods and interactions between food components, the role of water in determining the thermal and physical properties of foods may not be easily identified, and in situ determination of the properties of foodstuffs at pressures above atmospheric pressure may be advisable. Denys and Hendrickx (1999) applied a line heat source probe method for measuring thermal conductivity in a pilot scale high-pressure unit and reported thermal conductivity values of commercially canned tomato paste and apple sauce at pressures up to 400 MPa and temperatures 30 °C and 65 °C. The authors also reported experimentally measured values of the density and thermal expansivity of the

same products at high pressure (Denys *et al.*, 2000b). However, there is still a lack of data at low and subzero temperatures under high hydrostatic pressure.

2.3.5 Subzero treatment in the liquid state

The required cooling and heating steps during pressure supported phase transition processes implies a subzero treatment of the products in the liquid state of water, also affecting food related components. Furthermore, low-temperature non frozen storage under pressure appears to be applicable to prolonging the shelf life of certain foods, as compared with refrigeration, while avoiding the damage caused by freezing. However, enzyme activities are likely to limit potential storage times (Kalichevsky *et al.*, 1995). Charm *et al*. (1977) studied fish quality and stability of the enzymes horseradish peroxidase and red-crab trypsin on storage at –3 °C under 24 MPa (sufficient to prevent freezing). In general, pressure inhibition of enzyme activity occurred below a certain critical temperature, depending on the enzyme. Cod fillet stored under these conditions for 36 days had a perceived storage time of 7 days at 1 °C under ambient pressure, as compared with 6 days for a product that went through a similar period of frozen storage. Samples stored at 1 °C under ambient pressure were unacceptable after 9 days. The authors pointed out that a significant energy saving could be made using pressure storage rather than freezing. Deterioration due to freezing and thawing effects is also avoided. More recently, studies focusing on more extreme pressures and temperatures were carried out. Ooide *et al*.(1994) examined the change of the contents of nucleic acid related substances and drip volumes from the muscle of carp and chicken after non-freezing preservation under subzero conditions (-8 °C, 110 MPa and –15 °C, 170 MPa for 50 days). Enzymatic degradation of the nucleic acid related substances occurred at –8 °C as at 5 °C refrigeration, though their rates were slower. However, no changes were observed when storing the product at –18 °C in a frozen condition. They concluded that the technology could preserve meat for a long time without a decline of texture, but attention should be paid to enzyme activity which under these conditions may be a potential problem. Enzymatic degradation of compounds related to nucleic acids (ATP, ADP, IMP and AMP) was only slightly slower under high-pressure conditions than under refrigerated storage, whereas it was significantly reduced by freezing. Recently, the iso-rate contour diagram of lipoxygenase inactivation as a function of pressure and temperature was determined including subzero temperatures (Indrawati *et al.*, 2000). In the entire pressure-temperature domain studied (200 to 700 MPa and –10 to 60 °C), an increase in pressure at constant temperature enhanced the lipoxygenase inactivation rate, whereas at constant pressure, an increase in reaction rate was obtained by either increasing or decreasing temperature at 20 °C. Deuchi and Hayashi (1990; 1992) showed that mechanical and rheological properties of agar gels could be maintained by non-frozen storage at –20 °C and 200 MPa for 12 days. They also kept uncooked fruits and meats, microorganisms (baker's yeast and ten kinds of bacteria) and freeze-sensitive enzymes at subzero temperature (-5 to –20 °C) with application of pressure (50 to 200 MPa) for a few days or weeks. Strawberries and tomatoes maintained their fresh taste, texture and colour on storage. Raw pork also could be successfully stored, avoiding drip losses after thawing. Enzymes

that are inactivated by freezing (catalase, β-amylase, cathepsin and lactate dehydrogenase) generally had reduced activity after non-frozen storage, but were not inactivated. Microbial counts of most microorganisms in ground beef (coli forms, enterobacteriaceae, Gram-positive and Gram-negative psychrofiles, enterococci and lactic acid bacteria) were reduced by storage under 200 MPa and –20 °C, and in some cases more than by freezing. Yeast and some bacteria were completely inactivated by such pressurisation at subzero temperature. Takahashi (1992) studied the high pressure inactivation (100-400 MPa, 20min) of several species of microorganisms in sodium phosphate buffer (pH 7.0) at 20 °C and –20 °C. In most cases, except for *S. aureus*, microbial inactivation was greater at –20 °C than at 20 °C. Inactivation ratios were of 8 or more log cycles at 300-400 MPa and 20 °C, or at 200-300 MPa and –20 °C. While freezing (–20 °C) of a yeast suspension at atmospheric pressure for 3 h did not cause significant inactivation, the rate of pressure inactivation of *Saccharomyces cerevisiae* in 0.85% NaCl was markedly increased at –20 °C or –10 °C, as compared to 0, 5 and 20 °C (Hashizume *et al.*, 1995). Other areas of study that benefit from the extension of the liquid area towards low temperatures are cold denaturation of proteins (Zang *et al.*, 1995; Foguel and Weber, 1995) and gelation of food proteins (Dumoulin *et al.*, 1998). Kolakowski *et al*. (2001) reported an enhancement of exposure of the hydrophobic zones of β-lactoglobulin to water when lowering the temperature under pressure. They concluded that it is likely that low temperatures minimise the loss of native structure induced by pressurisation and reduce subsequent aggregation reactions under high pressure. Takahashi *et al*. (2001) studied the preservation of rat livers by supercooling under high pressure. Liver grafts were pressurised up to 5, 10, 20, 30, 40, 50 and 70 MPa, and preserved for 60 min at 0 °C or 5 h at 0 °C and –2 °C, respectively. Compression rates varied from 0.03 to 1.44 MPa/s. Their results demonstrated that rat livers could tolerate a hydrostatic pressure of 30 MPa for 60 min at 0 °C and maintained the functional integrity to sustain life even after transplanted, though it did not tolerate the same pressure for 5 h. The authors concluded that the structural destruction of liver grafts observed by scanning microscopy was due to an extrinsic force generated during the compression and decompression processes rather than due to the strength per se of hydrostatic pressure. However, it is still to be verified whether or not hypothermia below zero degrees would really contribute to prolonging the preservation time of livers, whereby avoiding the effects of freezing and thawing and the toxicity of antifreeze agents as well.

2.3.6 Special applications

Pressurisation of a food product at room temperature may induce formation of ice VI at pressures ≥ 900 MPa. This process can be defined as pressure induced freezing, which in principle can be obtained when increasing the hydrostatic pressure on a non-frozen product beyond the melting pressure of ice III, ice V, ice VI or ice VII (Figure 2.14). Due to the positive slope of these melting curves, following the opposite pathway should result in melting of the mentioned high pressure ices and can be defined as pressure shift thawing. Since these processes are more of theoretical interest

no experimental results are reported in the literature. However, the expected phase transformations might include phase transition steps analogous to pressure shift freezing and pressure induced thawing, respectively.

The effect of freezing-induced pressurisation on aqueous suspensions of various microorganisms was studied by Hayakawa *et al.* (1998). Suspensions (0.5 ml) were packed in sealed polyethylene pouches and the pouches placed in a pressure-resistant vessel filled with water (~20 ml). Pressure was generated by the volume expansion of water when the vessel was placed in a freezer at –20 °C for 24 h. The exact pressure was not determined, but was most probably between 140 and 180 MPa. Inactivation ratios were ≥5 log cycles for the vegetative forms of *Saccharomyces cerevisiae*, *Zygosaccharomyces rouxii*, *Aspergillus oryzae, Aspergillus niger*, *Lactobacillus brevis*, and *E. coli*. The inactivation ratio for *S. aureus* was about 4 log cycles. Freezing controls (24 h, -20 °C at 0.1 MPa) of microbial suspensions revealed little inactivation. Pressure controls were not reported, but significant microbial inactivation (especially in yeasts) can be expected when processing at 140 up to 180 MPa at 20 °C for 24 h.

Water vitrification without ice crystal formation does not cause structural damage and the critical cooling rate to achieve vitrification is reduced under pressure as compared to atmospheric pressure (Studer *et al.*, 1995). Consequently, high pressure is used in preparation techniques for microscopy examination of small samples (Roy *et al.*, 1997; Thijssen *et al.*, 1997). However, samples must be stored below the devitrification temperature (-133 °C) to avoid the formation of ice I and can then be examined under a microscope at about –170 °C, or freeze-substituted in the presence of a fixative agent (Lonsdale *et al.*, 1999).

The conversion of ice III to ice I is reported to be explosive near the triple point (water/ice I/ice III) but slower at –30 °C (Bridgman, 1912). Pressure shifting between ice polymorphs I, III and V (in the range 160-460 MPa, at –25 °C) has been envisaged as a way of disrupting *E. coli*, with shifts between ice I and ice III (in the range 160-225 MPa) proving the most successful (Edebo and Hedén, 1960; Hedén, 1964). However, its application to cellular food systems (plant and animal tissues) seems dubious as the associated volume change (>17%) will lead to severe tissue or textural damage, on the other hand its application might be of interest for certain foods like ice cream, frozen concentrates of fruit juice or other similar food systems.

2.3.7 Requirements for the technical equipment

The technical demands on a high-pressure system are mainly defined by the planned working pressure, the working temperature, the required throughput and the properties of the product (Van den Berg *et al.*, 2002). The high pressure thawing process does not place any additional requirements on the materials used in high pressure systems when compared to current high pressure system applications since temperatures above 0 °C are used with moderate pressure. Therefore, existing high-pressure systems can be used for both experimental use and in the transition to industrial usage (Olsson, 1995; Deplace, 1995). In the investigation of high pressure

supported phase change processes in the low temperature range (high pressure supported freezing and storage) the special material qualities needed for the pressure vessel, the seal systems and the pressure transmitting medium need to be examined and modified accordingly. Essential unit-specific aspects have to be considered also with regard to scaling-up to industrial usage. Examples of experimental plants (vessel volume between a few millilitres to a litre) are given in Table 2.5.

Table 2.5: Examples of experimental high pressure units working in the subzero temperature range

High Pressure - Low Temperature Units							Measurement		
System (company), Operator	Material	Temperature range [°C]	Pressure range[MPa]	Internal volume (diameter)	Pressure transmitting medium	Cooling system	Thermo-couples inside	Pressure gauge	Measuring rate [Hz]
single vessel (ACB, France), Levy *et al.* (1999)	stainless steel, copper-beryllium stopper	≥ -30	≤ 300	1000 ml (80 mm)	propanediol/ water (55/45,v/v)	external (cooling circuit in vessel wall)	type T (2x)	2	≤ 10
single vessel (Uhde, Germany) Amanatidou *et al.*, (2001)	special steel	≥ -40	≤ 360	600 ml (56 mm)	glycol/ ethanol (80/20,v/v)	external (cooling tubes around the vessel)	type T (11x) or Pt100 (2x)	1	≤ 10
single vessel (EPSI, Belgium), Denys *et al.* (1997)	special steel	≥ -35	≤ 600	590 ml (50 mm)	polyglycol	external (cooling tubes around the vessel)	type K (7x)	1	< 0.04
single vessel (Kobe Steel Ltd., Japan), Fuchigami *et al.* (1997)	special steel	≥ -30	≤ 400	40 ml (25 mm)	poly-ethylene glycol	external (directly inserted in cooling bath)	type n.s. (2x)	1	n.s.
multi vessel (UNIPRESS, Poland), Arabas *et al.* (1998)	copper-beryllium	≥ -50	≤ 700	5 x 4.1 ml (13 mm)	pentane/ hexane or silicon oil	external (directly inserted in cooling bath)	type K (5x)	5 + 1	≤ 1

n. s.: not specified

The relevant working temperature of high pressure supported freezing is in a range as low as -40 °C. In this range, the steels conventionally used for high pressure vessels tend to crack because of their temperature dependent flexibility (rigidity). Therefore, special alloys like Copper-Beryllium (high thermal conductivity, non-magnetic) (Knorr *et al.*, 1998) or certain other elastic alloys, which are not suitable for direct contact with the treated foods because of their toxicity- and corrosion-effects, are used in place of steel. Using specific plastic materials is also conceivable. However, the low thermal conductivity which may be expected from these materials can impose additional/special demands on the temperature-controlling system. Generally, the temperature controlling system is to be adapted to the specificity of the high pressure vessel. The temperature of

the vessel is usually controlled by external heating/cooling jacket or tubes wrapped around the vessel (possibly integrated into the vessel wall) and connected to a Cryostat. Vessels with a larger diameter can also be cooled by internally wound cooling tubes or by using Peltier elements. However, improving the rate of heat transfer in that way will cause the decrease of the usable vessel volume. A reduction in the necessary cooling capacity is possible when vessels of a smaller size (and diameter) are directly inserted into the coolant-bath of the cryostat. In multi-vessel systems a nearly equal temperature can be achieved in all of the connected high pressure vessels (Arabas *et al.*, 1999). This is particularly important in the determination of inactivation kinetics (of enzymes or microorganisms). However, to ensure accurate control of the temperature (e.g. during a pressure shift freezing process) further influences on the effective process temperature in the high pressure vessel must be considered: (i) influence of the starting temperature on the process duration (possible pre-cooling), (ii) the temperature of the pressure transmitting medium before the vessel entrance (needed for compression), (iii) effects on the quality of the test product caused by the time span between introduction in the pressure transmitting medium and attainment of the working pressure (avoiding early, partial freezing), (iv) influence of the pressure build-up rate and particular properties of the pressure transmitting medium (temperature rise due to compression).

The pressure holding time can be shortened in pressure supported freezing processes by reducing the system temperature at the beginning of the process. However, pre-cooling a pressure vessel requires a sufficiently fast pressure increase after inserting the product into the receptacle in order to avoid unwanted partial freezing before, say, the actual pressure-shift-freezing (i.e., the time between inserting the product into the medium and pressure-build-up should be as minimum as possible). Therefore, suitable lock systems, such as frame or bayonet locks (Van den Berg *et al.*, 2002) which allow for fast handling, should be chosen. Also, the material of the seals must be adapted to the low temperatures; suitable seal systems could be conical metal to metal seals or polymerised epoxy seals (e.g. Polyurethane).

In choosing the pressure transmitting medium the specific desirable qualities should be researched with regard to a possible unwanted phase transition (fluid to solid). Under these circumstances, pure water is unsuitable. Therefore, alcohol, oils or synthetic mixtures or combinations of these, even without water are employed directly as a medium (Table 2.5). In industrial food processing, the use of edible oils could also be conceivable considering their thermophysical qualities as a pressure transmitting medium. To prevent unwanted migration of the pressure transmitting medium to the treated food certain packaging materials (e.g. multi layer films) (Fradin *et al.*, 1998; Amanatidou *et al.*, 2000) must be used, also affecting the heat transfer coefficient.

Special demands are placed on the measurement of temperature and pressure in experimental research (investigation) of high pressure supported phase transitions. The product-specific limits can be determined via recording of pressure and temperature changes in the pressure vessel, although the course of events under high pressure can be represented more precisely with faster data recording rate. To assess temperature fields, a Multi-Thermo-Couple (e.g. co. Unipress) can be used

for a simultaneous measurement of up to 7 temperatures (thickness of the thermocouple tips less than 0.2 mm) in the high pressure receptacle. On account of the complexity of a high pressure-(low temperature) plant, the design of the system should be carried out problem-specifically around the process parameters of pressure, temperature and time to implement a controlled and efficient process. Consequently, during this study the high pressure units were developed, evaluated and adapted to the relevant questions (together with the companies Uhde, Germany and Unipress, Warsaw) ensuring accuracy and novelty of the experimental set-ups.

3 MATERIAL AND METHODS

3.1 Test Samples

3.1.1 Potato tissues

Potato was chosen as an example for plant tissue for the high pressure processing experiments at low temperatures. Due to seasonal restrictions of availability, different types of potato (*Solanum tuberosum* cv Bintje, cv Santé and cv Sieglinde) with comparable specific qualities according to processing criteria were used for the investigations. The potatoes, purchased from the local market (co. Krohn, Berlin), had an initial water content of about 77%, wet basis. Cylindrically shaped specimens were cut from the potato tubers immediately before the experiments. In accordance with the planned set of experiments, the cylinders had a length of 40 mm and varying diameters (9.8, 13 mm) or a length of 50 mm and diameters of 20, 32 and 38 mm. The deviation of radial and axial dimensions from the prescribed value was approximately less than 1%. The sample consisted of cell tissue as homogeneous as possible, avoiding significant amounts of the surface layer and the inner marrow of tuber. A schematic drawing of the sample preparation is shown in Figure 3.1. Due to its special characteristics and to ensure consistency of the results to be obtained, potato was used as test material in all experiments regarding the characterisation of various high pressure – low temperature processes.

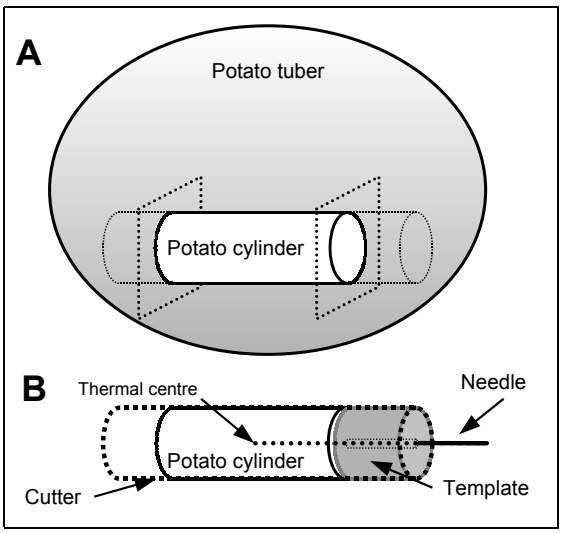

Figure 3.1: Sample preparation steps: A, cut of cylindrically shaped sample from the potato tuber using a special cutter. B, inserting precise holes for the tip of a thermocouple with a thin needle (diameter 0.6 mm) guided by a special tool.

3.1.2 Fish fillets

The fish used for thawing experiments was either caught by the fishery research vessel "Walther Herwig III" (cod, *Gadus morhua*, whiting, *Merlangius merlangius*, redfish, *Sebastes marinus*, haddock, *Melanogrammus aeglefinus*) around Faroer Islands or collected from the aquaculture farm

"Petersen Forellensee" in Krogaspe, Schleswig-Holstein (salmon, *Salmo salar*, rainbow trout, *Oncorhynchus mykiss*) in Autumn 2001. Shortly after catching the fish, it was slaughtered, filleted, skinned in pre rigor condition, and the skinned fillets were inserted into a steel cylinder (42 mm diameter, 200 mm length) and air blast frozen, on board or ashore, to a core temperature of -30 °C. Samples were frozen-stored in the cylinders at -24 °C until use. Before thawing experiments, frozen fish fillets were removed from the steel cylinder and vacuum-packed using a PE film.

3.1.3 Microorganisms

The inactivation kinetics of *Listeria innocua* BGA 3532 as a non-pathogenic indicator for *L. monocytogenes* (Kamat and Nair, 1996) was investigated. The stock culture of the bacteria obtained from BgVV (Bundesinstitutes für gesundheitlichen Verbraucherschutz und Veterinärmedizin, Berlin, Germany) was inoculated in two different mediums: ¼-strength-Ringer solution (Merck 15525, Darmstadt, Germany) and baby-food (Früh-Karotten mit Kartoffeln, HIPP GmbH & Co, Pfaffenhoffen, Germany), in order to compare bacterial inactivation in a model solution with that in a food matrix. The strains of *Listeria* appertains to the family of the *Listeriaceae*. From the food technological point of view *Listeria innocua* is important, because of its ubiquitous occurrence and its use as biological indicator for evaluating the safety of processed products with respect to the pathogen species *L. monocytogenes* and *L. ivanovii*. *Listeria* occurs in earth, plants and in faeces and therefore is able to contaminate foods such as meat, fish, milk, vegetables and fruits as well as related food products (Weber, 1996). The clinical picture of a Listeriose infection is described by complaints similar to flu up to brain dermatitis, and can also lead to premature birth or miscarriages. However, an infection conventionally can be avoided by short-term heating of the relevant products and by subsequent prevention of re-contamination (Baumgart, 1990).

3.2 High pressure units

3.2.1 Multi-vessel-system

The inactivation experiments were carried out in a special multi-vessel apparatus (U111;UNIPRESS; Warsaw, Poland). The apparatus, with a maximum operating pressure of 700 MPa at temperatures between -50 °C and +150 °C, consisted of five high pressure vessels immersed in a fluid-bath, and individually connected to a high pressure pump (Figure 3.2).

The pressure transmitting medium was silicon oil (type 6163, Huber, Germany). The hydraulic circuit of the apparatus was designed such that different pressures could be simultaneously maintained for different treatment times in the five vessels at a set temperature of the fluid bath. Each high pressure vessel set consisted of the following main assemblies: (a) A vessel body set made of Cu-Be alloy, with a mounting plate, for mounting the vessel in a bath; (b) An upper plug set which mainly incorporated the metal sheathed high-pressure type K thermocouples along with the high pressure sealing, consisting of an anti-extrusion ring, rubber O-ring and retaining ring; and

(c) A bottom plug which mainly incorporated a double electric feed-through and a manganin pressure gauge C12, a capillary tube (standard ¼ HP) and the sealing rings; The sample tube is introduced into the sample space.

The High-Pressure System of the apparatus consisted of a high-pressure intensifier, 700 MPa of piston cylinder type, which was operated from a hydraulic power unit with oil under pressure up to 70 MPa, and other auxiliaries including seven manually operated valves (SITEC, Maur/Zürich, Swiss), connectors, capillary tubes etc. The hydraulic power unit (MANNESMANN REXROTH POLSKA Ltd., Warsaw, Poland) consisted of a radial piston oil pump (fixed displacement, pressure 70 MPa, size 0.4 cm^3); an electric motor, controlled by a general-purpose Inverter Freqrol (MITSUBISHI, Japan) for varying the output of the oil pump; a block of hydraulic valves; and an oil tank with filter.

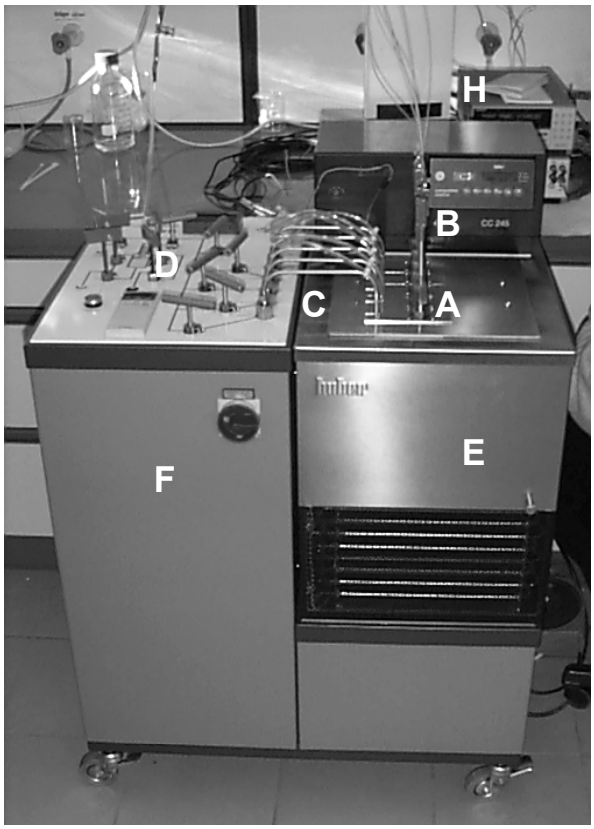

Figure 3.2: Multi-vessel system: A: Upper plugs of the vessels; B: Thermocouples; C: Connectors; D: Hand valves; E: Thermal bath; F: Rack for pump and intensifier; H: Measurement system.

High pressure is measured directly inside each of the five vessels by means of a manganin pressure gauge MPG10 (UNIPRESS). The gauge is mounted to the bottom plug of the vessel and protected by a metal cup. The manganin pressure gauge is connected to electrical feed-throughs of the bottom plug. Electric wires passing through the electric feed-through are linked (through standard connectors) to the 4-wire Scanner Card Model 7067 (KEITHLY). Low (oil) pressure in the hydraulic power unit is measured with strain gauge pressure transducer PE300 and displayed on the control desk. Temperature is measured directly inside each vessel by means of high pressure sheathed thermocouple type K. The thermocouple set is mounted to the upper plug of the vessel. The thermocouples are linked (through special connectors) to the Thermocouple Scanner Card

Model 7057 (KEITHLEY). Scanner Cards 7067 and 7057A are inserted into the slots of the High Density Switch System Mainframe 7001 (KEITHLEY) which co-operate with a high performance 6 ½ digit Multimeter 2000 (KEITHLEY). Both units are controlled via GPIB interface by a PC 486 equipped with GPIB card. A computer program "U111" enabled the monitoring of pressure and temperature in the high pressure sample vessels.

3.2.2 Low temperature system I

To investigate the phase transitions during relevant high pressure – low temperature processes one vessel of the multi-vessel-system was disconnected and adapted to an experimental set-up as show in Figure 3.3. The pressure was generated manually using a spindle. Pressures above 200 MPa were obtained by repeated compression cycles. In this way a pressure build – up to 400 MPa took less than 2 minutes. Decompression was accomplished either in a slow way via the spindle or within seconds via hand valve. The pressure transmitting medium was silicone oil (Type 6165, Huber, Germany). To control the temperature the whole pressure vessel was placed in a cryostat, type Haake K75-DC5 (Haake, Germany) or in a thermostat, type Lauda RUK 50–D (Lauda, Germany). The change from one bath to the other was accomplished in less than one minute. A thermocouple type K was inserted through the upper plug to measure the temperature in the centre of the sample. More thermocouples were used to measure the temperature of the cooling/heating bath and the outer surface of the vessel.

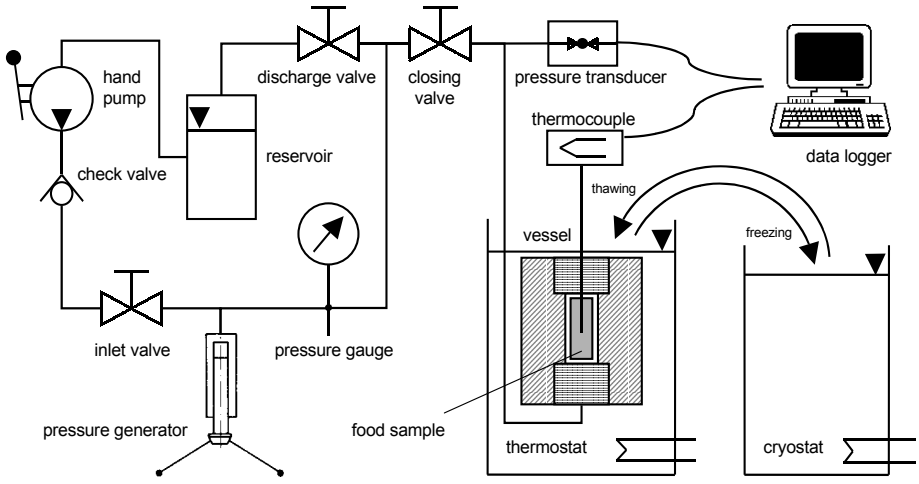

Figure 3.3: The schematic diagram of the high pressure apparatus 'low temperature system I' for subzero (°C) temperature operation.

The measured voltages at the tips of the thermocouples and the pressure were digitally converted and recorded with the help of an STB-TC Panel (ANALOG DEVICES, Norwood, MA, USA), which is a screw termination panel that supports the direct connection of 16 low-level differential analog input voltage signals or 15 thermocouples. The low level signals were then supplied to an RTI-820 Modular Analog/Digital Input/Output Board Panel (ANALOG DEVICES, Norwood, MA, USA), which measured the low-level voltage of a thermocouple through a menu-driven application software. The thermocouples were calibrated and also adjusted for room- temperature variation

errors. The measurements were digitally recorded using the software Cronolog Quick, version 2.02 (Amtech Automatisierungs-, Meß- und Testtechnologien GmbH, Berlin, Germany) which enabled precise monitoring of the phase transition processes. Depending on the planed treatment a measurement rate of 0.5 to 10 Hz was selected.

3.2.3 Low temperature system II

This high pressure unit has been developed during the studies on demands derived from the experimental investigations and allows the measurement of volume changes under high hydrostatic pressure up to 1.0 GPa in a temperature range from – 50 °C to 150 °C. The unit mainly consists of a pressure medium reservoir, a hand piston pump, high pressure intensifier, the high pressure vessel and a temperature control system (Figure 3.4). The capacity of the hand piston pump could be either set to 2.5 ml per stroke (for fast pressure build up) or to 0.5 ml per stroke (slow pressure built-up) with a maximum pressure of 63 MPa. The high pressure intensifier was provided with output pressure gauge (Type EBM6045-1000, 1.0 GPa, KGT Kramer, Germany) and with piston position gauge (Inductive gauge –50 mm to + 50 mm, PIZ100, Peltron Ltd., Poland), which guaranteed easy and complete monitoring of the pressure cycle. The high pressure intensifier was connected to the hand pump with elastic hoses.

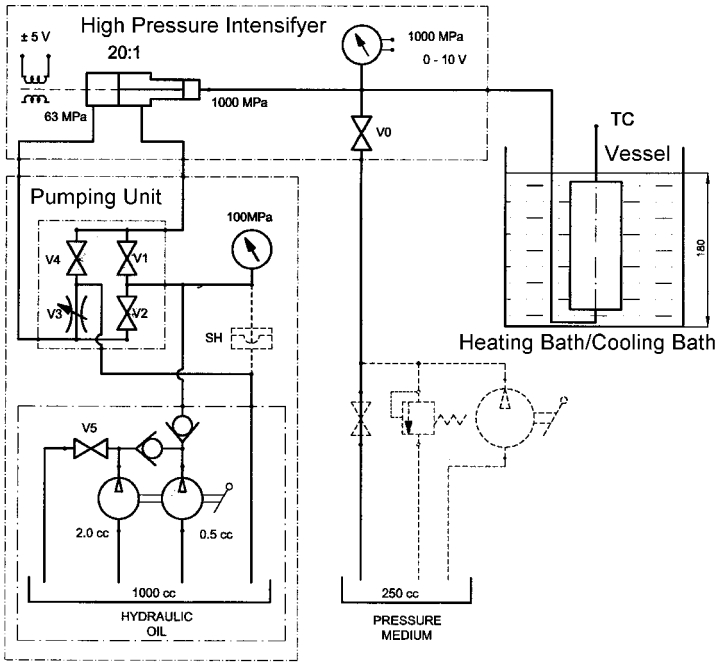

Figure 3.4: The schematic diagram of the high pressure apparatus 'low temperature system II' for subzero (°C) temperature operation.

The vessel was an externally piped small cylindrical pressure vessel made of high strength beryllium copper alloy similar to those described in section 3.2.1 'multi-vessel-system'. The vessel body (outer diameter: 50 mm, inner diameter: 13 mm, height: 130 mm) incorporated two seats with two-start metric threat for faster operation. The bottom closure served for supplying the vessel from the hand pump through a capillary tube (3/16'' connectors, 0.6 mm, 1.0 GPa). The upper closure

was used for loading the vessel and for introducing different types of temperature probes (Figure 3.5).

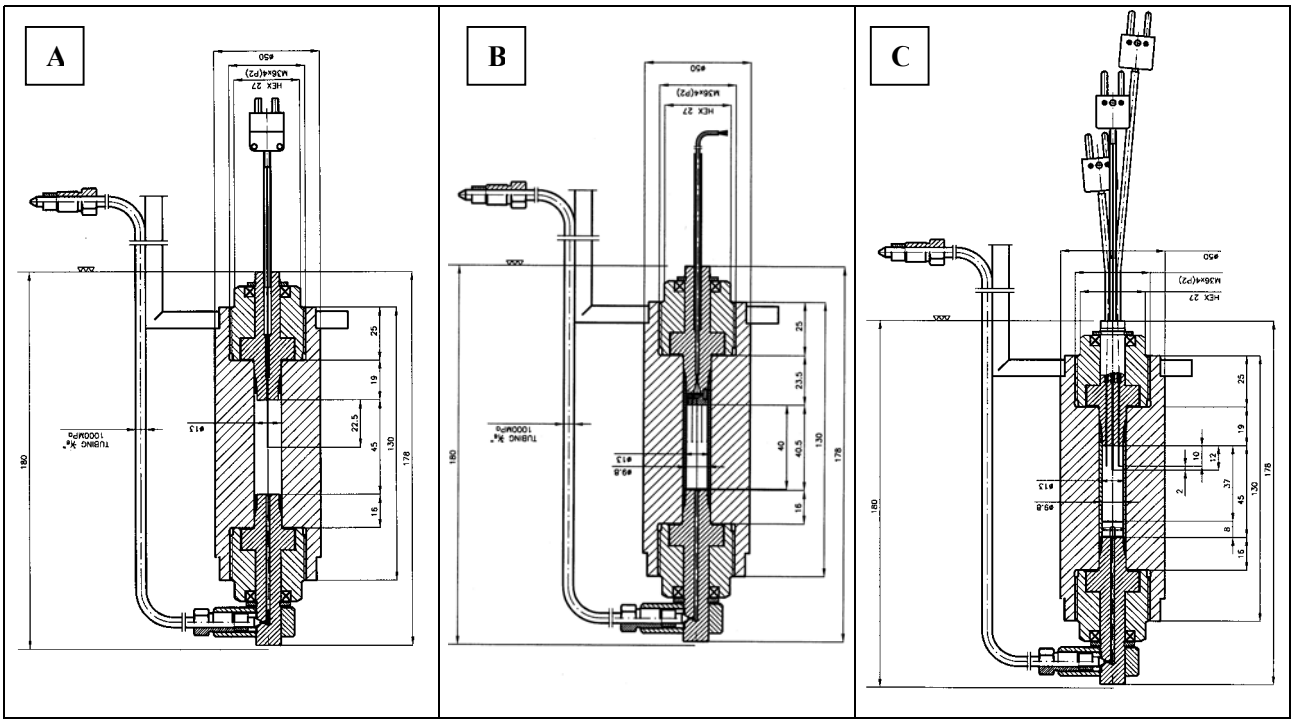

Figure 3.5: Sectional view of the high pressure vessel connected to the 'low temperature system II' with different upper plugs. A, plug with single thermocouple; B, plug with multi-thermocouple (7 x type T) and sample holder; C, plug with three thermocouples and sample container with floating piston.

The basic assembly (Figure 3.5a) incorporated a plug with soldered single sheathed thermocouple with tip located in the middle of the inner volume used for quality assessment of potato tissue (section 3.4.1). The second assembly (Figure 3.5b) incorporates a plug with seven wire-type thermocouples (type T, thickness 0.3 mm). Thermocouples were prepared for measuring the temperature distribution in the middle cross section of a solid sample. Two of the thermocouples monitored the boundary temperature of the sample, on the thermal centre and the four others were positioned in between at diameter 4.5 mm. The solid sample of length 40 mm was contained in a stainless steel cylinder (diameter: 9.8 mm, thickness: 1.5 mm) to prevent convection on the sample surface. The samples (potato cylinders) was prepared using a special cutter (for shaping the sample and making holes for the thermocouples accurately). The third assembly (Figure 3.5c) incorporated a plug with three soldered sheathed thermocouples (type K, thickness: 0.5 mm), located at different levels. A sample container with floating piston was screwed on the plug and sealed with rubber O-ring for studies on phase transitions of liquid samples (e.g. water, silicone oil, etc.). All elements, the thermocouples, the pressure gauge and the piston position gauge were connected to the measurement system as described for 'low temperature system I' (section 3.2.2).

3.2.4 Pilot scale system I

A schematic drawing of the high pressure vessel (Uhde GmbH, Hagen, Germany) especially used for the thawing of potato experiments is shown in Figure 3.6.

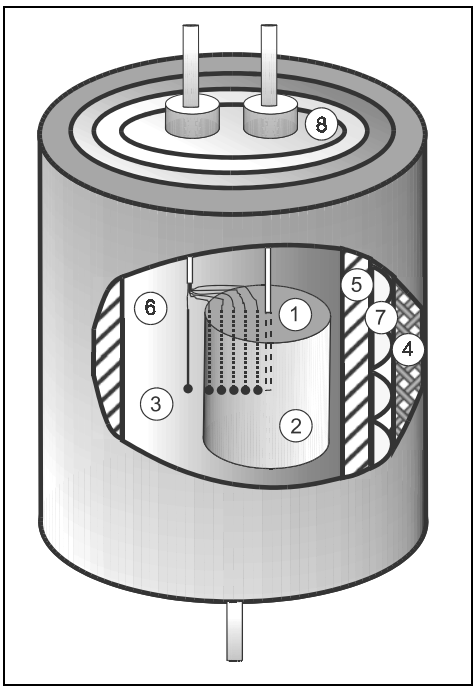

Figure 3.6: Schematic drawing of the experimental arrangement. 1: potato cylinder; 2: thermocouple (Pt 100); 3: multi-thermocouple; 4: insulation; 5: pressure vessel; 6: pressure medium (silicone oil); 7: cooling tubes; 8: upper seal.

The high pressure apparatus, which had a maximum design pressure of 360 MPa, mainly consisted of the vessel (5) and the plug (8) with the fit-throughs for the pressure release valve and the multi-thermocouple (3). The volume of the vessel was 600 ml (internal diameter 56 mm, height 250 mm), consequently it was used for scale-up evaluations of pressure supported thawing of potato tissue. The plug also consists of a rigid thermocouple Pt-100 (2) which in this context served as a pin for holding the potato cylinder (1).The vessel was filled with the pressure transmitting medium (6) which is a silicone oil (Type 6165, Huber, Germany). The fluid mix was chosen specifically for its low freezing point, which is necessary for the subzero operations involved in high pressure-thawing and freezing. The temperature in the vessel was controlled externally by flexible tubes (7) coiled around the vessel and connected to a cryostat (DC5-K75, HAAKE, Karlsruhe, Germany). The medium in the cryostat was a polyhydrocarbon (Synth 60, HAAKE, Karlsruhe, Germany) with an operating temperature of –60 to 40°C. A high pressure reciprocating pump (DSXHW, Haskel Ltd., California, USA) pumped the pressure medium into the vessel from a reservoir. The pressure in the vessel was measured using a pressure-transducer (HP28, Intersonde Ltd., Watford, England) connected near the inlet to the vessel. The temperature field in the sample during thawing can be measured using a specially designed multi-thermocouple fit-through designed by UNIPRESS, Warsaw, Poland (Figure 3.7).

It consisted of seven T-type thermocouples (copper-constantan) i.e., fourteen wires each of 0.12 mm thickness, microscopically drawn through a hole in a plug (03) and housed within a metal body

(01). The plug was provided with special seals (04) to prevent leakage under high pressures (up to 500 MPa). The fit-through was connected to the high pressure vessel using a HP ¼ connector (05). The wires were soldered at the tip to form the ”hot-junctions“ of the thermocouples. The other ends of the thermocouple wires were connected to a screw termination panel. It was this unique construction which made it possible to measure the temperature at various points in the sample during thawing under high hydrostatic pressure.

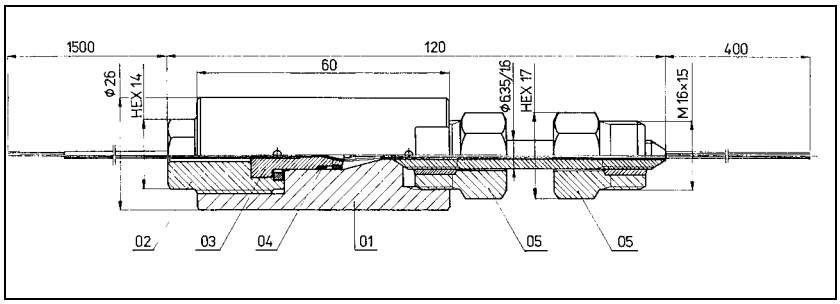

Figure 3.7: Section of the multi-thermocouple high pressure cell (UNIPRESS; Warsaw). 1: cell body; 2: plug screw; 3: plug with 7 thermocouples; 4: seals; 5: HP 1/4 connector.

3.2.5 Pilot scale system II

This high pressure unit was similar to the one ‘pilot system I’ described before, but the vessel had an extended height so that the inner volume increases to 1.6 l. The unit was used to investigate the effects of high pressure thawing on fish fillets. Instead of the above described flexible tubes coiled around the vessel a heating/cooling jacket was built for better control of the temperature. The jacket was connected to a thermal bath (type RUK 50–D, Lauda, Germany) via insulated flexible tubes. Two thermocouples (type K, thickness: 1.0 mm, (response time 70 ms) was placed inside the vessel to measure the temperature of the medium and if required the temperature of the sample. Pressure gauge, measurement system and high pressure pump were the same as described above.

3.3 Process evaluation

3.3.1 Phase transition points

At atmospheric conditions, the precise determination of the product dependent freezing and/or melting points is possible with the aid of different analytical methods (Hemminger and Höhne, 1984). Compared to Differential Scanning Calorimetry (DSC) under high hydrostatic pressures (Le Bail *et al.*, 2001), a more feasible method of measurement at high pressure levels is the Thermistor-Cryoscope method (Chen *et al.*, 1996, Chen and Chen, 1996) with which the temperature of the sample is recorded over time while cooling below the freezing point. In this case, the crystallisation temperature is derived by the relatively long temperature plateau which follows the nucleation on account of latent heat being released. If the latent heat of fusion is dissipated to a large extent, the temperature of the sample decreases in accordance with the defaulted ambient temperature. In the same way the freezing and/or melting point of foods was determined at high hydrostatic pressure.

The temperature change in the centre of a sample related to the phase transition was then plotted versus time and/or pressure.

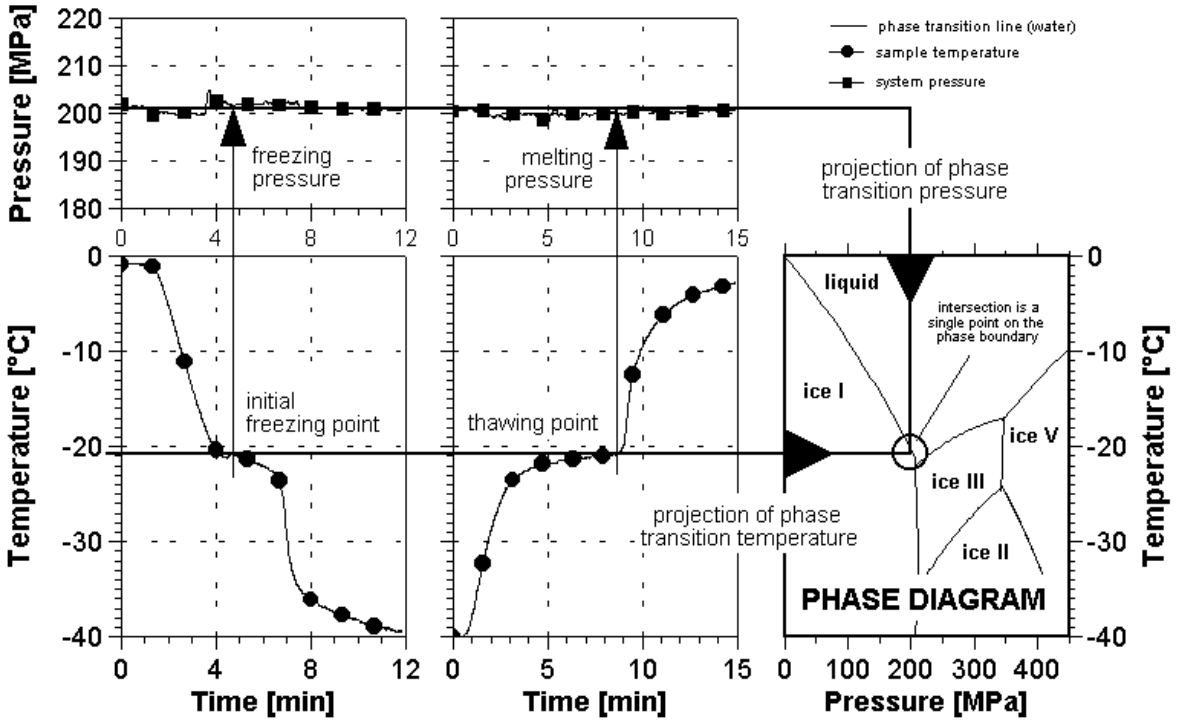

Figure 3.8: Simultaneous detection of temperature and pressure data during freezing and thawing of potato tissue and determination of single phase boundary points by projecting the data pairs to the *pT*-diagram.

Figure 3.8 shows a typical freezing and thawing curve obtained at a constant pressure of 200 MPa. The projection of the freezing/melting point of potato tissue and the corresponding pressure value to the *pT*-diagram leads to a single point of the phase transition line. The slope of the phase transition line was then obtained by extrapolation. To ensure a comparable cooling/heating rate the bath temperature of the tempering units was set 25 K below/above the expected melting point at the selected pressure values calculated using the equations given for water (Wagner *et al.*, 1994). Single freezing/melting points were determined at pressure levels between 0.1 and 450 MPa. The temperature stability at the phase boundary offered a different approach to the experimental description of the equilibrium line. Using the measurement system of the high pressure units 'low pressure system I and II', the shift of the phase transition temperature in the centre of a sample was recorded during manual change of the system pressure, so that the slope of the phase boundary was determined. Besides the slope of the melting curves, characteristic density changes resulting in pressure increase (freezing to ice I) or decrease (freezing to ice III or ice V) identified the ice polymorphs obtained.

3.3.2 Description of melting curves

For pure water the International Association for the Properties of Water and Steam (IAPWS) accepted the definition of melting curves given by Wagner *et al.* (1994). Wagner fitted the parameters of Simon equations to the available experimental data and reached high conformity for pressures up to 20 GPa. The melting pressure of ice I (p_{ml}), ice III (p_{mIII}) and ice V (p_{mV}) can be calculated using the following internationally adopted equations:

$$p_{mI} = \left[1 - \alpha \times 10^6 \left(1 - \Theta^{\beta}\right) + \chi \times 10^6 \left(1 - \Theta^{\delta}\right)\right] \times p_N \tag{3.1}$$

$$p_{mIII} = \left[1 - \alpha \times \left(1 - \Theta^{\beta}\right)\right] \times p_N \tag{3.2}$$

$$p_{mV} = \left[1 - \alpha \times \left(1 - \Theta^{\beta}\right)\right] \times p_N \,, \tag{3.3}$$

in which α, β, χ, δ are fitting constants and Θ is the normalised temperature quotient:

$$\Theta = \frac{T_m}{T_N} \tag{3.4}$$

The parameters obtained by fitting procedure are given in Table 3.1.

Table 3.1: The parameters for pure water according to Wagner *et al.* (1994)

	Phase Boundary		
Parameter	Ice I/liquid	Ice III/liquid	Ice V/liquid
T_N [K]	273.16	251.165	256.164
P_N [MPa]	$6.11675*10^{-4}$	209.9	350.1
α	0.626000	0.295252	1.18721
β	-3	60	8
χ	0.197135	-	-
δ	21.2	-	-
Temperature range [K]	273.16 to 251.165	251.165 to 256.164	256.164 to 273.31

To define the melting curves of potato tissue in a first step the specific values of T_N (equations (3.1) to (3.3)), had to be adapted taking into consideration the lower freezing/melting point of potato tissue compared to that of pure water due to dissolved components. This adaptation led to a simple parallel shift of the calculated melting curve of pure water towards lower temperature values and allowed to prove whether the phase boundary of potato tissue is parallel to that of pure water or not. Available equations were fitted to the experimental data with a non-linear regression procedure in TableCurve2D (SPSS Inc., Chicago, IL, USA). The accuracy of fit of the model was assessed using the term FSE (Fit Standard Error) between the experimental and predicted value.

3.3.3 Calculation of phase transition times

3.3.3.1 Modelling

The temperatures at various points in the sample were plotted against time to obtain the master freezing/thawing curves. The experimental curves were then re-calculated using the finite difference scheme discussed in Chapter 2. Figure 3.9 presents a schematic view of the radial, one dimensional heat balancing at the different volume elements within the cylindrical sample. Radial symmetrical one dimensional heat conduction was assumed to describe correctly the situation inside the middle part of an extended potato cylinder. The iterative calculations were performed by an algorithm with the help of Mathcad PLUS 6.0 (Mathsoft Inc. Ltd., Massachusetts, USA). The final equations used to generate the temperature-time curves are given in section 2.1.6 (eqn. 2.31, eqn. 2.36, eqn. 2.42).

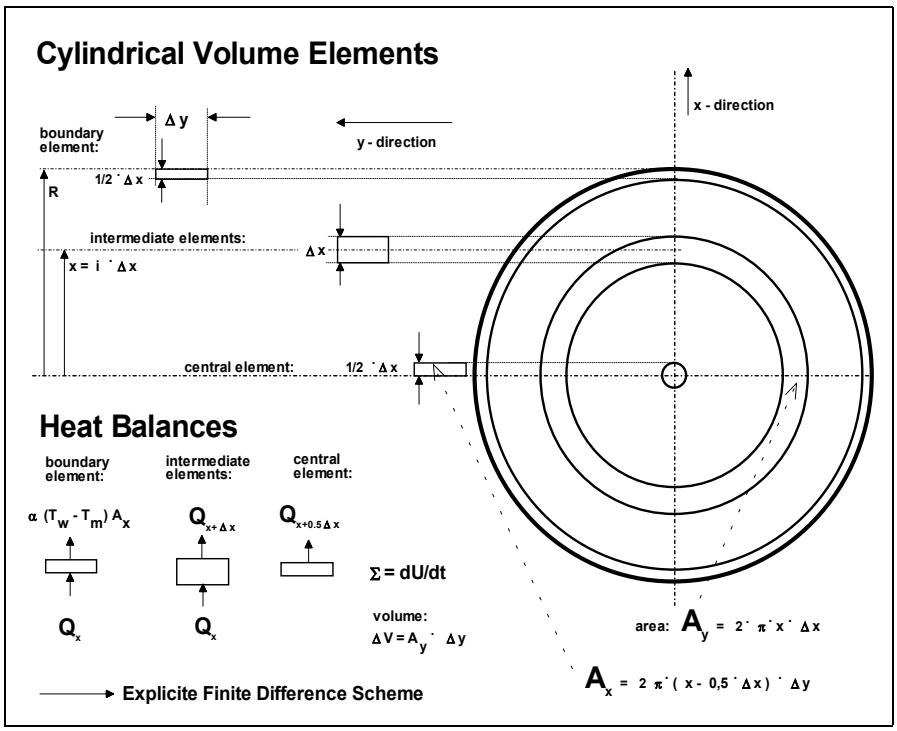

Figure 3.9: Schematic view of the radial, one-dimensional heat balancing at the different volume elements within the cylindrical sample.

3.3.3.2 Thermodynamic properties

The algorithm requires the determination of thermal conductivity, heat capacity and density of the potato samples at the different experimental conditions. As long as there are no available data in the literature for potato properties at high pressures, the model itself was used as a tool to give back the corresponding values for each experimental condition. Taking a previous set of data obtained with an atmospheric pressure freezing experiment as start point, modification coefficients were included into the numerical schema to give back the values that better fit with the experimental curves.

Then, the thermophysical properties for this material must be expressed as a function of the temperature at time step t-Δt. The freezing temperature, T_f, supposes an inhomogeneous point. For

this reason, constant values were used for $T \geq T_f$ and the cumulative Weibull distribution (equations 3.5 and 3.6) was used to calculate thermal conductivity and density at temperatures below the freezing point. According to the parameters b and c the shape of the function varies between maximum and minimum values of the quantities under consideration, which where estimated from the literature (Ross *et al.*, 1977, Chizhov, 1993);

$$\lambda(T) = \lambda_{\min} + (\lambda_{\max} - \lambda_{\min}) \cdot \left[1 - \exp\left(-\left(\frac{T - T_f}{b} \right)^c \right) \right], \tag{3.5}$$

$$\rho(T) = \rho_{\min} + (\rho_{\max} - \rho_{\min}) \cdot \left[\exp\left(-\left(\frac{T - T_f}{b} \right)^c \right) \right] \tag{3.6}$$

Following the approach of Cleland and Earle (1984) the heat capacity was modelled by assuming a hypothetical change in specific heat capacity around the freezing temperature. Since the sharp peak in c_p at T_f seems to affect the plateau of the freezing curves (where the phase transition occurs), a modification of the distribution Weibull function was used as follows:

$$c_p(T) = c_{p,\min} + (T - T_f - T_{\min}) \frac{c_{p,\max} - c_{p,\min}}{T + T_{\min}} + a \left(\frac{T_f - T}{b} \right)^c \frac{c}{T_f - T} \exp\left(-\left(\frac{T_f - T}{b} \right)^c \right) \tag{3.7}$$

Since thawing thermodynamically differs from freezing the values for the parameters for Eqns 3.5 and 3.6, 3.7 were set by the trial and error method selectively for freezing and thawing. Figure 3.10 shows typical model curves for density, thermal conductivity and specific heat as a function of temperature at atmospheric pressure.

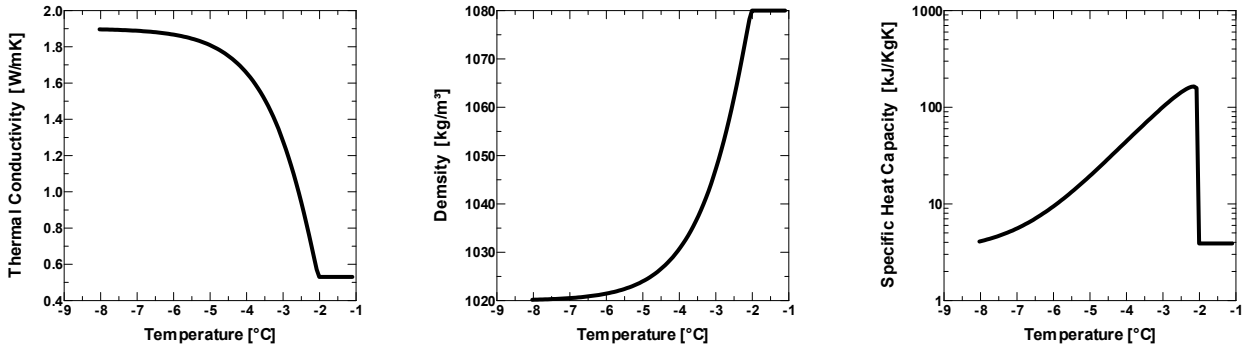

Figure 3.10: Thermal conductivity, density and specific heat as functions of temperature calculated to implement the phase change into the heat balance for freezing at atmospheric pressure.

3.3.3.3 Stability criteria

In eqns. 2.31, 2.36 and 2.42, the temperature at a position or node and at a new time $t+\Delta t$ is calculated from the temperatures of this node and of those in its immediate neighbourhood at time t,

the starting time. This is called the explicit method, because the temperature at a new time can be calculated explicitly from the temperatures at the previous time. In this method the calculation proceeds directly from one time increment to the next until the final temperature distribution is calculated at the desired final time. The temperature distribution at the initial time and the boundary conditions must however be known.

Once the value of Δx has been selected, then the time increment Δt may be chosen such that certain stability criteria are satisfied. Stability means that the errors in the solution do not grow exponentially as the solution proceeds but damp out.

For example, in Eqn 2.31, the value of the *Fo* must be as follows:

$$1/\mathrm{Fo} \geq 4 \tag{3.8}$$

If the above condition is not satisfied, then the second law of thermodynamics is violated. It is also important for the convergence of the finite difference solution that $1/Fo$ must be ≥ 4. Convergence means that the solution of the differential equation approaches the exact solution of the partial differential equation as Δt and Δx go to zero with *Fo* fixed. The general thumb rule to be followed in fixing the criteria is that the coefficient of T_m in the iterative equation should be positive. Accordingly in eqn. 2.36, the value of *Fo* must be such that,

$$1/\mathrm{Fo} \geq 2 \tag{3.9}$$

And in eqn. 2.42,

$$1/\mathrm{Fo} \geq \mathrm{Bi} + (1-\Delta x/4) \tag{3.10}$$

Hence, for the finite difference solution to be stable and convergent, it is necessary that all three of the above criteria are satisfied. eqn. 3.9 is already implied if eqn. 3.8 is satisfied. Therefore the value of Δt must be so chosen that,

$$1. \quad \frac{1}{Fo} = \frac{\Delta x^2}{\alpha \Delta t} \geq 4 \quad i.e., \quad \Delta t \leq \frac{\Delta x^2}{4\alpha} \tag{3.11}$$

$$2. \quad \frac{1}{Fo} = \frac{\Delta x^2}{\alpha \Delta t} \geq Bi + \left(1 - \frac{\Delta x}{2R}\right) \quad i.e., \quad \Delta t \leq \frac{\Delta x^2}{\alpha\left[Bi + \left(1 - \frac{\Delta x}{2R}\right)\right]} \tag{3.12}$$

For a given value of *Fo*, smaller values of Δx mean smaller values of Δt. Using smaller sizes of Δt and Δx increases the accuracy in general but greatly increases the number of calculations required. Hence, a digital computer is ideally suited for this type of calculation.

3.3.3.4 Treatment & procedure

Potatoes were cut into cylindrical shape samples of 40 mm length and 9,8 mm diameter to perform the freezing experiments using the apparatus ‘low temperature system II’. Three holes were bored into the cylinder with a thin needle to insert the tip of a thermocouple into the sample centre and

two additional thermocouples near the surface in the sample. Conductive heat transfer was assumed, since the sample fits exactly to the sample holder. A first experiment at atmospheric pressure was performed to ascertain how much lower the freezing temperature is for potatoes with respect to pure water levels. Then, the freezing process was performed for the following constant pressure levels: 140, 210, 225, 240, 255, 270 and 300 MPa. Additionally, a pressure-shift freezing process was run. Freezing experiments were, performed at least twice, to better ensure their validity. In all the experiments, the samples were first tempered in a heating bath to a temperature level 25°C higher than the theoretically expected level for the freezing point in each case, and then placed in the cooling bath, in which the temperature level was maintained 25°C lower than the expected freezing points. The freezing curves were performed until a 1°C difference was observed between the bath and the sample centre temperatures. In every experiment, the sample temperature was recorded at three different points: once in the sample centre and twice in sample wall, in diametrical opposite points. Also, the temperature of the high-pressure vessel external wall and the bath temperature were recorded. An average value from the two wall temperatures was taken for further calculations in the mathematical model. During phase change, pressure was controlled, either increasing (when ice III is obtained) or decreasing (when ice I crystallises). Beneath the initial freezing temperatures, these tendencies in pressure indicate which ice modification is obtained.

The model used here was also applied to freezing process in which ice III is obtained, with a one-step modelling schema. This model has been implemented in a spread sheet with the help of Visual Basic program tool. The way this model is applied permits that a one-step calculation follows the experimental jump to the corresponding freezing point, also after significant supercooling as ice III is obtained.

Besides pressure, the diameter of the sample (20, 32 and 38 mm) was the variable parameters for the thawing experiments. The temperature of the pressure transmitting medium was maintained at 10°C for all the thawing experiments. The pressures selected were 0.1, 50, 100, 150, 200, 250 and 300 MPa. Each of the three mentioned cylinder sizes were thawed under the above mentioned pressures using the apparatus ‘pilot scale system I’.

The tips of the multi-thermocouple were inserted into the sample at various randomly selected radial distances, ensuring that the tips were placed exactly equidistant from the top and bottom of the cylinder. Two of the thermocouples were also held outside the sample, with the help of aluminium wires, for the purpose of measuring the temperature of the pressure-transmitting medium. The thermocouples were marked by differently coloured isolations for proper identification. The sample was then fixed on to the Pt-100. Tiny wooden projections fixed around the sample ensured that the sample, when placed inside the vessel, would stay equidistant from the walls of the vessel. The sample was then frozen with liquid-nitrogen-vapours. It was found previously that directly immersing the sample into the liquid nitrogen resulted in severe cracking of the sample. As soon as the temperature near the centre of the sample (as observed on the screen) reached –30°C, the plug, with the sample was placed into the vessel and sealed tight. The pressure

was then built up to the required level and the sample was allowed to thaw in the vessel. When the temperature at all points in the sample reached nearly the same temperature of the medium (10°C), the pressure in the vessel was gradually released by opening the pressure-release valve. After a short while, ensuring that the sample is fully thawed, the programme was stopped. The sample was then taken out of the vessel and all the thermocouples were carefully removed from it. The sample was then cut axially at the centre and the distances of the thermocouple-positions from the edge were accurately measured.

The heat transfer coefficient, h at the surface of the sample was found to have a significant influence on the rate of thawing. Since h is a function of the Grasshoff number which in turn is a function of the temperature difference Δt between the sample surface and the fluid film at an infinitesimally small distance from surface of the sample, h had to be modelled as a function of the changing Δt. For this, the temperature distribution in the pressure-transmitting medium had to be modelled as a linear approximation of the temperatures from the two thermocouples placed outside the sample. Thus Δt was calculated as the difference between the surface temperature (obtained from the finite difference algorithm) and the temperature in the fluid at zero distance from the surface of the sample (obtained from the linear approximation), and h was subsequently modelled as a function of Δt.

The value of the melting point was obtained by visual interpretation of the master thawing curves. The peak parameter in the function for c_p was so that the re-calculated thawing curves fit closely with the experimental thawing curves. The same was repeated for all the pressures. Having modelled c_p and λ at all the pressures for a particular size, the thawing curves were predicted for the other sizes also, and these were compared with the corresponding experimental curves.

3.4 Quality assessment

3.4.1 Plant derived tissue

3.4.1.1 High pressure treatments

Cylindrical samples were cut from potatoes (*Solanum tuberosum* cv. Sieglinde) purchased from a local market. Samples with a diameter of 13 mm and a length of 40 mm were used for the experiments. A thermocouple type K was inserted through the upper plug to measure the temperature in the centre of the sample during the high pressure treatment in the apparatus ‘low temperature system I’. The pressure was generated manually using a spindle (Figure 3.3). Pressures above 200 MPa were obtained by repeated compression cycles. In this way a pressure build–up to 400 MPa took less than 2 minutes.

Freeze–thaw cycles at constant pressures of 0.1 MPa, 200 MPa, 320 MPa and 400 MPa were carried out. Two thermal baths were used, one was tempered to a temperature 20 °C above the expected phase transition (0 °C at 0.1 MPa, –20 °C at 320 MPa, –15 C° at 400 MPa), the other 20

°C below. The phase boundaries of potato tissue were examined as mentioned before. In this way, the initial temperature gradient between the bath and the vessel were similar for each treatment and thus, comparable cooling and heating rates were realised. The vessel was tempered to the starting point, compressed and placed in the cooler bath until it approached the temperature of the bath after freezing. Then the sample was heated and thawed using the heating bath and finally decompressed. The change from one bath to the other was accomplished in less than one minute. The pressure was held constant during the pressure holding time using the spindle. The spindle also allowed release of the pressure in a controlled and gradual manner. For the equilibration of the sample temperature to the bath temperature, a difference of ±1 °C was tolerated. The experiments at 0.1 MPa (control sample) were carried out in the same experimental set-up with opened valves to keep constant ambient pressure.

Pressure-shift freezing was carried out, starting at 250 MPa and –27 °C. After freezing, when the temperature approached –27 °C, conventional thawing followed. To examine direct crystal transformations between the ice modifications I and III, the samples were compressed, frozen at a constant pressure value of 320 MPa and decompressed within a few seconds at a temperature of –40 °C. Afterwards, the temperature of the sample was raised to –20 °C in order to get the same starting temperature for thawing, as at ambient pressure. In the opposite direction, the sample was frozen at ambient pressure, tempered to –40 °C, compressed to 320 MPa, thawed under pressure, and decompressed (preventing freezing to ice I).

High pressure treatments without phase transitions were performed as follows. Processes at 250 MPa and temperatures of 20 °C, 0 °C and –27 °C were carried out in combination with pressure holding times of 1 h, 6 h and 24 h. A pressure drop less than 5 MPa during a pressure holding time of 24 h was deemed acceptable for the relevant experiments. The vessel was placed in a bath tempered to the desired temperature. For treatments at 20 °C the sample was compressed when the sample temperature approached 20 °C (±2 °C) and decompressed after the holding time. For the treatments at 0 °C and –27 °C the pressure build-up was started during the cooling but above 0 °C. In these cases the vessel was heated at the end of the pressure holding time to prevent undesired freezing of the sample during decompression.

3.4.1.2 Impedance measurement

Impedance measurement and evaluation of the data was carried out according to the method described by Angersbach et al, (2002), using the same equipment (Electronic Manufacture Company, Mahlsdorf, Germany). The electrodes of the measuring system were adapted to the diameter of the sample (13 mm). The extent of cell membrane permeabilisation was expressed as percentage fractional pore area according to the following equation:

$$F_p = \frac{2l_m\left(\frac{\varphi_h^i}{\varphi_h^{treat}}\varphi_l^{treat} - \varphi_l^i\right)}{l_c\left(\varphi_h^i - \frac{\varphi_h^i}{\varphi_h^{treat}}\varphi_l^{treat}\right)}, \tag{3.13}$$

where l_m and l_c represent the thickness of the membrane and length of the cell respectively and F_p was determined in treated sample by measuring the complex conductivity of initial intact ($\varphi^i{}_l$ and $\varphi^i{}_h$) and high pressure treated samples ($\varphi^{treat}{}_l$ and $\varphi^{treat}{}_h$) at low frequencies (3 kHz) and high frequencies (12.5 MHz) of AC. Starting instantly after the treatment, the conductivity of each sample was measured in the same way every 30 seconds for at least 6 hours. During this measurement, the temperature of the sample was kept at 20 °C in a climatic chamber. The fractional pore area F_p [%] was calculated from the conductivity data before and after the treatment. The difference indicates the area fraction of the cytoplasmic membrane that changed its complex conductivity, i.e. the area that was permeabilised. Equal permeabilisation of all cells was assumed to simplify the model used. High pressure treatments without phase transitions were repeated twice and high pressure treatments with phase transitions were carried out threefold (two experiments for freezing at 200 MPa).

3.4.1.3 Texture measurement and analyses

After the high pressure treatment the potato cylinders were cut transverse into 3 or 4 cylindrical pieces with a length of 10 mm, depending on the state of the sample. In this way 7 to 12 texture measurements could be done for each treatment. The samples were subjected to a uniaxial compression of 9 mm between two parallel plates using a texture analyzer TA.XT2 (Stable Micro Systems, Godalming, UK) which recorded the force–deformation data. The deformation rate was 1 mm/s.

From the force-deformation curves, the true stress and the true strain were calculated. These values give a more realistic impression of the deformation than the apparent stress and strain, because they consider the deformation of the sample. Deviations between the true strain and the apparent strain are not negligible considering large deformations of foodstuffs (Calzada and Peleg, 1978, Pons and Fiszman, 1996).

True compressive stress σ_c [N/mm²] was calculated using the following equations:

$$\sigma_c = \frac{F}{A}, \tag{3.14}$$

$$A = \frac{A_i \cdot h_i}{h_i - \Delta h} \qquad \text{(assuming volume incompressibility)}, \tag{3.15}$$

where F [N] is the force, A_i [mm²] is the cross sectional area of the cylinder before compression, A [mm²] is the cross sectional area of the cylinder at a deformation of Δh, h_i [mm] is the initial height

of the cylinder before compression, Δh [mm] is the difference of the height of the sample before compression and during compression

True compressive strain ε_c [-] was calculated as follows:

$$\varepsilon_c = \ln\left(\frac{h_i}{h_i - \Delta h}\right) \tag{3.16}$$

The first local maximum in the true stress – true strain plot was defined as failure stress σ_f and the associated strain was defined as failure strain ε_f.

3.4.1.4 Colour measurement and visual appearance

In order to evaluate the optical appearance of the potato cylinders, they were cut in two pieces in the longitudinal direction. Digital photographs were taken form one half under constant light and constant camera parameters every 10 minutes for two hours. The middle section of each picture was cut out using picture editing software. Colour measurements (Minolta CR200) were carried out as triple determination in the same frequency using the other half of the cylinder. The lightness value L^* of the $L^*a^*b^*$ colour space is given, like it was done by Sapers *et al.* (1989). Enzymatic browning mainly influences this value.

3.4.1.5 Thermal analyses

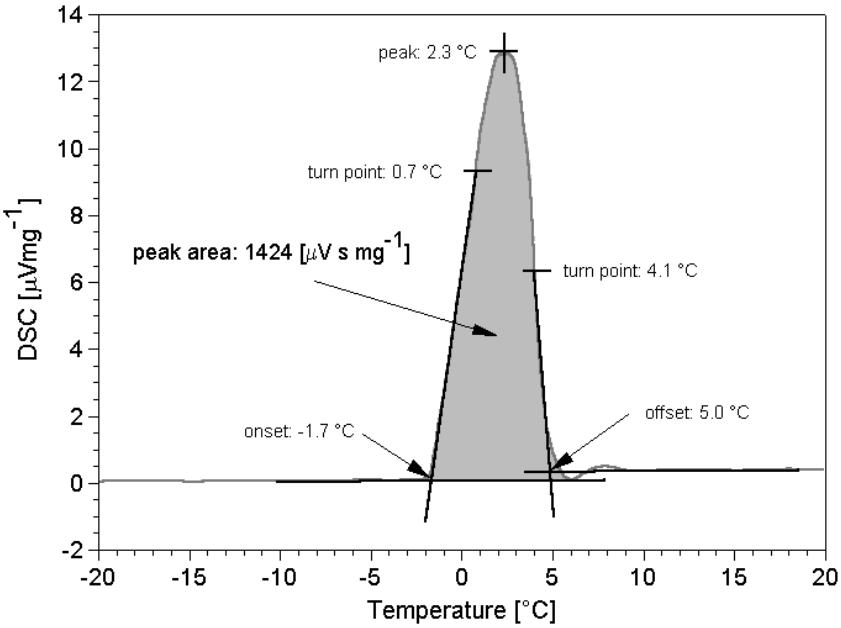

Figure 3.11: Typical endothermic peak due to melting of pure water and peak analysis.

Differential scanning calorimetry (DSC) was used to determine the enthalpy of fusion of potato tissue at ambient pressure. The measurements were performed by a simultaneous device TG-DTA/DSC (STA 409C, Netzsch, Germany) equipped with a TG-DSC-sample holder (with attached thermocouple type Ni-Cr / Constantan) and an oven with winding heater (attached thermocouple

type Pt-Rh / Pt). The potato samples (12 ± 3 mg) were weighed (± 0.01 mg) into 30 µl aluminium pans and sealed hermetically. At least quadruplicate samples were heated under continuous He-atmosphere from -50 to 50 °C at a heating rate of 2.0 $Kmin^{-1}$, with an empty sealed pan as reference. Calibration of the instrument was carried out using common standard materials within the relevant temperature range. In the first step the melting enthalpy of pure distilled water was carried out. All DSC-thermograms obtained were evaluated using a basic software provided by the DSC equipment supplier (Netzsch, Germany). A typical thermogram for water is given in Figure 3.11.

3.4.2 Animal derived tissue

3.4.2.1 Thawing experiments

In order to evaluate high pressure assisted thawing and the storing of foodstuffs, and to estimate the industrial potential of these processes, the transportable high pressure unit 'pilot scale system II' was used. The vessel pressure and the inner vessel temperature were measured in the sample surrounding medium as described above. The temperature of the cooling circuit was set to 15 °C. The data were recorded via computer and a measurement rate of 0.5 Hz was selected. The end of the phase change process was indicated by a slight pressure increase due to density changes of the sample. In preliminary experiments a type K thermocouple was fixed in the thermal centre of the cylindrical sample after an adequate hole had been drilled using a boring machine to evaluate the temperature history of the fish probe and to estimate the pressure holding time required for completion of the phase transition. Then, a pressure holding time of 60 min was applied in all high pressure experiments to ensure complete phase transition. The thawing under atmospheric conditions was performed either using the pressure vessel at 0.1 MPa or a water bath (Haake 6P, Karlsruhe, Germany), equipped with a thermostat (Haake D1), was used to thaw the fish samples. Then, the temperature of the circulating water was set to 15 ± 0.5 °C.

3.4.2.2 Water holding capacity

Expressible moisture was determined using a modification of the filter paper press method as described by Detienne & Wicker (1999). Samples prepared from sliced fillet portions (20 mm diameter, 15 mm thick) were pressed between paired filter sheets (Schleicher & Schuell 2043 A, 7x7 cm) and parallel plates using a texture analyser TA.XT2 (Stable Micro Systems, Godalming, UK). A 25 kg load cell and a crosshead speed of 1.7 mms^{-1} were used. Samples were pressed to 75 % deformation and held at that point for 15 s. WHC was defined as the expressible moisture, calculated as % = 100 (initial weight – final weight) / initial weight.

3.4.2.3 Thawing loss

The thawing loss was determined by weighing samples prior to and after thawing. Thawed samples were unwrapped and weighted. The surface drip was removed using filter paper. Each experimental value represents the mean of three determinations.

3.4.2.4 Sensory tests

Sensory analysis was performed in duplicate by a panel consisting of three trained judges, except for the haddock samples. Raw fillets were tested immediately after thawing and cooked fillets sealed in PE film after heating for 10 minutes in water at 80 °C. Modified Quality Index Method (QIM) schemes according to Warm *et al*. (1998) were used for quality assessment of thawed and cooked fillets. In the former, the following parameters have been assessed (in brackets the demerit points are given): texture (0-3), odour (0-2), colour (0-3), gaping (0-3) and in the latter: odour (0-4), colour (0-4), flavour (0-4), texture (0-4). For each species used, the QIM scheme has to be adapted to a description of the single scores of individual quality parameters. The scores for all the characteristics are added to give an overall sensory score, the so-called 'quality index'. QIM gives scores of zero for very fresh fish and increasing values as the fish deteriorates.

3.4.2.5 Texture analyses

Hardness was measured with a texture analyser TA.XT2 (Stable Micro Systems, Godalming, UK) by compressing the samples (20 mm diameter) prepared by the use of a cork borer to 75 % using a flat-ended probe (50 mm diameter). The crosshead speed was set at 1.7 mms^{-1}. The measurements were repeated at least nine-fold.

3.4.2.6 Colour changes

Colour measurements have been performed on intact fillets after thawing and boiling according to Schubring (1998) using a tristimulus colorimeter CR 300 (MINOLTA). In the CIE Lab system, L^* denotes lightness on a 0 to 100 scale from black to white; a^*, (+) red or (-) green; and b^*, (+) yellow or (-) blue. ΔE, the colour difference, denotes the square root of ($\Delta L^2 + \Delta a^2 + \Delta b^2$). Measurements were repeated twelve-fold at least.

3.4.2.7 Calorimetric analyses

Protein denaturation was determined using differential scanning calorimetry. The measurements were performed by a Perkin Elmer DSC 7 device equipped with a Perkin Elmer Intra cooler II as described by Schubring (1999). The fish samples (15 ± 3 mg) were weighted (± 0.1 mg) into 30 µl aluminium pans (BO 169 320) and sealed. At least quadruplicate samples were heated from 25 to 95 °C at a scanning rate of 10 $Kmin^{-1}$, with an empty sealed pan as reference. The transition temperature (T_{max}) was recorded.

3.4.2.8 Viable count of microorganisms

Aliquots (10 g) of the thawed fillets were prepared under sterile conditions and homogenised by a Stomacher for 2 min in 90 ml sterile NaCl Pepton solution. Subsequently, a decimal dilution series of the homogenate was made, from which each of 3 replicates were spread plated (0.2 ml) on Standard I Agar dishes. The dishes were incubated at 20°C for 3 days, then the black colonies (specific spoiling organisms: *Shewanella putrefaciens*) and the other colonies for total viable count (TVC) were counted and calculated in 1 g fillet samples.

3.4.2.9 Parasites

The potential of high pressure to inactivate fish parasites was estimated using nematodes extracted from fresh fish caught by the fishery research vessel "Walther Herwig III" on the Atlantic Ocean. A variety of parasites have been identified in raw fish. Most of the scientific literature describes methods to control the most significant parasites of concern in the western world, such as anisakid parasites (nematodes). According to Bier (1976), Goldsmid and Speare (1997) and Reilly and Kaferstein (1997) the descriptions of the life cycles of the parasites can be summarised as follows. *Anisakiasis* is a disease that includes infections by all ascaroid nematodes having larval stages in aquatic hosts. The main nematodes known to have caused disease in humans are *Anisakis simplex* and *Pseudoterranova decipiens*. These nematodes reach sexual maturity in the intestinal tract of marine mammals. Eggs are expelled into the intestinal tract and then are expelled in the faeces. In the water the eggs embryonate and undergo at least one moult. The larvae that hatch may infect a small crustacean that may in turn be ingested by a fish (that is, rockfish, herring, mackerel, and salmon). When an infected fish is consumed by another fish, the larvae may penetrate the viscera and infect the new fish host. Marine mammals (such as dolphins, seals, and so on) or humans may become infected from eating the infected intermediate host. In humans, these nematodes do not normally mature, but the worms can migrate from the gastrointestinal tract, becoming embedded in the gastrointestinal mucosa and causing tissue reaction and discomfort (that is, gastric pain, diarrhoea, vomiting).

For the experiments the nematodes were separated from the guts of fresh fish (pre rigor) and for each sample about 100 living organisms were packed directly in a flexible sterile bag filled with digestive solution or stuffed before into a piece of fish fillet and then forced to high pressure treatment at 150 (30 and 60 min) and 200 MPa (30 and 60 min) at 15 °C. After high pressure application the status of the nematodes was evaluated by using UV light and by visual inspection of their mobility. According to Karl *et al*. (1995) a fluorescentic white colour of the larvae (maybe due to protein denaturation) in a UV chamber indicates an inactivation of the nematodes. Additionally the mobility of the high pressure treated larvae was visually evaluated in petri dishes and controlled after 24 h storing the sample at room temperature, to estimate possible recovery of the nematodes.

3.4.2.10 Statistical analysis

The results were statistically evaluated using the software package STATISTICA (StatSoft, Inc. (1996), Tulsa, OK, USA).

3.4.3 Inactivation of microorganisms

3.4.3.1 Sample preparation

In order to obtain cells in the stationary phase the growth behaviour of *Listeria innocua* at 30 °C was determined (Figure 3.12). A 48-hour Standard-I-nutrient-broth culture of *L. innocua* grown at 30°C was inoculated into 27 ml of Ringer solution (pH 6.7) and in 90 g of babyfood (pH 5.3) to

obtain a population of about 10^7 to 10^8 CFU/ml at the beginning of the process. The cell suspensions were dispensed in 1.5-ml portions in sterile plastic cryovials (1.5 ml capacity; Nunc GmbH & Co. KG, Wiesbaden, Germany) and pressurised. The vials were kept at 4°C during handling before and after pressurisation for periods that did not exceed 1.5 h.

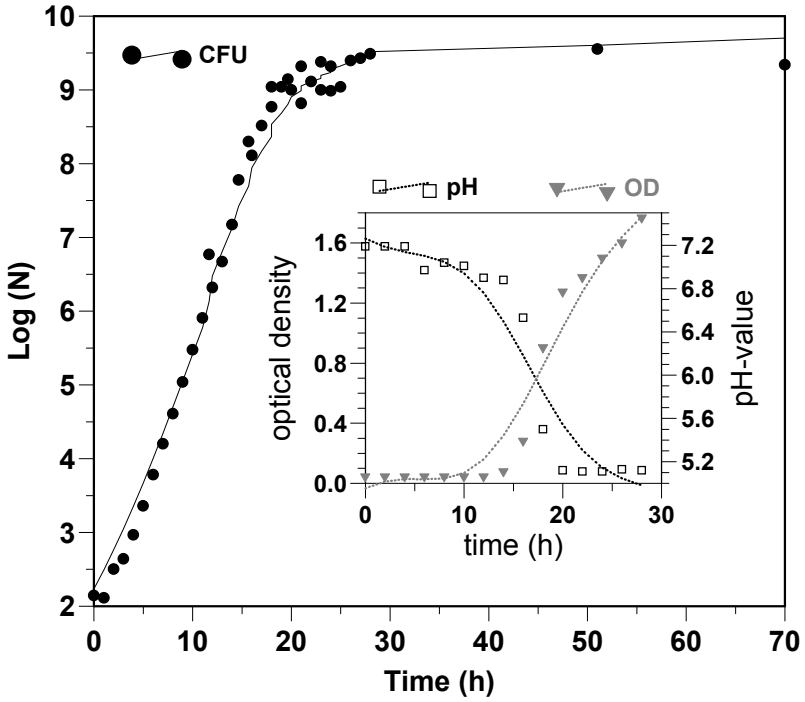

Figure 3.12: Growing behaviour of *Listeria innocua* during cultivation at 30 °C derived from colony forming units (CFU), changes of optical density (OD) and pH-value. Stationary phase was reached after 30 h.

3.4.3.2 Treatment

The inactivation experiments were carried out at temperatures of –30, –20, –10, 0, 10, 20, 30 and 40 °C. The pressures and treatment times selected were as follows: 200 MPa (10, 30, 60, 90 and 120 min); 250 MPa (5, 10, 15, 20 and 30 min); and 300 MPa (2, 5, 10, 15 and 20 min). The pressurisation times reported in this study did not include the come-up and come-down times. All experiments were performed in triplicate. For the experiment, a cryovial was placed in one of the vessels, the vessel was sealed tight and the required pressure was built up in it. After the required treatment time, the pressure in the vessel was released gradually, the vial was taken out, marked and kept at 4°C. The cell suspensions were then enumerated for viable cells.

3.4.3.3 Enumeration of viable cells

The cell suspension in each vial was serially diluted in ¼ strength sterile Ringer solution (Merck 15525, Darmstadt, Germany) and 0.1-ml portions were surface plated on bacteriological agar (agar no. 1, Unipath-Code L11, Basingstoke, England) supplemented with peptone from meat (5 g/l) (Merck 7214, Darmstadt, Germany) and dry extract of meat (3 g/l) (Merck 3979, Darmstadt, Germany). The plates were incubated at 30 °C for 2 days and then enumerated for viable cells.

3.4.3.4 Regression analysis

In this study, the microbial inactivation was explained by a mathematical model based on *n*th order kinetics according to Ananta *et al*., (2001). The general form of the *n*th order kinetic is shown in eqn. (3.17):

$$\frac{du}{dt} = -k \cdot u^c \tag{3.17}$$

where u is the concentration of the microorganism of consideration, k is the rate constant and c is the reaction order of the reaction. Substituting the left-hand side of eqn. (3.17) with $\log N/\log N_0$ and further transformation into the common presentation of $\log(N/N_0)$ versus time results in the following mathematical expression, which should correctly fit the experimental data:

$$\log\left(\frac{N}{N_0}\right) = \left(e^{-k \cdot t} - 1\right) \cdot \log N_0, \qquad \text{for c = 1, and} \tag{3.18}$$

$$\log\left(\frac{N}{N_0}\right) = \left(\left(-k \cdot t + k \cdot t \cdot c + 1\right)^{1/1-c^{-1}}\right) \cdot \log N_0, \qquad \text{for c} \neq 1. \tag{3.19}$$

This model is derived empirically and has no mechanistic background of real molecular reactions underlying inactivation of vegetative cells.

Two model parameter can be yielded from the regression analysis, i.e. k and $c \cdot k$ is not identical with the real rate constant of the *n*th order reaction, from which this equation is derived, because u in the original equation (eqn. 3.17) was substituted by $\log N/\log N_0$; however, at constant c the apparent rate constant k is the characteristic value of each survival curve, which directly represents the cell-inactivating effect of each *pT*-combination. The proposed model was fitted to the experimental survival data with the non-linear regression procedure in TableCurve2D (SPSS Inc., Chicago, IL, USA) using the Person estimation method whose iteration procedure minimises the following expression:

$$\sum_{i=1}^{n} \ln\left(\sqrt{1 + |u_i - \hat{u}_i|}\right), \tag{3.20}$$

where $u_i = \log N/\log N_0$ experimental; $\hat{u}_i =$ calculated; and n = number of data points in the survival curves. The accuracy of fit of the model was assessed using the term FSE (Fit Standard Error) between the experimental and predicted value.

The pre-selection of suitable reaction order was performed by testing a series of reaction orders between 1 and 3 with an incremental step of 0.5. For each survival curve, a table of results of the curve-fitting procedure from each tested reaction order was sorted with ascending fit standard error. The reaction order, which yielded the least fit standard error in the minority of the examined survival curves was selected. This reaction order was further applied in the proposed model to calculate the rate constants. The generation of data for predicted survival curves was made with *MathCad* software (MathSoft Inc., Cambridge, MA, USA). A *pTk*-diagram (Yayanos, 1998), which

explains how both T and p influences the rate constant k, was derived from the kinetic data of the regression analysis. The data for the *pTk*-plot were generated using *Plot-It* graphics and scientific package (Scientific Programming Enterprises, Haslett, MI, USA).

4 RESULTS AND DISCUSSION

4.1 Processing criteria for controlled pressure-supported phase transitions

4.1.1 Introduction

Phase transitions in the form of pressure-assisted freezing, pressure-shift freezing, pressure-assisted thawing and pressure induced thawing were investigated using plant derived tissue in the form of potato cylinders. An attempt is made here to explain in detail about the phenomena of high pressure-supported phase transitions, which also serves the purpose of clarifying questionable notions upon which some of the previous research in the area is centred about.

It is a common and natural expectation that the sample under consideration undergoes transition from one phase to another (be it liquid to solid, solid to liquid or to a different solid form) if it has crossed the equilibrium line between the two phases and exists with regard to pressure and temperature in a region where the latter phase is stable. But this has been established by Knorr *et al.* (1998) and reinstated by the present study as not necessarily true. This means that one may not, for instance, have water at conditions such as –30°C and 300 MPa (a region where ice III is stable) and arrive at the conclusion that the water exists as ice III. A close examination of the phase transition experiments with potato throws more light on these statements.

4.1.2 Phase transition lines of plant tissue

An interesting prospect that arises from the nature of the freezing and thawing curves is that of tracing the phase transition lines of foods at constant pressure levels or by manipulating pressure build-ups and pressure releases. An attempt was therefore made to obtain the phase transition lines ice I/liquid, ice III/liquid and ice V/liquid of potato by freezing and thawing it under pressure. In either case the ambient bath temperature was set at –25°C below the expected freezing point and the sample was cooled under pressure to equilibrium temperature. Then, before the pressure was released the sample was thawed under pressure by immersing the high pressure vessel in the heating bath (set to temperature 25 °C above the expected melting point). The temperature stability at the phase boundary offered a different approach to the experimental description of the equilibrium line. Using a suitable measurement system, the shift of the phase transition temperature in the centre of the sample was additionally recorded during manual change of the system pressure, so that the slope of the phase boundary could be determined.

4.1.2.1 Melting curve ice I

An essential step in the modelling of freezing and thawing processes is the determination of the real phase transition temperature that is dependent on both the specific properties of the considered material and the working pressure (Denys *et al.*, 2002). Since no data for melting curves of plant

tissues at high pressure levels were available, one aim of this study was to determine the phase boundaries of potato tissue. In the first step, freezing and melting points of potato tissue were detected along the melting curve of ice I. The experimental data for the melting pressure were plotted versus phase transition temperature in Figure 4.1. Compared to pure liquid water the phase boundary shifts towards lower temperature values (about 1.1 °C).

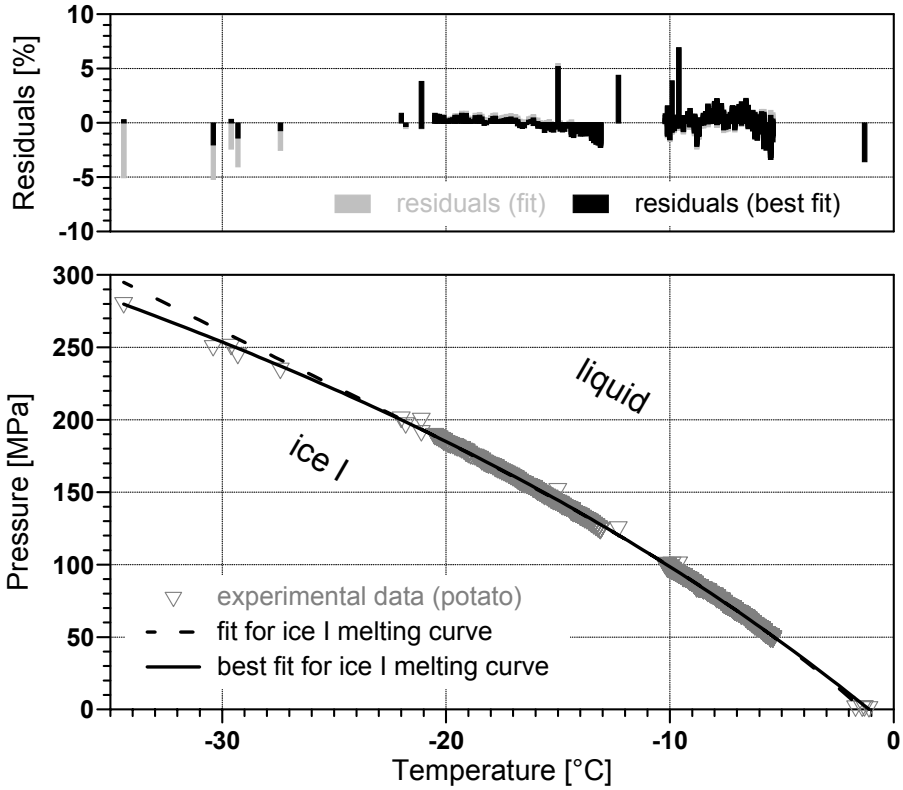

Figure 4.1: Predicted and experimental melting curves of ice I in potato tissue. The percentage difference between the predicted and the experimental melting pressure is quantified by the residuals.

To quantify the difference the melting curve of pure ice I (calculated according to (Wagner *et al.*, 1994)) was shifted parallel by fitting the initial freezing temperature (fit), taking into account the freezing point reduction due to solvable components in the potato tissue water (Table 4.1). The residuals indicate the difference of the calculated melting curve and the experimental data obtained. It can be seen that the melting points of potato follow the slope of the shifted melting curve of pure water indicating a convergent pressure dependency.

Table 4.1: Model parameters for pure water but shifted T_N to evaluate the melting curve of ice I in potato

Parameter	Value
T_N [K]	271.79
P_N [MPa]	6.11675×10^{-4}
α	0.626000
β	-3
χ	0.197135
δ	21.2
Temperature range [K]	271.79 to 249.79
Fit Std Error	1.15

Table 4.2: Best fitting parameters to describe the melting curve of ice I in potato

Parameter	Value
T_N [K]	272.05
P_N [MPa]	0.0049776
α	0.17477715
β	-0.74833239
χ	0.050198807
δ	11.014122
Temperature range [K]	272.05 to 238.66
Fit Std Error	0.93

However, at pressure levels above 210 MPa where freezing to ice III was expected, formation of only ice I was indicated and the model overestimated the melting pressure. This behaviour can be explained by the range of validity of the model. Since Wagner *et al.* (1994) fitted the parameters of the model within the range of thermodynamic stability of the single melting curves, the calculations for the melting pressure of ice I are not valid beyond the triple point at 209.9 MPa and –22 °C. To improve the model in the extended range, all the parameters were fitted to the experimental data (best fit), resulting in high conformity of experimental data and calculated values as indicated by a Fit Standard Error (FSE) of 0.93, especially in the region where ice III is thermodynamically stable. The regression parameters are given in Table 4.2.

4.1.2.2 Melting curve ice III

To obtain the melting curve of ice III for potato tissue, the steps as described before were carried out. The calculated and experimental melting pressures are plotted versus phase transition temperature in Figure 4.2. To estimate the similarity of the melting curves of ice III for pure water and potato, the initial freezing point at the triple point of liquid/ice I/ice III was shifted to lower temperatures leading to satisfying precision with residual values lower than 7% (Figure 4.2). However, the general slope of the experimental curve was slightly different and results in overestimation of the melting pressure in the middle part of the phase boundary while near the triple points at 209.9 MPa and –22 °C (liquid/ice I/ice III) and the shifted water model underestimated the melting pressure.

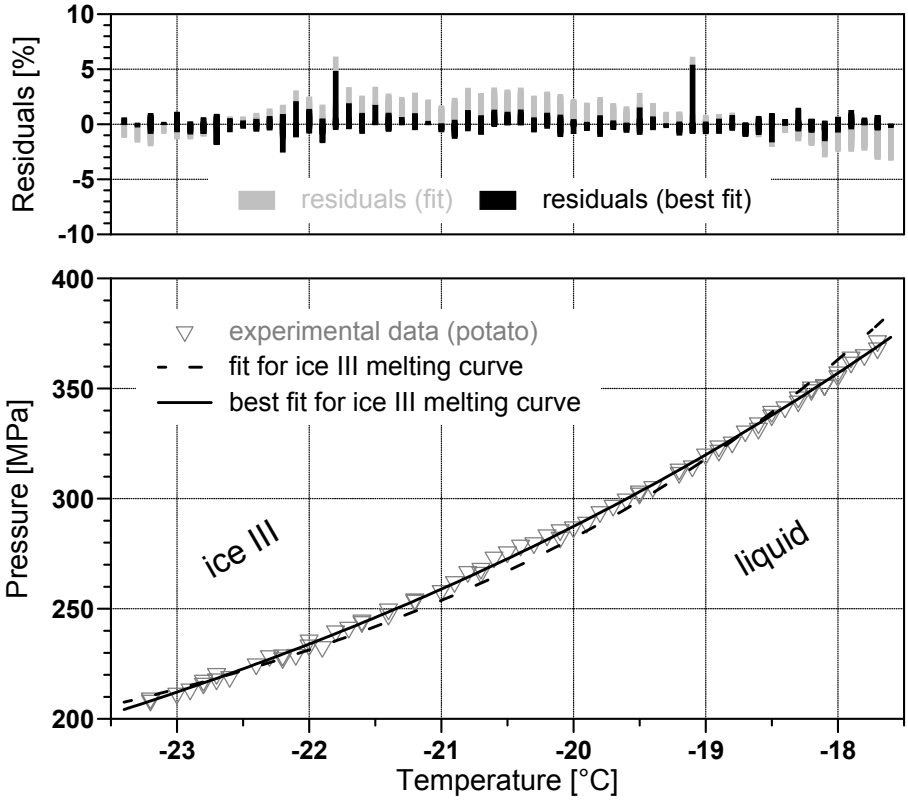

Figure 4.2: Predicted and experimental melting curves of ice III in potato tissue. The percentage difference between the predicted and the experimental melting pressure is quantified by the residuals.

This led to a FSE value of 4.69 as given in Table 4.3. Consequently all model parameters were fitted to the experimental data (Table 4.4) resulting in a better conformity as indicated by the residuals (≤ 5%) and the FSE.

Table 4.3: Model parameters for pure water but shifted T_N to evaluate the melting curve of ice III in potato

Parameter	Value
T_N [K]	249.91
P_N [MPa]	209.9
α	0.295252
β	60
Temperature range [K]	249.91 to 254.91
Fit Std Error	4.69

Table 4.4: Best fitting parameters to describe the melting curve of ice III in potato

Parameter	Value
T_N [K]	249.88
P_N [MPa]	206.8
α	0.68866823
β	34.519028
Temperature range [K]	249.88 to 255.46
Fit Std Error	1.81

4.1.2.3 Melting curve ice V

Figure 4.3 shows a comparison of the experimental data and the calculated melting pressure for ice V by shifting the initial freezing temperature (fit) to a value of -18.7 °C which is about 1.7 °C lower than that of pure water and subsequent fitting of all model parameters (best fit).

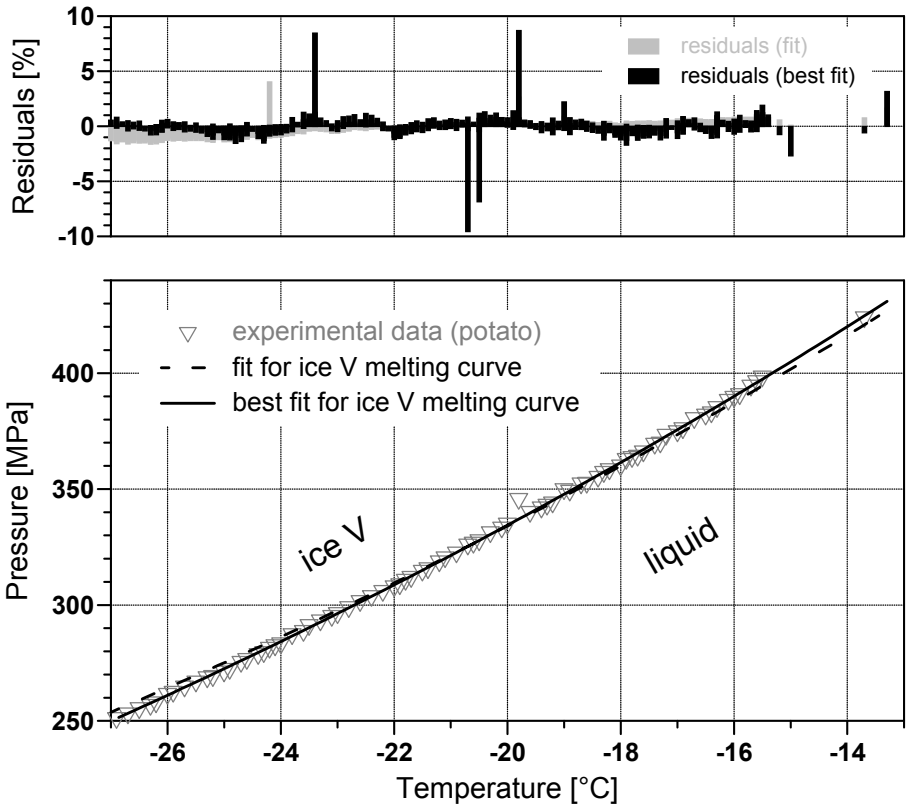

Figure 4.3: Predicted and experimental melting curves of ice V in potato tissue. The percentage difference between the predicted and the experimental melting pressure is quantified by the residuals.

The regression parameters are given in Table 4.5 and 4.6. Interestingly, phase transition points were obtained far below the stability area of ice V which is marked by the triple point (liquid/ice III/ice V) at 350.1 MPa and –17.0 °C. Nevertheless, the calculated values show high conformity with the experimental data, except with some single melting coordinates, which might be attributed to differences in the biological material. Fitting all the model parameters does not significantly improve the precision of the calculated melting curve by visual inspection, but can be seen by comparison of the FSE values in Table 4.5 and 4.6.

Table 4.5: Model parameters for pure water but shifted T_N to evaluate the melting curve of ice V in potato

Parameter	Value
T_N [K]	254.40
P_N [MPa]	350.1
α	1.18721
β	8
Temperature range [K]	256.40 to 271.54
Fit Std Error	2.37

Table 4.6: Best fitting parameters to describe the melting curve of ice V in potato

Parameter	Value
T_N [K]	254.23
P_N [MPa]	348.9
α	1.3080857
β	7.5643531
Temperature range [K]	254.23 to 259.66
Fit Std Error	1.29

4.1.2.4 Solid-solid phase boundary

Figure 4.4A illustrates an attempt to trigger the solid-solid transformation in potato tissue during pressure release starting from ice III.

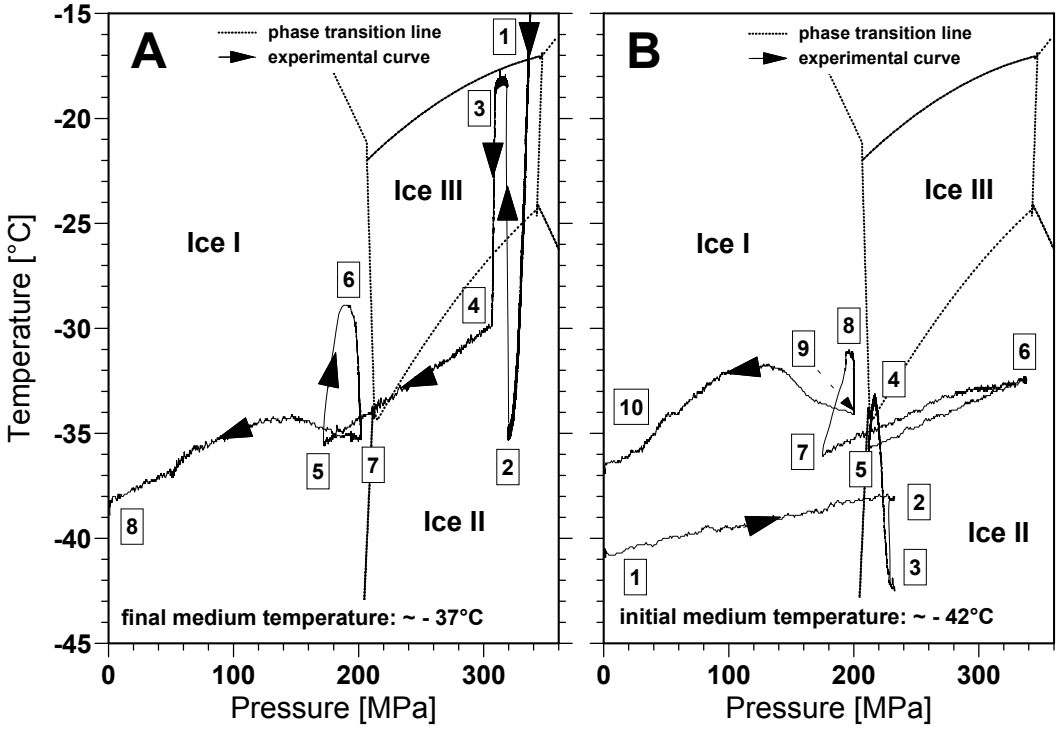

Figure 4.4: Freezing experiment on potato tissue to trigger solid-solid transformation. A: Evolution of the sample temperature (centre) during freezing to ice III and subsequent de-pressurisation plotted vs. pressure on the phase diagram of pure water. B: Temperature (sample centre) plotted vs. pressure during pressure cycle at low temperature (≤ –30 °C), indicating solid-solid transformation (ice I – ice III – ice I). Directions of the pathways are marked by arrows and numbers.

In the first step the nucleation point to ice III was reached by cooling the sample (liquid state) pressurised at 320 MPa (step 1 to 2). The phase transition was clearly indicated by a jump in temperature which did not exceed the melting curve of ice III (step 2 to 3) and a nearly constant temperature value during freeing to ice III (removal of latent heat of fusion) at step 3. The decrease in pressure indicates that the phase change coincided with a volume contraction of the sample, which is in agreement with the different specific densities of liquid and ice III. A high degree of supercooling was always obtained before freezing to high pressure ices. After the freezing was accomplished, the sample was cooled to –30 °C (step 3 to 4). On pressure release (step 4 to 5), a jump in temperature and pressure (step 5 to 6) was encountered beyond the ice I/ice III phase boundary, which indicates a transformation from ice III to ice I. The nature of the jump is such that it does not reach the ice I/liquid line. Had it been so, then the formation of ice III could have been ruled out, since such a jump (to the ice I/liquid line) would imply a transition from liquid to ice I (e.g. pressure shift freezing). The nature of the jump therefore serves as an indicator of the (exothermic) crystallisation of ice III. The shape of the 'loop' (steps 5, 6, 7) indicates that the

transformation occurs along the ice I/ice III phase boundary. Step 7 to 8 marks the de-pressurisation.

Figure 4.4B shows the temperature at the centre of the sample plotted vs. pressure for an experiment where the pressure was built up on a deeply frozen sample (step 1 to 2). At a pressure of about 230 MPa, the sample temperature suddenly dropped from –38 °C to –42°C (step 2 to 3). This drop clearly indicates an endothermic transformation from ice I to ice III, since formation of ice II would have resulted in an exothermic event. The sample was sufficiently frozen to ensure that it contained no metastable water. The temperature then increased (step 3 to 4) according to the surrounding medium temperature and the pressure decreased, indicating the ongoing formation of ice III (due to the higher density of ice III). This transformation occurs close to the ice I/ice III phase boundary. After the phase transformation is complete, the sample is subcooled (step 4 to 5) and the pressure was then manually built up (step 5 to 6) and released (step 6 to 7) to see if any further temperature jump or drop occurs. Expectedly, during pressure release, the characteristic loop (step 7, 8, 9) occurred again which indicated recrystallisation to ice I and therefore confirmed the initial crystallisation of ice III. Since the exact slope of the phase boundaries ice I/ice III and ice III/ice V was not detectable with the experimental procedure a straight vertical slope was assumed for potato tissue starting from the relevant triple points. However, no indication for ice II formation was obtained within the range of investigation, neither during cooling from ice III nor during pressure build-up from ice I.

4.1.2.5 Phase diagram

The determination of the phase transition lines of foods is significant with respect to attempts at modelling pressure supported phase transitions. Such a model would inevitably require knowledge about the dependence of freezing temperature on pressure. Foods are expected to exhibit depressions in the freezing temperature at all pressures owing to the presence of solutes and the food matrix and not all the water in the food is freely available. The experiments described above demonstrate that phase transition lines can be traced using the Thermistor-Cryoscope method and the dynamic method of pressure-manipulations. It however remains a challenge to tactfully conduct the manipulations to obtain the equilibrium points between all the different solid forms. Figure 4.5 summarises the experimentally determined phase boundaries for water-ice and ice-ice transitions in potato tissue. The triple point liquid/ice I/ice III at 210.9 MPa and – 23.1 °C is shifted to lower temperature as compared to the analogue triple point for pure water at 209.9 MPa and –22 °C. The triple point liquid/ice III/ice V at 363 MPa and – 18.2 °C is shifted to lower temperature and higher pressure as compared to the analogue triple point for pure water at 350.1 MPa and –17 °C. The experimental data showed a high degree of supercooling before liquid-solid transition was obtained when triggering ice III and ice V. The transformation along the extended melting curves of ice III and ice V was significant as indicated by the broken lines. The fact that it was possible to prolong the equilibrium lines beyond the triple point into the region of instability, thus realising equilibrium

points between two unstable phases, was also reported by Bridgman (1912) in his experiments to determine the phase diagram and by Evans (1967a).

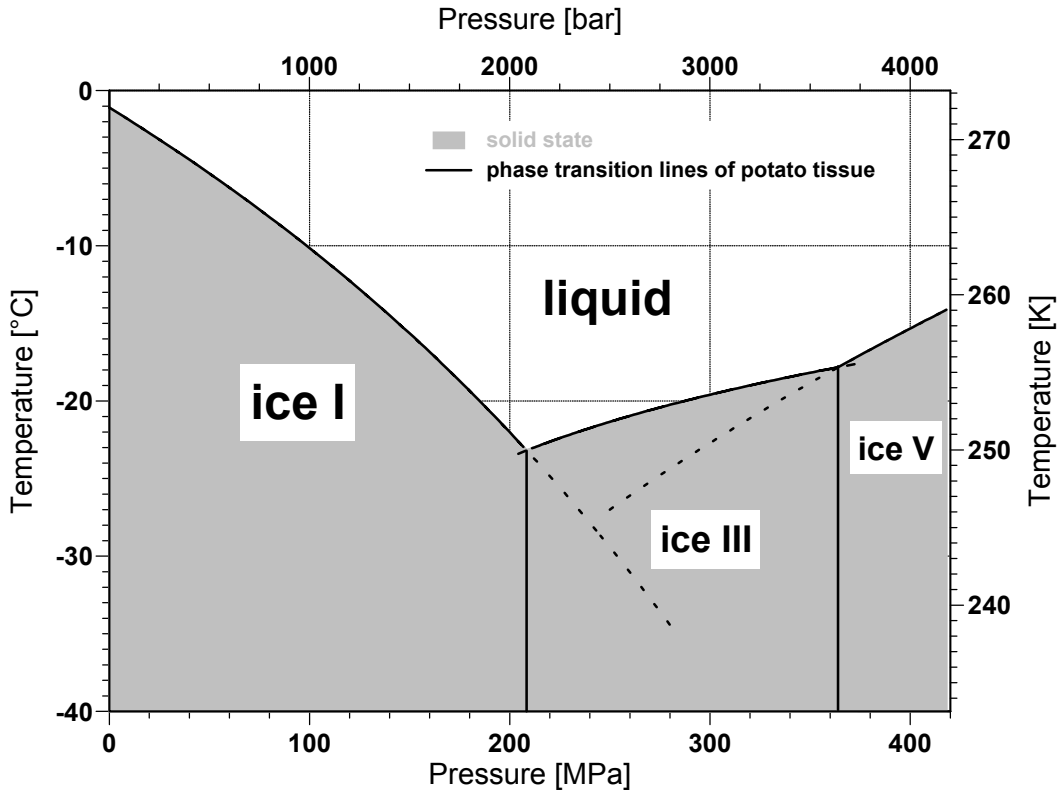

Figure 4.5: Phase diagram of potato tissue as derived from -experimental results.

Besides the above described model to calculate the melting pressure for a certain phase transition temperature, the pressure dependency of the phase transition points can be described by simple polynomial equations as follows:

$$T_{m(iceI)} = -1.083 - 0.08091 \cdot p - 7.471^{-5} \cdot p^2 - 2.199^{-7} \cdot p^3, \quad (4.1)$$

$$T_{m(iceIII)} = -36.14 + 0.0785 \cdot p - 7.769^{-5} \cdot p^2, \quad (4.2)$$

$$T_{m(iceV)} = -53.81 + 0.1259 \cdot p - 7.431^{-5} \cdot p^2. \quad (4.3)$$

These equations were obtained by simple regression procedure.

4.1.2.6 Liquid-solid contour plot

As outlined above, the melting curves of different ice polymorphs in foods can be described by specific equations, but for modelling implementations and process design it might be of interest to describe the liquid-solid phase boundary over a wide pressure range by a single equation. In order to find such an equation describing the liquid-solid contour within the range of experimental data a fitting procedure was applied using the software packet TableCurve2D (SPSS Inc., Chicago, IL,

USA). As a result the following relation of pressure level p_m and melting temperature T_m [°C] was obtained:

$$T_{m_{potato}} = \frac{k_1 + k_3 p_m + k_5 {p_m}^2 + k_7 {p_m}^3 + k_9 {p_m}^4 + k_{11} {p_m}^5 + k_{13} {p_m}^6 + k_{15} {p_m}^7 + k_{17} {p_m}^8 + k_{19} {p_m}^9}{1 + k_2 p_m + k_4 {p_m}^2 + k_6 {p_m}^3 + k_8 {p_m}^4 + k_{10} {p_m}^5 + k_{12} {p_m}^6 + k_{14} {p_m}^7 + k_{16} {p_m}^8 + k_{18} {p_m}^9 + k_{20} {p_m}^{10}} \quad (4.4)$$

The model coefficients are given in Table 4.7.

Table 4.7: Values of the 20 coefficients of eqn. (4.4) fitted with the results calculated according to Wagner et al (1994) but using optimised parameters for potato tissue. (FSE: 0.05)

Symbol	Value	Symbol	Value	Symbol	Value
k_1	-1.09657573	k_8	8.86749e-009	k_{15}	-1.9994e-015
k_2	-0.02683753	k_9	1.33848e-007	k_{16}	5.03938e-021
k_3	-0.05051507	k_{10}	-2.3904e-011	k_{17}	1.70829e-018
k_4	0.000314777	k_{11}	-5.2997e-010	k_{18}	1.90288e-023
k_5	0.001709429	k_{12}	4.00545e-014	k_{19}	-6.2937e-022
k_6	-2.1109e-006	k_{13}	1.31449e-012	k_{20}	-1.176e-026
k_7	-2.0541e-005	k_{14}	-3.594e-017		

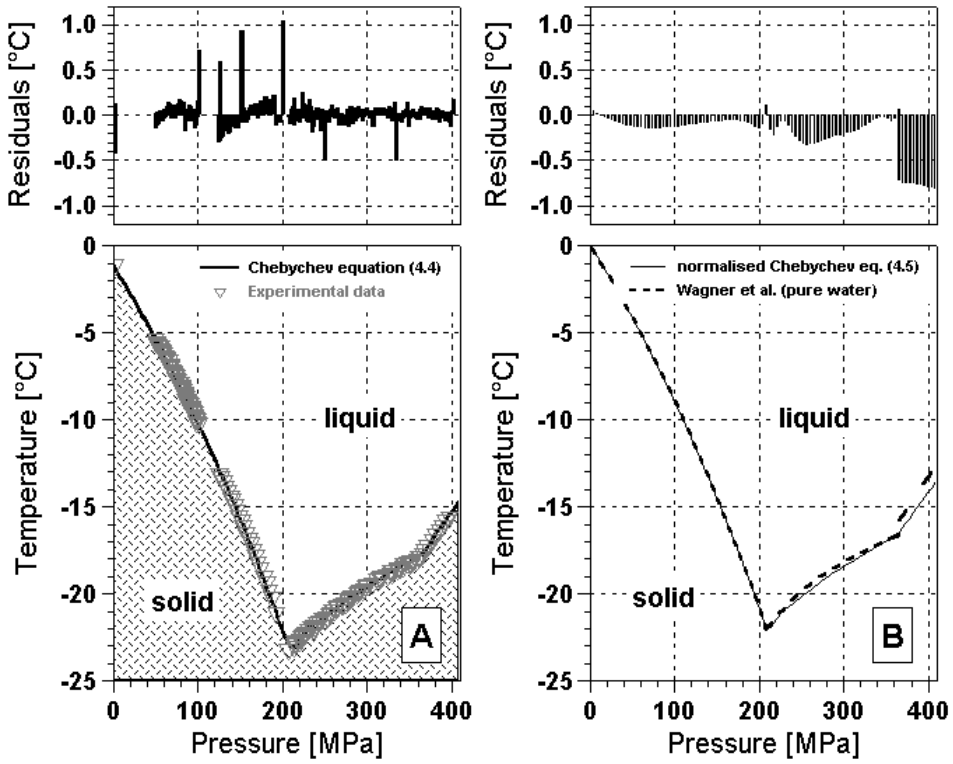

Figure 4.6: Liquid-solid contour plot. A: Experimental and predicted data for potato tissue (eqn. 4.4). B: Normalised contour plot according to eqn. 4.5 (initial freezing point at 0.0 °C) compared to the phase boundary of pure water. The divergences can be estimated by the residuals given.

In Figure 4.6A a comparison of experimental and the calculated (eqn. 4.4) phase contour is presented. As indicated by the residuals the model fits with high accuracy. The maximum divergence of about 1 K is obtained near the triple point liquid/ice I/ice III because of the sudden

change in sign (- to +) of the slope there. However, the contour plot is defined by the staring point, precisely the freezing point of potato tissue at atmospheric pressure (-1.1 °C). Assuming similar shapes of the contour plots for different foods with analogous pressure-dependent freezing point depression, equation 4.4 can be modified into a general form with respect to the freezing point at 0.1 MPa:

$$T_{m_{food}} = \left(\frac{k_1 + k_3 p_m + k_5 {p_m}^2 + k_7 {p_m}^3 + k_9 {p_m}^4 + k_{11} {p_m}^5 + k_{13} {p_m}^6 + k_{15} {p_m}^7 + k_{17} {p_m}^8 + k_{19} {p_m}^9}{1 + k_2 p_m + k_4 {p_m}^2 + k_6 {p_m}^3 + k_8 {p_m}^4 + k_{10} {p_m}^5 + k_{12} {p_m}^6 + k_{14} {p_m}^7 + k_{16} {p_m}^8 + k_{18} {p_m}^9 + k_{20} {p_m}^{10}} \right) + 1.1 + T_{m_{food},0.1MPa} \quad (4.5)$$

Then, the normalised form (equation 4.5) allows the prediction of freezing/melting temperatures of different food materials at high pressure levels up to 400 MPa when the relevant freezing point at ambient pressure is known. Figure 4.6B compares the normalised contour plot (set to initial freezing point of 0.0 °C) with the melting curves of pure water. It can be seen that the general slopes are nearly analogous, but especially along the melting curve of ice V the freezing point depression of food is slightly more pronounced as compared to melting curve ice I and ice III. However, the residuals do not exceed 1 °C.

4.1.3 Modelling high pressure supported freezing of plant tissue

4.1.3.1 Relevant aspects

In all freezing experiments, the sample temperature was recorded at three different points: one in the sample centre and at two points in sample wall, in diametrically opposite points. Also, the temperatures of the high pressure vessel external wall and the bath temperature were recorded. An average value from the two wall temperatures was taken for further calculations in the mathematical model. In Figure 4.7, an example of all the temperatures recorded is shown. The phase transition times were calculated from the time at which the wall temperature jumps (showing the beginning of nucleation) until the sample core temperature had reached –5°C with respect to the plateau temperature. The freezing time begins when the bath temperature goes to negative values and finishes when the sample core temperature reaches –18°C with respect to the corresponding plateau.

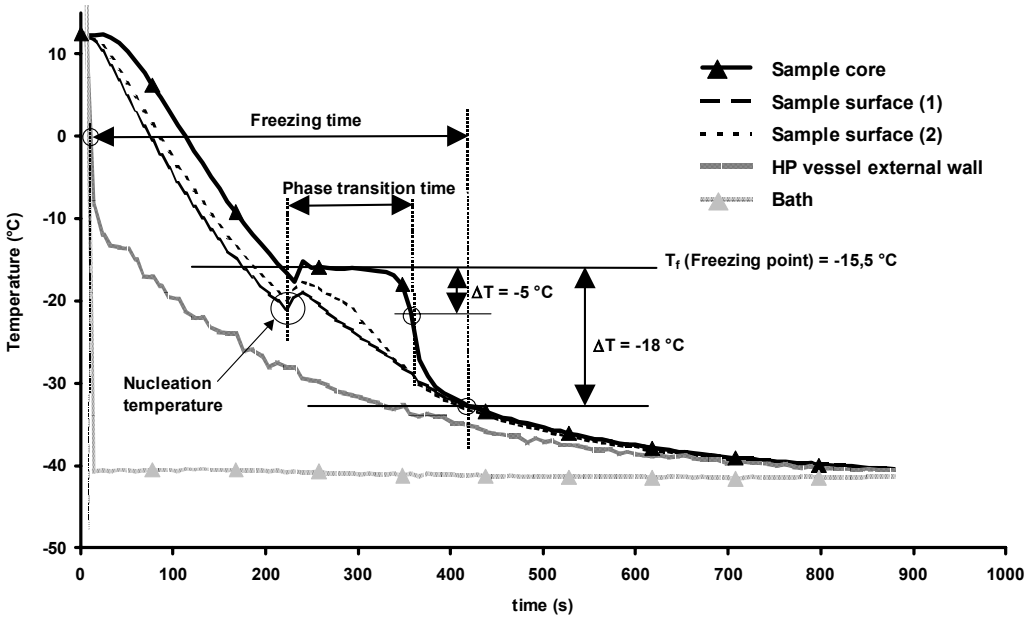

Figure 4.7: Example for measured temperature profile during freezing to ice I at 140 MPa, with the definitions of phase transition and freezing time.

4.1.3.2 Pressure assisted freezing to ice I

For pressure-assisted freezing to ice I a typical temperature evolution plotted vs. time (A) and pressure (B) is shown in Figure 4.8. The initial sample temperature was 20 °C and the sample was inserted at 0.1 MPa into the high pressure vessel pre-cooled to a temperature of –20 °C. The pressure was built up without significant delay to prevent freezing before reaching the target pressure level of 100 MPa (step 1 to 2). During the cooling step (2 to 3) the pressure decreased due to increasing specific density of the fluid matrix. A small degree of supercooling was necessary to trigger crystal formation. The local temperature at the centre then quickly (within a fraction of a second) returned to the pressure-dependent equilibrium of liquid water and ice I (step 3 to 4) in a manner which can be coined as a 'jump'. After the initial crystallisation occurrence of the jump the sample started freezing gradually (step 4). During this process the pressure level was not stabilised by external manipulation and therefore, an increase in pressure (~ 15 MPa) was observed during the freezing due to the increase in specific volume associated with the formation of ice I. This change in pressure could be used in addition to the temperature monitoring as an indicator for the freezing process. The temperature also decreased with increasing pressure as the system shifted to the new equilibrium condition. Consequently during the experiments described below the cooling step was controlled using two fluid baths and during cooling the pressure was held constant to obtain temperature profiles at required conditions. At step 5 the sample was completely frozen and the pressure was released reaching step 6.

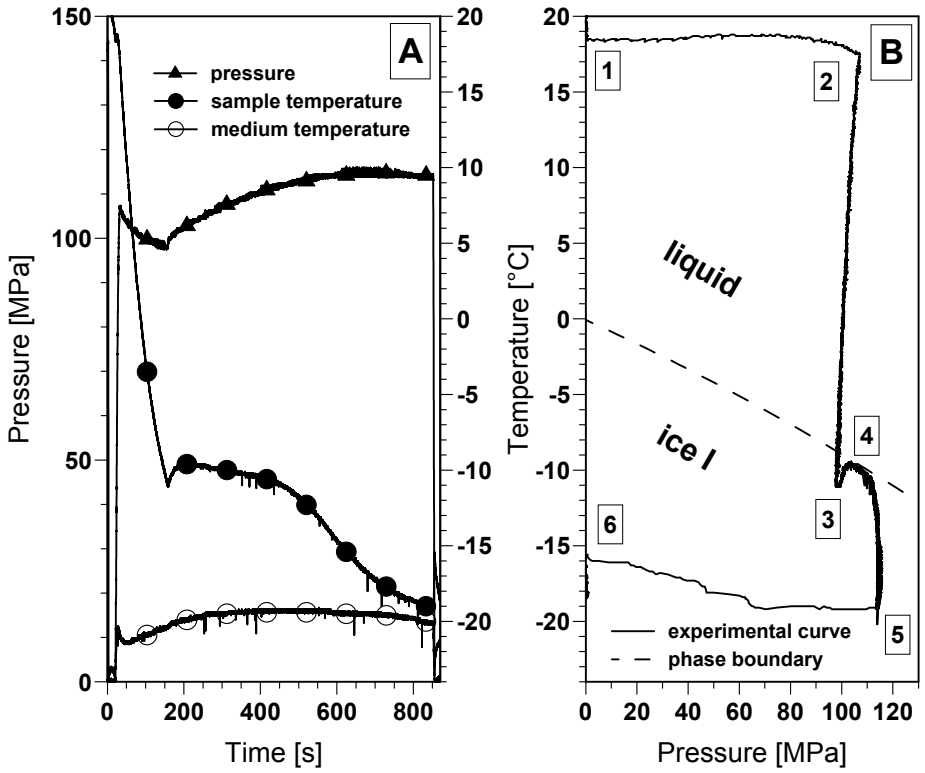

Figure 4.8: Changes in pressure and sample temperature during pressure-assisted freezing of a potato cylinder without pressure stabilisation. A: Pressure and temperature vs. time. B: Temperature (sample centre) vs. pressure.

The experiment at atmospheric pressure allows to set the thermal properties considering data reported by Cleland and Earle (1984) for predicting the temperature history precisely (Figure 4.9 and 4.10a). Based on this estimation procedure the thermal properties were shifted according to the freezing point depression at high hydrostatic pressure to fit the experimental curves. Figure 4.9 gives an example of this strategy. The experimental value of the freezing point of potato at 0.1 MPa was derived from the experiments and was found to be –1.1 °C. One of the critical operating factors is the temperature difference between the plateau and the cooling medium. Therefore, to set up the next experiments at high pressure, the expected plateau temperatures along the melting curve of ice I were calculated with the polynomial equation 4.1 described in section 4.1.1. Then, the temperature of the freezing medium was always set to a temperature 25 °C lower than the expected phase change and the initial temperature was set to a value 25 °C higher than the expected phase transition point ensuring comparable cooling rates. For higher ice polymorphs the above steps were executed accordingly.

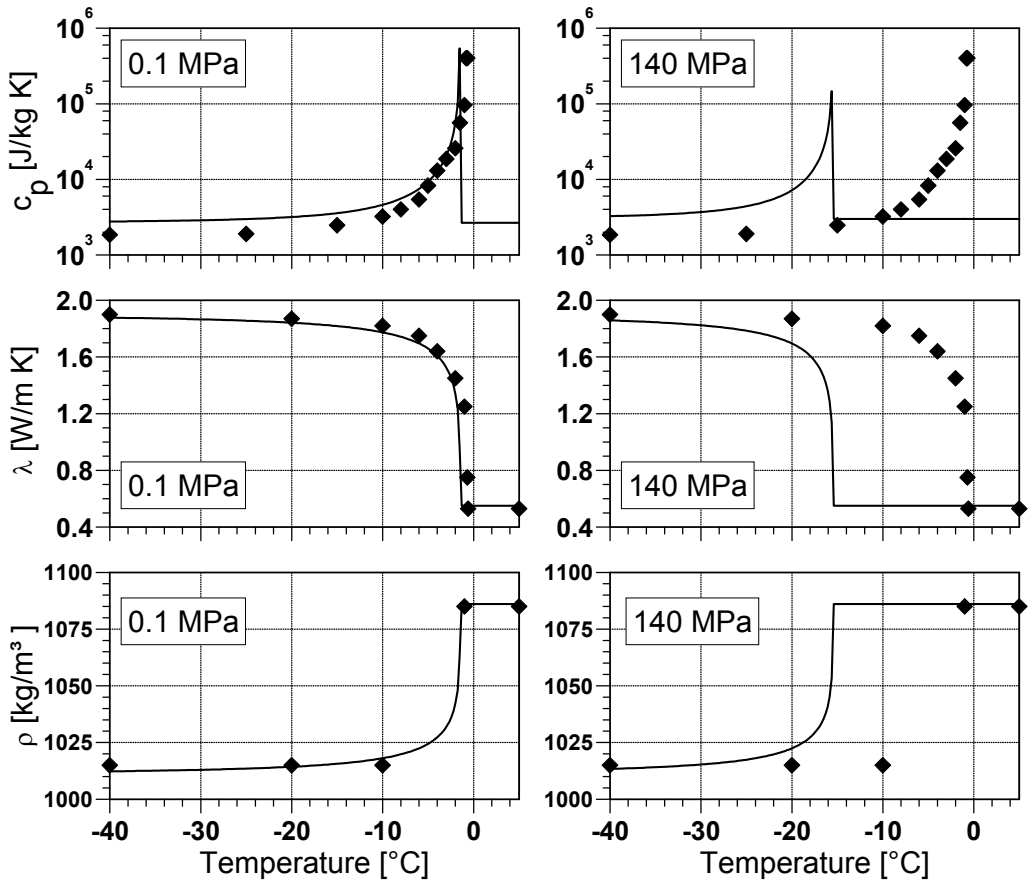

Figure 4.9: Specific heat (c_p), thermal conductivity (λ) and density (ρ) as functions of temperature in the freezing range at ambient pressure (0.1 MPa) and high pressure (140 MPa); calculated data (—) and reference data (—◆—) (Cleland and Earle, 1984).

In order to better compare the effect of the supercooling phenomenon, and the nucleation of a higher ice modification, pressure-assisted freezing experiments were planned. Ice I is obtained (as expected from the phase diagram) after a weak degree of supercooling. In Figure 4.10, these freezing curves to ice modification I and the mathematical model application are shown. After the water phase diagram, the triple point liquid/ice I/ice III is expected to appear at a pressure level of 209 MPa. As described above it is assumed that an experiment carried out at 209 MPa still leads to formation of the ice modification I and not ice III. The obtained results, in Figure 4.10c, show a freezing temperature of around –24.5 °C that is 1.5 °C lower than that expected for potatoes. In this case, the higher volume of the sample after freezing, clearly shows that ice I was obtained. In this near region of the triple point liquid/ice I/ice III, a weak supercooling peak is obtained, and after short running through a metastable liquid phase, ice I is formed. In this process, as the enthalpy of fusion is lower, the processing time also is expected to be lower, with respect to the same freezing process run into the stable liquid/ice I transition zone (140 MPa). As the highest damages are caused during the phase transition, the lower this transition time, the better product quality. However, also volume changes must be taken into account, which are higher near the triple point (~13 %) as compared to lower pressure levels.

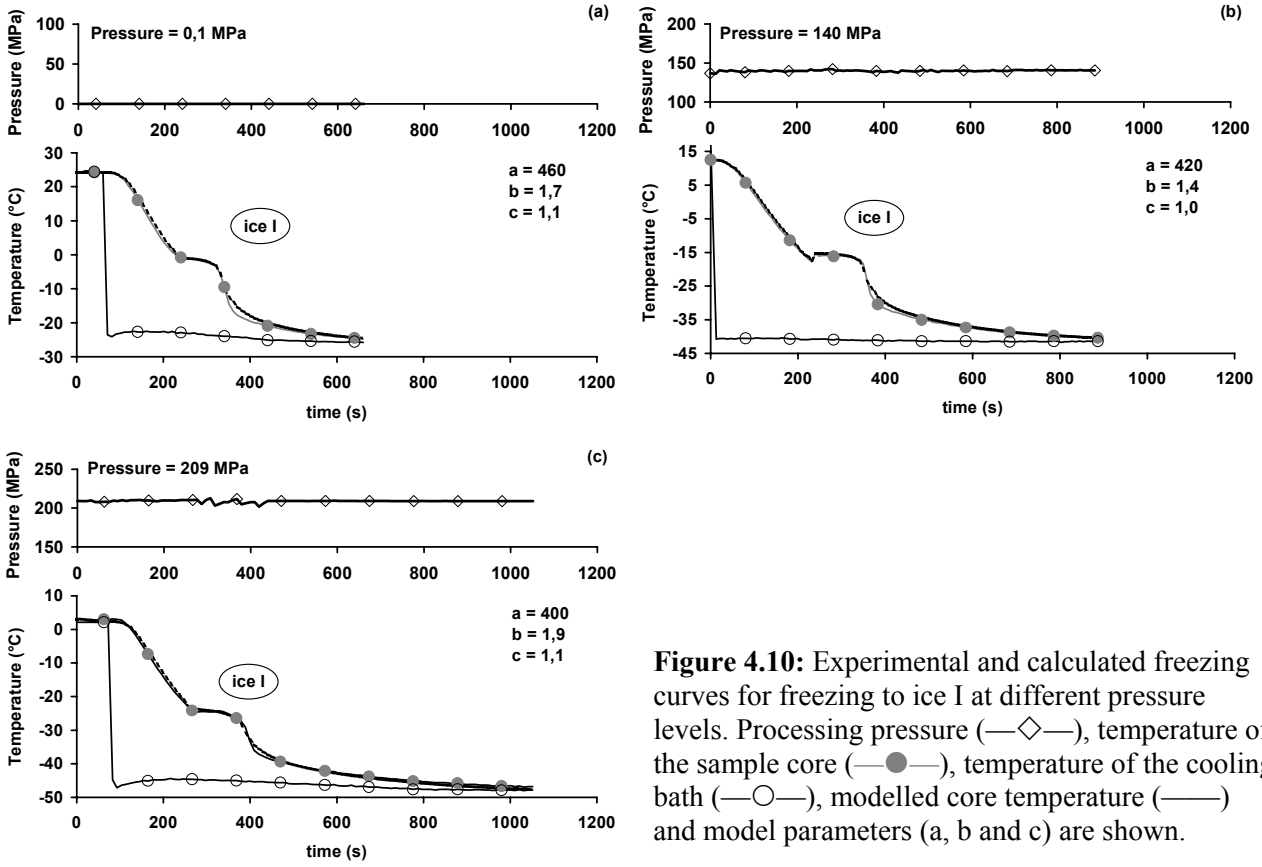

Figure 4.10: Experimental and calculated freezing curves for freezing to ice I at different pressure levels. Processing pressure (—◇—), temperature of the sample core (—●—), temperature of the cooling bath (—○—), modelled core temperature (——) and model parameters (a, b and c) are shown.

4.1.3.3 Pressure assisted freezing to ice III

At a pressure level of 255 MPa, the formation of ice modification III was already clearly achieved. In Figure 4.11a, this can be observed, as the ice III is clearly obtained, after the supercooling phenomenon, with a clear horizontal temperature plateau. The freezing temperature experimentally recorded was –21.0°C for 255 MPa, which is 1.3°C lower than the corresponding value for pure water, after regression data of Wagner *et al.* (1994). So, this temperature is still in the range of difference between potato and water as predicted by the calculations. A degree of supercooling of 11,3°C is obtained here. With earlier plateau, and higher degree of supercooling, again ice III is obtained at 270 MPa (Figure 4.11b), with a freezing temperature experimentally recorded of –20.5°C, which is again 1.3°C lower than the corresponding value for pure water (after phase diagram interpolation, see above). The degree of supercooling in this case is around 15.0°C. In the case of pressure-assisted freezing at 300 MPa (Figure 4.11c), the freezing temperature is –20.0 °C given by the clear plateau obtained after the nucleation of ice modification III, which is 1.8°C lower than the corresponding value for pure water. A degree of supercooling of around 18.5°C, significantly higher than the one obtained at 255 MPa, can be seen. Here it is remarkable that, between the freezing curves at 255 and 300 MPa, the higher the pressure, the higher the degree of supercooling, and therefore, the shorter the plateau time. But also, when a higher degree of supercooling occurs, there is a longer tempering or pre-cooling time before nucleation starts. At 300 MPa, the enthalpy of fusion is higher than the one at 255 MPa (both corresponding to ice III), and

therefore, the phase transition time must be higher. All these effects together lead to shorter plateau times at higher pressures.

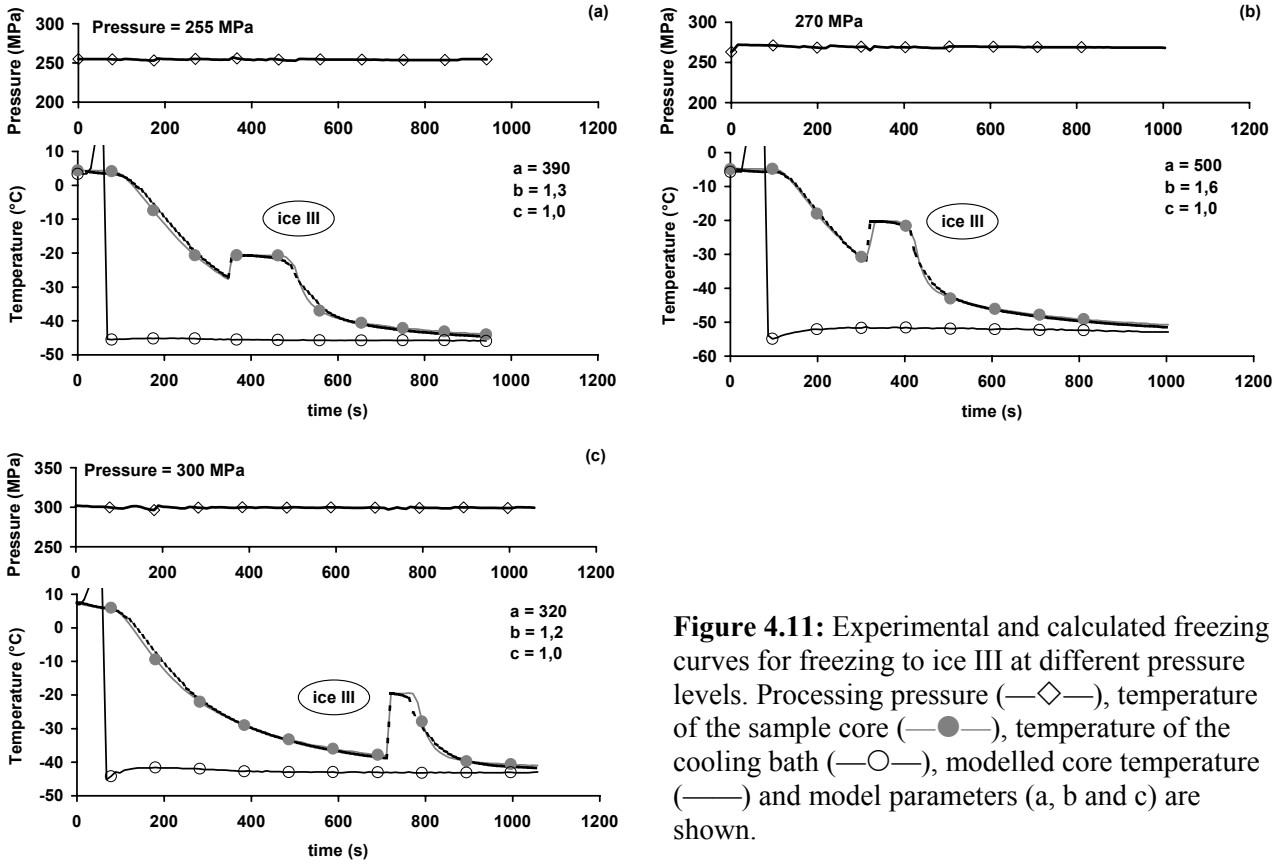

Figure 4.11: Experimental and calculated freezing curves for freezing to ice III at different pressure levels. Processing pressure (—◇—), temperature of the sample core (—●—), temperature of the cooling bath (—○—), modelled core temperature (——) and model parameters (a, b and c) are shown.

4.1.3.4 Pressure assisted freezing in metastable zones

During pressure-assisted freezing at a pressure level of 225 MPa, usually the ice modification III is expected to be obtained, as stated by the phase diagram, but according to Evans (1967b), ice I is obtained through the prolonged melting curve ice I. In this study what was obtained was a set of experiments in which the instability of this region led to different results. Therefore, in Figures 4.12a-c, three different experimental freezing curves are shown for the same pressure level (225 MPa) in which ice I is obtained (4.12a), ice III (4.12b) or a mixture of both ice modifications (4.12c). The behaviour when ice I is obtained can be explained as follows: in the area where theoretically ice III is to be reached, at this pressure level, a metastable zone of liquid is still obtained, in agreement with the data described in section 4.1.1. Therefore it is assumed that a prolongation of the ice I phase transition curve gives the new freezing points for this area. This assumption can be proved by comparing the experimental freezing point when ice I is still obtained to the one calculated from an extrapolation of the ice I phase transition curve. This comparison resulted in differences no greater than 1.5 °C and the different experimental results confirm this prolongation of ice I phase transition curve. The corresponding experimental freezing temperatures are, –27.5 °C for ice I and –23 °C for ice III (the expected being –26.0 °C and –22.1 °C, respectively). Additionally, in Figure 4.12c a double plateau is observed. In this case, an

explanation becomes more difficult. Nevertheless, a possible reason for this behaviour is that first, as freezing runs, the nucleation temperature corresponding to ice I is reached, and then, this aggregation state is crystallised. But, at the same time, just after ice I nucleation starts, the wall temperature in the sample reaches the nucleation line of ice III. The whole sample then starts an ice III nucleation, and the second jump to the corresponding ice III plateau is observed.

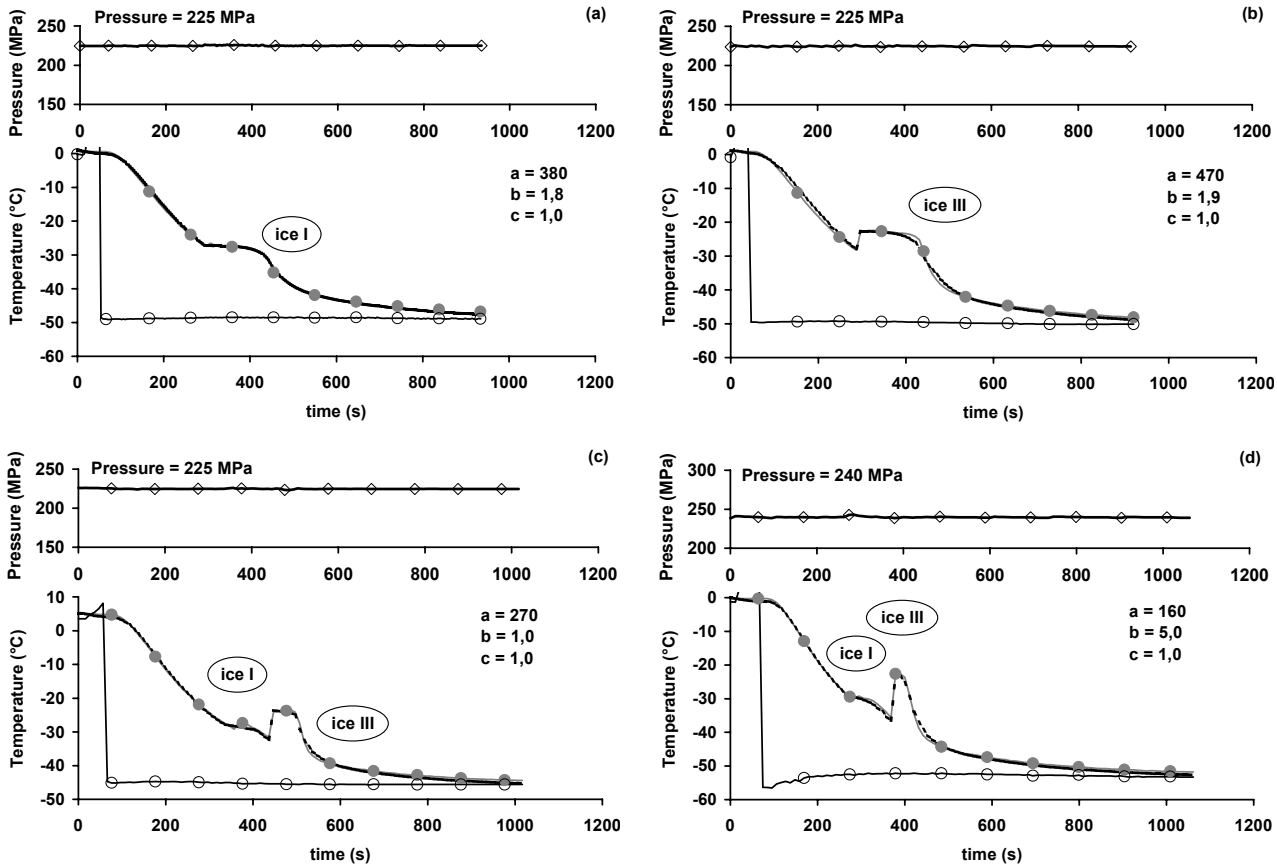

Figure 4.12: Experimental and calculated freezing curves for pressure-assisted freezing through a metastable range at different pressure levels. Processing pressure (—◇—), temperature of the sample core (—●—), temperature of the cooling bath (—○—), modelled core temperature (——) and model parameters (a, b and c) are shown.

In the case of 240 MPa, similar results to those shown in Figure 4.12c are obtained (Figure 4.12d). A first freezing point, given by a (not specially marked) plateau, is obtained for a temperature assumably for ice modification I, and after further supercooling, ice III 'plateau' is observed. This double freezing plateau clearly states the evidence of a metastable phase in this region. This metastable phase gives no clear freezing patterns, but unstable freezing curves in which both ice modifications I and III are suspected to be obtained. No further predictions can be made about which ice modification will first nucleate, when freezing occurs in the metastable area. However, in all experimental cases (especially formation of ice III) nucleation occurs not before cooling below the extended melting curves of ice I or ice V, respectively. Especially significant is the unstable freezing curve obtained here, as no clear plateau is observed, for ice I, or for ice modification III, and no clear freezing points can be taken from the experimental data, either from ice I freezing point, or from ice III. In this experiment for 240 MPa, the expected freezing temperatures are –

27.3°C and –21.4°C for ice I and ice III, respectively. The experimental freezing temperatures are slightly lower than those expected from inter- and extrapolation of the potato-adapted phase transition curves: –29.5°C and –23°C for ice III and ice I, respectively.

4.1.3.5 Pressure shift freezing

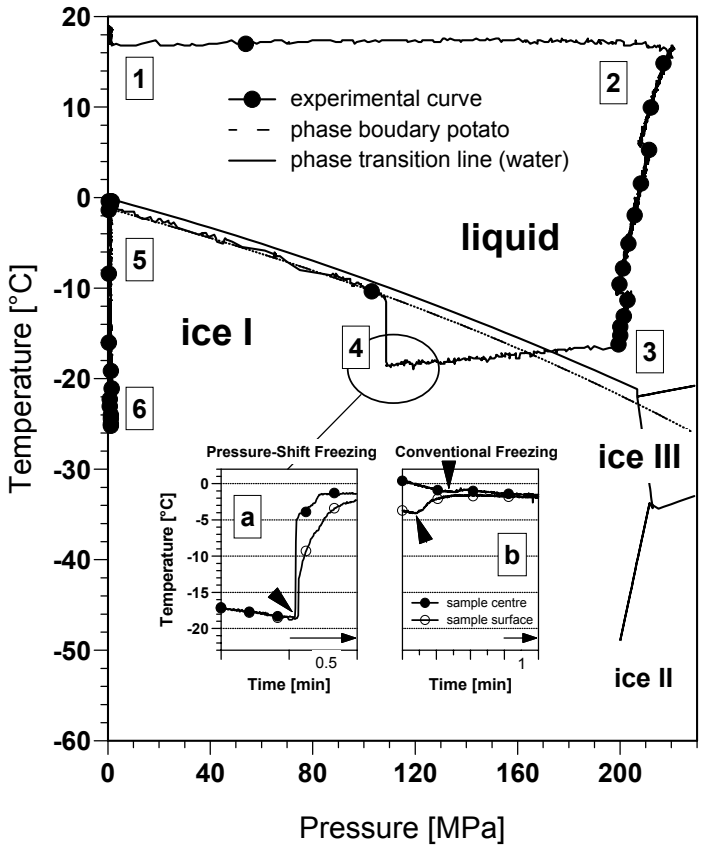

Figure 4.13: Evolution of sample temperature during pressure-shift freezing of a potato cylinder plotted vs. pressure on the phase diagram of water. Processing steps are indicated by numbers.
Insert: Comparison of crystallisation step initiated by pressure shift freezing (a) and conventional freezing (b). The sample temperature (centre and surface) is plotted vs. time. Nucleation is marked by arrows.

A typical example for pressure-shift freezing is shown in Figure 4.13. The crystallisation is initiated by the pressure release (step 4) after the unfrozen sample has been pressurised (step 1 to 2) and cooled at 200 MPa to –18 °C (step 2 to 3). At some point during the pressure release (step 3 to 4), the temperature suddenly increased with a jump (step 4 to 5) to the equilibrium freezing point corresponding to the pressure at that point. The product at this point had reached the high degree of supercooling required to start rapid ice nucleation and release of the latent heat of fusion. Considering the rate of pressure release and the inability of the simultaneous removal of the latent heat, the product follows the phase equilibrium line till the freezing point at ambient pressure is reached (step 5). After completion of crystallisation, the sample temperature approached the temperature of the immersion medium (step 5 to 6). The almost simultaneous temperature jump in the centre and at the edge of the sub-cooled sample (Figure 4.13a) indicates the regular beginning of crystallisation over the sectional view of the sample (independent of radial distance) due to

expansion, whereas the crystallisation during conventional freezing is delayed in the sample centre as compared to the sample surface (Figure 4.13b). This observation is in agreement with reported results for pressure shift freezing of emulsions. Levy *et al.* (1999) observed the uniform nucleation throughout an oil-in-water emulsion by the simultaneous rise of temperature according to pressure shift freezing.

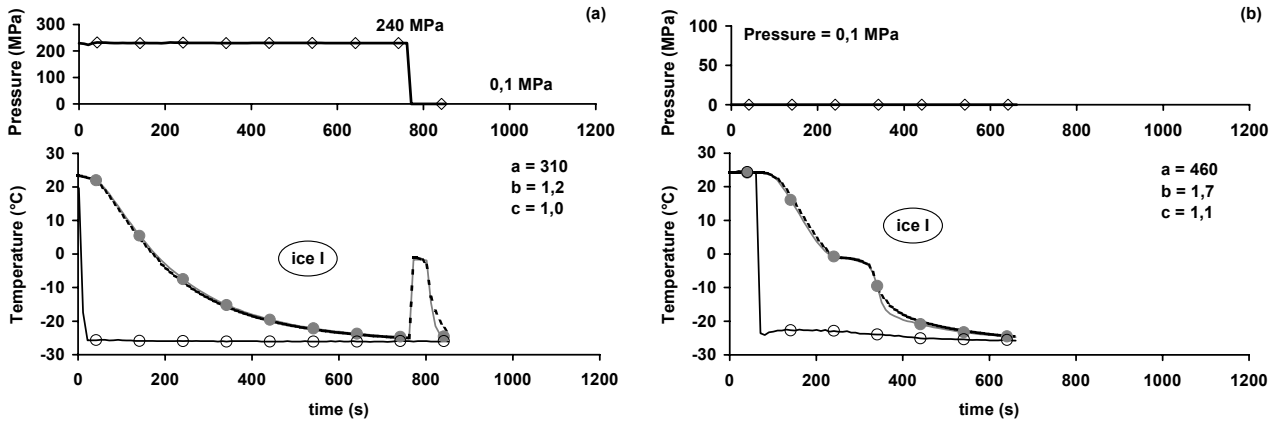

Figure 4.14: Experimental and calculated freezing curves for pressure-shift freezing (a) and conventional freezing (b). Processing pressure (—◇—), temperature of the sample core (—●—), temperature of the cooling bath (—○—), modelled core temperature (——) and model parameters (a, b and c) are shown.

An experiment was carried out in order to compare pressure-assisted freezing experiments with the pressure-shift freezing. The application of this process for potato cylinders is shown in Figure 4.14a. In this case, ice I is also obtained, and the pressure release leads to supercooling, but this time due to pressure-shift and not due to further temperature decrease. This experiment provides a tool to discuss the effect of the pressure change or the pressure range in which each process is carried out, with respect to the phase transition time, i.e., the freezing plateau time in the freezing curve. When comparing this experiment with the corresponding one at atmospheric pressure (Figure 4.14.b), we can clearly state that the freezing time by pressure-shift is higher than by atmospheric pressure, but the phase transition time is much shorter here, due to this controlled 'supercooling' effect (provoked by the pressure release).

4.1.3.6 Discussion on temperature profiles

The experiments' organisation, experimental and predicted data and model parameters are summarised in Table 4.8. The phase transition and freezing times for the different experiments carried out are given. From these results, it can be derived that the freezing time grows with pressure (that is equivalent to the ice modification) and cooling phase prior to freezing. The phase transition time ('plateau' time) reaches a maximum for ice modification I above 209 MPa (metastable zone) and has its minimum for pressure-shift freezing and pressure-assisted freezing to ice III.

The temperature profiles in the Figures 4.10, 4.11, 4.12 and 4.14 show a good agreement between the experimental and the predicted curves, after application of the developed one-step model. Also,

when a double plateau both for ice I and ice III is obtained, this model is able to follow in one step the double jump, and therefore might be taken as a good label to study the mechanisms. The model was first performed just trying to reproduce the experimental data using the temperature profile of the sample wall as the feeding start point for the mathematical schema. Then, an approach to these wall temperature profiles was used to validate the model, using the nucleation temperatures both for ice I and ice III as indicator for the temperature jumps until the freezing plateau. In this way, the model was first adjusted to fit the experimental profiles and then, using estimation equations for the nucleation points, the sample centre temperature profiles were reproduced as shown. When freezing to ice III, a high degree of supercooling is obtained, and, therefore, a higher temperature gradient is reached. This temperature gradient is the one reached between the temperature of sample wall just before nucleation starts and the temperature of the sample centre during phase transition (removal of latent heat). Then, a shorter phase transition time is expected for these experiments. Here, also using the same one-step schema for the mathematical model, a good agreement with the experimental freezing curve can be observed.

Table 4.8: Experiments organisation, experimental data and model parameters: a, b, c and T_f are the model parameters shown in equations (3.5), (3.6) and (3.7). Phase transition time (s) and freezing time (s) are the phase transition and freezing times, respectively, as defined in section 4.1.3.1. Additionally, the experimental freezing temperature (T_f^{exp}) is also shown. In the cases (no. 9) and (no. 10), the phase transition time is calculated from the nucleation time of ice I until the time in which temperature has reached –18°C with respect to the ice III freezing temperature.

Experiment			**Experimental results**					**Model parameters**			
No	Figure	Process	P (MPa)	T_f^{exp} (°C)	Ice modif.	Phase transition time (s)	Freezing time (s)	a	b	c	T_f(°C)
1	fig.10a	AF	0.1	-1.0	I	88	390	460	1,7	1,1	-1,0
2	fig.10b	PAF	140	-16.0	I	118	390	420	1,4	1,0	-15,4
3	fig.10c	PAF	209	-24.5	I	109	595	400	1,9	1,1	-23,7
4	fig.11a	PAF	255	-20.8	III	156	590	390	1,3	1,0	-20,6
5	fig.11b	PAF	270	-20.5	III	102	740	400	1,6	1,0	-20,0
6	fig.11c	PAF	300	-20.0	III	76	845	320	1,2	1,0	-19,6
7	fig.12a	PAF	225	-27.5	I	144	760	380	1,8	1,0	-27,0
8	fig.12b	PAF	225	-22.9	III	150	511	470	1,9	1,0	-22,7
9	fig.12c	PAF	225	-27.5/-23.5	I / III	328	671	270	1,0	1,0	-27,7/-23,7
10	fig.12d	PAF	240	-29.5/-23.0	I / III	158	443	160	5,0	1,0	-29,3/-22,9
11	fig.14a	PSF	PSF	-1.8	I	37	820	310	1,2	1,0	-1,1

In the experiments at 225 and 240 MPa, the metastable ice I solid phase is obtained, in a region where ice III is thermodynamically stable and there are two experiments (Figure 4.12c and d) in which a ‘double plateau’ is obtained. This means that during the freezing process, ice I (or a mixture of both ice I and ice III) is first obtained, and then, when the nucleation line of ice III is reached, the freezing curve jumps to the freezing temperature corresponding to ice III. A physical explanation can be given by possible simultaneous existence of different ice modifications according to Hasselton *et al.* (1995) or a liquid – solid (ice I) mixture is first obtained, and this residual liquid in mixture nucleates further to ice III, as the temperature decreases. As the core

temperature after the second jump to ice III is higher than the corresponding freezing temperature for ice I, it can be assumed that all the ice I first nucleated transforms again to liquid and then further nucleation to ice III occurs. A solid (ice I) – solid (ice III) transformation is not notably indicated by the obtained results, since it must be accompanied by a temperature decrease in the thermal history due to the endothermic process. However, solid-solid transition cannot be excluded since the endothermic effects during ice I–ice III transformation might be compensated by an exothermic jump, due to liquid-solid transition (liquid-ice III).

A fact that should be mentioned here is the existence of the supercooling phenomenon when ice III is obtained and the non-existence or the weakness of this supercooling when ice I is obtained. Evans (1967a) described this weakness of supercooling when ice I crystallises at higher pressure levels. The results reported showed that nucleation is enhanced by pressure, and the supercooling initially necessary to nucleate ice I falls from –6.5 °C (at pressures below 100 MPa) to virtually zero between 150 and 250 MPa. Since, nucleation is one of the major kinetic factors affecting freezing for a liquid-to-solid transformation to take place, it is necessary for the presence of a 'seed' upon which the solid phase can grow. Without this seed, growth is not possible, as the molecules in the liquid phase do not easily align into the configurations required for the solid (Reid, 1993).

4.1.3.7 Supercooling and instantaneously formed ice

When studying the freezing time and the phase transition, the effect of the phase transition on food quality must be discussed, as this quality is directly related to the cell modifications and disruptions due to the formation of ice crystals. The faster the process of nucleation and propagation of the crystals, the lower the negative effects of the freezing process on food products' quality. This rate of phase transition process is directly related to the degree of supercooling. The positive influence of applying high pressure on the time required to release latent heat was reported by Denys *et al.* (1997). This was explained for pressure-shift freezing as a combined effect of both the larger temperature gradient between the high-pressure medium and the sample and the higher nucleation rate (as a consequence of a higher degree of supercooling). To better estimate this effect for pressure-assisted freezing, both pressure and the degree of supercooling are related, as shown in Figure 4.15a.

In real freezing situations, it is heterogeneous nucleation that comes into play, where the presence of a catalytic template reduces the requirements for assembly of the critical nucleus, and nucleation increases in probability at higher temperatures. But the initiation of nucleation and subsequent freezing are limited by other kinetic constraints such as the 'mass –transfer-limited growth of the first kind'. The lack of nuclei will prevent ice forming even though it is the thermodynamically favoured species. The system will therefore supercool, and the isotherm that delineates the location of the freezing temperature will move in towards the centre of the object that is being cooled. The outer regions will become progressively more supercooled. At some point, nucleation will occur and initiate ice growth up to the position of the freezing temperature isotherm. The amount of ice that can form is determined by the amount of heat removed during the supercooling. Since this heat

has been already removed, ice growth is rapid, and crystal size is small (Reid, 1993). The extent of supercooling is known to be dependent on a number of factors including the size and shape of the vessel, on the materials in contact with the solid phase, on the element of time, the rate of cooling etc. (Bridgman, 1912).

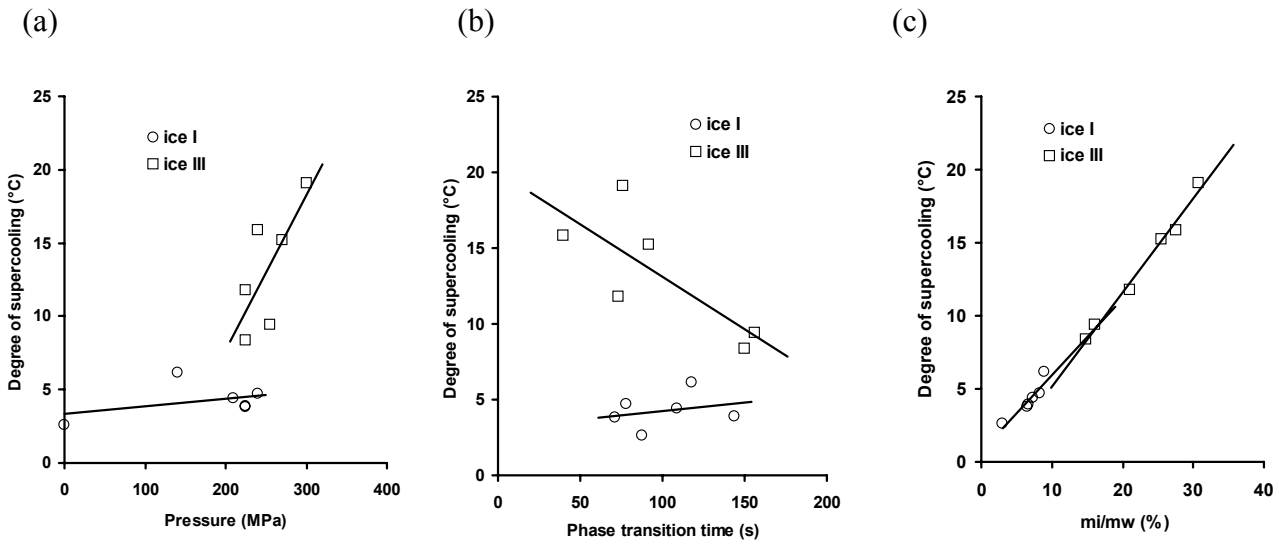

Figure 4.15: Correlation between supercooling before freezing (to ice I and ice III) and (a): pressure level; (b): phase transition time; (c): ice content instantaneously nucleated (m_i/m_w).

However, in view of faster and uniform nucleation, it was reported that crystallisation occurs more homogeneously and that a better product is obtained in terms of texture (Fuchigami *et al.*, 1997a and 1998a). It should be noted that, since the sample has to be brought into the liquid state at negative temperature, the total time required for a high-pressure freezing process is larger compared to a classical freezing. As mentioned before, a higher degree of supercooling is assumed to lead to a shorter phase transition time, as the temperature gradient is then higher. Therefore, a correlation is expected between these two variables: phase transition time and degree of supercooling. In Figure 4.15b, the experimental results for this correlation are shown.

It can be assumed that the effect of supercooling is not beneficially affecting the reduction of phase transition times when ice I is crystallised, but a slightly positive effect is reached when ice III nucleates. These assumptions may match with the calculation of instantaneous ice formed when the freezing temperature is first obtained after the supercooling. After the considerations of Otero and Sanz (2000a) and Chevalier *et al.* (2000b), the amount of ice instantaneously formed in a freezing process can be described after a heat balance (eqn. 2.46, section 2.3.4). Taking the parameters with the corresponding values adapted for potato and the different pressures experimented, the results given in Figure 4.15c are obtained.

From the Figure 4.15 a correlation can be described: the higher the pressure, the higher the supercooling degree, especially for ice III crystallisation (Figure 4.15a). Therefore, the higher the degree of supercooling, the shorter the phase transition time, also clearly for ice III (Figure 4.15b), and finally, the amount of ice instantaneously formed in the freezing processes is always growing

(both for ice I and ice III) as long as it does the degree of supercooling (Figure 4.15c). It should be mentioned that the instantaneous amount of ice with respect to the degree of supercooling for each pressure agree with those presented by Otero and Sanz (2000). Therefore, a direct relation seems to exist between pressure, degree of supercooling, shortening of phase transition time, amount of ice instantaneously formed in the freezing processes and consequently realisable increase in product's quality.

4.1.4 High pressure supported thawing of plant tissue

4.1.4.1 Temperature evolution during pressure-assisted thawing

The reverse direction of the processing steps in pressure-assisted freezing results in pressure-assisted thawing. In Figure 4.16 the temperature of the sample centre is plotted vs. time and pressure to show the typical processing steps in pressure-assisted thawing. As expected the frozen sample was thawed at lower temperatures than under atmospheric conditions. Step 1 to 2 involves adiabatic heating and inward heat transfer. A drop in temperature was then observed during continued pressurisation (step 2 to 3) indicating that the work of compression was transferred into melting energy on decreasing temperature levels along the extended phase transition line liquid/ice I. The temperature decrease along the phase transition line could be explained in terms of the fast changing equilibrium (caused by the increasing pressure). Step 3 to 4 is the actual thawing process accompanied by a pressure decrease of about 30 MPa due to the higher density of the liquid state as compared to ice I. Even after the thawing is complete, the sample is allowed to remain in the vessel. This further heating of the sample (step 4 to 5) is to ensure that the sample doesn't undergo recrystallisation on pressure release. After the temperature at the centre of the sample has nearly reached the temperature of the medium, the pressure is released (step 5 to 6).

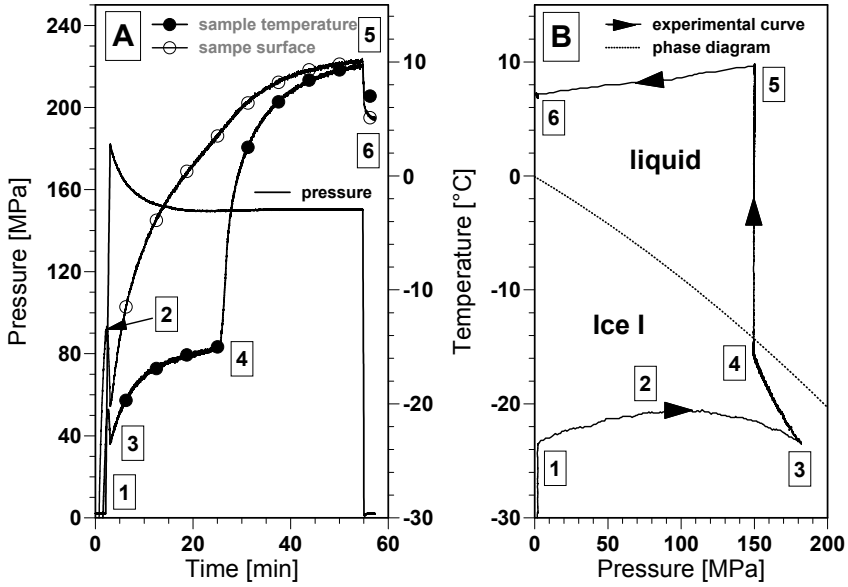

Figure 4.16: Pressure assisted thawing of a cylindrical potato sample (dia: 32 mm). A: Pressure and temperature vs. time; B: Temperature (sample centre) vs. pressure. Processing steps are indicated by ciphers and/or arrows.

4.1.4.2 Modelling thermophysical properties

The thawing of potato cylinders at high hydrostatic pressure was modelled with the objective of predicting the thawing times. An explicit finite difference scheme developed by Marek and Götz (1995) was used for the model. Radial symmetrical one-dimensional heat conduction with convection at the surface was assumed to describe the situation in the potato cylinder. The cylinder was split into several ring elements which were categorised as the central element, the intermediate elements and the boundary element. The final iterative equations (2.31, 2.36, 2.42) used for these elements are as described in section 2.1.6.

It was also required to model the behaviour of the thermophysical properties namely, the apparent specific heat c_p and the thermal conductivity λ in the vicinity of the pressure dependent melting point. In earlier experiments it was found that changes in density did not significantly affect the calculations. Therefore, the density was set to a constant value of 1080 kg m^{-3} for recalculating the thawing curves. Two statistical distributional functions namely, the Density Weibull function and the Cumulative Weibull function were used to model c_p and λ respectively. The parameters in these functions, especially the peak parameter in the former were altered according to the pressure, so as to obtain a close fit of the predicted curves with the experimental ones.

Table 4.9: Parameters of the Cumulative Weibull distribution used to predict thermal conductivity, λ.

Parameter	Denotation	Value						
		0.1 MPa	50 MPa	100 MPa	150 MPa	200 MPa	250 MPa	300 MPa
b	Scale	2.1	2.1	2.1	2.1	2.1	2.1	2.1
c	Shape	2.7	2.7	2.7	2.7	2.7	2.7	2.7
λ_{min}	λ (if $T>T_f$)	0.55	0.55	0.55	0.55	0.55	0.55	0.55
T_f	Freez. temp.	-1.5	-5.5	-10.5	-15.7	-22.1	-28.5	-20.2

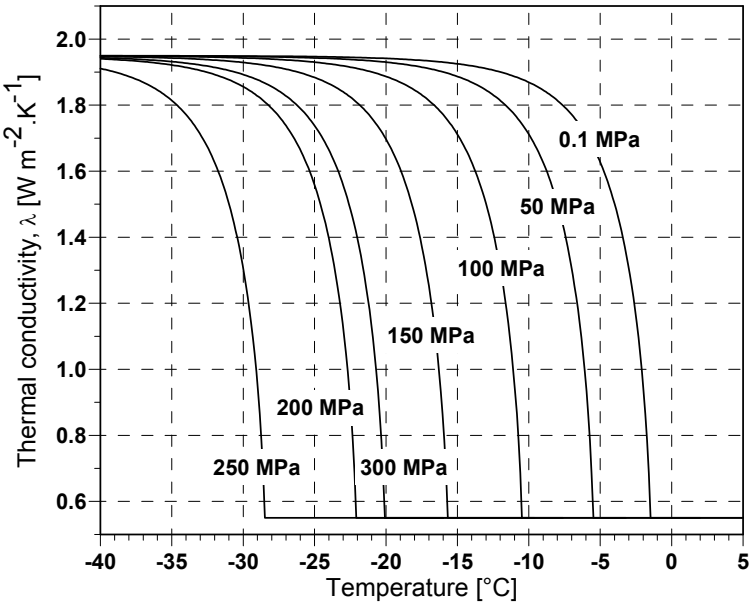

Figure 4.17: Thermal conductivity as a function of temperature at different pressure levels

The Cumulative Weibull function (eqn. 3.5) was used with the parameters in Table 4.9 to predict the thermal conductivity. The Density Weibull function (eqn. 3.7) along with the parameters in Table 4.10 was used to predict the apparent specific heat. Figures 4.17 and 4.18 show the thermal conductivity λ and the apparent specific heat c_p respectively modelled as a function of temperature on different pressure levels.

Table 4.10: Parameters of the Density Weibull distribution used to predict specific heat, c_p.

Parameter	Denotation	Value						
		0.1 MPa	50 MPa	100 MPa	150 MPa	200 MPa	250 MPa	300 MPa
a	Peak	$2.26*10^5$	$2.18*10^5$	$2.16*10^5$	$2.14*10^5$	$2.08*10^5$	$2.20*10^5$	$2.21*10^5$
b	Scale	2.1	2.1	2.1	2.1	2.1	2.1	2.1
c	Shape	2.7	2.7	2.7	2.7	2.7	2.7	2.7
$c_{p,min}$	c_p(if $T>T_f$)	$3.6*10^3$	$3.6*10^3$	$3.6*10^3$	$3.6*10^3$	$3.6*10^3$	$3.6*10^3$	$3.6*10^3$
T_f	Freez. temp.	-1.5	-5.5	-10.5	-15.7	-22.1	-28.5	-20.2

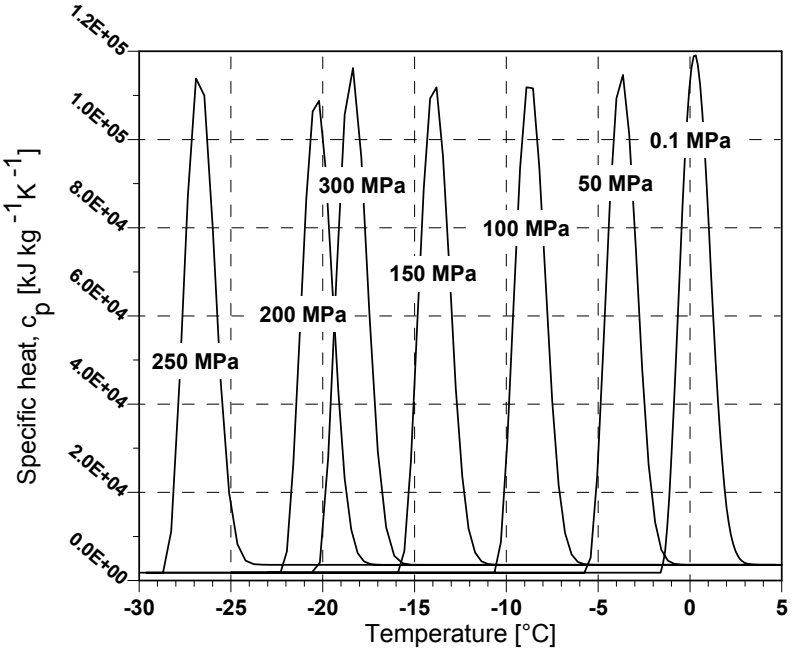

Figure 4.18: Apparent specific heat c_p as a function of temperature at different pressure levels.

The melting enthalpy of potato tissue ΔH_{potato} was determined at atmospheric pressure using a DSC method. A typical thermogam is presented in Figure 4.19. It should be mentioned that temperature values were not calibrated, since this was not required for this study. The endothermic peak for potato tissue was compared to pure water and the melting enthalpy for potato was then derived from the ratio of the peak areas:

$$\Delta H_{potato} = \frac{A_{potato}}{A_{water}} \cdot \Delta H_{water} \,. \tag{4.6}$$

The area of the water peak A_{water} is equivalent to a value of 334 kJ kg^{-1} (ΔH_{water} at 0.1 MPa). Compared to that value the peak area for potato tissue A_{potato} is equivalent to a value which is about 30 % lower. The melting energy of potato obtained by the experiments is 238 kJ kg^{-1} (Table 4.11)

which is in agreement with data reported in literature (Polley *et al.*, 1980). The enthalpy of melting was assumed to be equivalent to the peak area of the apparent specific heat in the model. Consequently this area was expected to decrease with pressure due to the reduction of the melting energy required at a certain pressure level.

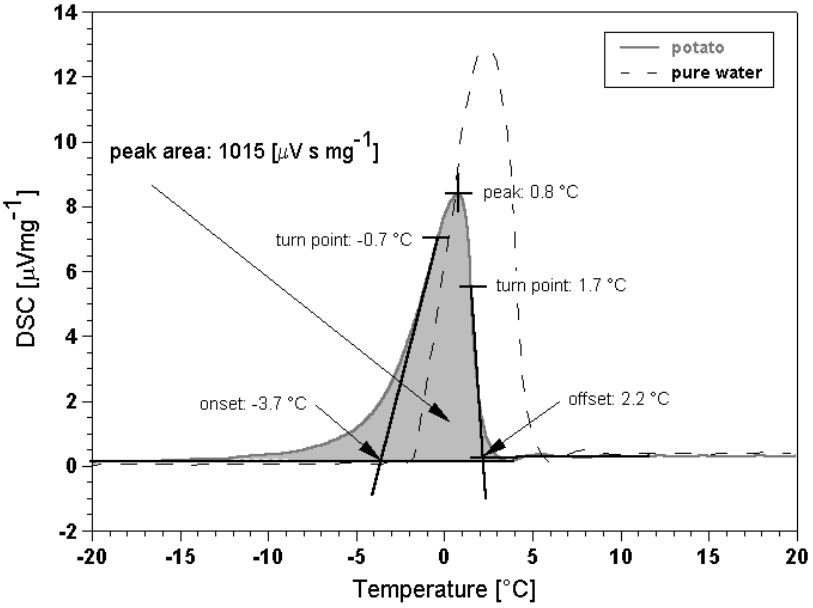

Figure 4.19: Typical endothermic peak due to melting of potato compared to pure water.

Table 4.11: Values derived from analysing the experimental DSC thermograms.

Sample	Weight	Onset (°C)	Peak (°C)	Offset (°C)	Peak area (A)	Average A	Enthalpy (ΔH)
water	9.58	-1.7	1.6	3.4	1431	1438.5±8.2	334 kJ kg^{-1}
	9.58	-1.7	1.6	3.6	1444		
	10.39	-1.6	2.2	4	1447		
	13.98	-1.4	2.3	4.7	1432		
potato	16.8	-3.7	1	2.5	1026	1026.3±8.7	238 kJ kg^{-1}
	15.66	-3.7	0.8	2.2	1015		
	17.59	-3.4	1	2.7	1036		
	19.41	-3.8	1.1	2.9	1028		

It was found from some preliminary trials with the modelling that the predicted curves were several minutes faster than the experimental ones. This was because (a) the surface heat transfer coefficient h was assumed constant at a relatively high value of 110 W m^{-2} and (b) a regression curve of the temperature at a distance of around 8 mm from the surface of the cylinder during the thawing process was implemented as the medium temperature T_∞ in the calculations. The values of both h and T_∞ were sufficiently high as to yield faster thawing curves and also the heat transfer coefficient changes according to the temperature difference dT between the boundary element and that of the fluid in its vicinity. It was therefore felt necessary to model the temperature of the medium at an infinitesimally small distance from the surface of the cylinder. For this purpose, all the thawing experiments were performed with at least two thermocouples placed at pre-determined locations

outside the sample. The required T_∞ was then obtained by extrapolation of a linear approximation of these temperature profiles. The surface heat transfer coefficient, h was then incorporated into the model as a function of *dT* as follows:

$$h = \frac{Nu \cdot \lambda_b}{2 \cdot R}, \text{ with} \tag{4.7}$$

$$Nu = 0.47 \cdot (Gr \cdot \Pr)^{0.25}, \text{ and} \tag{4.8}$$

$$Gr = \frac{9.81 \cdot \beta \cdot \rho^2 (2 \cdot R)^3 \cdot dT}{\eta^2}, \tag{4.9}$$

where h: surface heat transfer coefficient, [W m^{-2} K^{-1}]; λ_b: thermal conductivity of bulk fluid, [W m^{-1} K^{-1}]; R: radius of the cylindrical sample, [m]; Nu: Nusselt number for the sample, [-]; Pr: Prandtl number for the fluid, [-] ; Gr: Grashof number of the fluid [-]; β: volumetric coefficient of expansion, [K^{-1}]; ρ: density of the fluid, [kg m^{-3}]; g: acceleration due to gravity, [m s^{-2}]; η: dynamic viscosity of the fluid, [kg m^{-1} s^{-1}]; dT: positive temperature difference between wall and bulk fluid, [K].

Such a modification was found to give highly satisfactory and comparable thawing times.

4.1.4.3 Calculation of pressure-assisted thawing times

As explained in Chapter 2, high hydrostatic pressure has a profound impact on the rate of thawing of foods. The most important effect is certainly the depression of the melting point as the pressure increases. The lower the melting point compared to the temperature of the surrounding medium, the greater is the gradient of temperature and faster is the thawing. Theoretically, at all pressures above atmospheric and up to 210 MPa, the sample is expected to thaw at decreasing temperatures. But according to the results described before it has been found that the thawing temperatures are further lowered up to nearly 300 MPa, owing to the prolongation of the ice I/liquid line. Apart from the melting point depression, there is also a reduction in the latent heat at higher pressures.

A thawing curve can be defined as being composed of three stages (for the central element):

(a)The *pre-thawing stage* that exists between the moment the frozen product is subjected to the thawing process up to the moment at which the ice just begins to melt (heating or pressurisation to the melting point). This stage is characterised by a steep increase in the temperature for pressure-assisted thawing.

(b) The *thawing stage* which is the period during which the temperature at the considered location (especially the centre) is almost constant because the heat supplied causes the phase change from ice to liquid.

(c) The *increase to medium temperature stage* during which the temperature is increased from the temperature at which all the ice has been converted to liquid to the intended final temperature. This stage is characterised by an S-shaped curve.

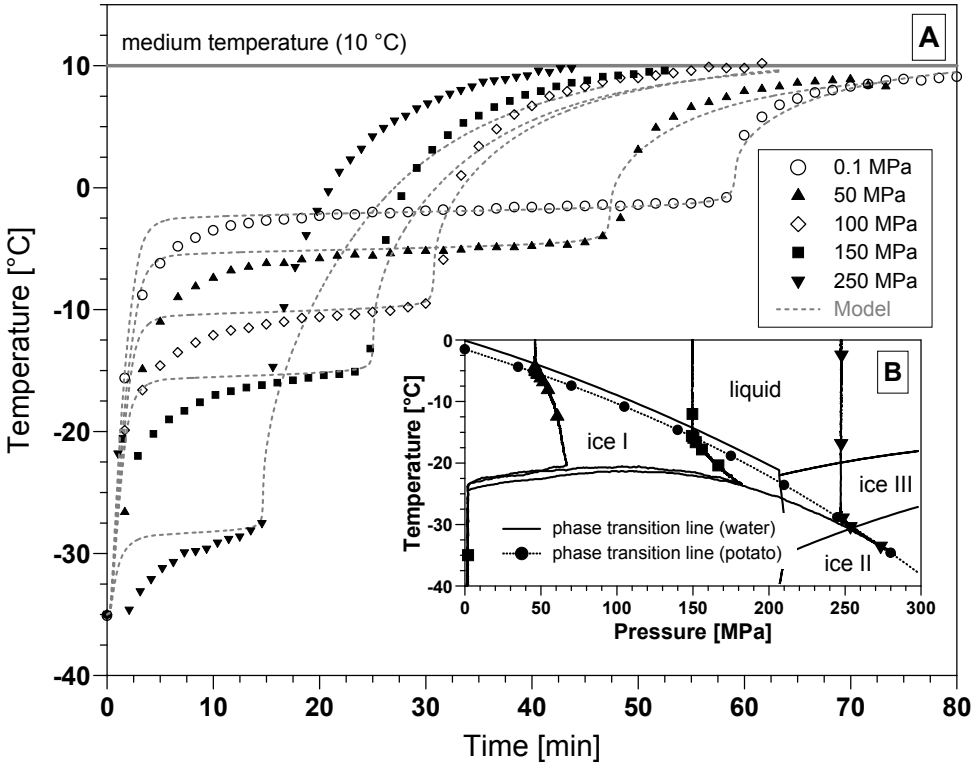

Figure 4.20: Temperature of the sample centre during pressure assisted thawing of potato cylinders (32 mm dia) at different pressure levels. A: Experimental and modelled temperature evolution indicating thawing time reduction enhanced by high pressure at constant pressure transmitting medium temperature. B: Temperature and pressure evolution plotted to the phase diagram of pure water. Phase transition at 250 MPa occurs along the extended melting curve of ice I in potato tissue.

Figure 4.20 shows a comparison between the thawing times of a potato cylinder (dia: 32 mm; length: 50 mm) at various hydrostatic pressures. Measured and calculated temperatures at the centre of the sample are shown. The figure very clearly depicts the fact that thawing times are greatly reduced by high hydrostatic pressure. At 250 MPa, for instance, the centre temperature of the sample reached the medium temperature in 50% of the time required at atmospheric pressure. The effect of high pressure on thawing times is more clearly evident on comparing the duration of the actual thawing process under various pressures. The phase transition time is presented by the temperature 'plateau' (the region of the curve where the temperature is nearly constant over time). The time of actual thawing is therefore the time corresponding to the 'corner' following the plateau. It can be observed from Figure 4.20 that, whereas it took 60 min for the sample to actually thaw under atmospheric pressure, an application of 100 MPa reduced the actual thawing time to 30 min. The thawing time was further reduced to 15 min at 250 MPa. The recalculated curves show a good agreement with the experimental data. The curves were first recalculated for the 32 mm diameter for all pressures (0.1, 50, 100, 150, 200, 250, and 300 MPa) and then the predictions were validated for the other sizes as well. The insert in Figure 4.20 shows the temperature evolution vs. pressure for selected thawing curves and clearly indicates the phase transition along the extended melting curve ice I for pressure assisted thawing at 250 MPa.

4.1.4.4 *Impact of sample size*

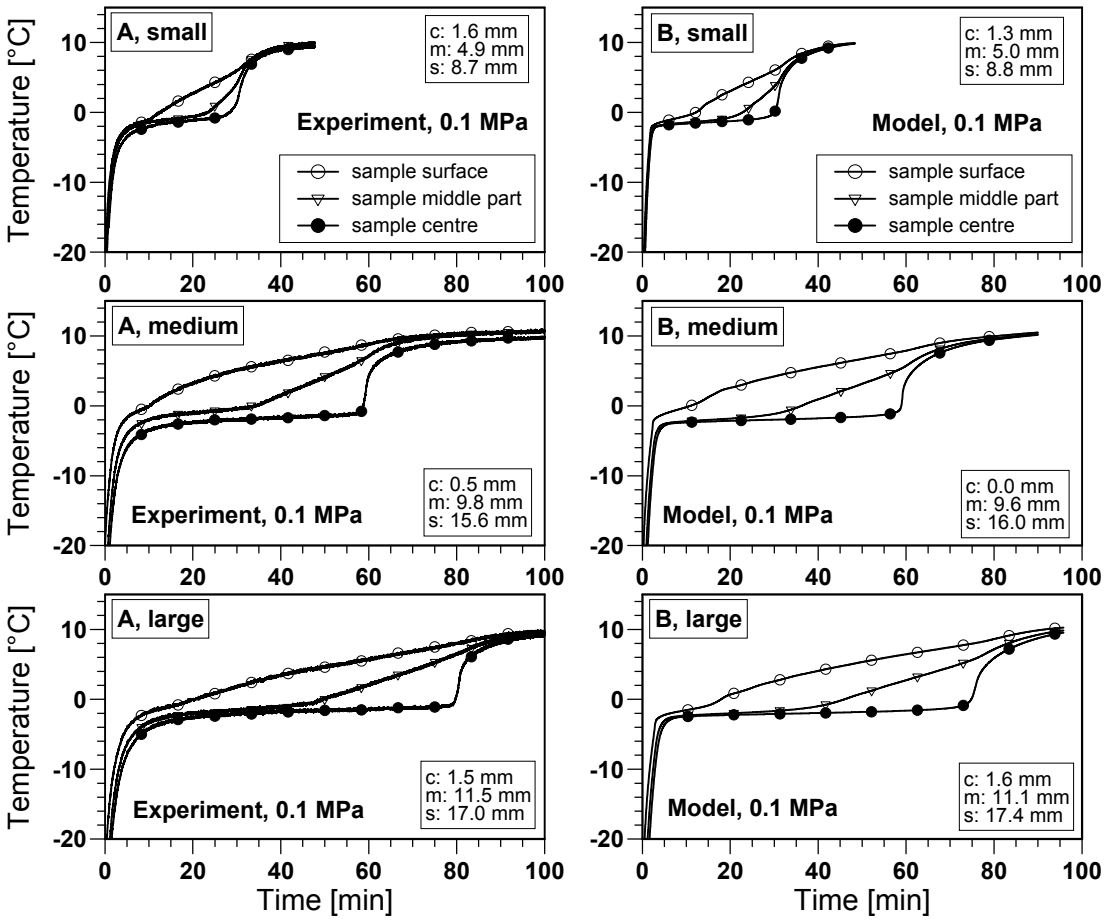

Figure 4.21: Comparison of experimental (A) and calculated thawing curves for small (20 mm dia), medium (32 mm dia), and large (38 mm dia) potato cylinders at 0.1 MPa. The temperature evolution was measured and calculated for comparable positions in the sample defined by c (sample centre), m (sample middle part) and s (sample surface).

The predicted curves from the model thus developed were compared with experimental curves obtained by thawing three different sizes (diameters: 20, 32 and 38 mm; length: 50 mm) of potato cylinders. Figures 4.21, 4.22 and 4.23 show the experimental and recalculated curves at 0.1, 150 and 250 MPa. In general, it can be observed that a good level of agreement exists between the numerical simulation and experimental data. It can be seen that the size of the sample significantly affects the thawing time at 0.1 MPa, but the effect of size on the thawing curves decreases with increasing effective temperature gradient due to increasing pressure. At ambient pressure the phase transition was completed in the centre of the large potato cylinder after 80 min, which means about 50 min delay compared to thawing the central element of the small cylinder. At 250 MPa the liquid state in the centre of the large potato cylinder was already reached after 16 min, that is just about 10 min more than the time required to thaw the small cylinder at the sample centre. As a result, it is proved that pressure-assisted thawing provides an interesting tool to significantly reduce the phase transition step, especially in large sample sizes since this process enhances the heat transport by increased effective temperature gradients and reduced values of melting enthalpy.

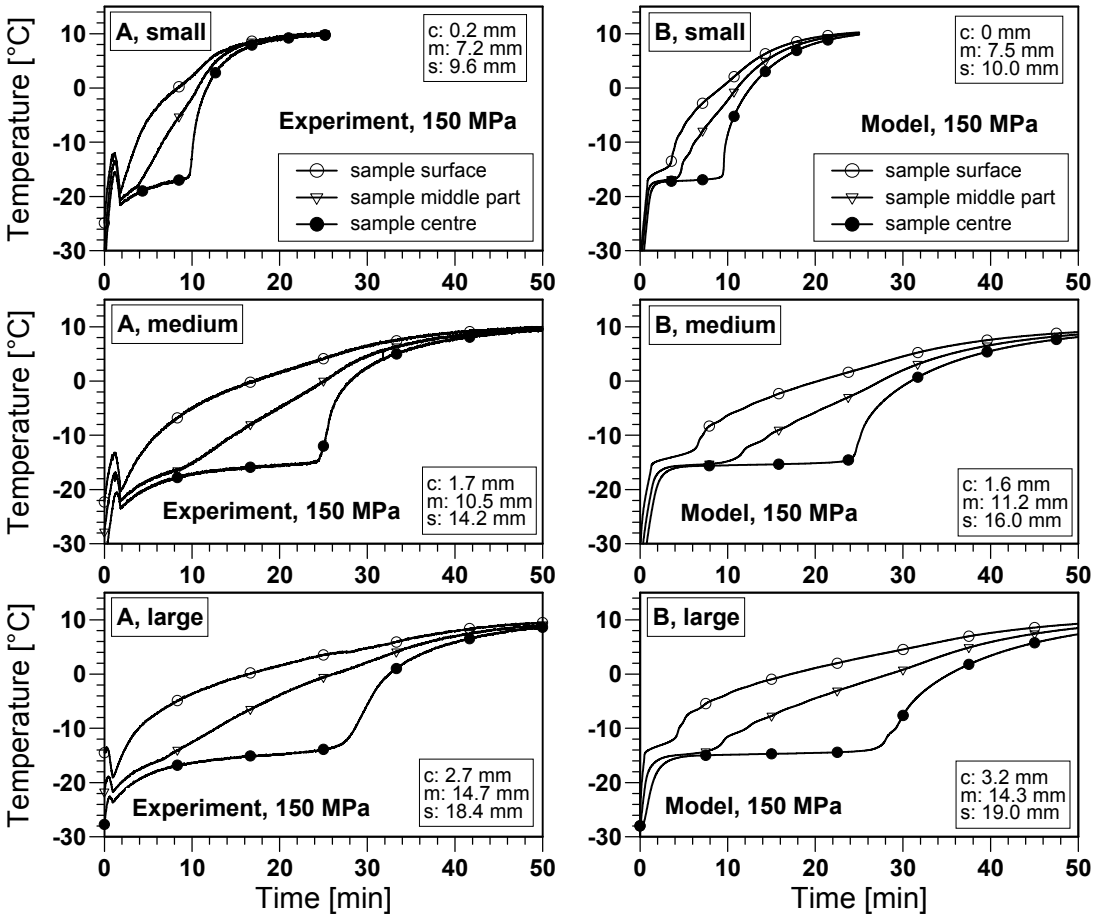

Figure 4.22: Comparison of experimental (A) and calculated thawing curves for small (20 mm dia), medium (32 mm dia), and large (38 mm dia) potato cylinders at 150 MPa. The temperature evolution was measured and calculated for comparable positions in the sample defined by c (sample centre), m (sample middle part) and s (sample surface).

The experimental temperature changes are well fitted by the model under all the pressures considered. However, there exists a discrepancy between the curves in the pre-thawing stage, especially towards the end of it. This can be explained by the following reasons. Firstly, the heating of the sample during the time period of half to one minute between inserting the sample in the vessel and the beginning of pressure build-up is not taken into account in the modelling. Secondly, as the pressure increases, the temperature in the sample drops because of the work of compression being converted into melting energy. This pressure-induced thawing step is more pronounced at higher pressure levels. Moreover the pressure after attaining the peak value drops until the final value is reached, owing to the equilibration of the pressure transmitting medium (which had undergone adiabatic heating) to the walls of the vessel. It is the melting point corresponding to the final value of pressure which is incorporated into the model and for these reasons the comparison with the model should not be taken into account until this final value of the pressure is attained.

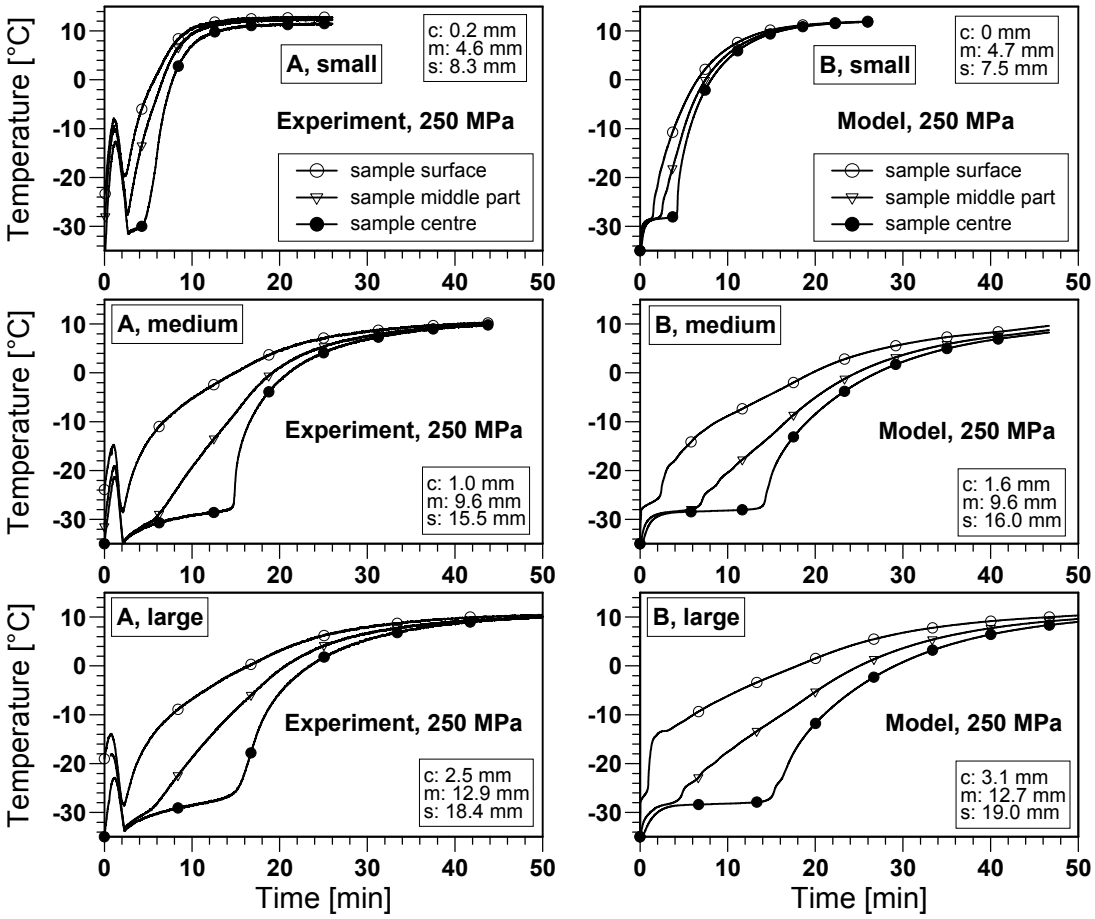

Figure 4.23: Comparison of experimental (A) and calculated thawing curves for small (20 mm dia), medium (32 mm dia), and large (38 mm dia) potato cylinders at 250 MPa. The temperature evolution was measured and calculated for comparable positions in the sample defined by c (sample centre), m (sample middle part) and s (sample surface).

The slenderness of the thermocouples used and the method adopted for placing them in the sample ensured that the exact surface temperatures were measured. This was corroborated by the nearly close agreement found between the calculated and experimental temperatures even at the surface of the cylinder. The slight dissimilarity between the curves during the 'increase to medium temperature' stage suggests that the parameters which decide the value of the apparent specific heat c_p and the thermal conductivity λ may not be correctly defined for temperatures above the freezing point.

4.1.4.5 Prediction of thawing profiles

With the description of the thermophysical properties the thawing time at different pressure levels can be predicted by calculated temperature profiles. Figure 4.24 shows the calculated temperature profiles during thawing of potato cylinder (32 mm dia) at 0.1, 150 and 250 MPa. This representation of the moving 'thawing' front can be used to predict the thawing times. For example, at 150 MPa, the central element of the sample reaches the unfrozen state about 35 min earlier than at 0.1 MPa.

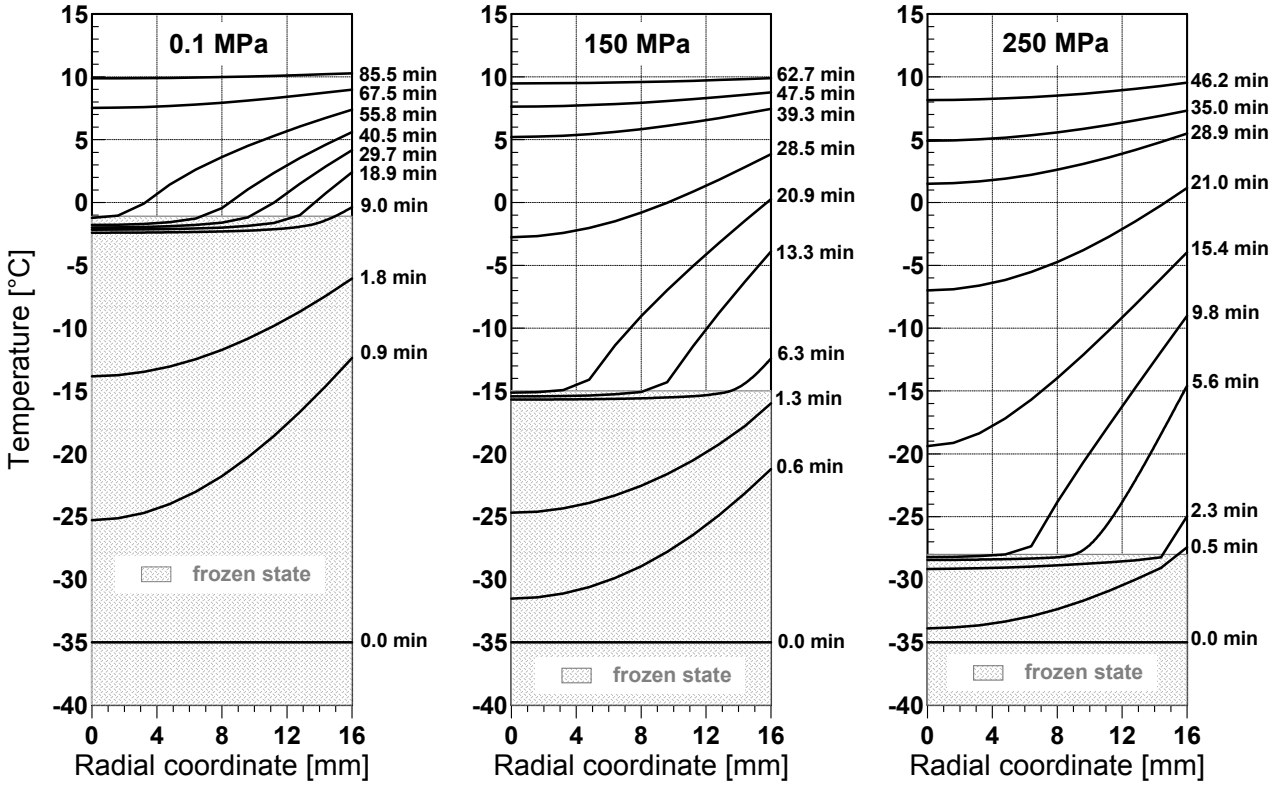

Figure 4.24: Predicted temperature profiles of a potato cylinder during high pressure-assisted thawing at different pressure levels.

4.1.4.6 Pressure assisted and pressure induced thawing

Theoretically, in the pressure-assisted thawing process from ice I, the phase transition occurs under constant pressure by increasing the temperature. In the pressure-induced thawing process, the phase transition is initiated and completed by a pressure increase. For high pressures up to 250 MPa, the samples started thawing during the pressure built-up and continued after the pressure build-up was stopped. In case the case of 50 MPa, a small amount of heat was necessary for thawing to commence. In contradiction to the defined pressure-induced thawing process (E-D-C-B-A in Figure 1.1), the temperature in the centre of the sample did not cross the ice I/liquid line, because of time dependence of heat transfer. The curves passed considerably beyond the ice I/ice II transition curve so as to arrive at the smooth prolongation of the ice I-liquid curve. This behaviour agrees with the observations documented in literature (Bridgman, 1912).

However, in Figure 4.25 the differentiation of pressure-assisted and pressure-induced thawing is clearly indicated near the surface in the sample. At 50 MPa the thawing process clearly starts in the outer layer of the sample due to heating under pressure (pressure-assisted thawing), while during the pressure build-up to 250 MPa the sample temperature (edge) crossed the phase boundary (pressure-induced thawing). The decrease in pressure during thawing clearly indicates a volume contraction of the sample during melting, which is characteristic of ice I as only ice I has a lower density than liquid water. Dependent on sample size, medium temperature and initial sample temperature a part of the required melting energy can be received. The experimental thawing curves

in Figure 4.23 indicate that the main phase transition occurs during the pressure holding time, but pressure-induced thawing can be seen in random parts of the samples.

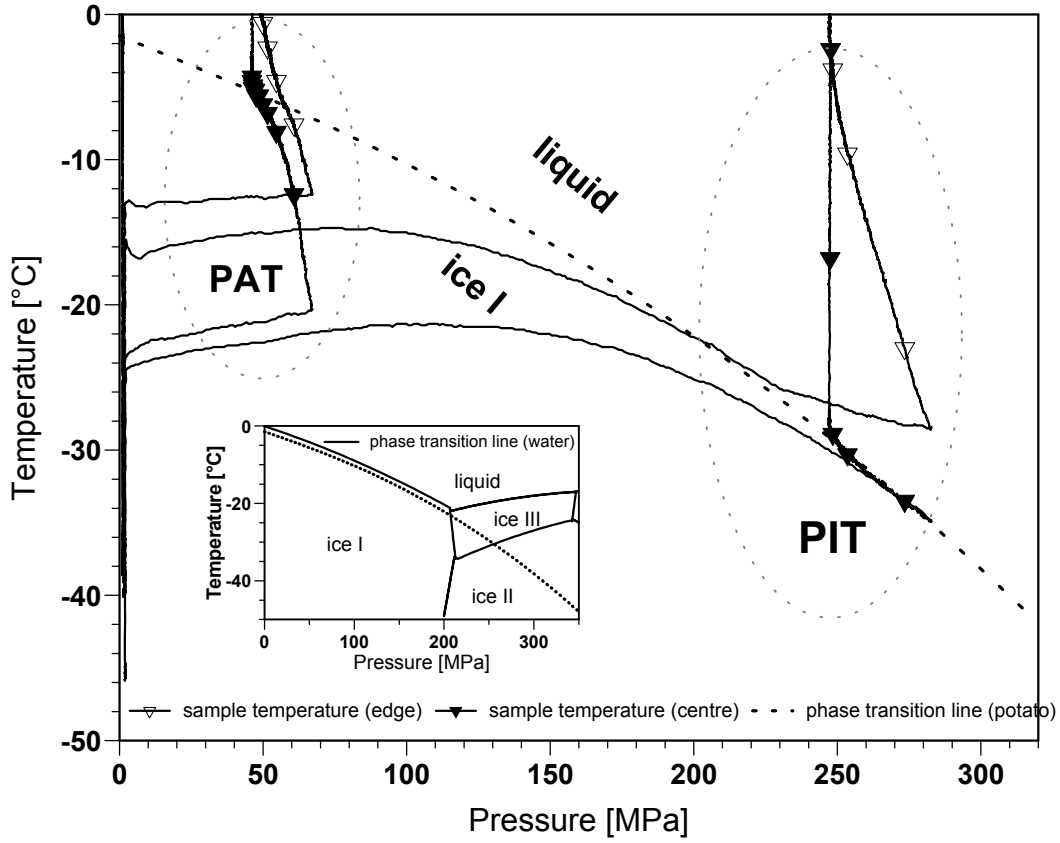

Figure 4.25: Differences between pressure-assisted thawing (PAT) and pressure-induced thawing (PIT) of a potato cylinder (32 mm dia) indicated at the random element of the sample. Temperature changes at the centre and the edge of the sample are plotted versus pressure. Insert: Extended melting curve for potato tissue (ice I) compared to the phase transition lines of pure water.

With respect to real processes, pressure-assisted thawing could be defined more clearly as each pressure-supported thawing process in which no melting of ice takes place during the pressure increase and phase transition is provoked by a temperature gradient at constant pressure. On the other hand, pressure-induced thawing, should be defined as every process in which a melting of ice is 'induced' during the pressurisation, leading to a temperature decrease.

4.1.4.7 Critical parameters for pressure supported melting

Due to the results obtained, it could be expected that further reduction of thawing times could be attained on pressurisation above 250 MPa. The first non-homogeneity of the thawing curve occurred on further pressure build-up, in a region where ice II is stable (Figure 4.26).

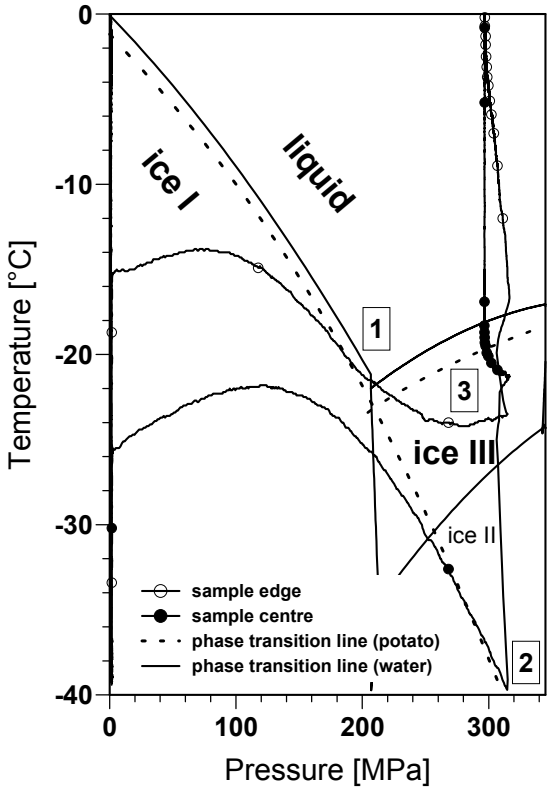

Figure 4.26: Pressure-supported thawing of a potato cylinder (32 mm dia) at 300 MPa on the *pT*-diagram of water. Temperature of the sample (edge and centre) is plotted vs. time. 1: Temperature at the edge crosses the phase boundary during pressure build-up (pressure-induced thawing). 2: Nucleation to ice III. 3: Thawing of the sample (centre) at nearly constant pressure at the melting curve of ice III (pressure assisted thawing).

During pressurisation thawing of the outer layer was again obtained (point 1), but here at 310 MPa and –40 °C (point 2), a jump in the temperature, to nearly the ice III/liquid line (point 3) was encountered. The non-homogeneity in the form of the jump suggests the probable transformation from ice I to an other phase form, which was absent in the other thawing experiments at lower pressures. The curve (sample centre) clearly indicates a change (drop) in pressure combined with the jump of temperature. The pressure drop could be explained by a volume decrease associated with transformation from ice I to ice III. Since pressurisation couldn't be stopped immediately, the pressure increases a little further. However, a possible change from ice I to ice III should be endothermic, and not exothermic as shown in the figure. This goes to suggest the existence of a metastable liquid phase between ice I and ice III. Since the thawing curve proceeds for a while along the ice I/liquid line, some amount of liquid could be expected, and just this amount of liquid crystallises to ice III, while there still remains some ice I. The transition therefore, is from ice I $\rightarrow$ liquid (metastable) $\rightarrow$ ice III $\rightarrow$ liquid. On the other hand, it can also be argued that ice III was never formed considering the fact that the subsequent thawing was accompanied by a pressure decrease, which implies, as explained before, that it is ice I, which undergoes melting. But this pressure decrease could be attributed to (a) the temperature decrease associated with the equilibration of the medium (after quasi adiabatic heating of the medium during pressure build-up) to the walls of the vessel since the sample volume was small compared to the volume of the pressure transmitting medium. Considering the transformation from the solid to the liquid, it was found here as it has been found in other attempts before, that it is impossible to superheat a

crystalline phase with respect to the liquid and according to Bridgman (1912), higher ice modifications could behave similar to liquid water in this point.

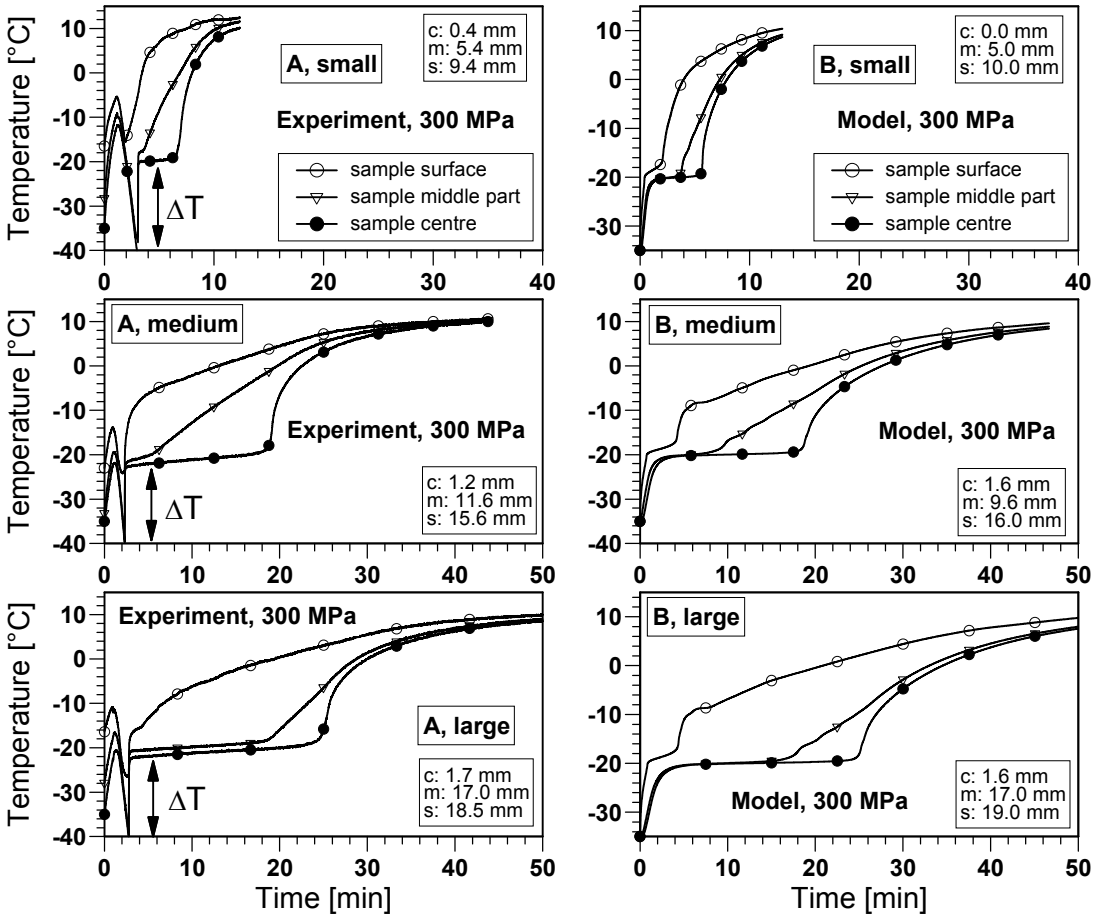

Figure 4.27: Comparison of experimental (A) and calculated thawing curves for small (20 mm dia), medium (32 mm dia), and large (38 mm dia) potato cylinders at 300 MPa. The temperature evolution was measured and calculated for comparable positions in the sample defined by c (sample centre), m (sample middle part) and s (sample surface). The double headed arrow marks the temperature jump from the extended melting curve ice I to the melting curve ice III reducing the effective temperature gradient about 20 K.

However, as shown in Figure 4.27 and 4.28, at about 300 MPa the thawing time was slightly higher than at 200 MPa, owing to the higher amount of latent heat as well as the higher thawing temperature. This non-homogeneity in the dependence of thawing time on pressure supports the theory that a solid form other than ice I exists between the transition from ice I to water during thawing at pressures above 300 MPa (Figure 4.26) and that the nucleation point of ice III is reached around –40°C. The thawing curves in Figure 4.27 clearly show that the nucleation point is a critical value in pressure-supported thawing processes, since the effective temperature gradient (sample centre and pressure transmitting medium) is significantly reduced after the temperature jump resulting in prolonged phase transition times. This critical point seems to be independent of the sample size and the experimental results imply a high degree of reproducibility.

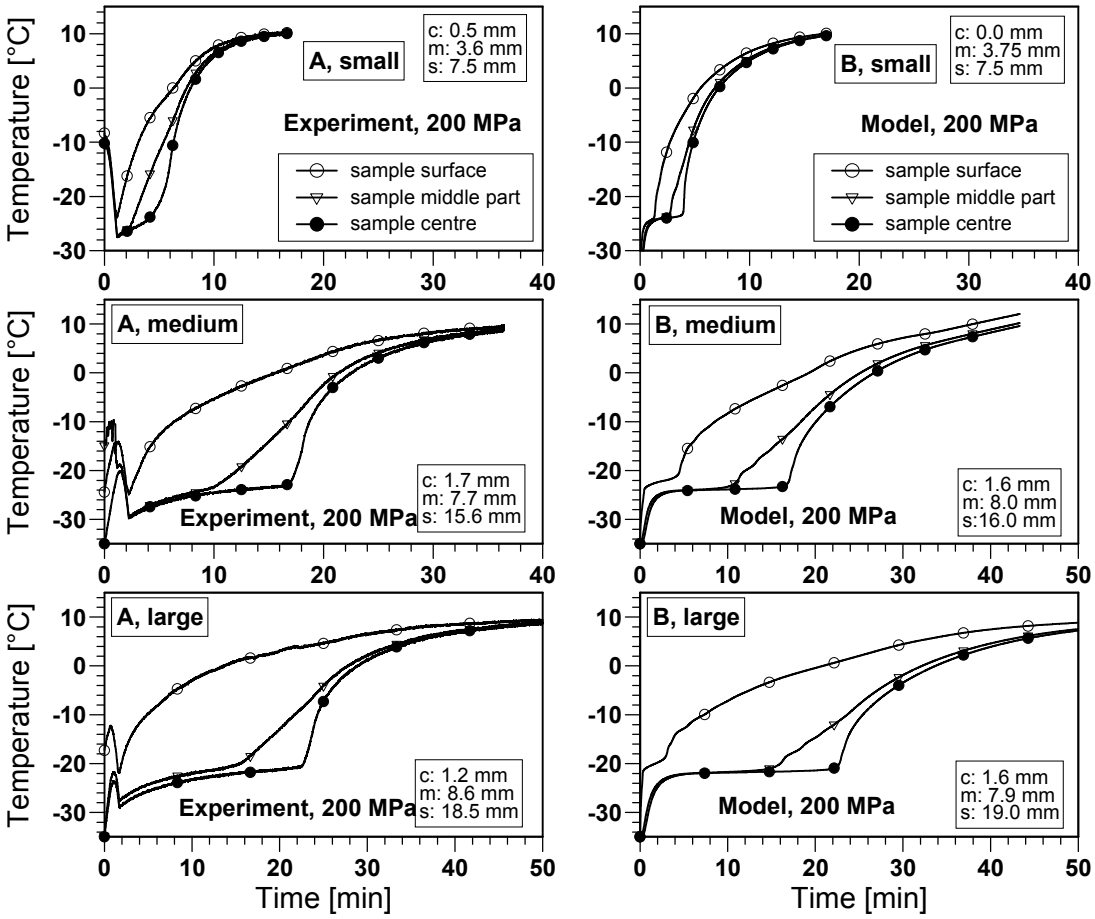

Figure 4.28: Comparison of experimental (A) and calculated thawing curves for small (20 mm dia), medium (32 mm dia), and large (38 mm dia) potato cylinders at 200 MPa. The temperature evolution was measured and calculated for comparable positions in the sample defined by c (sample centre), m (sample middle part) and s (sample surface).

4.2 Quality and safety aspects of high pressure - low temperature processes

4.2.1 Impact of high pressure-low temperature processing on plant tissue

4.2.1.1 Characteristic pressure and temperature plots

To clarify the experimental observation of phase transitions, selected processes are summarised in Figure 4.29-4.31. As an example for a high pressure treatment without phase transition, a pressure-temperature plot is given in Figure 4.29.

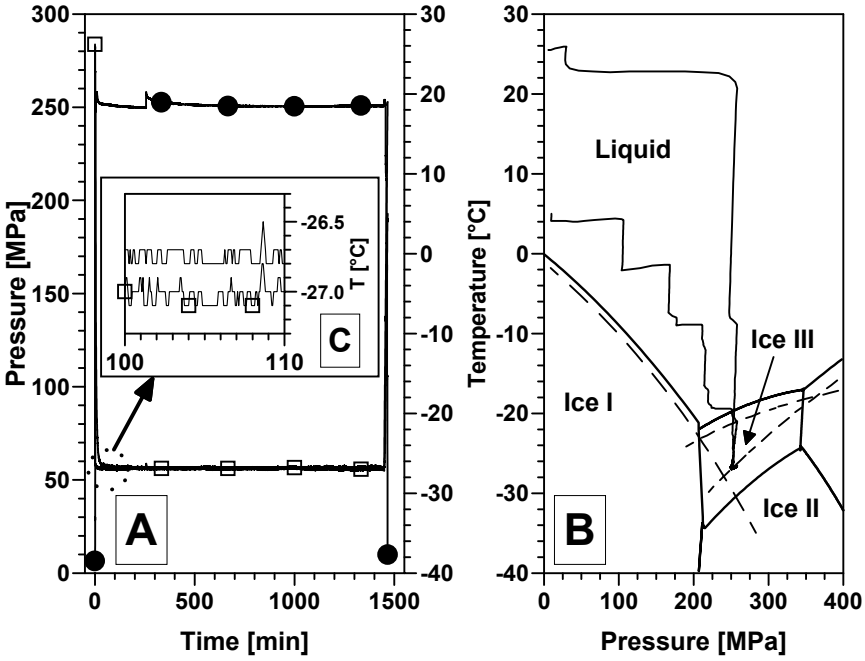

Figure 4.29: Typical temperature and pressure history for high pressure treatment of potato at 250 MPa and –27 °C without freezing. Processing pressure (—●—), temperature of the sample core (——), temperature of the cooling bath (—□—). A: Graph of temperature and pressure versus time. B: Graph of sample temperature versus pressure (solid lines: phase boundaries of pure water; dashed lines: phase boundaries of potato tissue). C: Magnification of a detail (circle).

During the cooling to –28 °C at 250 MPa, water did not freeze to ice III as it could be expected. According to the data given before, to trigger the phase change, a degree of supercooling ≥ 15 °C with respect to the melting curve ice III was necessary. The sample temperature and the cryostat temperature converged, thus, the curves were only distinguishable when they were magnified (Figure 4.29 C). A phase transition would have resulted in observable pressure and temperature changes, thus the constant curves of the pressure and the sample temperature indicated the preservation of the liquid phase. The small peak in the pressure curve arose from an external adjustment of the system pressure. Beside the formation of ice III, freezing to ice I or ice V was possible in this pressure range but only at temperatures below the (extended) phase transition lines of potatoes of these ice modifications as mentioned before. Pure water showed a similar behaviour

in this pressure range regarding the metastable phases (Petrenko and Withworth, 1999). When the desired treatment time was achieved, the temperature of the sample was raised to prevent the formation of ice during the stepwise decompression.

The recorded data for pressure-shift freezing corresponded to the plots given by Levy *et al.* (1999), however a different onset point (250 MPa, -27 °C) was used to optimise the starting conditions. A lower temperature of the onset point led to a higher supercooling during decompression, hence a faster phase transition and a more advantageous crystallisation could be achieved (Denys *et al.*, 2002).

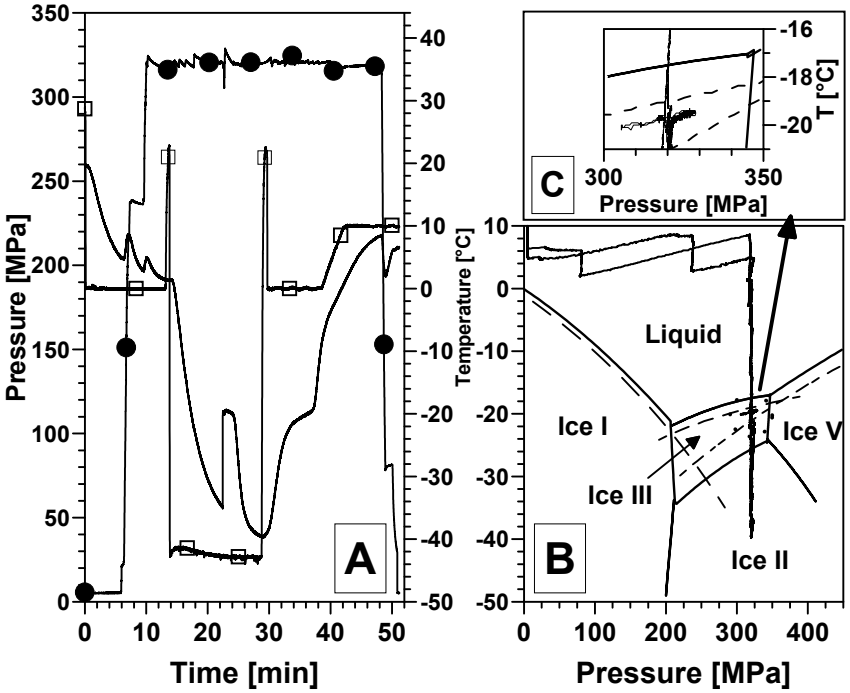

Figure 4.30: Typical temperature and pressure plots for freezing and thawing of ice III at a constant pressure of 320 MPa (potato sample). Processing pressure (—●—), temperature of the sample core (——), temperature of the cooling bath (—□—). A: Graph of temperature and pressure versus time. B: Graph of sample temperature versus pressure (solid lines: phase boundaries of pure water; dashed lines: phase boundaries of potato tissue). C: Magnification of a detail (circle).

To document the treatments with phase transitions at elevated pressures (200 MPa, 320 MPa, 400 MPa), one representative experiment at 320 MPa is shown in Figure 4.30. In this experiment the pressure was generated in two cycles during the pre-tempering at 0 °C, which could be identified by two small increases of the sample temperature caused by quasi-adiabatic compression. After the temperature equilibration the high pressure vessel was completely immersed in the cooling bath. During the cooling the pressure was manually kept constant by moving the piston of the pressure generating spindle. At an supercooling of 21 °C the nucleation took place causing a jump of the sample temperature to the freezing point of –19.5 °C at 320 MPa. The freezing point was detected by the formation of a temperature plateau at the equilibrium point of the liquid and the solid phase (Figure 4.30 A). At the beginning of the phase transition the pressure was briefly manipulated in order to record the phase transition line at the freezing point by changing the equilibrium condition.

As a result of the system response the sample temperature was shifted along the phase transition line when it was plotted versus the system pressure (Figure 4.30 B and C). In this way, the determination of the formed ice modification (ice III in this case) could be realised by comparing the recorded phase transition line with the known phase transition lines of water. After freezing and the equilibration of the temperatures, thawing was commenced by immersing the pressure vessel in the heating bath and the sample temperature approached characteristically the melting point of –19.6 °C. After the phase transition the sample temperature was increased to 10 °C to prevent freezing induced by decompression. In a similar manner, the experiments at 200 MPa and 400 MPa were carried out. At 200 MPa the formation of ice I was detected and at 400 MPa the formation of ice V, whereas at 320 MPa the formation of ice III as well as the formation of ice V was detected in independent experiments.

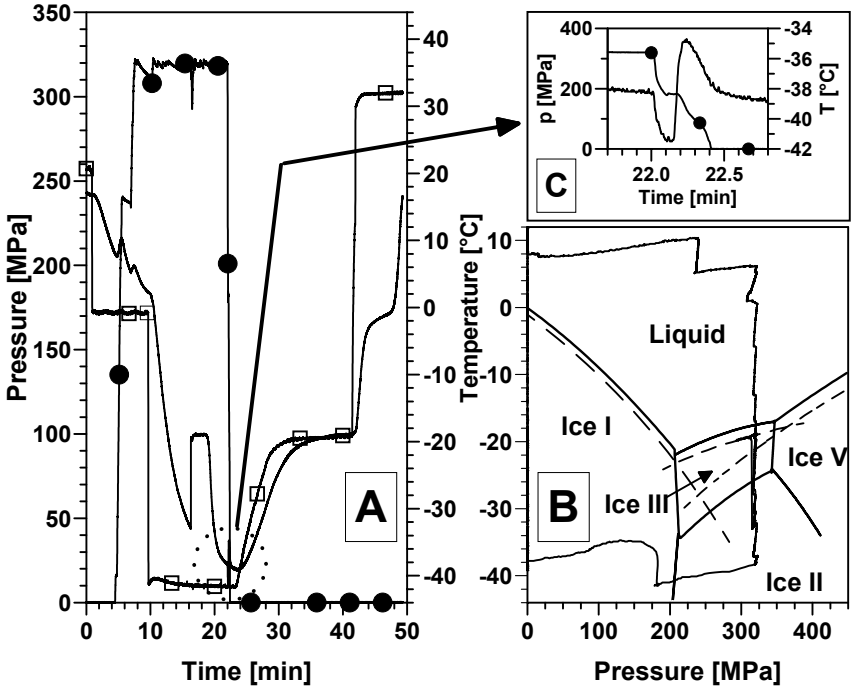

Figure 4.31: Typical temperature and pressure plots when freezing a potato at 320 MPa (ice III), followed by a fast pressure release and subsequent thawing at atmospheric pressure. Processing pressure (—●—), temperature of the sample core (——), temperature of the cooling bath (—□—). A: Graph of temperature and pressure versus time. B: Graph of sample temperature versus pressure (solid lines: phase boundaries of pure water; dashed lines: phase boundaries of potato tissue). C: Magnification of a detail (circle).

Taking into account these and numerous other experiments (data not shown), the formation of ice III from the liquid phase was only possible after a supercooling of at least 15 °C. The phenomenon of the formation of other ice polymorphs in the ice III-stability range was also recorded frequently. These results confirm the assumption (Teramoto and Fuchigami, 2000; Cheftel *et al.*, 2000; Denys *et al.*, 2002), that Fuchigami *et al.* (1997a, 1997b, 1997c, 1998b) did not accomplish phase transitions at –20 °C in this pressure range.

The pressure-temperature plot of a solid-solid phase transition obtained is shown in Figure 4.31. Firstly the sample was frozen to ice III. After completion of the freezing process, the pressure was

released within a few seconds by opening the valves of the system. Within the first seconds, the temperature decreased due to the quasi-adiabatic decompression. Beyond the phase transition line to ice I at about 200 MPa, a sudden exothermic crystal-transformation of ice III to ice I was obtained, indicated by an increase in sample volume and accompanying temperature increase. The rise of the sample volume was detected by the short constant pressure plateau during the ongoing decompression (Figure 4.31 C). At the same time an increase of the sample temperature was observed. After the decompression and the phase change, the vessel was tempered to –20 °C and finally thawed at ambient pressure. In the opposite direction, the phase change caused by the compression of ice I could be detected by a drop of the pressure and of the sample temperature. The ice formed could be identified as ice III by its melting point during thawing under pressure as mentioned in section 4.1.2.4.

4.2.1.2 Indication of phase transitions by impedance spectra

Figure 4.32 shows the change of the Fractional Pore Area subsequently after high pressure treatments without phase changes at different temperatures and for different pressure holding times. Generally a progressing increase of the permeabilised membrane area could be seen.

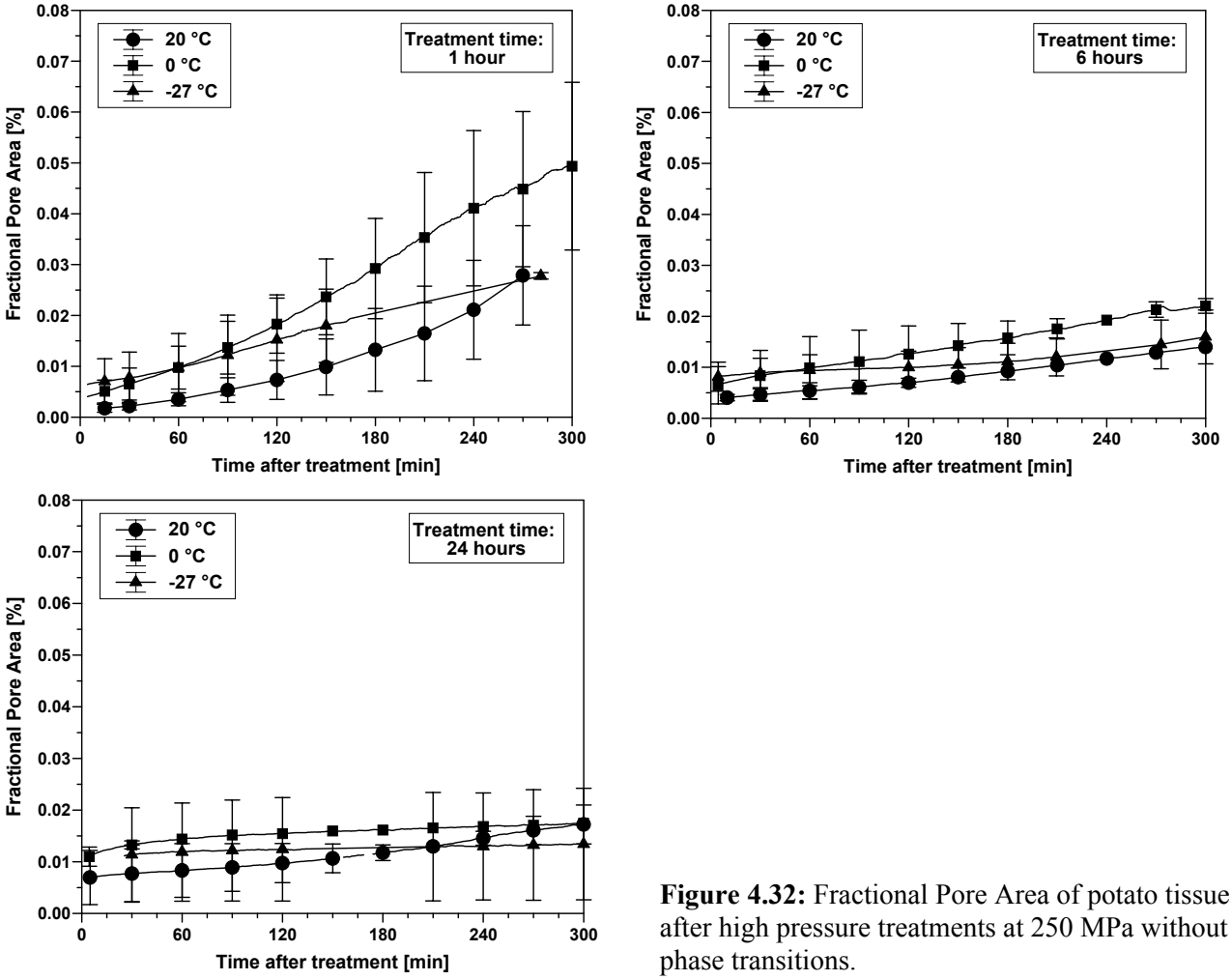

Figure 4.32: Fractional Pore Area of potato tissue after high pressure treatments at 250 MPa without phase transitions.

However, all values were associated with a very small impact on the cell membranes, compared to the data for treatments with phase transitions and the data reported by Angersbach *et al.* (2002). Lower treatment temperatures, as well as longer treatments, led to a small increase of the initial permeabilisation directly after treatment. The largest increase of the Fractional Pore Area was found after a pressure holding time of one hour, however, the individual influence of the sample had to be considered (cf. standard deviations). After longer pressure holding times a slower increase was detected. The influence of the treatment temperature was low after 1 hour and 6 hours. However, after high pressure treatments at 0 °C and –27 °C for 24 hours, no significant increase of the pore area was detected, while treatments at 20 °C for 24 hours still resulted in a low rise of the Fractional Pore Area.

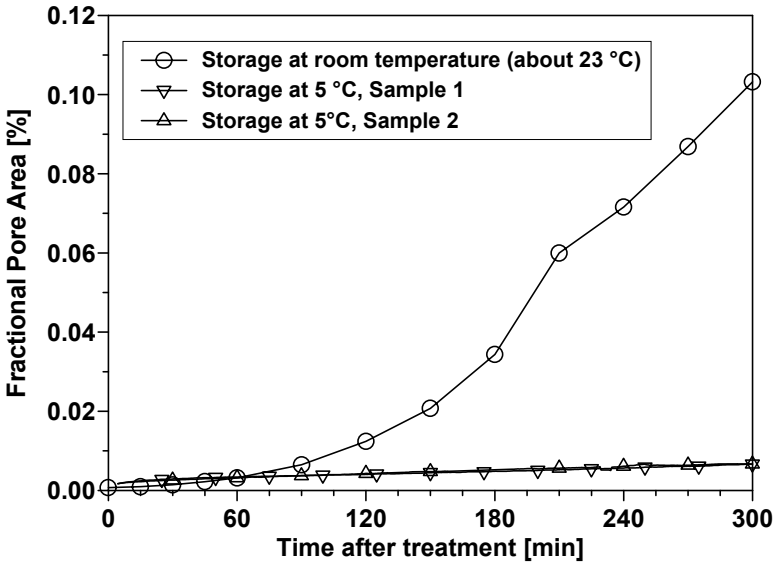

Figure 4.33: Influence of different storage temperatures on the Fractional Pore Area of potato tissue after high pressure treatment at 250 MPa and 20 °C for 30 minutes.

Figure 4.33 shows the influence of the storage temperature during the impedance measurements. At 5 °C, only a slow increase could be noticed, whereas samples stored at 23 °C during the measurement showed a significant increase. To amplify the effect of the onset value of a high pressure treated sample on the post-processing behaviour during storage, the measurement temperature was set to 20 °C.

To comparatively evaluate the effect of phase transitions on the impedance spectra, freeze-thaw cycles at constant pressures of 0.1 MPa, 200 MPa, 320 MPa and 400 MPa as well as pressure-shift freezing were carried out (Figure 4.34). The measurement of the Fractional Pore Area at values above 0.5 % was strongly influenced by small changes in the impedance characteristics of the sample material. Hence the standard deviation was only given in positive direction to improve the clarity of the diagram. The extent of the damage of the cellular membranes in comparison to the experiments without phase transitions underlined the strong influence of liquid-solid phase transitions on the sample material. Like before (Figure 4.32) an ongoing increase of the Fractional Pore Area was noticed. The influences of the different processes on the cell membrane were

distinguishable, with a freeze-thaw-cycle at 200 MPa being most destructive followed by a freeze-thaw-cycle at 0.1 MPa, pressure-shift freezing, freezing and thawing of ice V and freezing and thawing of ice III being least destructive. These results are in accordance with examinations which showed a decrease of the impedance of plant tissues after freezing at ambient pressure (Zhang and Willison, 1992a; Zhang and Willison, 1992b; Ohnishi *et al.*, 2002). The results for freezing to ice V were pooled, even though the formation of this ice was achieved at different pressures. The comparatively low standard deviations confirmed that the type of ice polymorph has a higher influence on the cellular membranes than the different pressure levels.

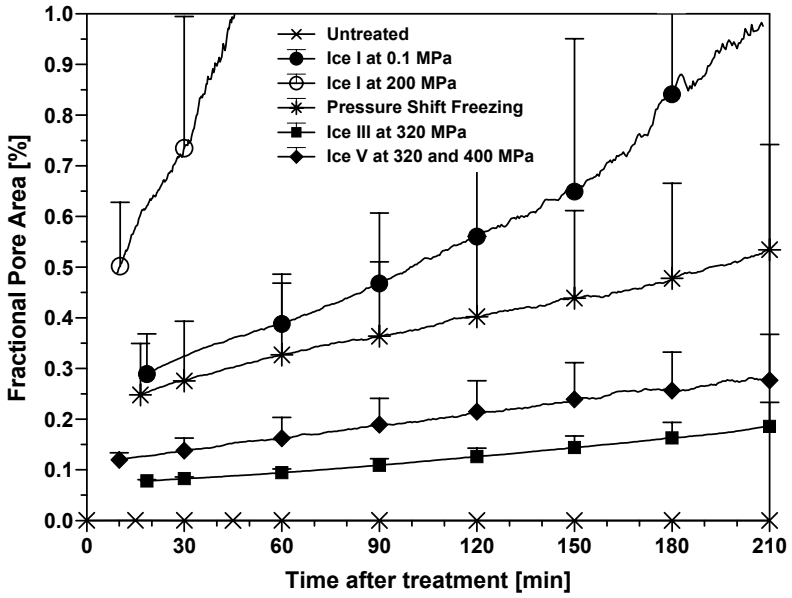

Figure 4.34: Fractional Pore Area after high pressure treatments with phase transitions. Determined ice polymorphs and the constant treatment pressure during the freeze-thaw cycles are given in the legend text.

4.2.1.3 Process induced changes of the cell membrane

The low initial extent of permeabilisation illustrated the comparatively low impact of high hydrostatic pressure in relation to thermal processes. Lower treatment temperatures increased the initial permeabilisation of the cellular membranes. This was attributed to the influence of a solidification of the membrane, since model membranes and membranes in bacteria showed a phase transition from the liquid-crystalline to the gel phase at low temperatures and elevated pressures (Winter and Czelik, 2000; Ulmer *et al.*, 2002). This solidification facilitates damaging of the membranes, caused by different compressibility of cell inclusions like starch granules or gas vacuoles.

After the treatment, the pore area increased, even after relatively short treatment times (Figure 4.32). (Dörnenburg and Knorr, 1997 and 1998) demonstrated the permeabilisation of plant cell cultures under pressure and showed an increasing release of intracellular substances to the medium after pressure treatment. These results agree well with the data given here. Kalchayanand *et al.* (2002) showed the decrease of the optical density and the cell counts of *Leuconostoc mesenteroides* after treatments with high pressure and a bacteriocin, which influenced the cell membranes. It was concluded from similarities between the treatments that high pressure permeabilised the cellular

membranes and caused cytolysis. The increase in pore area was interpreted in the same way as a result of autolytic enzymes in the treated potato cells. Kalchayanand *et al.* (2002) also found the hindering of the enzymatic, autolytic process at 1 °C. This agrees well with the very low increase of the pore area, when the sample was kept at 5 °C after treatment (Figure 4.33). Thus, the occurrence of enzymatic lysis, triggered by high pressure treatments in plant cells, was concluded. Most of the lysis did not seem to take place during the high pressure treatment itself, because the initial membrane damage increased only slowly during the high pressure treatments, like the Fractional Pore Area after different treatment times at one temperature level indicated. Beside the lytic reactions other reactions might be responsible for the deterioration of the membranes (for example drop of pH-value, etc.).

Long holding times and low temperatures resulted in a stabilisation of the membrane, i.e. less lytic reaction takes place. This could be caused by the (cold) denaturation of parts of the autolytic enzymes. No data are available on enzyme inactivation under pressure at very long treatment times or temperatures below –20 °C, but general data on the stability of proteins under pressure (Heremans and Smeller, 1998) and the inactivation kinetics of enzymes (Indrawati *et al.*, 1998; Indrawati *et al.*, 2000) showed that this can be stated. After the most extreme conditions in this study of 24 h treatment at –27 °C and 250 MPa, no reaction could be detected. Unpublished data seem to show that this inactivation is partly reversible and the Fractional Pore Area starts to rise after an intermission of several hours.

Freezing and thawing (with or without high pressure) resulted in a much stronger membrane disintegration than high pressure alone. This comprised the initial pore area as well as the further kinetics (Figure 4.34). In this case the extent of the initial membrane damage influenced the rate of increase of the pore area. A higher membrane damage led probably also to a higher release of autolytic enzymes, which increased the rate of reaction. The inactivation of autolytic enzymes was not likely in these experiments due to the relatively short pressure holding time.

Two factors seemed to influence the extent of membrane damage after a freeze-thaw cycle: the duration of the phase transition and the volume change of water during the transition. The volume increase of water during the transition from the liquid state to ice I is 0.09 cm^3g^{-1} at 0.1 MPa and rises to about 0.13 cm^3g^{-1} at 200 MPa. As a consequence, the extent of membrane damage increased from freezing and thawing at 0.1 MPa to freezing and thawing at 200 MPa. The formation of ice III at 320 MPa causes a volume change of –0.03 cm^3g^{-1} which means not only a smaller absolute value of the volume change, but also a decrease in volume. The resulting membrane damage is comparatively lower than after conventional freezing, but this phase transition seems also to cause stress to the membrane. The formation of ice V at 320 MPa and 400 MPa (–0.08 cm^3g^{-1} and –0.07 cm^3g^{-1} respectively) resulted in a higher damage than the formation of ice III, but the effect was less than after conventional freezing. This means that a phase change with a volume decrease was less destructive for the cellular membranes than with volume increase, but a larger negative change in volume was more destructive than a smaller negative change.

Beside the volume change, the dependency of the membrane damage on the phase transition time had to be considered. The formation of ice III (always) and ice V (usually) took place after a significant supercooling. This had the effect that the phase transition time is shorter than during the formation of ice I in which less supercooling occurred. In this way the osmotic gradient between intracellular and extracellular liquid, which occurs during freezing, was lower. This gradient can affect the integrity of the membrane (Steponkus, 1984). Since the positive effects of the smallest volume change and the largest supercooling both occurred during the formation of ice III, both effects could not be separated from each other. However, it can be argued that the phase transition time for the examined small samples (diameter 13mm) was relatively short and that in this case the effects of the volume change dominated. Due to supercooling, the effective phase transition time of the pressure-shift freezing process was also very short. It can also be assumed that, due to the higher temperature difference as compared to atmospheric conditions, more ice is formed instantly during the pressure release as calculated in section 4.1.2.7 and reported elsewhere (Thiebaud *et al.*, 2002). The damage of the membranes was less than during conventional freezing, although ice I was formed. This was due to the shorter phase transition time and the formation of smaller ice crystals as compared to conventional freezing. Micrographs of plant tissue materials in other examinations indicated this effect (Fuchigami *et al.*, 1997b; Fuchigami *et al.*, 1998a; Otero *et al.*, 1998; Otero *et al.*, 2000b).

4.2.1.4 Effects of phase transitions on textural properties

Figure 4.35 shows examples of the recorded force-deformation plots, re-calculated as true stress-true strain plots. The results for the mean failure stress and strain after the formation of ice V at 320 MPa or 400 MPa did not show significant differences (P>0.05) (Table 4.12), thus the results were pooled.

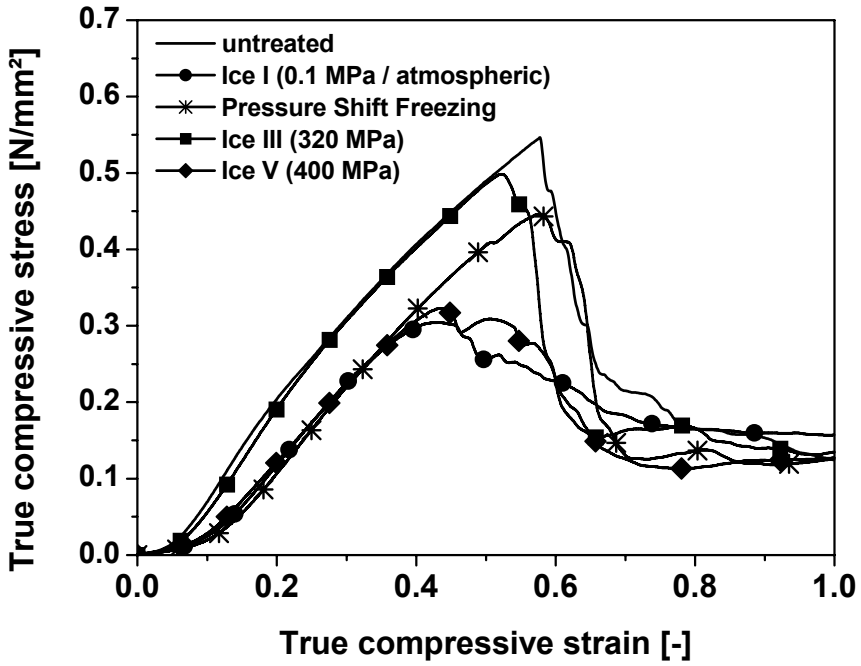

Figure 4.35: Examples of true stress – true strain plots of compression tests of potato cylinders (l=10mm, d=13mm). A true strain of $\varepsilon_c = 1.2$ corresponds to a compression of $\Delta h = 6.99$ mm.

Table 4.12: Results of compression tests of potato cylinders after high pressure phase transitions.

	Untreated	Ice I at 0.1 MPa	PSF	Ice III at 320 MPa	Ice V
No. of samples	12	11	10	8	7 at 320 MPa 8 at 400 MPa
Mean failure stress, σ_f [N / mm²]	0.53 ± 0.04 ++	0.28 ± 0.06 oo	0.43 ± 0.04 oo ++	0.48 ± 0.04 o ++	0.33 ± 0.05 oo
Mean failure strain, ε_f [-]	0.56 ± 0.04 ++	0.48 ± 0.05 oo	0.58 ± 0.06 ++	0.57 ± 0.04 ++	0.48 ± 0.06 oo

PSF: pressure shift freezing; Ice I at 0.1 MPa e.g. denotes a freeze-thaw cycle at a constant pressure of 0.1 MPa with the formation of ice I. Results for the formation of ice V were pooled, because there was no significant difference by T-test between the samples frozen at different pressures (P>0.05).

o P<0.01: Significant differences between tested sample and untreated sample by T-test.

oo P<0.001: Significant differences between tested sample and untreated sample by T-test.

+ P<0.01: Significant differences between tested sample and conventional frozen sample by T-test.

++ P<0.001: Significant differences between tested sample and conventional frozen sample by T-test.

This confirmed the assumption that under the selected experimental conditions, the type of ice mainly affected the cellular membranes. The failure stress showed more significant differences between the various treatments than the failure strain (Figure 4.36). Freezing at 0.1 MPa had the largest impact on the texture followed by freezing to ice V. Freezing to ice III and pressure-shift freezing resulted in a considerably lower softening. These two treatments showed significant differences in failure stress compared to the untreated sample and to the sample frozen at ambient pressure. The failure stress after freezing to ice V was only significantly different from the untreated sample. Regarding the failure strain, pressure shift freezing and freezing to ice III were very similar to the untreated sample, showing significant differences only to the conventional frozen sample. In contrast, the failure strain after freezing to ice V was nearly the same compared to freezing at 0.1 MPa. Other experiments indicated that high pressure treatments without phase transitions did not result in significant textural differences between the treatments (data not shown).

As soon as a certain deformation was reached, failure of the tissue in untreated potato cylinders occurred suddenly. This was indicated by the abrupt decrease of the curve after the peak in Figure 4.35. Pressure-shift freezing and freezing to ice III showed nearly the same stress-strain curves as the untreated sample. A certain softening of the tissue could be derived from the somewhat rounder shape of the peaks and the lower failure stress. Freezing to ice V was comparable to conventional freezing, since both processes resulted in round and comparatively low peaks. No significant difference was found between freezing to ice V at different pressure steps. This is in excellent agreement with the results of the impedance measurements. These observations are supported by the data given in Table 4.12.

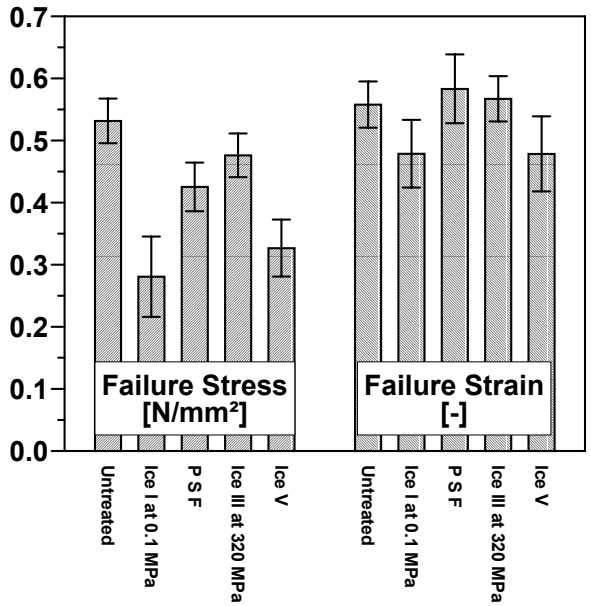

Figure 4.36: Influence of phase transitions under high pressure on the texture of potato cylinders determined by a compression test. (For abbreviations cf. to Table 4.12)

The comparison of the effects of phase transitions under high pressure showed certain differences between the state of the membranes as determined by impedance measurements and the textural properties. The texture of vegetable tissue depended on different interacting factors, freezing for example did not only cause damage to cellular membranes and consequently to the turgor pressure, but also influenced the (outer) cell wall polymers (Sahagian and Goff, 1996; Roy *et al.*, 2001). Pressure-shift freezing resulted in relatively high membrane damage, but preserved the texture very well. The textural advantages of pressure-shift frozen vegetable tissue were also reported by other authors (Otero *et al.*, 1998, Fuchigami *et al.*, 1997a). This showed that the formation of small ice crystals during pressure-shift freezing did not affect the framework of the cell walls significantly. Hence, the texture of tissues which depend mainly on the skeletal frame was preserved very well, like in the case of potatoes or carrots (Fuchigami *et al.*, 1997a). However, vegetables like Chinese cabbage depend more on the turgor pressure and the state of the voluminous vacuoles filled with gas. Hence their softness increased remarkably during pressure-shift freezing (Fuchigami *et al.*, 1998a). When freezing to ice V, a considerable discrepancy between the membrane structure and the texture was observed. In this case, different amounts of supercooling and the resulting differences of the freezing rates influenced the results. This means that the formation of dense ice polymorphs resulted in a low membrane damage, but the tissue may be softened due to osmotic water transport during the phase transition.

4.2.1.5 Evaluation of changes in colour and visual appearance

Figure 4.37 shows the macroscopic changes of the samples on the basis of digital pictures and the corresponding colour measurements. The untreated sample showed no detectable browning at the cutting surface, whereas the sample frozen and thawed at ambient pressure showed the highest extent of browning. Pressure-shift freezing showed the lowest extent of browning of all samples

that had been frozen. Freezing and thawing at 320 MPa showed a slightly decreased browning compared to conventional freezing and thawing. After the induction of a phase transition of ice I to ice III by compression, the sample showed browning comparable to the sample that was subjected to a freeze-thaw cycle at 320 MPa. All these samples showed no difference in the macroscopic shape, although the texture changed. In contrast, the phase transition of ice III to ice I by decompression had a detrimental effect on the sample structure. As a consequence, substantial shrinkage in combination with an enormous drip loss (about 50 % immediately after treatment) and an extensive softening and deformability were detected. However, the treatment did not result in a stronger browning than freezing at ambient conditions. Because of the shrinkage, the colour measurement had to be terminated after 100 minutes. The increase of the lightness value after 70 minutes resulted from the release of starch granules from the tissue. The impact of this solid-solid phase transition was too extensive to obtain reproducible data for texture and impedance characteristics, thus solid-solid phase transitions were not examined extensively in these experiments.

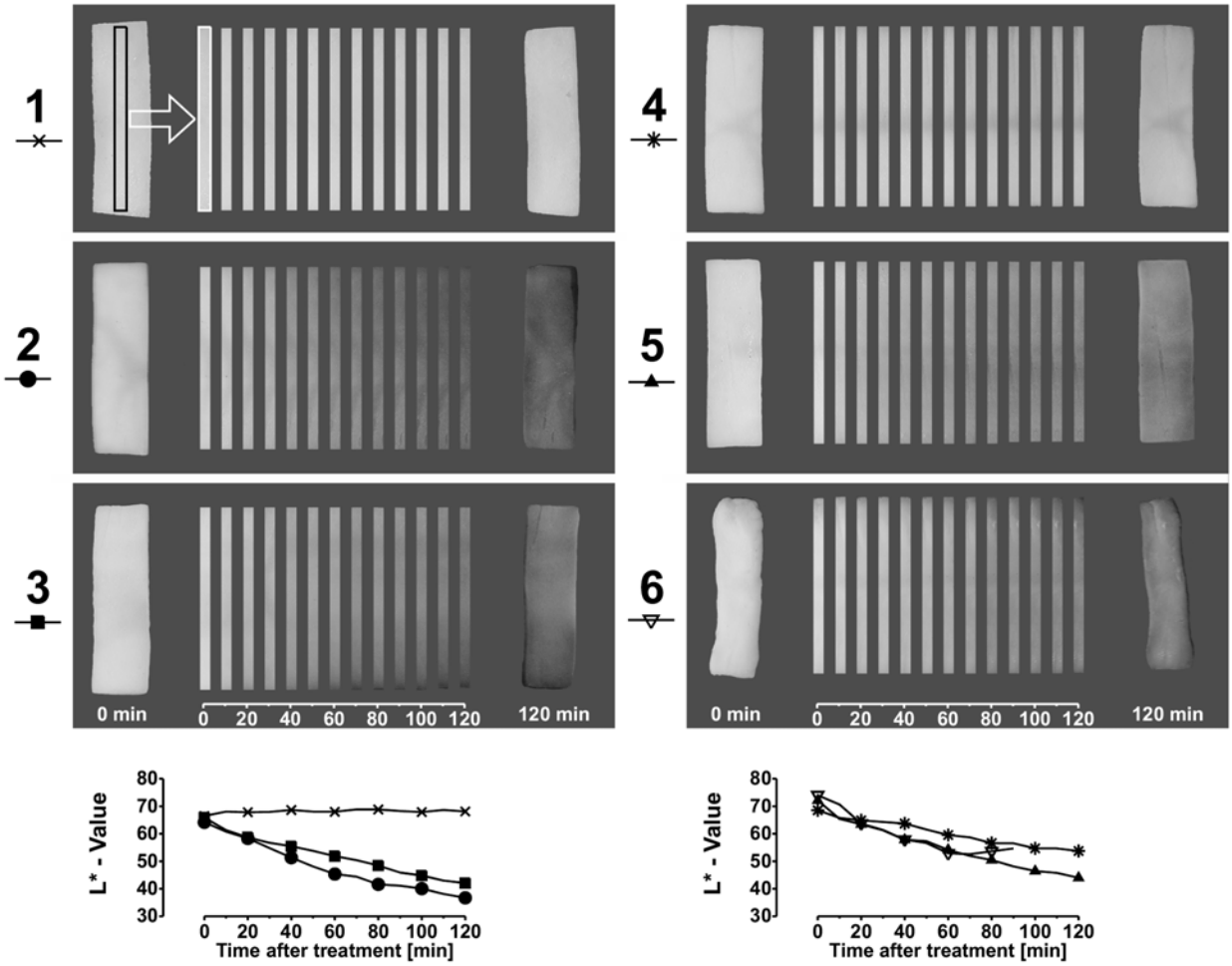

Figure 4.37: Influence of phase transitions under high pressure on visual appearance and evolution of lightness value L* of potato samples after treatment. **1:** Untreated sample; **2:** Freeze-Thaw-Cycle at 0.1 MPa (Ice I); **3:** Freeze-Thaw-Cycle at 320 MPa (Ice III); **4:** Pressure Shift Freezing with an onset point of 250 MPa and –27 °C; **5:** Freezing at 0.1 MPa, compression with phase transition; thawing at 320 MPa (Ice III); **6:** Freezing at 320 MPa (Ice III), decompression with phase transition, thawing at 0.1 MPa. (Luscher *et al.*, 2003)

High pressure treatments lead either to an activation or an inactivation of polyphenoloxidase (PPO) (Ludikhuyze and Hendrickx, 2002). To achieve considerable inactivation usually higher pressure – temperature combinations were required, but PPO from various plants differed in their activation / inactivation behaviour (Ludikhuyze and Hendrickx, 2002; Weemaes *et al.*, 1998; Palou *et al.*, 1999; Hernandez and Pilar Cano, 1998). In the high pressure – low temperature domain Indrawati *et al.* (1998) found only a slight, reversible inactivation of mushroom PPO. The data for potato PPO are not consistent regarding activation or inactivation (Ludikhuyze and Hendrickx, 2002) and only data at temperatures above zero are available. Dörnenburg and Knorr (1997) found a dependency of the production of polyphenols in cultured potato cell suspensions on the pressure dependent loss of compartmentalization in cultured potato cells. Due to the limited number of samples, results regarding (in-)activation of PPO could not be derived here. According to Dörnenburg and Knorr, 1997 it was assumed that at this pressure level the loss of compartmentalization of the cells influenced the browning reaction more than a possible pressure influence on the enzyme itself. It has to be pointed out that in this case tissue samples were examined and not extracts or enzyme solutions where no compartmentalization influences the browning reaction.

The browning of the treated samples was comparable, with the exception of the sample that was pressure-shift frozen (Figure 4.37). This showed a comparably good preservation of the natural structure, in the latter case, because the necessary PPO was not released totally. Hence, it can be concluded that the compartmentalization of the cells was not completely destroyed. However, freezing to ice III resulted in a higher browning, that was only slightly lower compared to conventional freezing. This was not in accordance with the results of the texture evaluation and the Fractional Pore Area, which showed better results than for pressure-shift freezing. The lower release of PPO during pressure-shift freezing might be related to the shorter overall process time. The macroscopic shape of the samples was not varying from the raw sample although softening occurred.

In this series of experiments also direct crystal transformations between the ice polymorphs I and III have been investigated. The results showed a clear dependency on the direction of the process. If the sample was frozen conventionally, cooled to about –30 °C and then compressed, a phase transition from ice I to ice III could be induced. Thawing under pressure excluded the influence of further phase transitions. The sample did not show significant macroscopic changes, and browning was comparable to the other samples frozen and thawed under high pressure. However, the process in the opposite direction gave a completely different result. After pressurisation of the raw sample and freezing under pressure, the phase transition from ice III to ice I was induced by pressure release. After thawing at ambient pressure, the sample showed an extensive destruction of the tissue. The potato cylinder (Figure 4.37 (sample 6)) shrunk due to an also extensive drip loss, and the textural appearance was extremely soft and deformable. This result was supported by the report of Edebo *et al.* (1960), who found even a cell disintegration of *E. coli* after repeated phase transitions of these ice modifications (ice I, ice III). This extreme influence was explained by

differences in the density of the solid states. A phase transition of ice III to ice I was accompanied by an explosive volume increase of about +0.19 cm^3 g^{-1}, which induced a disruption of the tissue structure. Due to the solid state of the surrounding water, the polymers and membranes had no possibility to act flexible like they would have done in the aqueous phase. In the opposite direction, the volume decreased during the phase transition, which was obviously less damaging to the tissue. Compared to the other samples, the browning of this heavily influenced sample was not increased. It might be the case that in all samples maximum browning was already achieved or that the PPO or its substrates were leaching from the tissue, due to the extensive drip loss.

4.2.2 Impact of high pressure thawing on animal tissue

4.2.2.1 Evaluation of the required processing time

To evaluate the processing time which ensures completion of the phase transition in pressure-assisted thawing processes at 200 MPa, the changes of the sample centre temperature was measured in preliminary experiments.

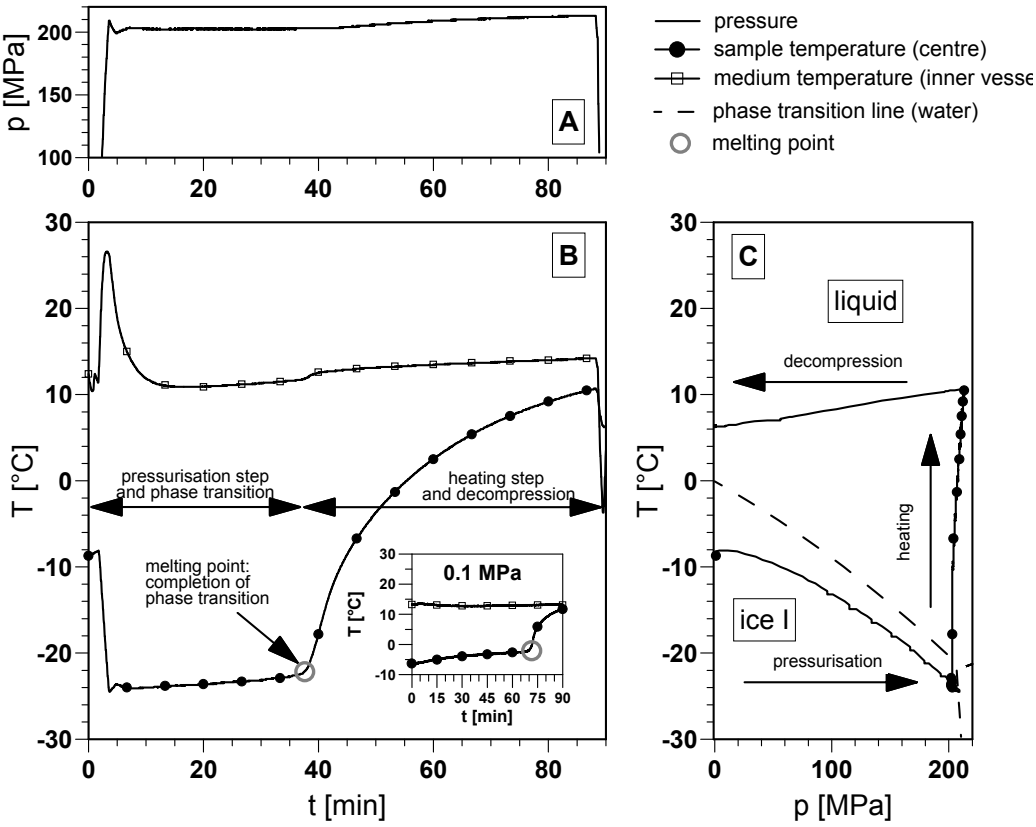

Figure 4.38: Typical pressure and temperature changes during pressure assisted thawing of fish, detected to ensure completion of the phase change. A: Pressure profile; B: Temperature history; C: Processing steps plotted to the *pT*-diagram of water. Insert diagram B: Temperature history for a conventional thawing process at 0.1 MPa.

As an example, Figure 4.38 shows typical pressure and temperature curves during pressure assisted thawing of salmon at 200 MPa. Due to the change of equilibrium conditions (liquid-solid) and the beginning of the thawing process, the sample temperature decreases during the pressure build-up

phase (pressure induced thawing in the first step). When reaching the selected working pressure the phase transition is completed under nearly constant pressure (pressure assisted thawing in the main step). Thus the required time for the phase transition process can be derived from the temperature plateau before reaching the melting point. Compared to ambient conditions and similar medium temperature, the plateau is reduced by approximately 50 % (Figure 4.38 B, insert). Since decompression is accompanied by a temperature decrease, sufficient heating is required to prevent unwanted crystallisation at atmospheric pressure. Consequently a pressure holding time of 60 min was applied in all high pressure experiments to ensure complete phase transition. The comparative evaluation of temperature and pressure plots, obtained during pressure-supported thawing, indicates analogous behaviour of animal derived tissue and plant based materials with respect to pressure dependent melting point depression.

4.2.2.2 Effects of thawing and subsequent heating on sensory attributes

The results of the sensory evaluation of thawed fillets (Table 4.13) show that colour as well as texture are most influenced by high pressure assisted thawing and that judges positively evaluated these changes for redfish, whiting and cod samples. The colour of salmon and rainbow trout changed due to protein unfolding induced by hydrostatic pressure, but the texture of the samples improved compared to the conventional thawing process.

Table 4.13: Sensory assessment using quality index method (QIM) of raw fillet as affected by thawing (n=6)

Species	Thawing	Texture	Odour	Colour	Gaping	Demerit points
Redfish	HP	0	0	0	0	0
	AP	1.0	2.0	0	0	3.0
Whiting	HP	1.0	0	0.75	0	1.75
	AP	1.25	0	2.0	0	3.75
Salmon	HP	0	0	1.75	0	1.75
	AP	0.25	0	0	1.0	1.25
Cod	HP	1.0	0	0	0	1.0
	AP	2.0	0	2.0	0	4.0
Rainbo w trout	HP	0	0	1.5	0	1.5
	AP	1.0	0	0	0	1.0

*HP: Thawing at 200 MPa; AP: Thawing at 0.1 MPa

Table 4.14: Sensory assessment using quality index method of thawed and subsequent heated fillets (n=6).

Species	Thawing /heating	Texture	Odour	Colour	Taste	Demerit points
Redfish	HP	2.5	0.75	0.25	1.0	4.5
	AP	1.25	0.75	1.75	0.75	4.5
Whiting	HP	2.25	0.5	0.5	3.0	6.25
	AP	0.75	0.75	1.0	0.25	2.75
Salmon	HP	2.25	1.25	1.0	1.25	5.75
	AP	1.25	1.0	0.5	0.75	3.5
Cod	HP	2.0	2.0	0	3.0	7.0
	AP	2.0	1.0	1.0	1.0	5.0
Rainbo w trout	HP	2.5	0	2.0	2.0	6.5
	AP	3.5	0	1.0	1.5	6.0

* HP: Thawing at 200 MPa; AP: Thawing at 0.1 MPa

However, when sensory assessment was performed on subsequently heated fillets differences in quality between high pressure thawed and conventional thawed fillets were more pronounced (Table 4.14). The judges evaluated a significant influence of the species regarding the quality of high pressure thawed fillets. Samples from whiting, salmon and cod were affected by pressure-assisted thawing and consequently got more demerit points (poorer quality), while the assessment of redfish and rainbow trout resulted in equivalent values for the pressure treated and conventionally thawed samples. The parameters affected most by high pressure were taste and texture, but for cod fish the influence on odour was more significant while no difference in texture was evaluated. It should be mentioned that relevant literature lacks in data regarding the influence of high pressure thawing on organoleptically evaluated quality parameters.

4.2.2.3 Pressure and heat induced changes in texture

The texture of fish fillet is influenced by high pressure-assisted thawing when compared with thawing under atmospheric conditions (Table 4.15). Hardness at 75% compression is higher in high pressure, compared to conventionally thawed fillet except for redfish and rainbow trout 1.

Table4.15: Hardness (N) of raw and heated fish fillet (mean ± standard deviation) as a function of thawing conditions (HP: Thawing at 200 MPa; AP: Thawing at 0.1 MPa)

Species	**Raw fillet**		**Heated fillet**	
	HP	AP	HP	AP
Redfish	$91.4^{a} \pm 12.1$	$85.5^{a} \pm 8.0$	$85.4^{a} \pm 9.9$	$59.1^{b} \pm 11.4$
Salmon	$43,4^{b} \pm 3.2$	$27.1^{a} \pm 5.8$	$61.0^{a} \pm 13.9$	$87.9^{b} \pm 22.7$
Whiting	$46.2^{b} \pm 5.6$	$37.5^{a} \pm 4.9$	$54.9^{a} \pm 5.7$	$74.8^{b} \pm 3.7$
Haddock	$67.0^{b} \pm 3.8$	$42.6^{a} \pm 9.6$	-	-
Rainbow trout 1	$43.2^{a} \pm 10.5$	$33.7^{a} \pm 8.1$	$58.8^{a} \pm 11.7$	$65.9^{a} \pm 9.9$
Rainbow trout 2	$43.8^{b} \pm 10.7$	$26.7^{a} \pm 3.5$	$74.4^{a} \pm 18.0$	$93.1^{b} \pm 16.9$
Cod	$56.0^{b} \pm 15.2$	$37.7^{a} \pm 6.7$	$41.7^{a} \pm 11.8$	$54.0^{a} \pm 11.0$

[a, b] Different superscripts in the same row indicate significant differences ($p<0.05$) between HP and AP-thawed fillet

This also became clear when both variants were visually compared (Figure 4.39). While the conventionally thawed samples appeared flabby, the high pressure thawed ones looked stiff (similar to samples in rigor). When hardness was measured on heated fillets, the influence of the thawing treatment was almost contrary to that of raw samples. Except redfish, fillets heated after conventional thawing were significantly harder compared to those thawed using high pressure. Cooked fillets were harder than the raw ones independently of the thawing treatment (except redfish (HP, AP) and cod (AP)).

Compared to the physical properties of unfrozen fish muscle, according to Yoshioka *et al.* (1996) high pressure thawed muscles showed a similar breaking stress to that of unfrozen carp muscle and elasticity was also maintained in the muscle. In heated carp muscle, small differences in the breaking stress were observed in high pressure thawing, while running water-thawed muscles were harder. Massaux *et al.* (1999a and 1999b) noted for pork a toughening caused by high pressure

thawing which increased with working pressure. While Zhao *et al.* (1998) did not find significant differences in the penetration force among beef samples thawed by conventional and high pressure processing, it has been reported by other authors that meat tenderisation was induced by high pressure thawing (Okamoto and Suzuki, 2001).

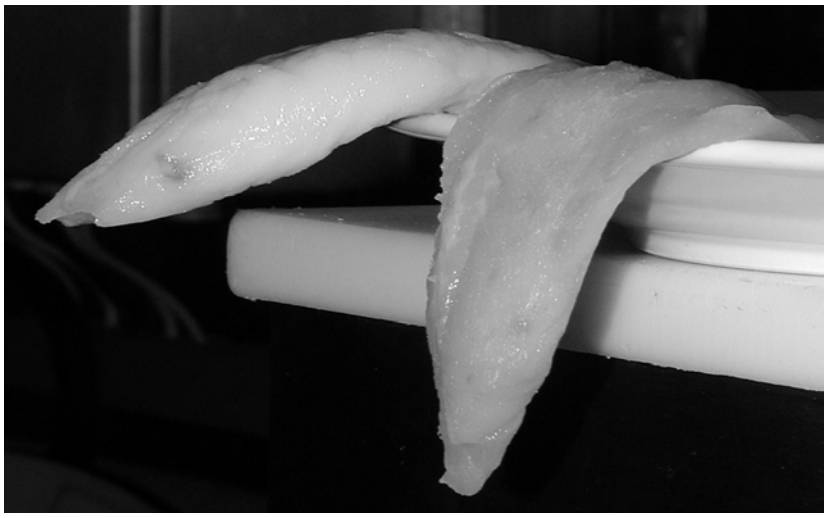

Figure 4.39: Visual appearance of Redfish fillets after different thawing at 200 MPa (left) and conventional thawing at 0.1 MPa (right).(Schubring *et al.*, 2003)

4.2.2.4 Evaluation of processing effects on colour and proteins

One of the most obvious quality changes caused by high pressure thawing was in colour. Discoloration as the consequence of pressure treatment was widely observed. Colour differences was measured on both the high pressure and conventionally thawed raw or cooked samples (shown in Table 4.16). These differences indicate a strong influence of high pressure treatment. Especially in raw fillets, significant colour changes (verified by very strong colour differences ΔE*) can be seen mainly caused by a strong increase in lightness (L*). Smaller but also uniform changes were monitored for both redness (decrease) and yellowness (increase). When thawing tuna using high pressure (50 to 150 MPa), an increase in all colour values (L*, a*, b*) was observed by Murakami *et al.*, (1992). This increase was stronger with increasing pressure. Furthermore, colour changes seem to be influenced by temperature, as lower temperatures caused stronger changes under the same pressure. These results were in agreement with the results of Yoshioka *et al.* (1996) on high pressure thawed carp muscle (100 to 300 MPa). Higher L* and b* values and a lower a* value were observed compared to conventionally thawed muscle. The differences were increased with increasing pressure. On the other hand, no visually recognisable colour changes have been reported for meat (Okamoto and Suzuki, 2001; Zhao *et al.*, 1998), while Massaux *et al.* (1999a) observed the same trends as seen here for pressure thawed pork at 200 MPa.

Table 4.16: Colour changes indicated by colour differences between high pressure thawed and conventionally thawed raw and subsequent heated fish fillets.

Species	Raw fillet				Heated fillet			
	ΔL*	Δa*	Δb*	ΔE*	ΔL*	Δa*	Δb*	ΔE*
Redfish	25.32	-1.38	2.66	25.50	0.67	0.25	-0.11	0.72
Salmon	20.45	-0.17	4.53	20.95	5.28	-4.53	-4.96	8.54
Whiting	21.15	-1.70	2.67	21.39	1.99	-0.31	-1.94	2.80
Rainbow trout 1	18.45	-3.28	1.48	18.80	-3.99	-3.60	-1.04	5.47
Rainbow trout 2	27.46	-7.44	0.01	28.45	6.86	-7.60	-5.68	11.71
Haddock	23.97	-1.55	3.80	24.32	-	-	-	-
Cod	15.84	-1.3	2.22	16.05	6.95	-0.05	-1.02	7.02

After heat treatment, the influence of high pressure on colour was obviously much smaller (Table 4.16). Compared to conventionally thawed fillet, L* increased from slight to high values except for one rainbow trout sample. Also except for redfish, a* and b* decreased. The colour difference ΔE* between cooked fillets previously thawed either by high pressure treatment or conventionally, varied from negligible (redfish) to significant (rainbow trout 2). Since the fresh-like character can be affected by high pressure, the changes in colour must be taken into consideration when applying high hydrostatic pressure to support the thawing of fish. This is particularly the case when thawed raw fish flesh loses its transparency (Yoshioka *et al.*, 1996). However, the colour changes induced by high pressure are marginal after heat treatment is applied, and therefore the post processing step must be considered during ongoing investigations to ensure optimal final product quality.

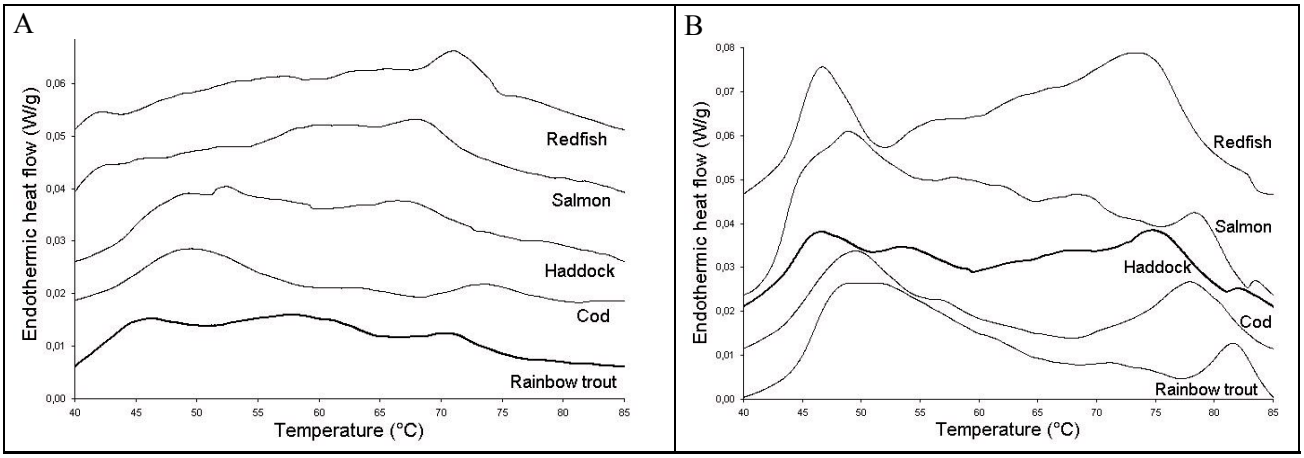

Figure 4.40: PE-DSC 7 measured curves of high pressure thawed (A) and of atmospheric pressure thawed (B) fish fillet

To comparatively evaluate the effect of high pressure thawing on proteins the DSC data for white fish muscle of both pressure thawed and conventionally thawed samples are presented in Figure 4.40. Independent of the species, there are remarkable differences between differently treated samples. Whereas the conventionally thawed muscles show pattern comparable to largely native proteins of fresh fish muscle, the pattern of high pressure thawed muscles confirm a denaturation of the muscle proteins as a result of applying high pressure. Single peaks, representing the different protein fractions like myosin, sarcoplasmic proteins and collagen, and actin (located in this

direction with increasing temperature and seen in curves of conventionally thawed muscle) disappeared almost completely in high pressure thawed samples. This behaviour, caused by denaturation, could explain the differences in texture and water binding capacity seen in the differently treated samples. These observations are in agreement with earlier reports (Angsupanich and Ledward, 1998). However, changes in pattern shown by Yoshioka *et al.* (1996) for high pressure thawed carp muscle were not as strong as in this study. As reported by Angsupanich and Ledward (1998) for fresh cod samples treated at 200 MPa for 20 min, almost all the myosin peak had disappeared. As the pressure increased further to 300 MPa, it was apparent that many of the sarcoplasmic proteins and actin were denatured.

4.2.2.5 Treatment effects on water loss and pH value

Water binding was characterised by measurements of drip loss during thawing and water loss after thawed samples were compressed to 75%. The drip loss may be reduced when thawing is assisted by high pressure, compared to thawing at atmospheric pressure, particularly for redfish, haddock and whiting (Figure 4.41). On the other hand, for salmon and rainbow trout, the same tendency was noted for differences between both treatments but was not significant, whereas for cod the thaw drip was slightly lower in conventionally thawed fillets.

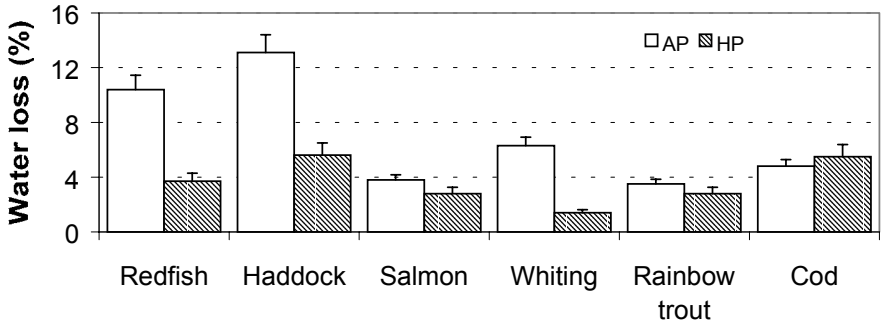

Figure 4.41: Thaw drip during thawing at 200 MPa and conventional thawing at 0.1 MPa.

However, when expressible moisture was determined by the compression method (a modified filter paper press method), the water loss for raw fillet was markedly higher in samples thawed under high pressure compared to those conventionally thawed (Figure 4.42). This result can be explained by a higher mass fraction of water remaining in the matrix after pressure-assisted thawing, resulting in comparatively high water loss caused by subsequent compression. The influence of the thawing treatment on the water holding behaviour of thawed-then-heated fillets was not completely clarified. While in redfish and salmon high pressure assisted thawing reduces the amount of expressible moisture, it increases in cod, rainbow trout and whiting. Thus, the reasons for these differences in water-holding capacity need further observation in which also mass changes at the single processing steps should be considered. The water loss during conventional and pressure assisted thawing of frozen seafood (Spingy dogfish and scallops) was investigated recently (Rouillé *et al.*, 2002). According to the authors the drip volume from thawing as well as drip volume from subsequent

cooking was significantly reduced by pressure-assisted thawing at 150 MPa in comparison to the conventional thawing process.

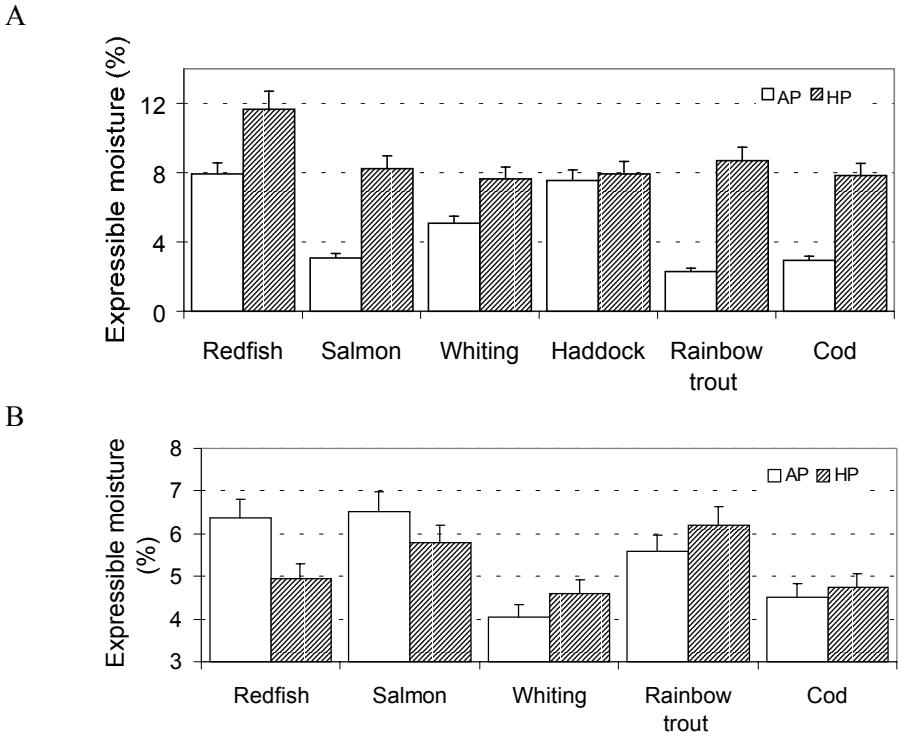

Figure 4.42: Water loss of fish fillets. A: Thawed at 0.1 MPa (AP) or at 200 MPa (HP). B: Heated after thawing at 0.1 MPa (AP) or at 200 MPa (HP).

Moreover, apart from differences in the physiological state of the fish, different pH values can be considered as a reason for variations in water binding. High pressure assisted thawing was connected with a slight increase in pH value independent of the fish species (Table 4.17). In this sense, it may be noted that self-ionisation of water is promoted by pressure. Furthermore, there is no example of ion formation from neutral molecules that is not associated with volume contraction (Tauscher, 1995). To this date, no further data has been found on the influence of high pressure on the pH of thawed fish compared to conventionally thawed fish.

Table 4.17: Influence of thawing at 200 MPa (HP) and 0.1 MPa (AP) on pH values.

Species	**pH values**	
	HP	AP
Redfish	6.62 ± 0.2	6.52 ± 0.3
Salmon	6.63 ± 0.1	6.56 ± 0.2
Whiting	6.22 ± 0.2	6.13 ± 0.1
Cod	6.78 ± 0.1	6.75 ± 0.1
Rainbow trout	6.39 ± 0.2	6.32 ± 0.2

4.2.2.6 Effect on microorganisms and parasites

The total viable count (TVC) as well as the number of specific spoilage microorganisms were significantly decreased in high pressure thawed fillets (Table 4.18). As pointed out by Cheftel *et al.* (2000), the risk of detrimental phenomena and microbial growth is markedly reduced by applying high pressure treatment for thawing. A shelf-life extension of two days was also obtained after high pressure treatment of 150 MPa for 10 min at 5 °C as compared to unpressurised vacuum-packed salmon. A further extension of the shelf-life was reached when salmon was subjected to high pressure treatment in the presence of a modified atmosphere, 50 % CO_2 and 50 % O_2 (Amanatidou *et al.*, 2000). Regarding the stability diagram of proteins and also for enzymes and microorganisms (Heremans, 2002), the state of native protein is stabilised at certain temperature-pressure combinations and can be affected by low temperatures, high temperatures or high pressures resulting in an elliptical shape. Cold denaturation of proteins might occur during pressure-assisted thawing of animal tissues at subzero temperatures. However, the preservation effects of high pressure (inactivation of unwanted microorganisms and enzymes) should be supported by low temperatures. To prove this assumption a detailed study on high pressure inactivation of *Listeria innocua* is presented in section 4.2.3 as an example.

Table 4.18: Influence of thawing treatment (HP: Thawing at 200 MPa; AP: Thawing at 0.1 MPa) on microbiological count (detection limit-50 CFU/g)

Species	**Total aerobic count (CFU/g)**		**Shewanella (CFU/g)**	
	HP	AP	HP	AP
Redfish	5.2×10^2	2.7×10^3	nd	nd
Salmon	nd	1.6×10^3	nd	nd
Whiting	nd	1.9×10^3	nd	nd
Rainbow trout	nd	7.2×10^3	nd	nd
Cod	nd	6.7×10^4	nd	3.3×10^2

nd-not detectable

Commonly frozen storage for not less than 24 h is required to ensure inactivation of parasites like nematodes in fresh fish or fish products. To evaluate the potential of high hydrostatic pressure to inactivate parasites, a set of experiments was carried out at 10 °C. For the experiments the nematodes were separated from the guts of fresh fishes and for each sample about 100 living exemplars were packed directly in a flexible sterile bag filled with digestive solution and then forced to high pressure treatment at 100 MPa (15 and 60 min), 150 (1, 5, 15, 30 and 60 min) and 200 MPa (1, 5, 15, and 30 min). After high pressure application the status of the nematodes was evaluated by using UV light and by visual inspection of their mobility. According to Karl *et al.* (1995) a fluorescentic white colour of the larvae (maybe due to protein denaturation) in a UV chamber indicates an inactivation of the nematodes. Additionally the mobility of the high pressure treated larvae was visually evaluated in Petri dishes and controlled after 12 h storage of the samples at room temperature, to estimate possible recovery of the nematodes.

Figure 4.43 gives an example for comparative evaluation of the colour changes in a UV chamber. The nematodes pressurised at 150 MPa (30 min) are fluorescentic white, while the untreated sample remains inconspicuous. The number of white coloured nematodes and number of active/moving nematodes after storage are given in Table 4.19. After a high pressure treatment at 100 MPa the nematodes did not significantly change their colour and most of them were still active after 12 h. Increasing pressure led to higher inactivation rates and complete inactivation after 60 min holding time at 150 MPa and pressure treatment 200 MPa for 5, 15 ad 30 min.

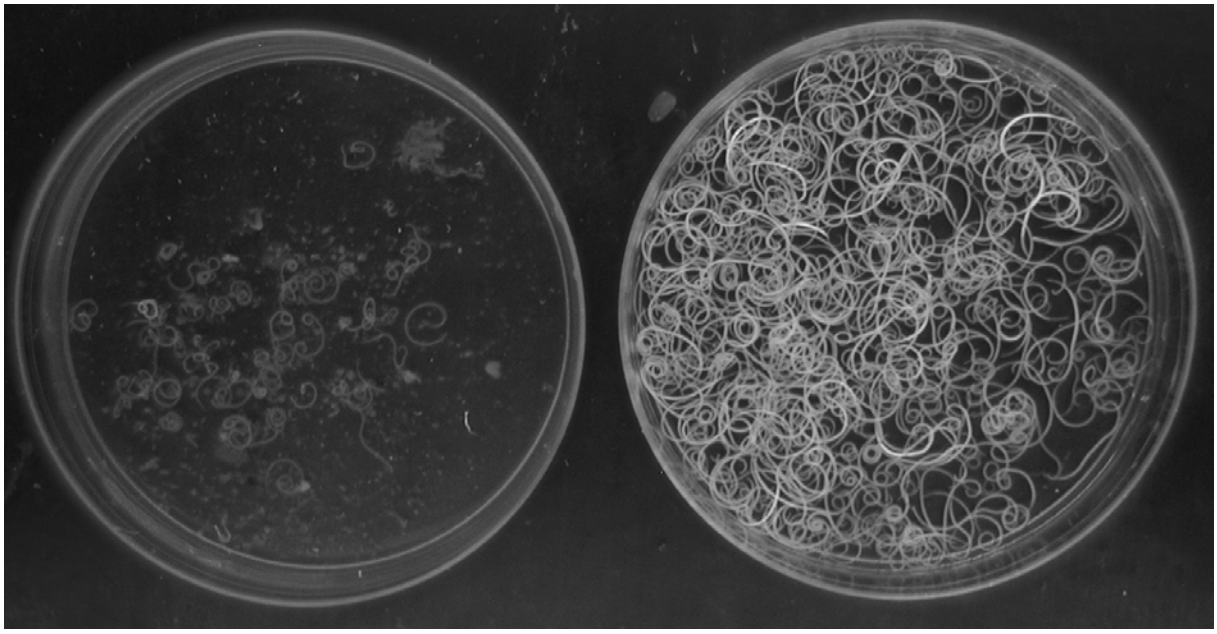

Figure 4.43: Viability evaluation by colour changes of nematodes in a UV chamber. Image of the control sample on the left; and pressurised sample (150 MPa, 30 min) on the right hand side.

Table 4.19: Evaluation of viable nematodes by inspection in UV chamber and detection of mobility after 12 h storage in digestive solution at room temperature.

Number of nematodes treated	Pressure (MPa)	Treatment time (min)	Nematodes with fluorescentic colour	Active/moving nematodes after 12 h
111	100	15	4	48
100	100	60	2	29
69	150	1	4	33
123	150	5	6	14
110	150	15	13	11
140	150	30	21	2
70	150	60	15	0
58	200	1	13	1
35	200	5	33	0
103	200	15	86	0
83	200	30	75	0

However, the differences of colour changes and the count of active nematodes are obvious. Since the indication of the state of the nematodes by colour changes lead to underestimation of the results

other methods must be explored for accurate investigation. Furthermore, the infective potential has to be considered in further studies. Nevertheless, the data obtained here are in agreement with a study on parasites (*Trichinella spiralis*) in pork meat (Nöckler *et al.*, 2001). According to the authors the larvae were affected at 150 MPa and completely inactivated at pressures of 200 MPa in a temperature range of 5 to 25 °C and pressure holding times equal or higher than 10 min.

4.2.3 Impact of high pressure-low temperature processing on microorganisms

4.2.3.1 Inactivation kinetics of Listeria innocua

The effect of high hydrostatic pressure on the inactivation kinetics of *Listeria innocua*, as an index for the pathogen *Listeria monocytogenes* was studied at subzero and elevated temperatures. An empirical model (Ananta *et al.*, 2001) was applied to model the inactivation kinetics. The non-linear regression method yielded a reaction order *c* of 1.5. The results of the performed regression analysis on the bacteria inactivation in Ringer solution are shown in Table 4.20. In order to facilitate the applicability of the model, it was more practical to use only one setting for the reaction order. The kinetic parameters derived from the model are, however, not applicable to systems with initial viable counts markedly deviated from the ones used in this study. This limitation results from the formulation of the model (eqn. 3.19), in which the regressively derived rate constant depends on the given initial viable count.

Table 4.20: Parameters and statistical analysis of the non-linear regression from the experimental curves for *Listeria innocua* in Figure 4.43. (FSE: Fit Standard Error)

T [°C]	p [MPa]	log N_o [CFU ml^{-1}]	k' [s^{-1}]	ln k' [s^{-1}]	FSE
-30	200	9.43	3.06e-4	-8.09	1.35
	250	9.43	1.11e-3	-6.80	1.43
	300	9.43	6.89e-4	-7.28	0.50
-20	200	9.40	5.11e-4	-7.57	1.07
	250	9.40	1.14e-3	-6.78	0.78
	300	9.40	1.89e-3	-6.27	0.57
-10	200	9.41	3.06e-4	-8.09	0.38
	250	9.41	7.96e-4	-7.14	0.90
	300	9.41	1.59e-3	-6.44	0.18
0	200	9.38	3.73e-4	-7.89	0.52
	250	9.38	1.07e-3	-6.84	0.37
	300	9.38	2.78e-3	-5.89	0.66
5	200	9.52	3.17e-4	-8.06	0.42
	250	9.52	7.69e-4	-7.17	0.45
	300	9.52	1.86e-3	-6.29	0.08
10	200	9.04	1.53e-4	-8.79	0.29
	250	9.04	7.58e-4	-7.18	0.21
	300	9.04	2.27e-3	-6.09	1.14
40	200	9.43	1.29e-4	-8.96	0.11
	250	9.43	9.83e-4	-6.92	0.12
	300	9.43	2.04e-3	-6.19	0.86

The experimental and calculated kinetic curves from the inactivation experiments with the microbes suspended in Ringer solution are presented in Figure 4.44. Since the initial bacterial counts were slightly different in each case, the final level of reductions were attained when indicated relative to N_0 were divergent.

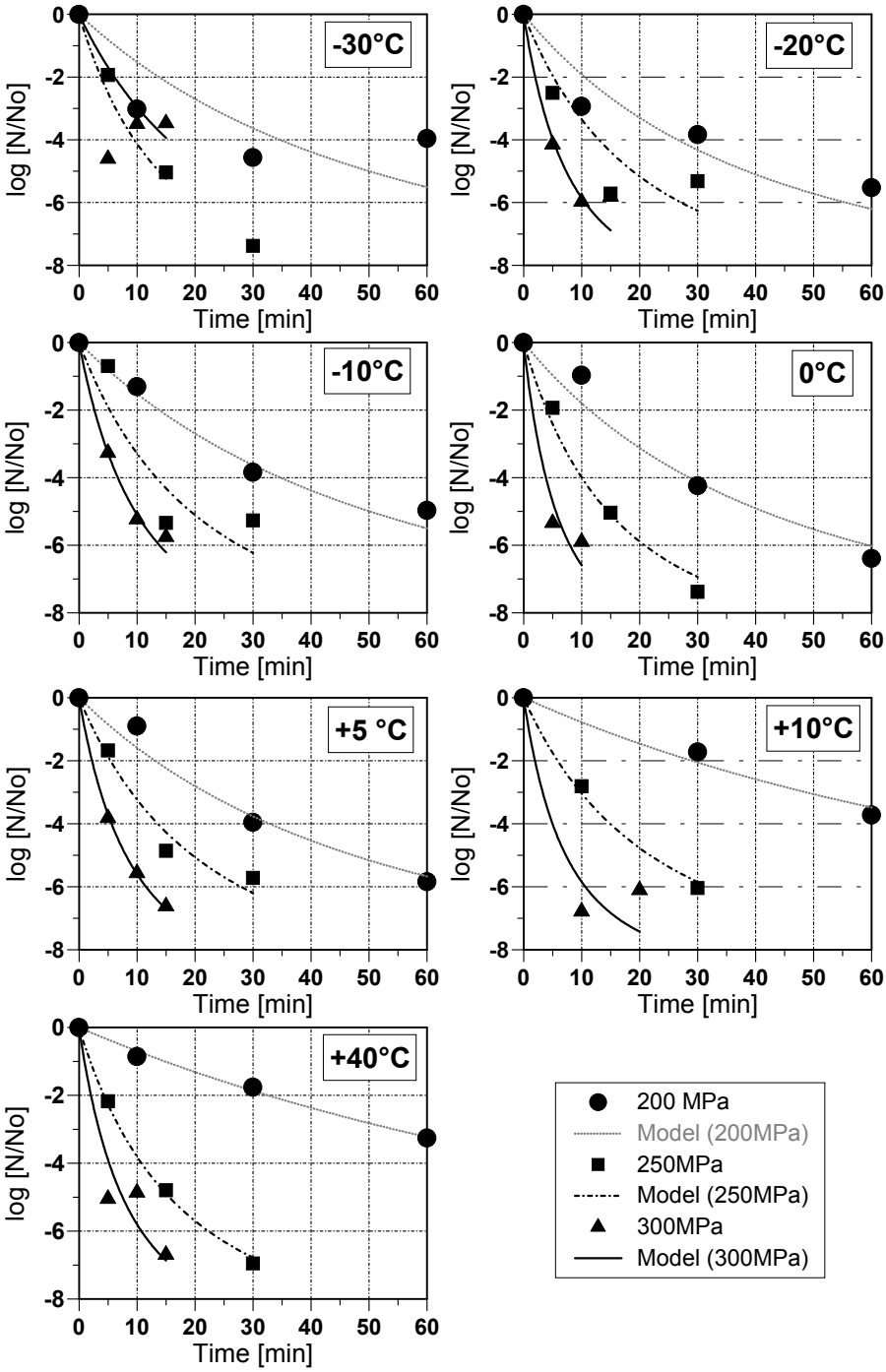

Figure 4.44: Inactivation kinetics of *Listeria innocua* in Ringer solution at subzero and elevated temperatures at different pressure levels. The ratio N/No is plotted logarithmically versus time. Lines obtained by fitting the model (eqn. 3.19) to the experimental data (symbols). The model parameters are given in Table 4.20.

According to the experimental data from the kinetic studies, it was shown that the inactivation curves exhibited a non-linear behaviour. From the results it can be seen that an increase of the pressure level applied led to higher inactivation rates. A pressure treatment at 200 MPa, for 60 min at 0 °C resulted in a 6 log cycle reduction of *Listeria innocua*, but the same reduction was obtained after 10 min when applying 300 MPa at 0 °C. However the inactivation curves showed no pronounced shoulder formation and the tailing effect was mainly noticeable at low pressures (200 MPa). It seems that lower temperatures shifted the inactivation rate to higher levels with a maximum at 0 °C. An irregularity of the temperature and pressure effectiveness was seen at –30 °C for 250 and 300 MPa, resulting in the assumption that the physical state of water (liquid or solid) may influence the inactivation kinetics under the tested conditions.

4.2.3.2 Bacteria inactivation in frozen solutions

Since formation of ice is known to reduce the water activity and lower water activity is known to induce protective effects on microorganisms (Smelt *et al.*, 2002), it could be expected that a change of the physical state of water may result in changes of pressure sensitivity of *Listeria innocua*. Consequently, a set of experiments was carried out starting from the frozen or the liquid state of the medium, but applying comparable process parameters along the phase boundary. Figure 4.45 (a, b) shows the comparison of the different inactivation kinetics. A reduction of about 6 log cycles was obtained after pressure treatment for 10 min at 300 MPa in both cases (frozen and liquid state). Contrary to expectations, the inactivation rate was slightly enhanced in the frozen state at 200 MPa and 30 min, but the final reduction values are similar for the frozen and the liquid matrices. As a result, it can be stated that the hydrostatic principle is not affected by the formation of ice, but it is likely that the observations may differ with size of the sample, initial working temperature and the media in which the microorganisms are suspended.

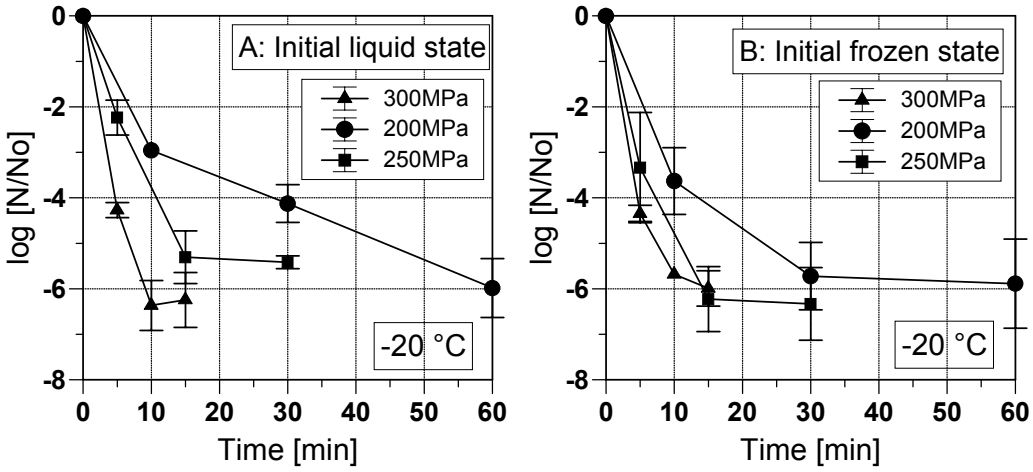

Figure 4.45: Effect of the initial physical state of water (liquid, solid) on the high pressure inactivation kinetics of *Listeria innocua* suspended in Ringer solution.

4.2.3.3 Influences of p,T-*combinations on the rate constant*

Using the kinetic data from the regression analysis (Table 4.20) a *pTk*-diagram was constructed to show the influence of pressure and temperature on the rate constant k'. The generated data are shown in Figure 4.46.

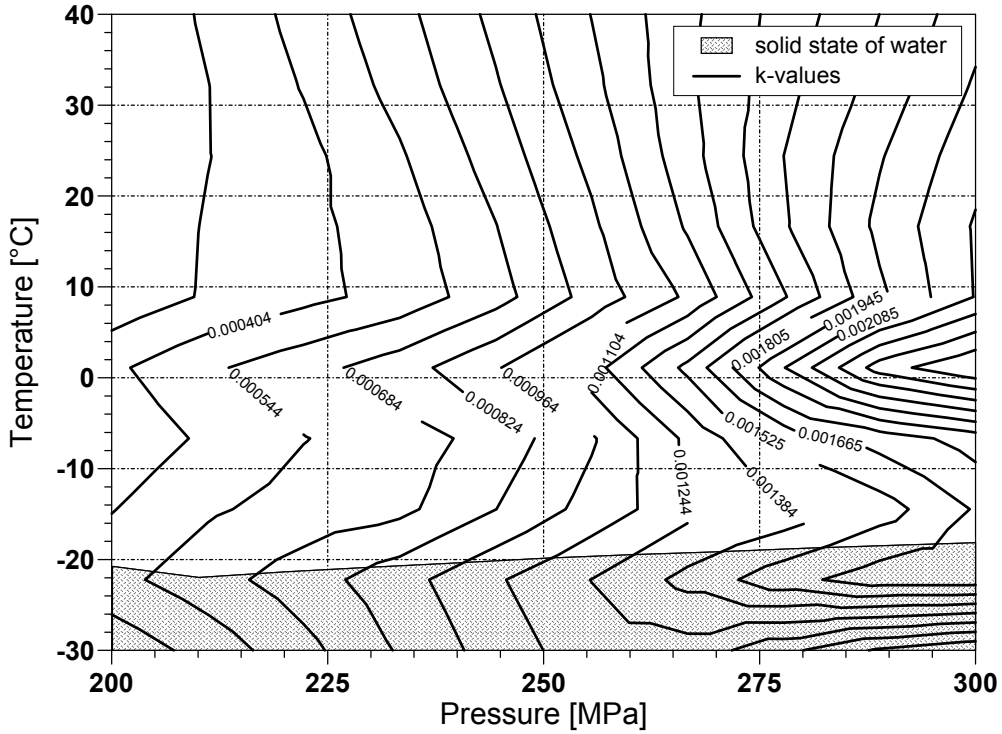

Figure 4.46: Effect of solid-liquid transition on the rate constant of *L. innocua* inactivation. The lines indicate *p,T*-combinations with constant inactivation rates.

As expected from the inactivation kinetics (Figure 4.44) the pressure level (within the range of consideration) affected the rate constant more than the temperature, leading to a more vertical slope of the curves in the *pTk*-plot. At 0 °C there is a significant change of the slope of the rate constant indicating accelerated inactivation at all pressure levels between 200 and 300 MPa. By implementing the phase boundary of pure water into the *pTk*-diagram of the *L. innocua* inactivation in Ringer solution, an effect of the physical state of water can be assumed to describe the divergent slope of the k-values near the phase transition line. However, this effect (more pronounced at pressures above 250 MPa) mainly derived form the experimental data in which the inactivation kinetics show irregular behaviour at –30 °C (Figure 4.44) and the subsequent estimation of the rate constant based on these data. The results of the experimental sets carried out to evaluate the protective effect of the solid state of water on *Listeria innocua* didn't support the assumption suggested above. Further investigations are required to provide more details on the effect of the solid state of water on the mechanical force transmission of high hydrostatic pressure and other mechanisms probably affecting the inactivation kinetics of microorganisms.

4.2.3.4 Pressure resistance of Listeria innocua *in food matrix*

The comparative evaluation of the effect of the matrix on the inactivation kinetics is shown in Figure 4.47 Though similar final levels of reductions were observed for both Ringer solution and baby food for the same temperature and pressure conditions, it was easier to inactivate the microorganisms suspended in baby food which had an initial concentration of ~10^7 CFU/ml as against ~10^9 CFU/ml in Ringer solution. The reason for this could be because of the pH of baby food (5.3) being lesser than that of Ringer solution (pH 6.75). However at low pressure (200 MPa) the inactivation curves showed pronounced shoulder formation at 10 °C and 0 °C when *L. innocua* was inoculated in baby food, as against Ringer solution. An explanation for this could be that the initial concentration suspended in the Ringer solution was two log cycles higher than that for baby food as mentioned before. The reduction in the former was therefore drastic in the first few minutes of treatment and then slowed down. It was also possible that a certain portion of the microorganisms were inactivated during the pressure build-up time itself, the effect of which was not taken into account in the present study.

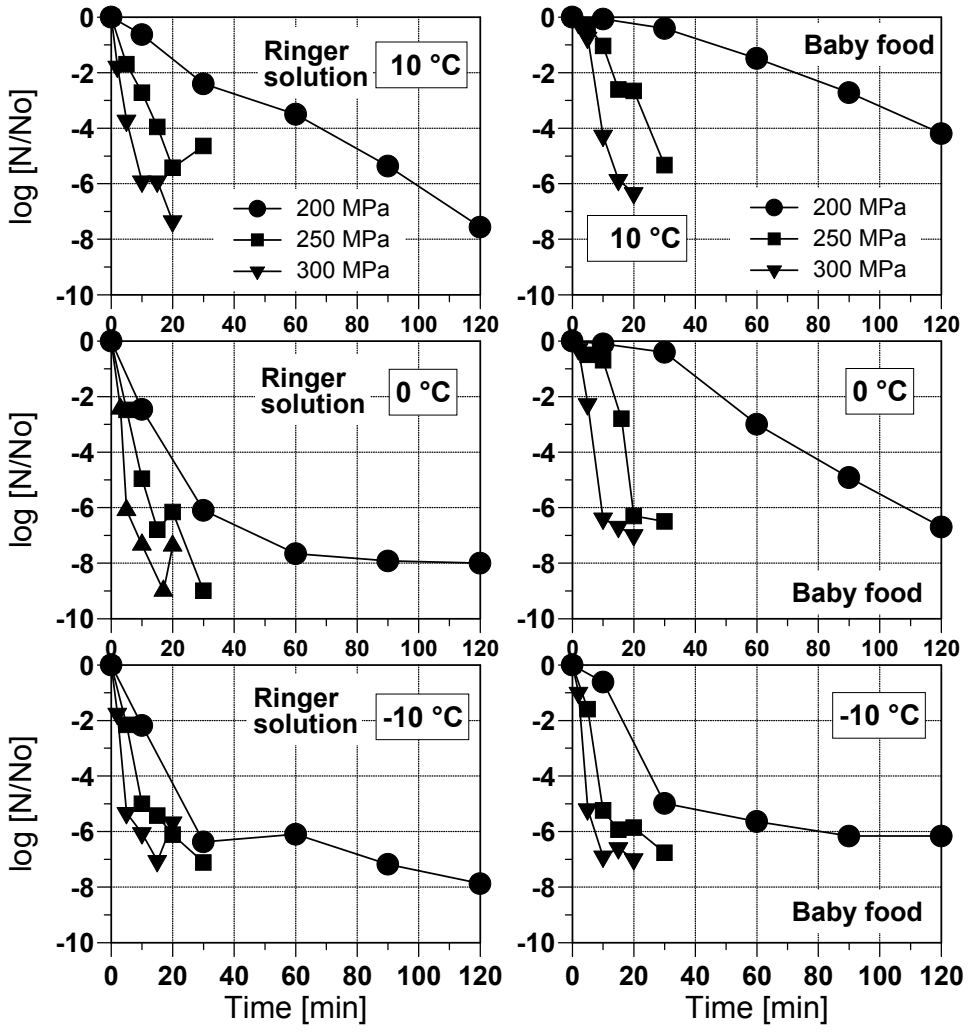

Figure 4.47: Comparison of inactivation kinetics of *Listeria innocua* in Ringer solution and baby food (carrot-potato puree) at 3 different pressures and temperatures. The ratio N/N_0 is plotted logarithmically versus time.

At 200 MPa and 10°C, low inactivation rates was observed even after 30 min whereas a combination of 300 MPa and –10 °C produced complete inactivation within 10 minutes. The inactivation at 0 and –10°C was in both cases greater than for that for elevated temperature and the highest inactivation rates was obtained at 0 °C for Ringer solution and –10 °C for baby food. Such a behaviour of the dependence of the inactivation on temperature corresponds with the dependence of protein denaturation with temperature (Heremans and Smeller, 1998) which goes to suggest that denaturation of proteins in the cell membranes of the microorganisms could be one of the major mechanisms causing inactivation. It can thus be expected that the high pressure supported phase transition processes which are normally associated with sub-zero temperatures can also benefit from the considerable amount of inactivation attained during the process. For example, thawing of a frozen product at 250 MPa for 40 min can cause complete microbial inactivation of the tested microorganism, *Listeria innocua* besides shortening the thawing time.

5 SUMMARY AND CONCLUSION

5.1 Modelling of high pressure supported water-ice transitions

This thesis provides a detailed study on modelling high pressure supported water-ice transitions in plant tissues. The first step in modelling of phase transitions was to identify the phase boundaries of the tissue water in potato during pressure supported freezing/thawing processes. Two parameters were primarily used to indicate the phase transitions: a variation in temperature evolution (temperature plateau) and a changing pressure level due to enthalpy changes and density changes. The melting curves of ice I, ice III and ice V were described by adapting a model for pure water according to Wagner *et al.* (1994), fitting precisely the experimental data. The next step was to evaluate and to model high pressure-supported freezing and thawing processes also considering crystallisation and melting of different ice polymorphs (ice I, ice III). The starting point in developing the model for calculating freezing/thawing times of plant based food materials was to recalculate the obtained experimental curves during freezing and thawing of potato at ambient conditions. The phase transition processes was modelled by introducing temperature dependent apparent specific heat c_P and thermal conductivity λ in the vicinity of the freezing/melting point into heat balances of the finite difference scheme (Marek and Götz, 1995). Data for temperature dependent c_P and λ of potato tissue at ambient pressure are available in literature from Cleland and Earle (1984). Modifications of these data were used to fit correctly the experimental freezing/thawing curves. Fitting the experimental freezing/thawing curves obtained during high pressure treatment made necessitated an additional modification of the values of the heat capacity c_P and the thermal conductivity λ of potato tissue, considering the decreasing freezing/melting point and the reduced latent heat (determined for potato tissue using DSC at 0.1 MPa). For the calculation further adaptation was necessary because no thermophysical data for potato at high pressure conditions were available. Therefore, continuous functions of temperature were used to empirically model the behaviour of either c_P or λ above and below the temperature level of the pressure dependent freezing/melting point. In the case of λ the cumulative Weibull distribution was used. An approximation of the apparent heat capacity c_P was obtained using the density Weibull distribution.

Freezing to ice I was calculated in good agreement with the experimental results below 209 MPa. In the pressure range between 209 and 240 MPa, no predictions have to be assumed for the ice I or ice III crystallisation, as the experimental results show different crystallisation steps for experiments run at similar pressure levels. When taking into consideration the experimental data obtained and data reported by (Evans, 1967b) the formation of ice I seems to be favourable in the first step. In this region no direct or clear correlation can be found between the freezing and phase transition times and the ice modification crystallised. An accurate control on bath temperature (to better control the temperature gradient) and the sample wall temperature (where the cooler point is reached, then, where nucleation starts) must be ensured, to better define the metastable area shown

here. However, high convergence of the experimental and the calculated data were obtained using the developed model. From a pressure level of 255 MPa and up to 300 MPa, the prolongation of the ice I melting curve as described for pure water (Bridgman, 1912) and a mixture of water and nucleating agents (Evans, 1967a) was just partly observed during freezing of potato tissue. In this case, a substantial supercooling (up to temperature levels of 20 °C) occurs, and ice III starts to nucleate at different temperature levels, depending on the pressure applied. A substantial degree of supercooling was always obtained before the nucleation of a higher ice modification (ice III, ice V). The higher or lower degree of supercooling depends on the thermodynamics of each experiment, and one must take into account parameters like: temperature of the sample at the surface (start of nucleation), temperature gradient between freezing point and bath temperature (cooling rate), thermophysical properties of the sample (pressure level), etc. The difference between the nucleation and the freezing temperatures (supercooling degree) can be assumed as a kinetic controlled phenomenon, in which the nucleation has not yet started when the freezing temperature is reached, although the thermodynamics will lead to such a nucleation, but an energetic barrier is still to be crossed. With respect to the degree of supercooling, a significant decrease in the phase transition time was reached when ice III is obtained. The high degree of supercooling before freezing to ice III is comparable to that of pressure-shift freezing and therefore positive effects to the processed food can be expected with regard to crystal size and distribution. This greater degree of supercooling together with the results of the phase transition times, indicate the consistency of the results, as shorter phase transition times are reached for higher degrees of supercooling. Shortening of phase transition times due to higher degree of supercooling was also reported for pressure shift freezing of model food (tylose-gel) (Denys *et al.*, 1997) and emulsions (Levy *et al.*, 1999).

When freezing, supercooling takes place because the kinetics of nucleation control the thermodynamics of the process; when thawing occurs there is no additional energy barrier (comparable to supercooling) that controls the process, and consequently a validation of the model was performed by calculation of the thawing times for different sample sizes using comparable model parameters in each pressure level applied. In the case of the thawing experiment the heat transfer coefficient has to be considered since the samples where inserted to a large vessel allowing for convection on the sample surface. The heat transfer coefficient was not considered in the freezing experiments, because there the sample was inserted to a sample holder fitting to the vessel and therefore only heat conduction was assumed. The calculated thawing curves fit well with the experimental curves for all sample sizes investigated. The thawing times were significantly reduced with increasing high pressure when compared to thawing at ambient pressure holding the surrounding medium temperature constant at 10 °C. It was also shown that the effect of the sample size decreases with increasing pressure and therefore with increasing effective temperature gradient ΔT. Furthermore, the prolongation of the ice I melting curve was clearly observed as described for pure water (Bridgman, 1912). However, the first non-homogeneity was obtained at a pressure level of 300 MPa, leading to extended thawing times compared to pressure-assisted thawing at 200 and 250 MPa. At 300 MPa the sample temperature enters the nucleation area of ice III (explained in the

following section). According to the results obtained the mechanisms during the pressure assisted thawing experiment can be explained by phase transition steps schematically indicated in Figure 5.1. During the pressurisation step the frozen sample reaches the melting curve of ice I and the sample surface liquefies while the sample centre remains in the frozen state (ice I). At a sample temperature (centre) of about –40 °C the nucleation area of ice III is entered and the water near the ice front of the sample (temperature near –40 °C) starts to form ice III indicated by sudden temperature increase. All liquid parts of the sample with a temperature lower than the freezing point of ice III under the given pressure also start to convert to ice III. Since overheating of ice seems to be impossible and the transformation of ice I to ice III was described as explosive (Bridgman, 1912), the frozen sample centre also is assumed to convert into ice III at the same time (probably initiated by the ice III-crystals at the sample surface). Consequently, the sample reaches the melting point of ice III uniformly accompanied by a sudden pressure drop, due to density decrease ($\rho_{ice\ I} < \rho_{liquid} < \rho_{ice\ III}$). Here, the sample (now transformed to ice III) continues the melting process since the surrounding medium temperature remains above the melting temperature of ice III and the process is accompanied by a density increase. However, the *pT*-coordinates where formation to ice III is initiated during pressure-supported thawing defines a critical pressure level p_c, which has to be considered when designing high pressure supported phase transition processes.

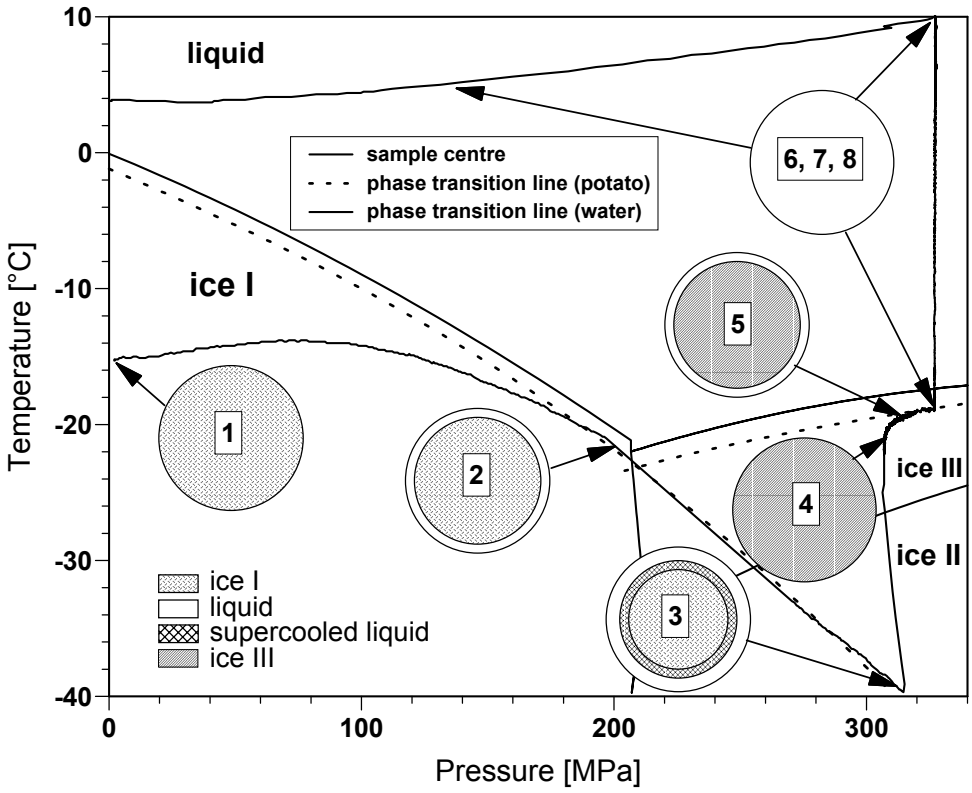

Figure 5.1: Scheme of proposed phase transition steps during pressure-supported thawing above 300 MPa ($p>p_c$). Sectional views at different processing steps are indicated by the circles on the *pT*-diagram of water. 1: Initial frozen state of the sample (ice I); 2: Melting at the surface; 3: Liquid layer reaches the nucleation point of ice III; 4: Complete transformation to ice III, initiated by the supercooled liquid layer; 5: Melting at the surface; 6: End of phase transition; 7: Warming of the thawed sample; 8: Pressure release.

5.2 Definition of metastable states in the phase diagram

The freezing/thawing curves, together with the corresponding pressure curves (both parameters *p* and *T* plotted versus time) give the different singular points of the modified phase diagram for potato, presented in Figure 5.2. From a pressure level of 209 MPa (triple point liquid/ice I/ice III), a prolongation of the ice I melting curve was observed, as the temperature of the plateau (part of the freezing/thawing curve indicating the freezing/melting point) was coincident to an extrapolation of the ice I melting curve, and not coincident to that of ice III melting points. These results gave an experimental prolongation for potato of the ice I melting curve in a metastable zone, as shown in Figure 5.2.

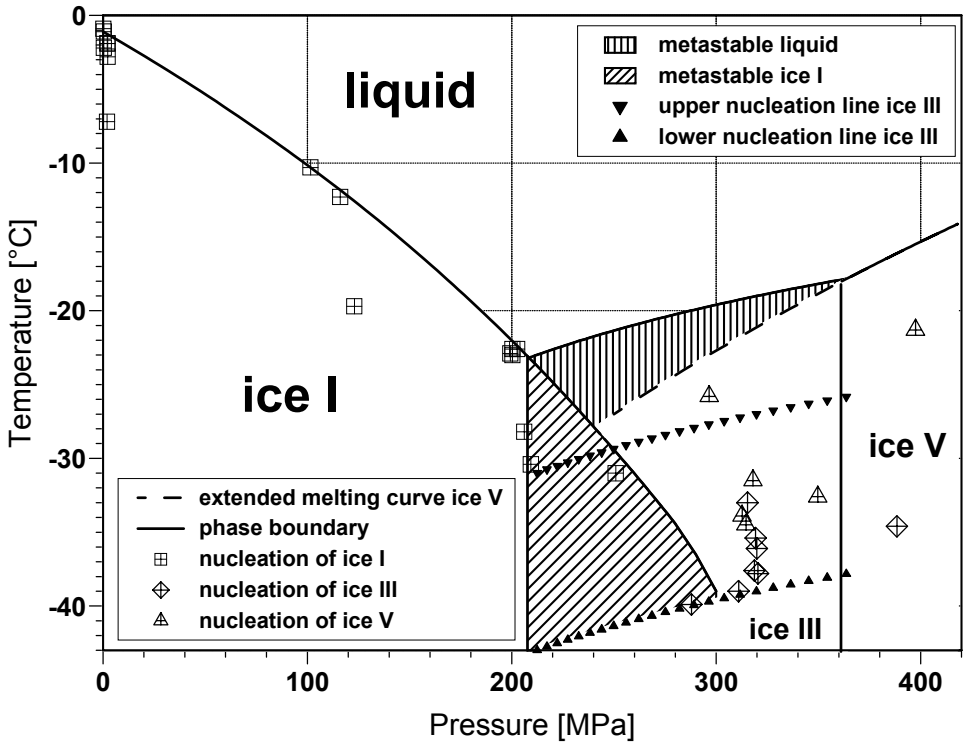

Figure 5.2: Selected freezing and nucleation points in the modified phase diagram for potato and metastable phases associated with the obtained experimental data. The range of ice III nucleation is defined between the upper and the lower nucleation line. The area of metastable liquid (long resting) indicates a region where no crystallisation was observed. Metastable liquid was also observed during pressure-supported thawing experiments, where ice I melted along the prolonged melting curve of ice I within the region of thermodynamic stability of ice III. The occurrence and the range of the metastable states is dependent on the direction of the phase transition. The indicated metastable state of ice I is defined for thawing, while the indicated metastable liquid is defined for cooling and storing.

On the other hand, the nucleation temperatures shown define the extent of the supercooling reached for each pressure level. This supercooling is higher for ice modification III and V arriving at values of around –20 °C. The differences of the experimental ice III nucleation temperatures, when compared to the better fit for ice I indicates the existence of a non-stable area between the indicated pressure levels (209 to 240 MPa).

Three different metastable phases are likely to be found in the modified potato phase diagram. As a definition, a metastable phase is one that exists in a pressure – temperature combination in which another phase is thermodynamically stable. Given the different metastable phases related to high pressure-supported processes, their definitions are given as follows:

- Metastable phase A (transient supercooled liquid): when a freezing process is carried out and the supercooling phenomenon appears, until the nucleation line for ice I or ice III is reached, we experimentally still have liquid phase, at temperatures lower than the theoretical phase boundary; in this case, a metastable liquid is reached.

- Metastable phase B (long resting supercooled liquid): according to the results obtained, there is a "long resting" or "significantly stable" region in which the liquid phase is still retained after keeping samples in this pressure/temperature levels for more than 40 hours.

- Metastable phase C (thermodynamically non-stable solid phase): at pressures above 209 MPa, when ice modification III is already the thermodynamically stable phase, ice I is still obtained when cooling below its prolonged melting curve. This metastable area can be extended when considering the direction of the phase transition process, i.e. pressurisation of a frozen sample (ice I). This definition is also applicable to metastable ice V in the region of ice III (Evans, 1967a), since formation of ice II seems to be inhibited in this range of investigation.

According to results shown in Figure 5.2 , the position of the metastable areas, both for ice I in the ice III domain and for the long resting liquid can be defined. In agreement with results reported by Evans (1967b), another prolongation (but in the case of ice V in the domain of ice III) was experimentally obtained, and schematically represented here. In Figure 5.2, only the metastable phases B and C are represented, as the metastable phase A is present in every case when the nucleation point is below the corresponding phase transition line: in a higher or lower degree, this supercooling phenomenon is always present when carrying out a pressure-assisted freezing operation. The prolongation of the phase transition lines of both ice I and ice V into the domain of ice III leads to a certain pressure range in which it can be ensured that ice III will nucleate. In this sense, when compared to the obtained nucleation points for ice I, a high dispersion of nucleation points is observed for ice III. This dispersion allows the definition of an area (Figure 5.2) whose upper and lower lines give the limits to ensure or to avoid the nucleation of ice III. In the cooling process, to ensure the nucleation of ice III a lower temperature than the one given by the lower line must be reached, and if this nucleation is to be avoided, the temperature of the sample must be always kept above the upper line of the defined area. Therefore, the better conditions to ensure the nucleation of ice III are working between (approximately) 280 and 300 MPa, and below –40°C.

5.3 Improvement in high pressure – low temperature processes

Since the nucleation temperature at a given pressure does not seem to be a constant value, it is necessary to define a range where nucleation might occur in order to predict the required conditions

for changing the physical state of a food sample. The prolongation of the melting curve of ice I as well as of the melting curve of ice V into the region of ice III define the extent of the liquid state where no crystallisation was observed. In agreement with all obtained data for potato tissue no nucleation took place in the region of the "long resting" metastable liquid phase area where the lowest temperature is defined at the theoretical triple point of liquid/ice III/ice V (Figure 5.3). The theoretical triple point liquid/ice I/ice V can be interpreted as optimised onset point for pressure supported phase transition processes. Compared to the triple point liquid/ice I/ ice III of pure water (-22 °C, 209 MPa) the onset temperature of pressure shift freezing can be lowered to -28 °C at a pressure of 240 MPa increasing the desired supercooling by about 30%. Regarding pressure supported thawing the effective temperature gradient (sample – surrounding medium) can be increased at a pressure of 240 MPa by decreasing the melting point about 6 °C. Consequently processing times could be significantly reduced. In the case of high pressure thawing further process accelerations are realisable at pressure levels below the critical value p_c at ~ 300 MPa. Furthermore, storage of biological material at higher pressure and lower temperature than expected seems possible, affecting enzymatic and microbial deterioration without damaging effects due to crystallisation.

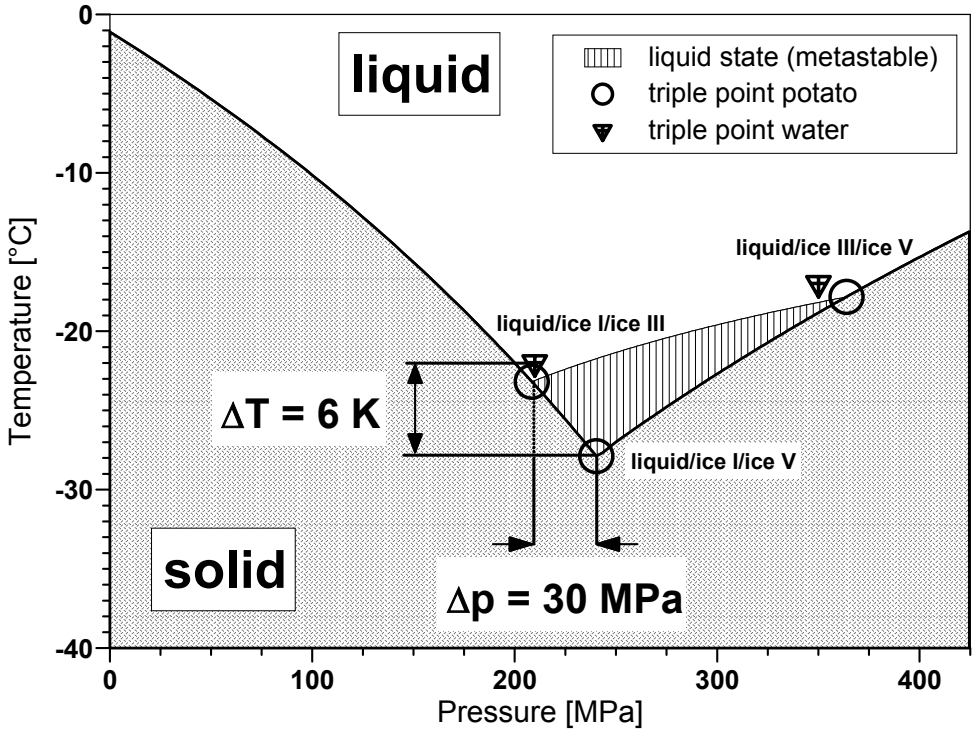

Figure 5.3: Improved onset conditions for pressure-supported freezing/storing/thawing of biological materials compared to previously accepted restrictions based on the phase boundaries of pure water.

However, controlling of pressure-supported freezing processes in combination with ice III formation is a challenge and ongoing experiments are necessary to characterise nucleation conditions. Tammann (1900) stated that the required high degree of supercooling before the nucleation of ice III starts is due to reaction inhibition by increased viscosity. The data reported by

Först *et al.* (2000) support this assumption, since the viscosity increases significantly with decreasing subzero temperatures at high pressure, especially at pressure levels above 200 MPa. To selectively form ice III Evans (1967a) suggested different agents capable of promoting nucleation. From food processing perspectives such additives are not desirable. Nevertheless, from the obtained data the intersection of the extended melting curve ice I and the lowest nucleation temperature conditions can be found to support ice III formation of the potato tissue water. The highest probability of obtaining ice III during pressure-assisted freezing seems to be around 280-300 MPa. To ensure the nucleation of ice III in different samples in a single charge, a temperature of about –40 °C must be reached. This extremely low temperature may lead to practical barriers for further industrial development of the technology. According to the experimental data generated at higher pressure levels (between 300 MPa and the triple point liquid/ice III/ice V at 360 MPa) the formation of ice V cannot be excluded.

A balance must be made when taking into account factors like the volume changes when ice modification I or III is obtained, together with overall freezing time and phase transition time. When freezing to ice I, the latent heat of fusion decreases with pressure supporting the freezing process when the surrounding temperature is lowered accordingly. On the other hand, volume changes due to liquid-solid transition of pure water increase with the pressure level starting from (approximately) +9 % at 0.1 MPa to +13 % at 209 MPa. From the point of view of volume changes, the ideal point lies near the triple point liquid/ice III/ice V (-3 %), but here formation of ice III is not guaranteed as explained before. And, while the phase transition time is shorter due to a higher degree of supercooling, the freezing time might be higher depending on the duration of the pre-cooling step. All these factors are to be considered together when a pressure-assisted freezing process is to be carried out. However, taking advantage of the “long resting” metastable liquid state requires the consideration of both, the critical process parameters in the processing concepts as well as the critical parameters regarding product quality and product safety.

5.4 Impact of process parameters on quality and safety aspects

Besides the investigation of critical process parameters the present study focused on the comparative evaluation of the impact of high pressure – low temperature processes on plant and animal tissues. The high pressure treatment of potato, as an example for plant based tissues, at 250 MPa and subzero temperatures (–28 °C) without phase transition resulted in a low deterioration of the cellular membranes. The state of the membrane was stabilised by high pressure when long holding times (more than 24 h) at subzero temperatures were applied, probably due to the (cold) inactivation of lytic enzymes. Freezing to ice polymorphs of a higher density than liquid water (especially ice III) resulted in a lower membrane damage than conventional freezing. Pressure-shift freezing and freezing to ice III resulted in an excellent preservation of textural characteristics. Short phase transitions (due to a large supercooling) as well as favourable volume changes improved the quality of biological samples. As a result, the phase change with the lowest extent of cellular

damage seems to be freezing to ice III at a pressure of about 360 MPa, close to the triple point liquid/ ice III/ ice V (specific volume change about –3 %) supporting the assumption presented above. This study points out the dependence of freezing damage on volume changes and freezing rates. Crystal transformations between ice I and other ice types demand further examination since these processes can dominate the quality of frozen biomaterials and define the maximum pressure for pressure assisted/induced thawing (around 300 MPa) as indicated by the results.

However, also the direction of the phase change must be considered since solid-solid transformation from ice I to ice III completely destroyed the original tissue matrix while the opposite direction of the solid-solid transformation had significantly minor effects on the biological material. An improvement and better control of high pressure supported phase transitions also demands detailed information on the nucleation mechanisms, since the type of the ice polymorph and supercooling influences the quality of frozen and thawed biological materials decisively. Influences of high pressure during the investigated phase transition processes on the membranes, texture and colour cannot be excluded completely. Especially the influence of enzymes on biomaterials during subsequent processing steps (after high pressure treatments) may not be neglected. More studies on enzymes, especially in their natural and partially permeabilised matrix, have to be carried out in the future to quantify these effects. However, in the case of phase transitions under pressure it is likely that the influence of the phase transition exceeds the influence of high pressure at this pressure level, regarding the quality of the material.

The evaluation of the effect of pressure-assisted thawing on an animal tissue was carried of using fish fillets as samples. It has been shown that by applying high pressure at 200 MPa the required phase transition time can be reduced by approximately 50 % compared to thawing at atmospheric pressure. As expected, the pressure dependent depression of the melting point was comparable to that of the potato taking into consideration the slightly lower melting point of -2.0 °C at ambient pressure. The sensory assessment of raw fillet by QIM revealed that the high pressure thawed samples were at least comparable to those thawed at ambient pressure. However, the demerits of cooked samples after high pressure treatment were higher compared to conventionally thawed ones particularly in taste and texture. Whereas the thaw drip was markedly reduced during high pressure thawing, the water binding ability measured later seems to be reduced compared to conventional thawing. The colour is influenced by high pressure thawing at 200 MPa which is related to an increase in lightness and consequently has to be considered when applying higher pressure levels. To retain the fresh character of a high pressure thawed fish product, pressure levels below 200 MPa seem to be favourable. The texture parameter hardness increased as a consequence of high pressure thawing, which can be an advantage when post rigor frozen fish fillets have to be processed. The microbial status of thawed fillets was improved when high pressure was used for thawing and it was shown that fish parasites (nematodes) were significantly affected by a high pressure treatment of 200 MPa increasing the product safety. The DSC measurements show that high pressure thawing at

200 MPa is connected with a remarkable denaturation of muscle proteins. This is assumed to be the reason for some quality deterioration observed of both the raw and cooked fillets.

Depending on the required characteristics of processed fish, the process parameters must be selected carefully (Murakami *et al.*, 1992; Amanatidou *et al.*, 2000). Therefore, further studies at different pressure levels are necessary. For designing new fish products an application of pressure levels above 200 MPa seems to be indispensable in order to form certain properties (e.g. modified gels) and to ensure pasteurisation of unwanted microbes or parasites. To obtain comparable properties of fresh fish pressure levels below 200 MPa are suggested depending on pressure holding time and working temperature. However, the various effects of high pressure on the different fish species and the impact of post thawing processing steps must be taken into consideration in each attempt to take advantage of high pressure technology and to improve the final quality of the product. However, the results obtained in this study clearly indicate the different effects of high pressure – low temperature on the quality of animal tissues when compared to plant tissue.

The potential ability of high pressure – low temperature processes to inactivate microorganisms at subzero temperatures was investigated on *Listeria innocua* which served as a non-pathogenic indicator for *L. monocytogenes*, in Ringer solution and babyfood and compared to inactivation kinetics at elevated temperatures. The inactivation kinetics was modelled using an empirical formula as described by Ananta *et al.* (2001) fitting the data obtained in ringer solution with good precision. A plot of the reaction rate constant into a *pT*-diagram clearly indicated the dominant effect of pressure when compared to the temperature effect within the range of investigation. However, a maximum of the rate constant was observed at low temperatures, i.e. at 0 °C.

The impact of the processing time t on the inactivation of *L. innocua* can be demonstrated for different log-cycle reductions using the following equation:

$$t = \frac{-\left[1-\left(1+\frac{\log\left(\frac{N}{N_0}\right)}{\log N_0}\right)^{(1-c)}\right]}{(-k+k\cdot c)}, \tag{5.1}$$

where N_0 is the initial count set to 10^9 (CFU ml^{-1}), N is the final reduction (CFU ml^{-1}), c is the reaction order of the reaction and k is the apparent rate constant (s^{-1}). The required processing time to inactivate a certain amount of the bacteria at 0 °C is plotted versus pressure in Figure 5.4.

While nearly complete inactivation (8 log-cycles) requires a treatment time of 3 h at 200 MPa, the same effect is obtained when applying a pressure of 250 MPa for just 1 h. A further shortening of the pressure holding time to about 50% (30 min) is obtained at a pressure level of 300 MPa. This effect of the pressure decreases with lower inactivation rates. However, freezing and thawing times increase with sample size resulting in extended treatment times to ensure complete phase transition also under high hydrostatic pressure (e.g. 60 min to thaw the fish samples at 200 MPa) and

therefore increasing the product safety with respect to *Listeria*. Increased pressure inactivation of microorganisms at subzero temperatures was also reported by Takahashi (1992) and Hayashi *et al.* (1998). The elliptical shape of the phase boundary in the *pT*-diagram reported for *S. cerevisiae* was not clearly obtained for *Listeria innocua*. Nevertheless such a slope indicates that the inactivation seems to be mainly due to protein denaturation than due to damages of the lipid membrane, since phospholipids change their phases mainly along linear phase transition lines in the *pT*-diagram (Heremans, 2002). Nevertheless, the inactivation rate was not significantly affected by the physical state of the water (solid or liquid) but enhanced when suspending the Listeria in carrot-potato puree with an pH of 5.3 as compared to Ringer solution (pH 6.7). A freezing/thawing cycle at ambient pressure did not remarkable affect the viable count of *Listeria innocua*.

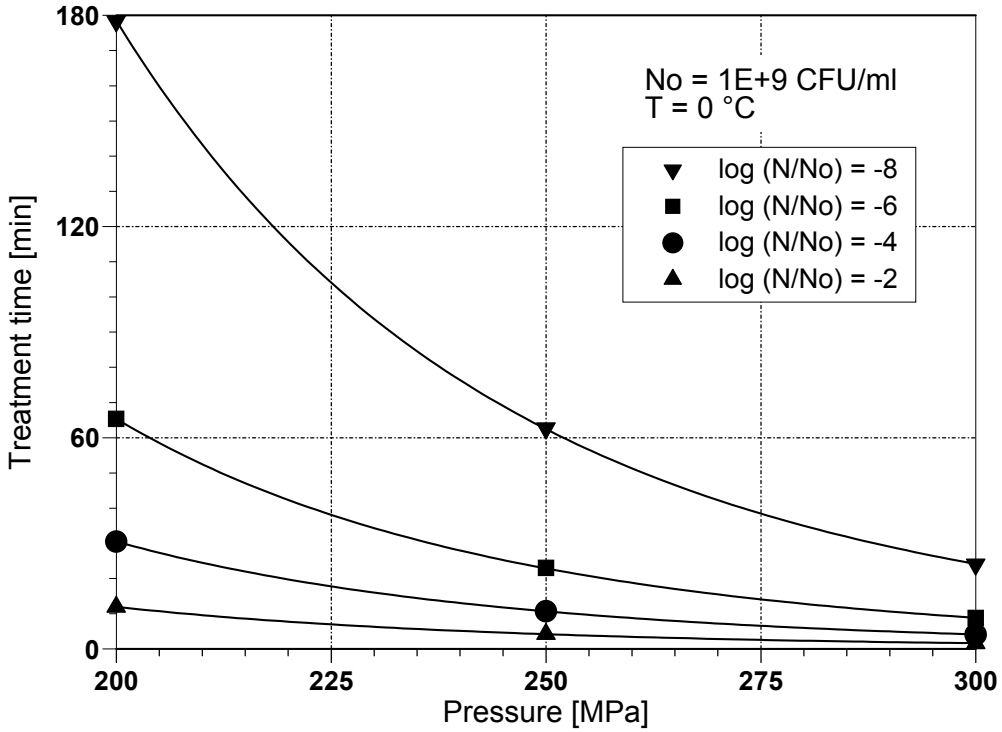

Figure 5.4: Impact of the pressure level on the required processing time to inactivate *Listeria innocua* at 0 °C, calculated (eqn. 5.1) for different log-cycle reductions and constant initial counts.

5.5 Perspectives of high pressure – low temperature processes

In the present work the potential of high pressure – low temperature combinations for food processing was investigated in detail considering processing criteria, as well as quality and safety aspects using different cellular biomaterials (plant tissue, i.e. potato; animal tissue, i.e. fish fillet and microorganisms, i.e. *Listeria innocua*) as test samples. Taking advantage of the observed effects of high hydrostatic pressure at low temperatures and summarising the results a ranking with respect to the potential of food industrial applicability of the high pressure – low temperature processes can be proposed as follows: pressure-induced thawing > pressure-assisted thawing > pressure-shift

freezing > storage under pressure at subzero temperatures without phase transition > pressure-assisted freezing to ice III/ice V > pressure-assisted freezing to ice I.

Compared to other HPLT-processes there are no further requirements on the technical equipment for pressure-induced/assisted thawing compared to existent high pressure units used in food processing, since the working temperature has to be adjusted above 0 °C. Furthermore, significant acceleration of the phase transition times can be reached at moderate pressure levels below 300 MPa. It was shown that melting occurs along the extended melting curve of ice I leading to improvements neglected so far. The pressure level is limited by a critical value where the thawing curves for potato shows an non-homogeneity, due to ice III formation resulting in a decrease of the effective temperature gradient and consequently lowering the thawing rate. Analogous behaviour was obtained by Zhao *et al.* (1998) when thawing beef samples at pressures higher than 280 MPa. Their data clearly indicates the validity of the critical process parameter for plant tissues also for animal tissues investigated here. Nevertheless, it should be mentioned here that none of the samples in their investigation thawed completely, since the maximum holding time was set to 30 min for samples of 55, 65 and 85 mm diameter and a medium temperature of about 25 °C. This can be seen as an example for the importance of accurately selecting the process parameters applied to ensure controlled and successful high pressure-supported phase transition processes. The ideal pressure-supported thawing process with respect to the process parameters seem to start at high initial temperatures (without thawing e.g. tempered by microwave), followed by fast pressure build-up to nearly 300 MPa (highest amount of liquefied ice) and keeping the sample at the pressure where the highest effective temperature gradient is reached until the sample is completely thawed, and finally pressure release after sufficient warming (to prevent recrystallisation). The application of pressure-supported thawing can be seen as most effective for large products which require low surrounding medium temperatures like fish and meat products.

Among all pressure supported freezing processes the pressure-shift freezing process seems to be the most favourable for industrial application. In this study it was indicated that this process allows for substantial and controlled supercooling leading to a high amount of water converting to ice during fast pressure release. This amount of instantaneously formed ice can be enlarged taking advantage of the metastable ‘long resting’ liquid phase experimentally observed during this work and ignored in former studies. Accordingly, lowering the temperature to –28 °C at 240 MPa the calculated triple point of liquid/ice I/ice III increases the freezing rate and results in formation of smaller ice crystals (Fuchigami *et al.*, 1997a; Otero *et al.*, 1998; Levy *et al.*, 1999). Since the cooling step under pressure requires more time for large samples an increase in product safety can be expected as shown by the generated data on high pressure inactivation of microorganisms, with a potential to replace conventional blanching steps prior to freezing. Also the retention of quality was indicated by the experimental results in this study. However, one drawback for industrial application is the absence of reliable pressure transmitting media which do not undergo unwanted solidification, demanding further investigations on liquids like edible oils, alcohol and/or others. While water can

be used during high pressure supported thawing of foods it is not applicable without cryoprotective additives in pressure-shift freezing processes. Also reliable packaging materials must be available to prevent possible migration of the pressure transmitting medium and re-contamination of the product. Here, especially multi-layer films seem to be favourable (Fradin *et al.*, 1998; Amanatidou *et al.*, 2000). The suppliers of high pressure units have to use special materials for the vessels allowing for subzero operation and the construction of certain facilities results in the main drawback, comparably high equipment costs. However the pressure level to be applied does not seem to be challenging since the required working pressure is below 250 MPa. To overcome the limitations of batch processing and to enhance the throughput, it was suggested to initiate the freezing in the high pressure vessel and to continue the freezing in a freezing room (Denys *et al.*, 1997). Also pressure-shift freezing seems to be more advantageous when applied to large and high value products.

On the other hand, storage under high pressure at low temperature seems to be applicable for small as well as for large sample sizes. During the storage at subzero temperatures without freezing an enhancement of product safety can be expected, due to the indicated inactivation effects on microorganisms also assumable for enzymes (Indrawati *et al.*, 1998). Nevertheless, more data on inactivation kinetics of enzymes and microorganisms are required to quantify the effects of relevant combination processes for food production. During high pressure storage plant based tissues retained preserved quality attributes after 24 h storage at –28 °C and 240 MPa, while animal derived tissues changed their characteristic appearance at 200 MPa due to protein denaturation resulting in changes of colour and texture. However, there is also a potential for controlled and selective modification of biomacromolecules since for instance different proteins are not affected equivalently by comparable *pTt*-conditions (Heremans, 2002). Formation of certain gel-structures and selective inactivation of enzymes and microorganisms can be assumed, demanding for further detailed studies especially in the low temperature range within the metastable ‘long resting’ liquid area. Furthermore, the influences on different food matrices must be characterised in further investigations. However, transferring the potential for improvements of product quality to industrial scale is a challenge, since continuous storage under high pressure at low temperature seems to be a cost-intensive technology.

Pressure-assisted freezing to ice I seems to be of minor industrial relevance since the required working temperatures must be significantly lower than for conventional freezing processes and the specific volume changes increase with increasing pressure (~ 13% at 200 MPa). Furthermore, it lacks the advantageous effects of pressure-shift freezing. Nevertheless, this process was described as a useful tool to study the impact of high pressure on phase transitions (Denys *et al.*, 2002). From the perspective of quality retention, freezing to higher ice modifications showed a certain potential since freezing is then accompanied by a volume decrease, showing less damaging effects on plant tissues. Due to the specific densities of ice III and ice V, the formation of ice III was more preferable. The smallest specific volume change (~ -3%) is obtained near the triple point liquid/ice

III/ice V when freezing to ice III, consequently defining the optimal *pT*-conditions, 360 MPa and –18 °C in the case of potato tissue. However, some critical parameters were observed in the present study which has to be considered in process design. First of all, a substantial degree of supercooling was indicated before nucleation of higher ice polymorphs, resulting in the necessity of working at temperatures below –40 °C to ensure the crystallisation. Additionally the formation of ice III was not guaranteed sufficiently near the mentioned triple point, but most probable in the pressure range between 280 and 300 MPa. As a consequence, it seems to be notable that the present study can be seen as the first detailed and successful study on ice III formation in foods, since the obtained results clearly indicate that the formation of ice III in former studies (Fuchigami *et al.*, 1997b; 1998a; 1998b) can be excluded. This remark is also supported by several critical reviews also discussing the crystallisation of ice III (Denys *et al.*, 2002; Cheftel *et al.*, 2000; Teramoto and Fuchigami, 2000). However, to successfully retain high quality after freezing to ice III, thawing must be also performed at adequate pressure, and before thawing the frozen product must be kept under suitable *pT*-conditions. These requirements lead to further difficulties when transferring this special technology to applicable process concepts. Another possibility of retaining the ice III crystals may be further lowering of the product temperature before pressure release, since low temperatures decreases the rate of re-crystallisation (Bridgman, 1912). However, the kinetics of this solid-solid transformation must be investigated in further studies. As demonstrated above, solid-solid transformation (ice III-ice I) at temperature levels around –35 °C results in nearly complete damage of the tissue matrix, which on the other hand can be a useful tool to inactivate microorganisms as reported by Edebo and Hedén (1960). Here, probably the most interesting processing concept can be found with respect to higher ice modifications. Pressurisation of a frozen matrix at -40 °C to about 400 MPa should result in transformation of the ice crystals from ice I to ice III to ice V and re-crystallisation in the opposite way during pressure release. According to the obtained results it can be assumed that such high pressure cycles may lead to effective disruption and inactivation of microorganisms while not affecting non-cellular food matrices e.g. ice cream. This assumption must be proved in detailed investigations, but is of certain industrial relevance since Walker *et al.* (1991) reported that factories in which frozen milk products are processed can harbour *Listeria monocytogenes* and thus can serve as a source of the pathogen in finished products (e.g. ice cream, ice milk, sherbet).

The European “Novel Foods” Directive (May, 1997) has introduced regulatory hurdles and slowed the introduction of new pressure-treated products (Tewari *et al.*, 1999). However, the evaluation of this legislation was envisaged after 5 years and since this process is not completed now the further progress with regard to new applications of high pressure in the low temperature region remains somewhat unclear. But, it can be expected that the relatively moderate pressures (for relevant processes mainly below 300 MPa) to be applied helps simplifying the demanded prove of substantial equivalence before introducing a high pressure product to the food market, since this pressure range is just slightly above the pressure level reached in commercialised processes (e.g. homogenisation at 200 MPa). Based on the results of this study substantial equivalence of high

pressure – low temperature processed and conventionally processed foods can be assumed for the materials investigated. Nevertheless, further studies on this topic might be necessary for acceptance of the European executives.

Furthermore, the results compiled in the present thesis can also serve as a useful tool for studying water-ice transitions at much higher pressure levels. Since pressure levels above 1.0 GPa was reported to improve the sterilisation effects at reduced temperatures and decreased treatment times (Heinz and Knorr, 2002) also a high pressure treatment at 1000 MPa at room temperature seems to be realisable without formation of ice VI. In this case, the quasi-adiabatic temperature increase can be compensated using dispersed ice fragments, for example, which counteracts the warming when absorbing melting energy. However, controlled and successful high pressure food processing concepts demand for detailed knowledge of critical processing parameters with respect to the technical equipment, the selected pressure transmitting medium, the product characteristics, the safety aspects and ultimately depend on the process target to be reached. In conclusion, the research described in this thesis contributes to the understanding and development of high pressure – low temperature processes and provides a source for innovative and improved processing strategies and product concepts.

6 REFERENCES

Agnelli, M. E., and Mascheroni, R. H. (2001). Cryomechanical freezing. A model for the heat transfer process. *Journal of Food Engineering*, 47, 263-270.

Amanatidou, A., Schlüter, O., Lemkau, K., Gorris, L. G. M., Smid, E. J., and Knorr, D. (2000). Effect of combined application of high pressure treatment and modified atmospheres on shelf-life of fresh atlantic salmon. *Innovative Food Science & Emerging Technologies*, 1, 87-98.

Ananta, E., Heinz, V., Schlüter, O., and Knorr, D. (2001). Kinetic studies on high-pressure inactivation of *Bacillus stearothermophilus* spores suspended in food matrices. *Innovative Food Science &. Emerging Technologies*, 2, 261-272.

Angell, C. A. (1982). Supercooled Water. In: *Water, a comprehensive treatise*, F. Franks, ed., Plenum Press, New York, 1-81.

Angersbach, A., Heinz, V., and Knorr, D. (1999). Electrophysical model of intact and processed plant tissues: cell desintegration criteria. *Biotechnology Progress*, 15, 753-762.

Angersbach, A., Heinz, V., and Knorr, D. (2002). Evaluation of process-induced dimensional changes in the membrane structure of biological cells using impedance measurement. *Biotechnology Progress*, 18(3), 597-603.

Angsupanich, K., and Ledward, D. A. (1998). High pressure treatment effects on cod (*Gadus morhua*) muscle. *Food Chemistry*, 63, 39-50.

Arabas, J., Szczepek, J., Dmowski, L., Heinz, V., and Fronberg-Broczek, M. (1999). New technique for kinetic studies of pressure-temperature induced changes of biological materials. In: *Advances in High Pressure Bioscience and Biotechnology*, H. Ludwig, ed., Springer-Verlag, Heidelberg, 537-540.

Arroyo, G., Sanz, P. D., and Prestamo, G. (1997). Effect of high pressure on the reduction of microbial populations in vegetables. *Journal of Applied Microbiology*, 82, 735-742.

Arthey, D. (1993). Freezing of vegetables and fruits. In: *Frozen food technology*, C. P. Mallett, ed., Blackie Academic & Professional, Glasgow.

Barry, H., Dumay, E. M., and Cheftel, J. C. (1998). Influence of pressure-assisted freezing on the structure, hydration and mechanical properties of a protein gel. In: *High pressure food science, bioscience and chemistry*, N. S. Isaacs, ed., Royal Society of Chemistry, London, 343-353.

Basak, S., and Ramaswamy, H. S. (1998). Effect of high pressure processing on texture of selected fruit and vegetables. *Journal of Textural Studies*, 29, 587-601.

Baumgart, J. (1990). In: *Mikrobiologische Untersuchung von Lebensmitteln*, Behr, Hamburg.

Bier, J. W. (1976). Experimental Anisakis: cultivation and temperature tolerance determination. *Journal of Milk and Food Technology*, 39, 132.

Biswal, R. N., Bozorgmehr, K., Tompkins, F. D., and Liu, X. (1991). Osmotic concentration of beans prior to freezing. *Journal of Food Science*, 56(4), 1008-1011.

Bridgman, P. W. (1912). Water, in the liquid and five solid forms, under pressure. *Proceedings of the American Academy of Sciences*, 47, 441-558.

Bridgman, P. W. (1914). The coagulation of albumen by pressure. *Journal of Biology and Chemistry*, 19, 511-512.

Bridgman, P. W. (1935). The pressure-volume-temperature relations of the liquid, and the phase diagram of heavy water. *Journal of Chemical Physics*, 3, 597-605.

Buchheim, W., Frede, E., Wolf, M., and Baldenegger, P. (1998). Solidification and melting of some edible fats and model lipid systems under pressure. In: *Advances in High Pressure Bioscience and Biotechnology*, H. Ludwig, ed., Springer-Verlag, Heidelberg, Germany, 153-156.

Calzada, J. F., and Peleg, M. (1978). Mechanical interpretation of compressive stress-strain relationships of solid foods. *Journal of Food Science*, 43(4), 1087-1092.

Cano, P. (1996). Vegetables. In: *Freezing effects on food quality*, L. E. Jeremiah, ed., Marcel Dekker, New York, 247-298.

Capri, G., Gola, S., Maggi, A., Rovere, P., and Buzzoni, M. (1995). Microbial and chemical shelf-life of high pressure treated salmon cream at refrigeration temperatures. *Ind. Conserve*, 70, 386-397.

Carlez, A., Rosec, J. P., Richard, N., and Cheftel, J. C. (1993). High pressure inactivation of *Citrobacter freundii, Pseudomonas fluorescens* and *Listeria innocua* in inoculated minced beef muscle. *Lebensmittel Wissenschaft und Technologie*, 26, 357-363.

Charm, S. E., Longmaid, H. E., and Carver, J. (1977). A simple system for extending refrigerated, nonfrozen preservation of biological material using pressure. *Cryobiology*, 14(5), 625-636.

Charoenrein, S., Goddard, M., and Reid, D. S. (1991). Effect of solute on the nucleation and propagation of ice. In: *Water relationships in foods*, H. Levine and L. Slade, eds., Plenum Press, New York, 191-212.

Cheftel, J. C. (1995a). Review: High-pressure, microbial inactivation and food preservation. *Food Science and Technology International*, 1, 75-90.

Cheftel, J. C. (1995b). Effect of high-pressure on meat: a review. *Meat Science*, 46(3), 211-236.

Cheftel, J. C., Levy, J., and Dumay, E. (2000). Pressure-assisted freezing and thawing: principles and potential applications. *Food Review International*, 16, 453-483.

Cheftel, J. C., Thiebaud, M., and Dumay, E. (2002). Pressure-assisted freezing and thawing of foods: a review of recent studies. *High Pressure Research*, 22, 601-611.

Chen, P., Dong Chen, X., and Free, K. W. (1996). Measurement and data interpretation of the freezing point depression of milks. *Journal of Food Engineering*, 30, 239-253.

Chen, X. D., and Chen, P. (1996). Freezing of aqueous solution in a simple apparatus designed for measuring freezing point. *Food Research International*, 29(8), 723-729.

Chevalier, D., Le Bail, A., Chourot, J. M., and Chantreau, P. (1999). High pressure thawing of fish (whiting): influence of the process parameters on drip losses. *Lebensmittel - Wissenschaft und Technologie*, 32(1), 25-31.

Chevalier, D., Le Bail, A., and Ghoul, M. (2001). Evaluation of the ice ratio formed during quasi-adiabatic pressure shift freezing. *High Pressure Research*, 21, 227-235.

Chevalier, D., Le Bail, A., and Ghoul, M. (2000b). Freezing and ice crystals formed in a cylindrical food model: part 2. Comparison between freezing at atmospheric pressure and pressure-shift freezing. *Journal of Food Engineering*, 46, 287-293.

Chevalier, D., Sentissi, M., Havet, M., and Le Bail, A. (2000c). Comparison of air-blast and pressure shift freezing on Norway lobster quality. *Journal of Food Science*, 65(2), 329-333.

Ching, H. L. (1984). Fish tapeworm infections (*Diphyllobothriasis*) in Canada, particularly British Columbia. *Canadian Medical Association Journal*, 130, 1125-1128.

Chizhov, V. E. (1993). Thermodynamic properties and thermal equations of the state of high-pressure ice phases. *Journal of Applied Mechanics and Technical Physics*, 34(2), 253-262.

Chourot, J.-M., Boillereaux, L., Havet, M., and Le Bail, A. (1997). Numerical modeling of high pressure thawing: application to water thawing. *Journal of Food Engineering*, 34, 63-75.

Christensen, C. M. (1984). Food texture perception. *Advanced Food Research*, 29, 159-199.

Chung, S. L., and Merritt, J. H. (1991). Freezing time predictions for brick and cylindrical-shaped foods. *Journal of Food Science*, 56(4), 1072-1075.

Cleland, A. C., and Earle, R. L. (1984). Assessment of freezing time prediction. *Journal of Food Science*, 49, 1034-1042.

Cleland, D. J., Cleland, A. C., and Earle, R. L. (1986). Prediction of freezing and thawing times for foods - a review. *International Journal of Refrigeration*, 9, 182.

Cui, Z. F., Dykkhuizen, R. C., Nerem, R. M., and Sembanis, A. (2002). Modeling of crypreservation of engineered tissues with one-dimensional geometry. *Biotechnology Progress*, 18, 354-361.

Czeslik, C., Reis, O., Winter, R., and Rapp, G. (1998). Effect of high pressure on the structure of dipalmitoylphosphatidylcholine bilayer membranes: A synchrotron-X-ray diffraction and FT-IR spectroscopy study using the diamond anvil technique. *Chemistry and Physics of Lipids*, 91, 135-144.

Darvall, J. G. (2000). Preservation of microorganisms. *Culture*, 21(2), 1-5.

Deardorff, T. L., and Throm, R. (1988). Commercial blast-freezing of third stage *Anisakis simplex* larvae encapsulated in salmon and rockfish. *Journal of Parasitology*, 74, 600-603.

Delgado, A. E., and Sun, D.-W. (2001). Heat and mass transfer models for predicting freezing processes - a review. *Journal of Food Engineering*, 47, 154-174.

Denys, S., and Hendrickx, M. E. (1999). Measurement of the thermal conductivity of foods at high-pressure. *Journal of Food Science*, 64, 709-713.

Denys, S., Schlüter, O., Hendrickx, M. E., and Knorr, D. (2002). Effects of high pressure on water-ice transitions in foods. In: *Ultra High Pressure Treatments of Foods*, M. E. G. Hendrickx and D. Knorr, eds., Kluwer Academic/Plenum Publishers, New York, 215-248.

Denys, S., Van Loey, A. M., and Hendrickx, M. E. (2000a). Modeling conductive heat transfer during high pressure thawing processes: Determination of latent heat as a function of pressure. *Biotechnology Progress*, 16, 447-455.

Denys, S., Van Loey, A. M., and Hendrickx, M. E. (2000b). A modelling approach for evaluating process uniformity during batch high hydrostatic pressure processing: combination of a numerical heat transfer model and enzyme inactivation kinetics. *Innovative Food Science & Emerging Technologies*, 1, 5-19.

Denys, S., Van Loey, A. M., Hendrickx, M. E., and Tobback, P. P. (1997). Modeling heat transfer during high-pressure freezing and thawing. *Biotechnology Progress*, 13(4), 416-423.

Deplace, G. (1995). Design of high pressure isostatic units for laboratory and industrial treatment of food products. In: *High Pressure Processing of Foods*, D. A. Ledward, D. E. Johnston, R. G. Earnshaw, and A. P. M. Hastings, eds., Nottingham University Press, Loughborough, 137-154.

Detienne, N. A., and Wicker, L. (1999). Sodium chloride and tripolyphosphate effects on physical and quality characteristics of injected pork loins. *Journal of Food Science*, 64, 1042-1047.

Deuchi, T., and Hayashi, R. (1990). A new approach for food preservation: use of non-freezing conditions at subzero temperature generated under moderate high pressure. In: *Pressure Processed Food: Research and Development*, R. Hayashi, ed., San-Ei Suppan Co., Kyoto, 37-51.

Deuchi, T., and Hayashi, R. (1991). Pressure application to thawing of frozen foods and to food preservation under subzero temperature. In: *High Pressure Science for Food*, R. Hayashi, ed., San-Ei Suppan Co., Kyoto, 101-110.

Deuchi, T., and Hayashi, R. (1992). High pressure treatments at subzero temperature: application to preservation, rapid freezing and rapid thawing of foods. In: *High Pressure and Biotechnology*, C. Balny, R. Hayashi, K. Heremans, and P. Masson, eds., Colloque INSERM, 353-355.

Devine, C. E., Bell, R. G., and Lovatt, S. (1996). Red Meats. In: *Freezing effects on food quality*, L. E. Jeremiah, ed., Marcel Dekker, New York, 51-84.

Dörnenburg, H., and Knorr, D. (1997). Evaluation of elicitor- and high - pressure - induced enzymatic browning utilizing potato (*Solanum tuberosum*) suspension cultures as a model system for plant tissues. *Journal of Agricultural and Food Chemistry*, 45(10), 4173-4177.

Dörnenburg, H., and Knorr, D. (1998). Monitoring the impact of high-pressure processing on the biosythesis of plant metabolites using plant cell cultures. *Trends in Food Science & Technology*, 9(10), 355-361.

Dumoulin, M., Ozawa, S., and Hayashi, R. (1998). Textural properties of pressure-induced gels of food proteins obtained under different temperatures including subzero. *Journal of Food Science*, 63(1), 92-95.

Edebo, L., and Hedén, C.-G. (1960). Disruption of frozen bacteria as a consequence of changes in the crystal structure of ice. *Journal of Biochemical and Microbiological Technology and Engineering*, 2(1), 113-120.

Edwards, M., and Hall, M. (1988). Freezing for quality. *Food Manufacture,* (3), 41-45.

Edwards, M. C. (1995). Change in cell structure. In: *Physico-chemical aspects of food processing*, S. T. Beckett, ed., Blackie Academic & Professional, London, 212-233.

Ehrenfest, P. (1933). *Proc. Acad. Sci. Amsterdam*, 36, 153.

El-Kest, S. E., and Marth, E. H. (1992). Lysozyme and lipase alter unfrozen and frozen/thawed cells of *Listeria monocytogenes*. *Journal of Food Protection*, 55, 777-781.

Erickson, M. C. (1997). Chemical measurements of frozen foods. In: *Quality in frozen food*, M. C. Erickson and Y.-C. Hung, eds., Chapman & Hall, New York, 340-356.

Eshtiaghi, M. N., and Knorr, D. (1996). High hydrostatic pressure thawing for the processing of fruit preparations from frozen strawberries. *Food Biotechnology*, 10(2), 143-148.

European Commission, E. (1991). Council Directive of 22 July 1991 laying down the health conditions for the production and the placing on the market of fishery products, (91/493/EEC). *Official Journal of the European Countries*, L268, 15-32.

Evans, L. F. (1967a). Selective nucleation of the high-pressure ices. *Journal of Applied Physics*, 38, 4930-4932.

Evans, L. F. (1967b). Two-dimensional nucleation of ice. *Nature*, 213, 384-385.

Feeney, R. E., and Yeh, Y. (1998). Antifreeze proteins: current status and possible food uses. *Trends in Food Science and Technology*, 9, 102-106.

Fennema, O. R., Powrie, W. D., and Marth, E. H. (1973). In: *Low-temperature preservation of foods and living matter*, Marcel Dekker, New York.

Fikiin, K. A. (1998). Ice content prediction methods during food freezing: a survey of the eastern european literature. *Journal of Food Engineering*, 38, 331-339.

Foguel, D., and Weber, G. (1995). Pressure-induced dissociation and denaturation of allophycocyanin at subzero temperatures. *The Journal of Biological Chemistry*, 270(48), 28759-28766.

Först, P., Werner, F., and Delgado, A. (2000). The viscosity of water at high pressures - especially at subzero degrees centigrade. *Rheologica Acta*, 39, 566-573.

Fradin, J. F., Le Bail, A., Sanz, P. D., and Molina-García, A. D. (1998). Behaviour of packaging materials during high pressure thawing. *Food Science and Technology International*, 4(6), 419-424.

Franke, K. (2000). A new approach for the numerical calculation of freezing and thawing processes of foods using a modified fictitious heat flow method. *Journal of Food Engineering*, 44, 23-29.

Franks, F. (1982). The properties of aqueous solutions at subzero temperatures. In: *Water, a comprehensive treatise*, F. Franks, ed., Plenum Press, New York, 215-338.

Franks, F. (1985). Complex aqueous systems at subzero temperatures. In: *Properties of water in foods*, D. Simatos and J. L. Multon, eds., Martinus Nijhoff Publishers, Dordrecht.

Fuchigami, M., Kato, N., and Teramoto, A. (1997a). High-pressure-freezing effects on textural quality of carrots. *Journal of Food Science*, 62(4), 804-808.

Fuchigami, M., Miyazaki, K., Kato, N., and Teramoto, A. (1997b). Histological changes in high-pressure-frozen carrots. *Journal of Food Science*, 62(4), 809-812.

Fuchigami, M., and Teramoto, A. (1997c). Structural and textural changes in kinu-tofu due to high-pressure-freezing. *Journal of Food Science*, 62(4), 828-832.

Fuchigami, M., Kato, N., and Teramoto, A. (1998a). High-pressure-freezing effects on textural quality of Chinese cabbage. *Journal of Food Science*, 63(1), 122-125.

Fuchigami, M., Teramoto, A., and Ogawa, N. (1998b). Structural and textural quality of kinu-tofu frozen-then-thawed at high-pressure. *Journal of Food Science*, 63(3), 1054-1057.

Fuji, T., Satomi, M., Nakatsuka, G., Yamaguchi, T., and Okuzumi, M. (1994). Changes of freshness indexes and bacterial flora during storage of pressurized mackerel. *Journal of Food Hygienic Society of Japan*, 35, 195-200.

George, R. M. (1997). Freezing systems. In: *Quality in frozen food*, M. C. Erickson and Y.-C. Hung, eds., Chapman & Hall, New York, 3-9.

Golden, D. A., and Arroyo-Gallyoun, L. (1997). Relationship of frozen-food quality to microbial survival. In: *Quality in frozen food*, M. C. Erickson and Y.-C. Hung, eds., Chapman & Hall, New York, 174-193.

Golden, D. A., Beuchat, L. R., and Brackett, R. E. (1988). Inactivation and injury of *Listeria monocytogenes* as affected by heating and freezing. *Food Microbiology*, 5, 17-23.

Goldsmid, J. M., and Speare, R. (1997). The parasitology of foods. In: *Foodborne microorganisms of public health significance*, A. D. Hocking, G. Arnold, I. Jenson, K. Newton, and P. Sutherland, eds., NSW: Aust Inst Food Sci and Technol Inc, North Sydney, 583-602.

Gould, G. W. (2000). Emerging technologies in food preservation and processing in the last 40 years. In: *Innovations in food processing*, G. V. Barbosa-Cánovas and G. W. Gould, eds., Technomic Publishing, Lancaster, 1-11.

Gould, G. W. (2002). The evolution of high pressure processing of foods. In: *Ultra High Pressure Treatments of Foods*, M. E. G. Hendrickx and D. Knorr, eds., Kluwer Academic/Plenum Publishers, New York, 3-21.

Grout, B. W. W., Morris, G. J., and McLellan, M. R. (1991). The freezing of fruit and vegetables. In: *Food freezing: today and tomorrow*, W. B. Bald, ed., Springer-Verlag, London, 113-122.

Gustafson, P. V. (1953). The effect of freezing on encysted *Anisakis* larvae. *Journal of Parasitology*, 39, 585-588.

Haas, G. J., Prescott, H. E., and D'Intino, J. (1972). Pressure freezing-air drying: a new technique to reduce deterioration in drying tissue. *Journal of Food Science*, 37, 430-433.

Hartel, R. W. (1998). Mechanisms and kinetics of recrystallization in ice cream. In: *The properties of water in foods ISOPOW 6*, D. S. Reid, ed., Blackie Academic & Professional, London, 287-319.

Haselton, H. T. J., Chou, I.-M., Shen, A. H., and Bassett, W. A. (1995). Techniques for determining pressure in the hydrothermal diamond-anvil cell: Behavior and identification of ice polymorphs (I, II, V, VI). *American Mineralogist*, 80, 1302-1306.

Hashizume, C., Kimura, K., and Hayashi, R. (1995). Kinetic analysis of yeast inactivation by high pressure treatment at low temperatures. *Bioscience Biotechnology & Biochemistry*, 59, 1455-1458.

Hauben, K. J. A., Wuytack, E. Y., Soontjens, C. C. F., and Michiels, C. W. (1996). High-pressure transient sensitization of *Escherichia coli* to lysozyme and nisin by disruption of outer-membrane permeability. *Journal of Food Protection*, 59(4), 350-355.

Hauck, A. K. (1977). Occurrence and survival of the larval nematode *Anisakis sp*. in the flesh of fresh, frozen, brined, and smoked pacific herring, *Clupea harengus Pallasi*. *Journal of Parasitology*, 63(3), 515-519.

Hawley, S. A. (1971). Reversible pressure-temperature denaturation of chymotrypsinogen. *Biochemistry*, 10, 2436-2442.

Hayakawa, K., Ueno, Y., Kawamura, S., Kato, T., and Hayashi, R. (1998). Microorganism inactivation using high pressure generation in sealed vessels under sub-zero temperature. *Applied Microbiology and Biotechnology*, 50, 415-418.

Hayashi, R., Kinsho, T., and Ueno, H. (1998). Combined applications of subzero temperature and high pressure on biological materials. In: *High Pressure Food Science, Bioscience and Chemistry*, N. S. Isaacs, ed., The Royal Society of Chemistry, Cambridge, UK, 166-174.

Hayden, R. I., Moyse, C. A., Calder, F. W., Crawford, D. P., and Fensom, D. S. (1969). Electrical impedance studies on potato and alfalfa tissue. *Journal of Experimental Botany*, 20, 177-200.

Hedén, C.-G. (1964). Effects of hydrostatic pressure on microbial systems. *Bacteriological Review*, 28(1), 14-29.

Heinisch, O., Kowalski, E., Goossens, K., Frank, J., Heremans, K., Ludwig, H., and Tauscher, B. (1995). Pressure effects on the stability of lipoxygenase: Fourier transform infrared spectroscopy and enzyme activity studies. *Zeitschrift für Lebensmittel Untersuchung Forschung*, 201, 562-565.

Heinz, V., and Knorr, D. (2002). Effects of high pressure on spores. In: *Ultra High Pressure Treatments of Foods*, M. E. G. Hendrickx and D. Knorr, eds., Kluwer Academic/Plenum Publishers, New York, 77-113.

Hemminger, W., and Höhne, G. (1984). In: *Calorimetry - fundamentals and practice*, Verlag Chemie, Weinheim, Germany.

Heremans, K. (1982). High pressure effects on proteins and other biomolecules. *Annual Reviews in Biophysics and Bioengineering*, 11(1-21).

Heremans, K. (2002). Effects of high pressure on biomaterials. In: *Ultra High Pressure Treatments of Foods*, M. E. G. Hendrickx and D. Knorr, eds., Kluwer Academic/Plenum Publishers, New York, 23-51.

Heremans, K., and Smeller, L. (1998). Protein structure and dynamics at high pressure. *Biochimica et Biophysica Acta*, 1386, 353-370.

Hernandez, A., and Pilar Cano, M. (1998). High - pressure and temperature effects on enzyme inactivation in tomato puree. *Journal of Agricultural and Food Chemistry*, 46(1), 266-270.

Hew, C. L., and Yang, D. S. C. (1992). Protein interaction with ice. *European Journal of Biochemistry*, 203, 33-42.

Houwing, H. (1969). The inactivation of herring nematodes (*Anisakis marina*) by freezing. *Bulletin of the International Institute of Refrigeration*, 6, 297-302.

Hung, Y.-C., and Kim, N.-K. (1996). Fundamental aspects of freeze-cracking. *Food Technology*, 50(12), 59-61.

Indrawati, Van Loey, A. M., Ludikhuyze, L. R., and Hendrickx, M. E. (2000). Kinetics of pressure inactivation at subzero and elevated temperatures of lipoxygenase in crude green bean (*Phaseolus vulgaris* L.) extract. *Biotechnology Progress*, 16, 109-115.

Indrawati, I., van Loey, A., Denys, S., and Hendrickx, M. (1998). Enzyme sensitivity towards high pressure at low temperature. *Food Biotechnology*, 12(3), 263-277.

Ingram, M., and Mackey, B. M. (1976). Inactivation by cold. In: *Inhibition and Inactivation of Vegetative Microbes*, F. A. Skinner and W. B. Hugo, eds., New York, 111-151.

Jones, E. (1997). Marketing frozen foods. In: *Quality in frozen food*, M. C. Erickson and Y.-C. Hung, eds., Chapman & Hall, New York, 426-441.

Jones, H. F., and Beckett, S. T. (1995). Fruits and vegetables. In: *Physico-chemical aspects of food processing*, S. T. Beckett, ed., Blackie Academic & Professional, London, 292-314.

Kalchayanand, N., Frethem, C., Dunne, P., Sikes, A., and Ray, B. (2002). Hydrostatic pressure and bacteriocin-triggered cell wall lysis of *Leuconostoc mesenteroides*. *Innovative Food Science & Emerging Technologies*, 3, 33-40.

Kalichevsky, M. T., Knorr, D., and Lillford, P. J. (1995). Potential food applications of high-pressure effects on ice-water transitions. *Trends in Food Science and Technology*, 6, 253-259.

Kalichevsky-Dong, M. T., Ablett, S., Lillford, P. J., and Knorr, D. (2000). Effects of pressure-shift freezing and conventional freezing on model food gels. *International Journal of Food Science and Technology*, 35, 163-172.

Kamat, A. S., and Nair, P. M. (1996). Identification of Listeria innocua as a biological indicator for inactivation of L. monocytogenes by some meat processing treatments. *Lebensmittel-Wissenschaft und -Technologie*, 29(8), 714-720.

Kamb, B., and Prakash, A. (1968). Structure of ice III. *Acta Crystallographica*, B24, 1317-1327.

Kamb, B., Prakash, A., and Knobler, C. (1967). Structure of ice V. *Acta Crystallographica*, 22, 706-715.

Kanda, Y., and Aoki, M. (1993a). Development of pressure-shift freezing method: Part I. Observation of ice crystals of frozen tofu. In: *High Pressure Bioscience and Food Science*, R. Hayashi, ed., San-Ei Suppan Co, Kyoto, 27-33.

Kanda, Y., and Aoki, M. (1993b). Behavior of ice under pressure. For the basis of high pressure sterilization under low temperature. In: *High Pressure Bioscience and Food Science*, R. Hayashi, ed., San-Ei Suppan Co., Kyoto, 24-26.

Kanda, Y., Aoki, M., and Kosugi, T. (1992). Freezing of tofu (soybean curd) by pressure-shift freezing and its structure. *Nippon Shokuhin Gakkaishi*, 39(7), 608-614.

Karino, S., Hane, H., and Makita, T. (1994). Behavior of water and ice at low temperature and high pressure. In: *High Pressure Bioscience*, R. Hayashi, S. Kunugi, S. Shimada, and A. Suzuki, eds., San-Ei Suppan Co, Kyoto, 2-9.

Karl, H., and Leinemann, M. (1989). Überlebensfähigket von Nematodenlarven (*Anisakis sp.*) in gefrosteten Herringen. *Archiv für Lebensmittelhygiene*, 40, 14-16.

Karl, H., Roepstorff, A., Huss, H. H., and Bloemsma, B. (1995). Survival of *Anisakis* larvae in marinated herring fillets. *International Journal of Food Science and Technology*, 29(6), 661-670.

Kennedy, C. J. (1998). Formulation of ice in frozen foods and its control by physical stimuli. In: *Properties of water in foods ISOPOW 6*, D. S. Reid, ed., Blackie Academic & Professional, London, 329-366.

Knorr, D. (1993). Effects of high-hydrostatic-pressure processes on food safety and quality. *Trends in Food Science and Technology*, 4, 370-375.

Knorr, D. (1995a). Hydrostatic pressure treatment of food: microbiology. In: *New methods of food preservation*, G. W. Gould, ed., Blackie Academic and Professional, London, 159-175.

Knorr, D. (1995b). High pressure effects on plant derived foods. In: *High Pressure Processing of Foods*, D. A. Ledward, D. E. Johnston, R. G. Earnshaw, and A. P. M. Hastings, eds., Nottingham University Press, Loughborough, 123-135.

Knorr, D. (1996). Advantages, opportunities and challenges of high hydrostatic pressure application to food systems. In: *High Pressure Bioscience and Biotechnology*, R. Hayashi and C. Balny, eds., Elsevier Science, Amsterdam, 279-289.

Knorr, D. (2000). Process aspects of high-pressure treatment of food systems. In: *Innovations in Food Processing*, G. V. Barbosa-Cánovas and G. W. Gould, eds., Technomic Publishing, Lancaster, 13-30.

Knorr, D., and Heinz, V. (1999). Recent advances in high pressure processing of foods. *New Food*, 2(3), 15-19.

Knorr, D., Schlueter, O., and Heinz, V. (1998). Impact of high hydrostatic pressure on phase transitions of foods. *Food Technology*, 52(9), 42-45.

Koch, H., Seyderhelm, I., Wille, P., Kalichevsky, M. T., and Knorr, D. (1996). Pressure-shift freezing and its influence on texture, color, microstructure and rehydration behaviour of potato cubes. *Nahrung-Food*, 40(3), 125-131.

Kolakowski, P., Dumay, E., and Cheftel, J.-C. (2001). Effects of high pressure and low temperature on β-lactoglobulin unfolding and aggregation. *Food Hydrocolloids*, 15, 215-232.

Lavety, J. (1991). Physico-chemical problems associated with fish freezing. In: *Food freezing: today and tomorrow*, W. B. Bald, ed., Springer-Verlag, London, 123-132.

Le Bail, A., Chevalier, D., Chourot, J. M., and Monteau, J. Y. (2001). High pressure calorimetry: Comparisons of two systems (differential vs. single cell), application to the phase change of water under pressure. *Journal of Thermal Analysis and Calorimetry*, 66, 243.253.

Le Bail, A., Chourot, J.-M., Barillot, P., and Lebas, J.-M. (1997). Le Congélation - décongélation à haute pression. *Revue Générale du Froid*, 972, 51-56.

Leistner, L. (2002). Update on hurdle technology. In: *Engineering and food for the 21st century*, J. Welti-Chanes, G. V. Barbosa-Cánovas, and J. M. Aguilera, eds., CRC Press, Washington, D.C., 615-629.

Levy, J., Dumay, E., Kolodziejczyk, E., and Cheftel, J. C. (1999). Freezing kinetics of a model oil-in-water emulsion under high pressure or by pressure release. Impact on ice crystals and oil droplets. *Lebensmittel - Wissenschaft und -Technologie*, 32(7), 396-405.

Li, B., and Sun, D.-W. (2002 a). Effect of power ultrasound on freezing rate during immersion freezing of potatoes. *Journal of Food Engineering*, 55, 277-282.

Li, B., and Sun, D.-W. (2002b). Novel methods for rapid freezing and thawing of foods - a review. *Journal of Food Engineering*, 54, 175-182.

Li, J., and Lee, T. C. (1995). Bacterial ice nucleation and its potential application in the food industry. *Trends in Food Science and Technology*, 6, 259-265.

Li, J., and Lee, T. C. (1998). Bacteria extracellular ice nucleator effects on freezing of foods. *Journal of Food Science*, 63(3), 375-381.

Lima, M., and Sastry, S. K. (1990). Influence of fluid rheological properties and particle location on ultrasound-assisted heat transfer between liquid and particles. *Journal of Food Science*, 55, 1112-1115.

Linton, M., McClements, J. M. J., and Patterson, M. F. (1999). Survival of *Escherichia coli* O157:H7 during storage in pressure-treated orange juice. *Journal of Food Protection*, 62, 1038-1040.

Londhal, L., and Goranson, S. "Quality differences in fast freezing." *19th International Congress of Refrigeration*, Sydney, 197-203.

Lonsdale, J. E., McDonald, K. L., and Jones, R. L. (1999). High pressure freezing and freeze substitution reveal new aspects of fine structure and maintain protein antigenicity in barley aleurone cells. *Plant Journal*, 17, 221-229.

Lopez-Caballero, M. E., Perez-Mateos, M., Borderias, J. A., and Montero, P. (2000). Extension of the shelf life of prawns (*Penaeus japonicus*) by vacuum packaging and high-pressure treatment. *Journal of Food Protection*, 63(1), 1381-1388.

Lowry, P. D., Gill, C. O., and Pham, Q. T. (1989). A quantitative method of determining the hygienic efficiency of meat thawing processes. *Food Australia*, 41, 1080.

Lüdemann, H.-D. (1994). Water and its solutions at high pressures and low temperatures. *Polish Journal of Chemistry*, 68, 1-22.

Ludikhuyze, L., and Hendrickx, M. E. G. (2002). Effects of high pressure on chemical reactions related to food quality. In: *Ultra High Pressure Treatments of Foods*, M. E. G. Hendrickx and D. Knorr, eds., Kluwer Academic/Plenum Publishers, New York, 23-51.

Ludikhuyze, L., Indrawati, I., Van den Broeck, I., Weemaes, C., and Hendrickx, M. (1998). Effect of combined pressure and temperature on soybean lipoxygenase: 1. Influence of extrinsic and intrinsic factors on isobaric-isothermal inactivation kinetics. *Journal of Agricultural and Food Chemistry*, 46, 4074-4080.

Luscher, C., Schlüter, O. and Knorr, D. (2003). High Pressure – Low Temperature Processing of Foods: Impact on Cell Membranes, Texture, Color and Visual Appearance of Potato Tissue. *Innovative Food Science & Emerging Technologies*, (in press)

Makita, T. (1992). Application of high pressure and thermophysical properties of water to biotechnology. *Fluid Phase Equilibria*, 76, 87-95.

Mallett, C. P. (1993). Editorial introduction. In: *Frozen food technology*, C. P. Mallett, ed., Blackie Academic & Professional, Glasgow.

Mallikarjunan, P., and Hung, Y.-C. (1997). Physical and ultrastructural measurements. In: *Quality in frozen food*, M. C. Erickson and Y.-C. Hung, eds., Chapman & Hall, New York, 313-339.

Mannapperuma, J. D., and Singh, R. P. (1988). Prediction of freezing and thawing times of foods using a numerical method based on enthalpy formulation. *Journal of Food Science*, 53(2), 626-630.

Marek, R., and Götz, W. (1995). In: *Numerische Lösung von partiellen Differentialgleichungen mit finiten Differenzen*, Moreno-Verlag, Buchenloe.

Martens, M., Scheerlinck, N., De Belie, N., and De Baerdemaeker, J. (2001). Numerical model for the combined simulation of heat transfer and enzyme inactivation in cylindrical vegetables. *Journal of Food Engineering*, 47, 185-193.

Martino, M. N., Otero, L., Sanz, P. D., and Zaritzky, N. E. (1998). Size and location of ice crystals in pork frozen by high-pressure-assisted freezing as compared to classical methods. *Meat Science*, 50(3), 303-313.

Mason, T. J. (1998). Power ultrasound in food processing - the way forward. In: *Ultrasound in food processing*, M. J. W. Povey and T. J. Mason, eds., Blackie Academic & Professional, Glasgow, UK.

Massaux, C., Bera, F., Steyer, B., Sindic, M., and Deroanne, C. (1999a). High hydrostatic pressure freezing and thawing of pork meat: quality preservation, processing times and high pressures treatment advantages. In: *Advances in High Pressure Bioscience and Biotechnology*, H. Ludwig, ed., Springer-Verlag, Heidelberg, 485-488.

Massaux, C., Bera, F., Steyer, B., Sindic, M., and Deroanne, C. (1999b). High hydrostatic pressure effects on freezing and thawing processes of pork meat. In: *Advances in High Pressure Bioscience and Biotechnology*, H. Ludwig, ed., Springer-Verlag, Heidelberg, 496-500.

Mertens, B. A. (1994). High pressure equipment for the food industry. *High Pressure Research*, 12, 229-237.

Meyer, E. D., Sinclair, N. A., and Nagy, B. (1975). Comparison of the survival and metabolic activities of psychrophilic and mesophilic yeasts subjected to freeze-thaw stress. *Applied Microbiology*, 29, 739-744.

Miles, C. A. (1991). The thermophysical properties of frozen foods. In: *Food freezing: today and tomorrow*, W. B. Bald, ed., Springer-Verlag, London, 45-65.

Miles, C. A., Morley, M. J., and Rendell, M. (1999). High power ultrasonic thawing of frozen foods. *Journal of Food Engineering*, 39, 151-159.

Miyawaki, O., Abe, T., and Yano, T. (1989). A numerical model to describe freezing of foods when supercooling occurs. *Journal of Food Engineering*, 9, 143-151.

Murakami, T., Kimura, I., Miyawaka, H., Sugimoto, M., and Satake, M. (1994). High pressure thawing of frozen fish. In: *High Pressure Bioscience*, R. Hayashi, S. Kunugi, S. Shimada, and A. Suzuki, eds., San-Ei Suppan Co., Kyoto, 304-311.

Murakami, T., Kimura, I., Yamagishi, T., Yamashita, M., Sugimoto, M., and Satake, M. (1992). Thawing of frozen fish by hydrostatic pressure. In: *High Pressure and Biotechnology*, C. Balny, R. Hayashi, K. Heremans, and P. Masson, eds., Colloque INSERM, 329-331.

Nöckler, K., Heinz, V., Lemkau, K., and Knorr, D. (2001). Inaktivierung von *Trichinella spiralis* in Schweinefleisch durch Hochdruckbehandlung. *Fleischwirtschaft*, 7, 85-88.

Ohlsson, T. (2000). Minimal processing of foods with thermal methods. In: *Innovations in food processing*, G. V. Barbosa-Cánovas and G. W. Gould, eds., Technomic Publishing, Lancaster, 123-140.

Ohnishi, S., Fujii, T., and Miyakawi, O. (2002). Electrical and rheological analysis of freezing injury of agricultural products. *International Journal of Food Properties*, 5(2), 317-332.

Ohshima, T., Ushio, H., and Koizumi, C. (1993). High pressure processing of fish and fish products. *Trends in Food Science & Technology*, 4(11), 370-375.

Okamoto, A., and Suzuki, A. (2001). Effects of high hydrostatic pressure-thawing on pork meat. *Nippon Shokuhin Kagaku Kogaku Kaishi*, 48(12), 891-898.

Olsson, S. (1995). Production equipment for commercial use. In: *High Pressure Processing of Foods*, D. A. Ledward, D. E. Johnston, R. G. Earnshaw, and A. P. M. Hastings, eds., Nottingham University Press, Loughborough, 167-180.

Ooide, A., Kameyama, Y., Iwata, N., Uchio, R., Karino, S., and Kanyama, N. (1994). Non-freezing preservation of fresh foods under subzero temperature. In: *High Pressure Bioscience*, R. Hayashi, S. Kunugi, S. Shimada, and A. Suzuki, eds., San-Ei Suppan Co., Kyoto, 344-351.

Otero, L., Martino, M., Zaritzky, N., Solas, M., and Sanz, P. D. (2000b). Preservation of microstructure in peach and mango during high-pressure-shift freezing. *Journal of Food Science*, 65(3), 466-470.

Otero, L., Molina-Garcia, A. D., and Sanz, P. D. (2002). Some interrelated thermophysical properties of liquid water and ice I: a user-friendly modelling review for food high pressure processing. *Critical Reviews in Food Science and Nutrition*.

Otero, L., and Sanz, P. D. (2000a). High-pressure shift freezing. Part 1. Amount of ice instantaneously formed in the process. *Biotechnology Progress*, 16, 1030-1036.

Otero, L., Sanz, P. D., de Elvira, C., and Carrasco, J. A. (1997). Modelling thermodynamic properties of water in the high-pressure-assisted freezing process. In: *High Pressure Research in the Biosciences and Biotechnology*, K. Heremans, ed., Leuven University Press, Leuven, Belgium, 347-350.

Otero, L., Solas, M. T., and Sanz, P. D. (1998). Contrasting effects of high-pressure-assisted freezing and conventional air-freezing on eggplant tissue microstructure. *Zeitschrift für Lebensmitteluntersuchung und -forschung*, A 206, 338-342.

Palou, E., Lopez-Malo, A., Barbosa-Canovas, G. V., Welti-Chanes, J., and Swanson, B. G. (1997). Effect of water activity on high hydrostatic pressure inhibition of *Zygosaccharomyces bailii*. *Letters in Applied Microbiology*, 24, 417-420.

Palou, E., Lopez-Malo, A., Barbosa-Canovas, G. V., Welti-Chanes, J., and Swanson, B. G. (1999). High-pressure treatment in food preservation. In: *Handbook of Food Preservation*, M. S. Rahman, ed., Marcel Dekker, New York, 533-575.

Panoff, J.-M., Thammavongs, B., Guéguen, M., and Boutibonnes, P. (1998). Cold stress responses in mesophilic bacteria. *Cryobiology*, 36, 75-83.

Patterson, M. F., and Kilpatrick, D. J. (1998). The combined effect of high hydrostatic pressure and mild heat on inactivation of pathogens in milk and poultry. *Journal of Food Protection*, 61(4), 432-436.

Pegg, D. E., Wusteman, M. C., and Boylan, S. (1997). Fractures in cryopreserved elastic arteries. *Cryobiology*, 34, 183-192.

Pething, R., and Kell, D. (1987). The passive electrical properties of biological system: their significance in physiology, biophysics and biotechnology. *Physics in Medicine and Biology*, 32, 933-970.

Petrenko, V. F., and Withworth, R. W. (1999). In: *Physiks of ice*, Oxford University Press, New York.

Pham, Q. T. (1985). A fast, unconditionally stable finite-difference scheme for heat conduction with phase change. *International Journal of Heat and Mass Transfer*, 28, 2079-2084.

Pham, Q. T. (1987). A note on some finite-difference methods for heat conduction with phase change. *Numerical Heat Transfer*, 11, 353-359.

Pham, Q. T. (1989). Effect of supercooling on freezing time due to dendritic growth of ice crystals. *International Journal of Refrigeration*, 12, 295-300.

Pham, Q. T. (1996). Prediction of calorimetric properties and freezing time of foods from composition data. *Journal of Food Engineering*, 30, 95-107.

Pham, Q. T. (2001). Modelling thermal processes: cooling and freezing. In: *Food process modelling*, L. M. M. Tijskens, M. L. A. T. M. Hertog, and B. M. Nicolai, eds., Woodhhead Publishing Limited, Cambridge, UK, 312-339.

Pham, Q. T., and Mawson, R. F. (1997). Moisture migration and ice recrystallization in frozen foods. In: *Quality in frozen food*, M. C. Erickson and Y.-C. Hung, eds., Chapman & Hall, New York, 67-91.

Polley, S. L., Snyder, O. P., and Kotnour, P. (1980). A compilation of thermal properties of foods. *Food Technology*, 11, 76-94.

Pons, M., and Fiszman, S. M. (1996). Instrumental texture profile analysis with particular reference to gelled systems. *Journal of Texture Studies*, 27(6), 597-624.

Pothakamury, U. R., Barbosa-Canovas, G. V., Swanson, B. G., and Meyer, R. S. (1995). The pressure builds for better food processing. *Chemical Engineering Progress,* (3), 45-53.

Préstamo, G., and Arroyo, G. (1998). High hydrostatic pressure effects on vegetable structure. *Journal of Food Science*, 63(5), 878-881.

Ramaswamy, H. S., and Tung, M. A. (1984). A review on predicting freezing times of foods. *Journal of Food Process Engineering*, 7, 169-203.

Reid, D. S. (1983). Fundamental physicochemical aspects of freezing. *Food Technology*, 37(4), 110.

Reid, D. S. (1993). Basic physical phenomena in the freezing and thawing of plant and animal tissue. In: *Frozen food technology*, C. P. Mallett, ed., Blackie Academic & Professional, Glasgow, 1-19.

Reid, D. S. (1997). Overview of physical/chemical aspects of freezing. In: *Quality in frozen food*, M. C. Erickson and Y.-C. Hung, eds., Chapman & Hall, New York, 10-28.

Reid, D. S. (1998). Freezing - nucleation in foods and antifreeze actions. In: *Properties of water in foods ISOPOW 6*, D. S. Reid, ed., Blackie Academic & Professional, London, 275-286.

Reilly, A., and Kaferstein, F. (1997). Food safety hazards and the application of the principles of the hazard analysis and critical control point (HACCP) system for their control in aquaculture production. *Aquaculture Research*, 28, 735-752.

Resurreccion, A. V. A. (1997). Sensory evaluation methods to measure quality of frozen food. In: *Quality in frozen food*, M. C. Erickson and Y.-C. Hung, eds., Chapman & Hall, New York, 357-376.

Robbers, M., Singh, R. P., and Cunha, L. M. (1997). Osmotic-convective dehydrofreezing process for drying kiwi fruit. *Journal of Food Science*, 62(5), 1039-1042.

Roos, Y., and Karel, M. (1990). Differential scanning calorimetry study of phase transitions affecting quality of dehydrated materials. *Biotechnology Progress,*(6), 159-163.

Roos, Y. H. (1992). Phase transitions and transformations in food systems. In: *Handbook of food engineering*, D. R. Heldman and D. B. Lund, eds., Marcel Dekker, Inc., New York, 145-197.

Ross, R. G., Andersson, P., and Bäckström, G. (1977). Thermal conductivity of nine solid phases of H_2O. *High Temperature - High Pressure*, 9, 87-96.

Rouillé, J., Le Bail, A., Ramaswamy, H. S., and Leclerc, L. (2002). High pressure thawing of fish and shellfish. *Journal of Food Engineering*, 53, 83-88.

Rovere, P. (2002). Industrial-scale high pressure processing of foods. In: *Ultra High Pressure Treatments of Foods*, M. E. G. Hendrickx and D. Knorr, eds., Kluwer Academic/Plenum Publishers, New York, 251-268.

Roy, S., Eckard, K. J., Lancelle, S., Hepler, P. K., and Lord, E. M. (1997). High-pressure freezing improves the ultrastructural preservation of in vivo grown lily pollen tubes. *Protoplasma*, 200, 87-98.

Roy, S. S., Taylor, T. A., and Kramer, H. L. (2001). Textural and ultrastructural changes in carrot tissue as affected by blanching and freezing. *Journal of Food Science*, 66(1), 176-180.

Rubens, P., Snauwaert, J., Heremans, K., and Stute, R. (1999). In-situ observation of pressure-induced gelation of starches studied with FT-IR in the diamond anvil cell. *Carbohydrate Polymers*, 39, 231-235.

Sahagian, M. E., and Goff, H. D. (1996). Fundamental aspects of the freezing process. In: *Freezing effects on food quality*, L. E. Jeremiah, ed., Marcel Dekker, New York, 1-50.

Sanz, P. D., de Elvira, C., Martino, M., Zaritzky, N., Otero, L., and Carrasco, J. A. (1999). Freezing rate simulation as an aid to reducing crystallization damage in foods. *Meat Science*, 52, 275-278.

Sanz, P. D., and Otero, L. (2000). High-pressure shift freezing. Part 2. Modeling of freezing times for a finite cylindical model. *Biotechnology Progress*, 16, 1037-1043.

Sanz, P. D., Otero, L., de Elvira, C., and Carrasco, J. A. (1997). Freezing processes in high pressure domains. *International Journal of Refrigeration*, 20, 301-307.

Sapers, G. M., Douglas, J., F.W., Bilyk, A., Hsu, A. F., Dower, H. W., Garzarella, L., and Kozempel, M. (1989). Enzymatic browning in Atlantic potatoes and related cultivars. *Journal of Food Science*, 54(2), 362-365.

Schubring, R. (1998). Determination of fish freshness by instrumental colour measurement. *Fleischwirtschaft International*, 26-29.

Schubring, R. (1999). DSC studies on deep frozen fishery products. *Thermochimica Acta*, 337, 89-95.

Schubring, R., Meyer, C., Schlüter, O., Boguslawski, S. and Knorr, D. (2003). Impact of high pressure assisted thawing on the quality of fillets from various fish species. *Innovative Food Science & Emerging Technologies*, 4, 257-267.

Schulson, E. M. (1999). The Structure and mechanical behavior of Ice. *The Member Journal of The Minerals, Metals & Materials Society (JOM)*, 51(2), 21-27.

Shi, X., Datta, A. K., and Mukherjee, S. (1999). Thermal fracture in a biomaterial during rapid freezing. *Journal of Thermal Stresses*, 22, 275-292.

Singh, R. P., and Heldman, D. R. (2001). In: *Introduction to food engineering*, Academic Press, London, UK.

Skrede, G. (1996). Fruits. In: *Freezing effects on food quality*, L. E. Jeremiah, ed., Marcel Dekker, New York, 183-246.

Slade, L., and Levine, H. (1991). Beyond water activity: recent advances based on an alternative approach to the assessment of food quality and safety. *CRC Critical Reviews in Food Science and Nutrition*, 30, 115-360.

Smelt, J. P., Hellemons, J. C., and Patterson, M. (2002). Effects of high pressure on vegetative microorganisms. In: *Ultra High Pressure Treatments of Foods*, M. E. G. Hendrickx and D. Knorr, eds., Kluwer Academic/Plenum Publishers, New York, 55-76.

Smelt, J. P. P. M. (1998). Recent advances in the microbiology of high pressure processing. *Trends in Food Science & Technology*, 9, 152-158.

Song, Y. C., Khirabadi, B. S., Lightfoot, F., Brockbank, K. G. M., and Taylor, M. J. (2000). Vitreous cryopreservation maintains the function of vascular grafts. *Nature Biotechnology*, 18, 296-299.

Steponkus, P. L. (1984). Role of the plasma membrane in freezing injury and cold acclimation. *Annual Review of Plant Physiology*, 35(543-584).

Studer, D., Michel, M., Wohlwend, M., Hunziker, E. W., and Buschmann, M. D. (1995). Vitrification of articular cartilage by high-pressure freezing. *Journal of Microscopy*, 179, 321-332.

Styles, M. F., Hoover, D. G., and Farkas, D. F. (1991). Response of *Listeria monocytogenes* and *Vibrio parahaemolyticus* to high hydrostatic pressure. *Journal of Food Science*, 56, 1404-1407.

Suzuki, K. (1960). Studies on the kinetics of protein denaturation under high pressure. *Reviews in Physics and Chemistry of Japan*, 29, 91-98.

Takahashi, K. (1992). Sterilization of microorganisms by hydrostatic pressure at low temperature. In: *High Pressure and Biotechnology*, C. Balny, R. Hayashi, K. Heremans, and P. Masson, eds., John Libbey Eurotext, Montrouge, 303-307.

Takahashi, T., Kakita, A., Takahashi, Y., Yokoyama, K., Sakamoto, I., and Yamashina, S. (2001). Preservation of rat livers by supercooling under high pressure. *Transplantation Proceedings*, 33, 916–919.

Tammann, G. (1900). Über die Grenzen des festen Zustandes IV. *Annalen der Physik*, 4(2), 1-31.

Tangwongchai, R., Ledward, D. A., and Ames, J. M. (2000). Effect of high-pressure treatment on the texture of cherry tomato. *Journal of Agricultural & Food Chemistry*, 48(5), 1434-1441.

Taniguchi, T., Stanley, H. E., and Ludwig, H. (2002). In: *Biological Systems Under Extreme Conditions: Structure and Function*, Springer-Verlag, Berlin.

Taniguchi, Y., and Suzuki, K. (1983). Pressure inactivation of α-chymotrypsin. *Journal of Physical Chemistry*, 87, 5185-5193.

Tant, M. R., and Wilkes, G. L. (1981). An overview of the nonequilibrium behavior of polymer glasses. *Polymer Engineering and Science,* (21), 874-895.

Tauscher, B. (1995). Pasteurization of food by hydrostatic high pressure: chemical aspects. *Zeitschrift für Lebensmitteluntersuchung und -forschung*, 200(1), 3-13.

Ter Minassian, L., and Pruzan, P. (1981). Thermodynamic properties of water under pressure up to 5 kbar and between 28 and 120°C. Estimations in the supercooled region down to -40°C. *Journal of Chemical Physics*, 75(6), 3064-3072.

Teramoto, A., and Fuchigami, M. (2000). Changes in temperature, texture and structure of Konnyaku (konjac gluomannan gel) during high-pressure-freezing. *Journal of Food Science*, 63(3), 491-497.

Tewari, G., Jayas, D. S., and Holley, R. A. (1999). High pressure processing of foods: an overview. *Sciences des Aliments*, 19, 619-661.

Thakur, B. R., and Nelson, P. E. (1998). High-pressure processing and preservation of food. *Food Review International*, 14(4), 427-447.

Thiebaud, M., Dumay, E. M., and Cheftel, J. C. (2002). Pressure-shift freezing of o/w emulsions: influence of fructose and sodium alginate on undercooling, nucleation, freezing kinetics and ice crystal size distribution. *Food Hydrocolloids*, 16(6), 527-545.

Thijssen, M. H., Mittempergher, F., Van Aelst, A. C., and Van Went, J. L. (1997). Improved ultrastructural preservation of *Petunia* and *Brassica* ovules and embryo sacs by high pressure and freeze substitution. *Protoplasma*, 197(199-209).

Tong, C. H., Lentz, R. R., and Lund, D. B. (1993). A microwave oven with variable continuous power and feedback temperature controller. *Biotechnology Progress*, 9, 488-496.

Ulmer, H. M., Herberhold, H., Fahsel, S., Gaenzle, M. G., Winter, R., and Vogel, R. F. (2002). Effects of pressure-induced membrane phase transitions on inactivation of HorA, an ATP-dependent multidrug resistance transporter, in *Lactobacillus plantarum*. *Applied and Environmental Microbiology*, 68(3), 1088-1095.

Van den Berg, R. W., Hoogland, H., Lelieveld, H. L. M., and Van Schepdael, L. (2002). High pressure equipment designs for food processing applications. In: *Ultra High Pressure Treatments of Foods*, M. E. G. Hendrickx and D. Knorr, eds., Kluwer Academic/Plenum Publishers, New York, 23-51.

Wagner, W., Saul, A. b., and Pruß, A. (1994). International equations for the pressure along the melting and along the sublimation curve of ordinary water substance. *Journal of Physical and Chemical Reference Data*, 23, 515-527.

Walker, R. L., Jensen, L. H., Kinde, H., Alexander, A. V., and Owens, L. S. (1991). Environmental survey for *Listeria spp.* in frozen milk products plants in California. *Journal of Food Protection*, 45, 178-182.

Warm, K., Boknaes, N., and Nielsen, J. (1998). Development of quality index methods for evaluation of frozen cod (*Gadus morhua*) and cod fillets. *Journal of Aquatic Food Product Technology*, 7(1), 45-59.

Weber, H. (1996). In: *Mikrobiologie der Lebensmittel. Milch und Milchprodukte*, Behr, Hamburg.

Weemaes, C., Ludikhuyze, L., van den Broeck, I., and Hendrickx, M. E. G. (1998). High pressure inactivation of polyphenoloxidases. *Journal of Food Science*, 63(5), 873-877.

Weingand-Ziadé, A., Renault, F., and Masson, P. (1997). Combined pressure/heat-induced inactivation of butyrylcholinesterase. *Biochimica et Biophysica Acta*, 1340(245-252).

Winter, R., and Czelik, C. (2000). Pressure effects on the structure of lyotropic lipid mesophases and model biomembrane systems. *Zeitschrift für Kristallographie*, 215, 454-474.

Wouters, P. C., Glaasker, E., and Smelt, J. P. P. M. (1998). Effects of high pressure on inactivation kinetics and events related to proton efflux in *Lactobacillus plantarum*. *Applied and Environmental Microbiology*, 64(2), 509-514.

Yayanos, A. A. (1998). Empirical and theoretical aspects of life at high pressure in the deep sea. In: *Extremophiles: Microbial Life in Extreme Environments*, K. Horikoshi and W. D. Grant, eds., Wiley-Liss, New York, 47-.

Yoshioka, K., Yamada, A., and Maki, T. (1996). Application of high pressurization to fish meat: changes in the physical properties of carp muscle resulting from high pressure thawing. In: *High Pressure Bioscience and Biotechnology*, R. Hayashi and C. Balny, eds., Elsevier Science B.V., 369-374.

Yuste, J., Mor-Mur, M., Capellas, M., Guamis, B., and Pla, R. (1998). Microbiological quality of mechanically recovered poultry meat treated with high hydrostatic pressure and nisin. *Food Microbiology*, 15, 407-414.

Zang, J., Peng, X., Jonas, A., and Jonas, J. (1995). NMR study of the cold, heat, and pressure unfolding of ribonuclease A. *Biochemistry*, 34(27), 8631-8641.

Zenker, M., Heinz, V., and Knorr, D. (2000). Hydrostatischer Hochdruck zur Erhöhung der mikrobiellen Sicherheit streichfähiger Rohwürste. Zeitschrift für Lebensmittel- und Verpackungstechnik, 45(2), 89-92.

Zhang, M. I. N., and Willison, J. H. M. (1992a). Electrical impedance analysis in plant tissues: The effect of freeze-thaw injury on the electrical properties of potato tuber and carrot root tissues. *Canadian Journal of Plant Science*, 72(2), 545-553.

Zhang, M. I. N., and Willison, J. H. M. (1992b). Electrical impedance analysis in plant tissues: in vivo detection of freezing injury. *Canadian Journal of Botany*, 70, 2254-2258.

Zhao, Y., Flores, R. A., and Olson, D. G. (1998). High hydrostatic pressure effects on rapid thawing of frozen beef. *Journal of Food Science*, 63(2), 272-275.

Zimmermann, U. (1982). Electric field mediated fusion and related electrical phenomena. *Biochimica et Biophysica Acta*, 694, 227-277.

LIST OF PUBLICATIONS

BOOK CHAPTER

Denys, S., Schlüter, O., Hendrickx, M.E.G., and Knorr D. (2002). Effects of high pressure on water-ice transitions in foods. In: *Ultra high pressure treatments of foods,* M.E.G. Hendrickx & D. Knorr, eds. New York: Kluwer Academic / Plenum Publishers. 2002, 215-248.

INTERNATIONAL JOURNALS

Knorr, D., Schlüter, O., and Heinz, V. (1998) Impact of high hydrostatic pressure on phase transitions of foods. *Food Technology*, 52 (9), 42-45.

Amanatidou, A., Schlüter, O., Lemkau, K., Gorris, L. G. M., Smid, E. J., and Knorr, D. (2000). Effect of combined application of high pressure treatment and modified atmospheres on shelf-life of fresh atlantic salmon. *Innovative Food Science & Emerging Technologies*, 1, 87-98.

Lee, D.-U., Schlüter, O., Heinz, V. and Knorr, D. (2000). High pressure treatment of liquid whole egg and advantages of low temperature application. *High Pressure Research*, 19, 521-526.

Ananta, E., Heinz, V., Schlüter, O., and Knorr, D. (2001). Kinetic studies on high-pressure inactivation of *Bacillus stearothermophilus* spores suspended in food matrices. *Innovative Food Science &. Emerging Technologies*, 2, 261-272.

Luscher, C., Schlüter, O. and Knorr, D. (2003). High Pressure – Low Temperature Processing of Foods: Impact on Cell Membranes, Texture, Color and Visual Appearance of Potato Tissue. *Innovative Food Science & Emerging Technologies*, (in press)

Schubring, R., Meyer, C., Schlüter, O., Boguslawski, S. and Knorr, D. (2003). Impact of high pressure assisted thawing on the quality of fillets from various fish species. *Innovative Food Science & Emerging Technologies*, 4, 257-267.

Schlüter, O., Urrutia Benet, G., Heinz V. and Knorr D. (2003). Metastable states of water and ice during pressure-supported freezing of potato tissue. *Biotechnology Progress*. (in press)

INTERNATIONAL CONGRESSES (PROCEEDINGS)

Schlüter, O., Heinz, V., and Knorr, D. (1998). Freezing of potato cylinders during high pressure treatment in *High Pressure Food Science, Bioscience and Chemistry*; Isaacs, N.S. Ed.; The Royal Society of Chemistry, Cambridge, 317-324.

Knorr, D., Heinz, V., Schlüter, O. and Zenker, M. (1998). The potential and impact of high pressure as unit operation for food processing, in *High Pressure Food Science, Bioscience and Chemistry*, ed. by Isaacs, N. S., University of Reading, UK.

Schlüter, O., George, S., Heinz, V. and Knorr, D. (1999). Pressure assisted thawing of potato cylinders. in Advances in *High Pressure Bioscience and Biotechnology*; Ludwig, H. Ed.; Springer-Verlag, Heidelberg, Germany, 475-480.

Schlüter, O. and Knorr, D. (2002). Impact of the metastable state of water on the design of high pressure supported freezing and thawing processes. ASAE Meeting Paper No. 026024. 2002. St. Joseph, MI, USA: ASAE.

Luscher, C., Schlüter, O., Heinz, V. and Knorr, D. (2003) Comparison of structural cell membrane changes induced by different high pressure processes at low temperatures, in *Advances in High Pressure Bioscience and Biotechnology*; Winter, R. Ed.; Springer-Verlag, Heidelberg, Germany, 351-354.

Schlüter, O., Heinz, V. and Knorr, D. Freezing kinetics due to ice III formation in potato tissue, in Advances in *High Pressure Bioscience and Biotechnology*; Winter, R. Ed. 2003; Springer-Verlag, Heidelberg, Germany, 425-430

INTERNATIONAL CONGRESSES (ORAL PRESENTATION / POSTERS)

Schlüter, O. and Knorr, D. (1998). Phase Transitions in Plant Tissues induced by Pressure Assisted Freezing and Pressure Assisted Thawing, Oral presentation, IFT Annual Meeting, 20. - 24. Juni 1998, Atlanta GA, USA.

Schlüter, O., George, S., Heinz, V. and Knorr, D. (1998). Pressure Assisted Thawing of Potato Cylinders, Poster presentation, Model-it Conference, Wagenningen, The Netherlands.

Schlüter, O., George, S., Heinz, V. and Knorr, D. (1998). Phase Transitions in Plant Tissues induced by Pressure Assisted Freezing and Pressure Assisted Thawing, Oral presentation, IIR/IIF Refrigeration Conference, 23. - 26. September, Sofia, Bulgaria.

Amanatidou, A., Schlüter, O., Knorr, D. and Smid, E.J. (1999). Antimicrobial activity of O_2 and CO_2 under pressure on food-related pathogens, Poster presentation, "Microbial stress symposium",Quimper, France.

Lee, D.-U., Schlüter, O., Heinz, V. and Knorr, D. (1999). High pressure treatment of liquid whole egg and advantages of low temperature application. Poster presentation. 37th European High Pressure Research Group Meeting, September, Montpellier, France.

Schlüter, O., Heinz, V. and Knorr, D. (2001). High Pressure and Phase Transitions of Food. Oral presentation, 4th High Pressure School, Warsaw, Poland.

Schlüter, O., Luscher, C. and Knorr, D. (2001). Liquid – Solid Phase Boundaries of Potato Tissue at Subzero (°C) Temperatures and Pressures up to 450 MPa. Poster presentation. European Conference on Advanced Technology for Safe and High Quality Foods - EUROCAFT, 5.-7. December, Berlin, Germany.

Schlüter, O. and Knorr, D., (2001). Process Indication during Pressure Freezing/Thawing. Oral presentation, 2nd Joint IFT/EFFoST Nonthermal Processing Workshop 2001, 9.-11.Dezember, Berlin.

Schlüter, O., Heinz, V. and Knorr, D. (2002). Optimisation of Pressure Supported Freezing/Thawing Processes by making Use of Metastable States of Water. Poster presentation. Symposium on Emerging Technologies for the Food Industry - EmerTec, 11.-13. March, Madrid, Spain.

NATIONAL SYMPOSIA (ORAL PRESENTATION / POSTERS)

Schlüter, O. Heinz, V. und Knorr, D. (1998). Phasenübergänge bei hochdruckunterstützten Gefrier- und Auftauprozessen am Beispiel pflanzlicher Gewebe, Vortrag, Interne Arbeitssitzung der Fachausschüsse Bioverfahrenstechnik und Lebensmittelverfahrenstechnik der GVC - VDI Gesellschaft Verfahrenstechnik und Chemieingenieurwesen, 19. und 20. Mai 1998, Baden-Baden.

Schlüter, O. Heinz, V. und Knorr, D. (1999). Kontrollierte Temperaturführung zur gezielten Beeinflussung von Hochdruckprozessen, Vortrag, Interne Arbeitssitzung des Fachausschusses Lebensmittelverfahrenstechnik der GVC - VDI Gesellschaft Verfahrenstechnik und Chemieingenieurwesen, 3. - 5. März, Zürich.

Schlüter, O., Luscher, C., und Knorr, D. (2001). Experimentelle Bestimmung und mathematische Beschreibung der Phasengrenzlinien von Lebensmitteln bei Gefrier- und Auftauprozessen unter hohem hydrostatischem Druck bis 450 MPa. GDL-Kongress Lebensmitteltechnologie 2001, 8. - 10. November, Berlin. Proceedings, 283-290.

Schlüter, O., Heinz, V. und Knorr, D., (2001). Untersuchung metastabiler Zustandsgebiete bei hochdruckunterstützten Phasenumwandlungen (flüssig – fest) und deren Bedeutung für die Prozessauslegung. Vortrag, GDL-Kongress Lebensmitteltechnologie, 8. - 10. November, Berlin. Proceedings, 291-300.

Angersbach, A., Heinz, V., Schlüter, O, Ananta, E, Knorr, D. und Bunin V. (2001). Sicherung der Reproduzierbarkeit von Populationszuständen bei der Untersuchungen von Mikroorganismen unter Nutzung einer elektro-optischen Messmethode. Vortrag, GDL-Kongress Lebensmitteltechnologie 2001, 8. bis 10. November, Berlin. Proceedings, 233-238.

Angersbach, A., Heinz, V., Schlüter und Knorr, D. (2001). Einsatz einer elektrophysikalischen Messmethode zur Charakterisierung des prozessbedingten Zustandes bei der technologischen Verarbeitung zellulärer Lebensmittel. Vortrag, GDL-Kongress Lebensmitteltechnologie 2001, 8. bis 10. November, Berlin.

Schlüter, O. und Knorr, D. (2002). Charakterisierung eines metastabilen Zustandsgebietes und seine Bedeutung für die Auslegung von Hochdruckprozessen im Gefrierbereich. Vortrag anläßlich der GVC Fachausschuss-Sitzung „Lebensmittelverfahrenstechnik“, 6. und 7. März, Weimar.